Diss. ETH No. 12988

Primordial noble gases in "Phase Q" in carbonaceous and ordinary chondrites studied by closed system stepped etching

A dissertation submitted to the

SWISS FEDERAL INSTITUTE OF TECHNOLOGY ZÜRICH

for the degree of

DOCTOR OF NATURAL SCIENCES

presented by

Henner Busemann

Diplom-Physiker, University of Hannover (Germany)

born May 31, 1967

citizen of Germany

accepted on the recommendation of

PD Dr. R. Wieler, ETH Zürich, examiner

Prof. Dr. A. N. Halliday, ETH Zürich, co-examiner

PD Dr. U. Ott, MPI Mainz, co-examiner

Zürich 1998

Contents

Leer - Vide - Empty

Abstract

The analysis of noble gases in meteorites provides insights into physical processes that have occurred in our solar system and even beyond. Noble gases have been incorporated or processed during the residence of the meteorites on Earth or in space, on the meteorite parent bodies, in the forming solar system and during nucleosynthesis in stars, outflows of which have contributed to the presolar molecular cloud. One of the most puzzling meteoritic noble gas components is the primordial gas that resides in an ill-defined carrier which has been named "phase Q". This almost mass-less, carbonaceous carrier contains most of the heavier primordial noble gases Ar, Kr and Xe, but only small amounts of the primordial He and Ne. All primordial noble gases are highly concentrated in HF/HCl-resistant residues. The noble gases trapped in phase Q are released upon oxidising with acids such as HNO_3. The typical large depletion, up to seven orders of magnitude, of the light noble gases relative to Xe and solar abundances, has been found in many meteorites of different chemical classes. Therefore, Q-gases and the presumably related noble gases found in ureilites are assumed to have been widespread in the early solar system. Not only the exact composition of the carrier phase is unknown, also the location where the gases have been trapped, as well as the origin of the Q-gases, are not yet known and are subject to debate.

The aim of this study is to better characterise especially the light Q-noble gases He and Ne in HF/HCl-resistant residues from meteorites of different chemical classes. Closed system stepped etching (CSSE), developed at ETH Zürich, appears to be the most suitable technique to analyse Q-gases, since up to now it is the only one capable of measuring He abundances as well as the He isotopic composition. This method also yields the most precise data for Ne. A large number of etch steps allows the separation of Q-gases and simultaneously released components such as cosmogenic and solar noble gases, or Ne-E(L) residing in presolar graphite. In this work, the HF/HCl-resistant residues of the chondrites CO3.4 Lancé, H3.7 Dimmitt, CV3 (ox.) Grosnaja, LL3.4 Chainpur and CM2 Cold Bokkeveld have been measured successfully. The analyses yielded these following results: All isotopic ratios in phase Q of the different meteorites are quite uniform, except for the $(^{20}Ne/^{22}Ne)_Q$ ratio. Most importantly, the $(^3He/^4He)_Q$ ratio is $(1.45 \pm 0.01) \times 10^{-4}$ for CV3 (ox.) Grosnaja and $(1.41 \pm 0.01) \times 10^{-4}$ for CM2 Cold Bokkeveld. These values are lower than the only available values for Q, measured in CV3 (ox.) Allende and CM2 Murchison (Wieler *et al.*, 1991; 1992), which must have been slightly compromised by cosmogenic He. The new data are also lower than the $^3He/^4He$ ratio of

$(1.66 \pm 0.05) \times 10^{-4}$, measured in the Jovian atmosphere (Mahaffy *et al.*, 1998). The mean $(^3He/^4He)_Q$ ratio of $(1.43 \pm 0.03) \times 10^{-4}$ obtained here has been used to determine the protosolar D/H ratio. The calculated value of $(2.3 \pm 0.5) \times 10^{-5}$ is in agreement with the ratio obtained from the Jovian atmosphere which has been assumed to have sampled unaltered protosolar hydrogen. Therefore, it appears to be possible that *both* He-Q and He in the giant planet *represent unaltered primordial pre-Deuterium-burning He*, slightly modified by fractionation. The protosolar D/H ratio is of importance to test the predictions of the standard Big-Bang nucleosynthesis theory by providing limits on cosmic parameters such as the baryon density.

As already suggested by precise earlier measurements (Schelhaas *et al.*, 1990; Wieler *et al.*, 1991; 1992), the $(^{20}Ne/^{22}Ne)_Q$ ratio is the least uniform isotopic ratio of the noble gases in phase Q. The data vary, on the one hand, between 10.05 ± 0.05 and 10.17 ± 0.03 for Cold Bokkeveld and Lancé, respectively, and on the other hand, between 10.6 ± 0.2, 10.60 ± 0.06 and 10.66 ± 0.04 for Dimmitt, Chainpur and Grosnaja, respectively. A correlation of the $(^{20}Ne/^{22}Ne)_Q$ ratio with the classification or the alteration history of the meteorites has not been found. However, the isotopic ratios of the other elements in all meteorites are rather similar. Thus, an unknown process probably accounts for the alteration of the originally incorporated Ne-Q. The Ar, Kr and Xe isotopic ratios for all five samples are identical within their uncertainties and similar to earlier Q determinations as well as to those found in ureilites.

This work provides the first evidence from noble gas data that Q consists of at least two carbonaceous carrier phases "Q_1" and "Q_2" with slightly distinct chemical properties. However, these sub-phases may well have incorporated noble gases from the same reservoir, which is indicated by the similar, characteristically increasing depletion of the lighter noble gases relative to Xe and solar abundances. The CSSE experiment on CM2 Cold Bokkeveld has yielded that phase Q_1 is enriched in He and Ne relative to phase Q_2 and Xe and might be related to presolar graphite, the carrier of the simultaneously released Ne-E(L). The elemental ratios of the heavier noble gases $(Ar/Xe)_Q$ and $(Kr/Xe)_Q$ reflect both thermal metamorphism and aqueous alteration. These parent body processes have led to larger depletions of Ar and Kr relative to Xe. In contrast, meteorites that suffered severe aqueous alteration, such as the CM chondrites, do not show depletions of He and Ne relative to Ar but rather the highest $(He/Ar)_Q$ and $(Ne/Ar)_Q$ ratios. This hints to a carrier phase Q_1, which is enriched in He and Ne and less susceptible to aqueous alteration than carrier phase Q_2.

The residues of Chainpur and Cold Bokkeveld contain significant amounts of Ne-E(L). The concentrations of 0.15 and 5.12×10^{-10} cm^3 STP ^{22}Ne-E(L)/g meteorite, respectively, confirm the suggestion of Huss (1997) that the ^{22}Ne-E(L) content, and thus the presolar graphite abundances, are correlated with the metamorphic history of the meteorites.

Kurzfassung

Die Analyse von Edelgasen in Meteoriten erlaubt Einblicke in physikalische Prozesse, die in unserem Sonnensystem und auch darüber hinaus ablaufen. Edelgase wurden während des Aufenthalts des Meteorits auf der Erde oder im Weltall, auf den Meteoritenmutterkörpern, im sich bildenden Sonnensystem und während der Nukleosynthese in Sternen, deren Produkte danach in die präsolare molekulare Wolke gelangt sind, eingebaut oder in ihrer Zusammensetzung verändert. Eine der rätselhaftesten meteoritischen Edelgaskomponenten ist jenes primordiale Gas, welches in einem nur sehr schlecht charakterisiertem Trägermaterial sitzt, der sogenannten „Phase Q". Dieser fast masselose kohlenstoffhaltige Träger enthält den Großteil der schweren primordialen Edelgase Ar, Kr und Xe, aber lediglich kleinere Mengen des primordialen He und Ne. Alle primordialen Edelgase sind in HF/HCl resistenten Rückständen der Meteorite enorm angereichert. Die in Phase Q enthaltenen Edelgase werden durch Oxidation mit Säuren wie z. B. HNO_3 freigesetzt. Die typische Verarmung der leichten Edelgase He und Ne um bis zu sieben Größenordnungen, im Vergleich zu solaren Häufigkeiten und auf Xe normiert, wurde in Meteoriten verschiedenster chemischer Klassen gefunden. Daher wird angekommen, daß die Edelgase der Phase Q und die vermutlich mit ihnen verwandten Edelgase aus Ureiliten im jungen Sonnensystem weitverbreitet gewesen sein mußten. Nicht nur die genaue Zusammensetzung des Trägermaterials „Phase Q" ist unbekannt, ebenso unbekannt und Gegenstand von Diskussionen sind der Ort, an dem die Edelgase eingebaut wurden, sowie die Herkunft dieser Edelgase.

Das Ziel dieser Arbeit ist die bessere Charakterisierung insbesondere der leichten Edelgase He und Ne aus Phase Q in HF/HCl resistenten Rückständen von Meteoriten aus verschiedenen chemischen Klassen. Es hat sich gezeigt, daß das Verfahren des „schrittweisen Oxidierens im Vakuum", das an der ETH Zürich entwickelt wurde, die am besten geeignete Methode zur Analyse der Q-Edelgase ist, und auch die bis jetzt einzige, mit der man sowohl He Konzentrationen als auch die He Isotopenzusammensetzung messen kann. Diese Technik brachte auch die besten Ergebnisse für Ne. Die grosse Anzahl von Schritten erlaubt die getrennte Bestimmung der Q-Edelgase und anderer ebenfalls freigesetzter Komponenten wie z. B. den kosmogenen und solaren Edelgasen oder auch dem Ne-E(L), das aus präsolarem Graphit stammt. Im Rahmen dieser Arbeit wurden die HF/HCl resistenten Rückstände der Chondrite CO3.4 Lancé, H3.7 Dimmitt, CV3 (ox.) Grosnaja, LL3.4 Chainpur und CM2 Cold Bokkeveld erfolgreich untersucht. Die Analyse brachte die folgenden Ergebnisse:

Abgesehen vom Verhältnis $(^{20}Ne/^{22}Ne)_Q$ sind alle Isotopenverhältnisse in Phase Q der verschiedenen Meteorite recht konstant. Als wichtigste Ergebnisse sind die $(^3He/^4He)_Q$ Verhältnisse von $(1.45 \pm 0.01) \times 10^{-4}$ für CV3 (ox.) Grosnaja und $(1.41 \pm 0.01) \times 10^{-4}$ für CM2 Cold Bokkeveld zu nennen. Diese Werte sind niedriger als die einzig sonst verfügbaren Werte für $(^3He/^4He)_Q$, gemessen in CV3 (ox.) Allende und CM2 Murchison (Wieler *et al.*, 1991; 1992), die jedoch offenbar durch kosmogenes He leicht beeinflußt wurden. Die neuen Daten liegen auch niedriger als das $^3He/^4He$ Verhältnis von $(1.66 \pm 0.05) \times 10^{-4}$, das in der Atmosphäre des Jupiters gemessen wurde (Mahaffy *et al.*, 1998). Das mittlere $(^3He/^4He)_Q$ von $(1.43 \pm 0.03) \times 10^{-4}$ wurde verwendet, um das protosolare D/H Verhältnis zu bestimmen. Der berechnete Wert von $(2.3 \pm 0.5) \times 10^{-5}$ stimmt mit dem Wert überein, der in der Atmosphäre des Jupiters bestimmt wurde. Von dieser wird angenommen, daß sie unveränderten protosolaren Wasserstoff aufgenommen hat. Daher erscheint es möglich, daß sowohl He-Q als auch das He im Jupiter lediglich leicht fraktioniertes, primordiales He aus der Zeit vor dem solaren Deuterium-Brennen repräsentieren. Das protosolare D/H Verhältnis ist wichtig, um die Voraussagen der Standardtheorie der Nukleosynthese im Urknall mit primordialen Elementverhältnissen einzugrenzen und so kosmische Parameter wie zum Beispiel die Baryonendichte zu bestimmen.

Wie bereits durch frühere Messungen angedeutet (Schelhaas *et al.*, 1990; Wieler *et al.*, 1991; 1992), ist das $(^{20}Ne/^{22}Ne)_Q$ Verhältnis das am wenigsten einheitliche Isotopenverhältnis der Edelgase aus Phase Q. Die Daten reichen von 10.05 ± 0.05 und 10.17 ± 0.03 für Cold Bokkeveld und Lancé bis zu 10.6 ± 0.2, 10.60 ± 0.06 and 10.66 ± 0.04 für Dimmitt, Chainpur und Grosnaja. Eine Korrelation der $(^{20}Ne/^{22}Ne)_Q$ Verhältnisse mit der Meteoritenklassifizierung oder mit der metamorphen Geschichte der Meteorite auf den Mutterkörpern konnte nicht festgestellt werden. Im Gegensatz dazu sind die Isotopenverhältnisse der anderen Elemente in allen Meteoriten sehr einheitlich. Wahrscheinlich sorgte also ein noch unbekannter Prozeß für die Variationen des ursprünglich eingebauten Ne-Q. Die Ar, Kr und Xe Isotopenverhältnisse der Q-Edelgase in allen fünf Proben sind innerhalb ihrer Fehlergrenzen identisch und sehr ähnlich zu bereits früher bestimmten Resultaten für Q und für die Ureilite.

Diese Arbeit liefert erstmals an Hand von Edelgasdaten Anhaltspunkte dafür, daß Phase Q aus mindestens zwei kohlenstoffhaltigen Trägern „Q1" and „Q2" mit leicht unterschiedlichen Eigenschaften besteht. Die sehr ähnliche charakteristische Verarmung der leichten Edelgase relativ zu Xe und den solaren Häufigkeiten läßt vermuten, daß diese „Unterphasen" Edelgase aus demselben Reservoir aufgenommen haben. Das Experiment mit dem CM2 Chondrit Cold Bokkeveld hat ergeben, daß die Phase Q1 gegenüber Phase Q2 an He und Ne relativ zu Xe angereichert ist und mit präsolarem Graphit, dem Träger des gleichzeitig freigesetzten Ne-E(L)

verbunden sein könnte. Die schweren Elementverhältnisse $(Ar/Xe)_Q$ and $(Kr/Xe)_Q$ reflektieren sowohl thermische Metamorphose als auch Alteration durch Wasser (aqueous alteration). Diese Prozesse auf den Meteoritenmutterkörpern führten zu grösseren Ar und Kr Verarmungen relativ zu Xe. Im Gegensatz dazu zeigen Meteoriten wie zum Beispiel die CM Chondrite, die lediglich „aqeous alteration" erfahren haben, keine Verarmung an He und Ne relativ zu Ar, sondern sogar the höchsten $(He/Ar)_Q$ und $(Ne/Ar)_Q$ Verhältnisse. Dies zeigt, daß die an He und Ne reichere Trägerphase Q_1 weniger empfindlich gegenüber „aqeous alteration" ist.

Die Rückstände von Chainpur und Cold Bokkeveld enthielten beträchtliche Mengen an Ne-E(L). Die Konzentrationen von 0.15 bzw. 5.12×10^{-10} cm^3 STP ^{22}Ne-E(L)/g Meteorit bestätigen den Vorschlag von Huss (1997), daß die ^{22}Ne-E(L) Konzentration, und somit auch die Konzentration des präsolaren Graphits, mit der metamorphen Geschichte der Meteorite korreliert.

1 Introduction

The two most fundamental questions in cosmochemistry are: What are the chemical compositions of all cosmic matter? What are the reasons for these compositions? The first question is tackled by chemical, physical or astrophysical examinations of all available cosmic "samples" or *reservoirs*, such as terrestrial rocks, meteorites, planets, atmospheres, stars, and the interstellar medium. To find the answer to the latter question, physical theories are needed that can account for the evolution of matter in the universe from Big-Bang and stellar nucleosynthesis to its current compositions in the reservoirs mentioned above.

One important link in the "evolutionary chain" between Big-Bang and the present is the development of our solar system from its birth in the proto-solar molecular cloud, 4.6 billion years ago, to its present state. A way to obtain information about many of the processes which led to the formation and the observed chemical compositions of the Sun, planets, asteroids, comets and meteorites is to study cosmic samples that are as primitive and unprocessed as possible. These samples show "fingerprints" of the primordial compositions in the solar system prior to secondary alterations and therefore can provide information about the processes involved. *Secondary processes can destroy this "memory" of former primordial reservoirs.* Examples are planetary events such as thermal alteration or differentiation into mantle and core caused by gravitation as well as simply the ability of most elements to chemically react. Unfortunately, components of a primitive origin often coexist with more evolved altered components which are more abundant and may swamp these primitive components.

Invaluable help to understand the conditions at the birth of our solar system is therefore provided by those archives which underwent only slight or no differentiation due to secondary planetary processes, i. e. **primitive, undifferentiated meteorites**. These meteorites, as well as some interplanetary dust particles (IDP), are assumed to be the least processed solar system material available, carrying information about formation and early evolution of the solar system. Once the secondary planetary processes have been accounted for, the *primary* solar system conditions such as (in)homogeneity in the starting elemental composition within different regions of the "solar nebula" or the cooling history can be reconstructed to better understand the history of matter from the Sun's parent molecular cloud to the first accretion of planetesimals.

To detect possible primordial differences in these samples, suitable analytical tracers need to be identified. For example, oxygen has become especially important, since it is a major, rock-forming element in the solar system *and* shows large systematic isotopic anomalies (Clayton *et*

al., 1973; Clayton, 1981). On the other hand, the analysis of elements that are especially rare, can detect even minute inhomogeneities relative to a reference isotopic composition. As already discussed above, most elements are chemically active and therefore are susceptible to secondary processes. The analysis of **noble gases** in the solar system (Ozima and Podosek, 1983) overcomes this difficulty and provides in many respects considerable advantages over the examination of chemically active and abundant elements. Since the noble gases helium, neon, argon, krypton, and xenon are chemically almost completely inert, they can remain in the gas phase, well-mixed and as atoms, while other elements already have formed compounds or have been condensed. Therefore, they are very rare on Earth and the planets, although they are not rare in the solar system as a whole ("solar" or "cosmic" abundances; Anders and Grevesse, 1989). Noble gases have a wide mass spectrum from 3 amu to 136 amu and consist of 23 isotopes. This leads to distinct physical properties of the various noble gas elements as, e. g. condensation temperatures, first ionisation potentials, (ion) radii, diffusion constants, solubility or adsorptive ability. The effects of each of these physical properties on a reservoir are therefore reflected in its noble gas composition.
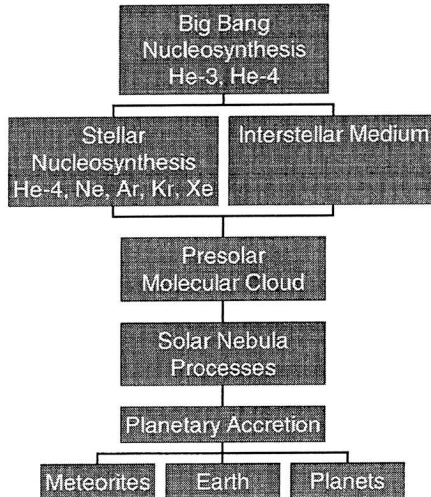
Figure 1.1: Scheme of the evolution of noble gases. The noble gas path from their "birth" in Big Bang and stellar nucleosynthesis into our solar system is roughly understood. However, no generally accepted explanation exists how elemental and isotopic compositions of different reservoirs within the solar system, e. g. of the planetary atmospheres or the Earth's mantle, were established. Unknown are also genetic relations between these components, and the "starting compositions" at the beginning of our solar system.

The most important of the many radiogenic noble gas isotopes, e. g. ^{4}He, ^{40}Ar, ^{129}Xe and also cosmic ray produced noble gas nuclides, are very well suited for chronology purposes in cosmo- and geochemistry. They may be lost upon relatively mild heating events which may not completely reset other parent-daughter isotope systems (Turner, 1988). However, noble gases are also ideal as tracers to discover differences between reservoirs, such as in primitive meteorites, planetary atmospheres, the Earth's mantle, or the Sun (Ozima and Nakazawa, 1980; Swindle, 1988; Pepin, 1992; Ozima et al., 1998).

In Figure 1.1, the universal evolution of the noble gases is schematically outlined. The noble gas "trace" begins with the primordial production of ^{3}He and ^{4}He in the Big-Bang (Alpher et al., 1948; Schramm and Turner, 1998) and leads to the stellar nucleosynthesis of the heavier noble gases in stars (Burbidge et al., 1957). Noble gases from several stellar sources contribute then to the interstellar medium and to our presolar molecular cloud. These individual noble gas components have thoroughly, but not completely, been mixed upon contraction of the molecular cloud fragment from which the Sun was formed, the solar nebula, and upon the formation of the Sun, and the subsequent mixing processes in the solar nebula (e. g. Cameron, 1962; Cassen, 1994; Sandford, 1996). However, mixing has not completely homogenised the preserved presolar reservoirs which is discussed in chapter 1.1.2.4. Finally, other noble gas components have been established during the accretion of the planetesimals in the early solar system and upon subsequent secondary planetary processes, e. g. degassing, impacts, radiogenic production or irradiation by cosmic rays (Pepin, 1992; Zahnle, 1993).

The complicated evolution of the noble gas inventory within the solar system is poorly understood. Large efforts have been made to determine the composition of *primordial*, terrestrial, planetary and solar noble gases. A meteoritic noble gas component is called primordial, if it existed in any form at the beginning of the solar system and was incorporated into the meteorite parent bodies. So far, no widely accepted model has been found to genetically connect all these reservoirs (Pepin, 1992; Zahnle, 1993). Possibly, a unique and homogeneously mixed "mother" noble gas component has existed in the gas phase and has then been incorporated into the first planetesimals (Ozima et al., 1998). This component could already have existed *prior* to the Sun (Huss and Alexander, 1987), but it may have been processed subsequently in the solar nebula. Unknown planetary processes could also mask this possible primordial component.

This study investigates the composition of a noble gas component which is likely to be related to this important primordial noble gas component described above. It resides in a carrier dubbed **"phase Q"** (Lewis et al., 1975) which is found in all classes of primitive meteorites and

which is described in detail in chapter 1.1.3. First, several other primordial noble gas components of solar (system) or presolar origin will be explained. In noble gas geochemistry, a *component* designates any compositionally well-defined reservoir of one element or more. A component may have a well-understood origin or it may simply be defined because it represents a widespread uniform composition (Ozima and Podosek, 1983).

1.1 Meteoritic noble gas components

Meteorites provide an extraordinary look on several of the physical processes mentioned above (see references in Kerridge and Matthews, 1988). They contain radiogenic or cosmogenic noble gas components which help to decipher origin, age and history of the meteorites and/or their parent bodies (Bogard *et al.*, 1984; Caffee *et al.*, 1988; Eugster *et al.*, 1997). Other noble gases reside in tiny grains which are remnants of older star generations (Anders and Zinner, 1993; Zinner, 1995; 1998a; 1998b). Meteorites also contain primordial gases probably incorporated into the precursors of the meteorite parent bodies during the formation of the solar system (Swindle, 1988; Pepin, 1992; Zahnle, 1993; Ozima *et al.*, 1998).

Most meteorites originate from the asteroid belt between Mars and Jupiter (Wetherill and Chapman, 1988). They are ejected from asteroid surfaces by impacts or formed by complete break-up of an asteroid due to a collision with another asteroid. Asteroids are much smaller than "normal" planets and became therefore less hot in their interiors. Some meteorites are thus the least altered material in our solar system and their incorporated noble gases underwent less severe alteration due to (thermal) metamorphism (McSween and Sears, 1988; Zolensky and McSween, 1988). The least processed *"unequilibrated" chondrites* (Sears and Dodd, 1988) are of special interest, since they remained more or less unchanged since their formation 4.56 Ga ago (Tilton, 1988). Chondrites are primitive meteorites containing distinctive *chondrules*, spherical objects having once being liquid (McSween, 1977). These unequilibrated chondrites provide the oldest material of our solar system available for examinations in terrestrial laboratories. In particular, they are a unique archive of noble gases sampled at the beginning of our solar system. If we can elucidate the original composition of these noble gases and the processes which subsequently modified them, we have gained important information about the evolution of our solar system. Towards this goal, we will need to separate the meteoritic noble gas components of different origin.

Historically, the distinction of a new noble gas component goes along with the discovery of elemental or isotopic anomalies relative to already known compositions, such as the terrestrial atmosphere. However, often a specific component can not be explained straightforwardly by a known process, e. g. by the nucleosynthesis in certain shells of a suitable star (chapter 1.1.2.4), or by a modification of a known reservoir. One important clue to the origin of a given noble gas component is therefore the identification of its *carrier*. A carrier phase can be a matrix of several mineral fractions, a single mineral, nanometer-sized mineral grains, but also a surface or labyrinth of "adsorption sites" within minerals which contains at least one distinct noble gas component.

The discovery, definition and characterisation of noble gas components is far from being completed. A survey of the most common components which are mentioned in this work, their carrier phases and their most important properties follows below: The noble gas components are divided here into two groups according to the mechanisms by which they are incorporated into meteorites: *In situ* produced noble gases are described in chapter 1.1.1, *trapped and primordial* noble gas components are presented in chapter 1.1.2. The primordial *noble gases of phase Q*, the main topic of this work, are discussed separately in more detail in chapter 1.1.3. Some of the most important features of the trapped and primordial components are summarised in Table 1.1 at the beginning of chapter 1.1.2. Unfortunately, no agreement in the naming has been reached. Every discovery of a carrier phase or a connection between noble gas components caused new names. First, components have been marked alphabetically ("He-A"), others are named according to their isotopic composition ("Xe-HL"), their formation ("Kr-s") or their carrier phase ("Q"). Synonyms for the noble gas components are therefore also given in Table 1.1.

1.1.1 In situ produced noble gases

Noble gas "components" discussed in this section are generated by nuclear processes within the meteorites. **Cosmogenic** as well as **radiogenic noble gases** result from numerous different single nuclear reactions.

1.1.1.1 Cosmogenic noble gases

Cosmogenic noble gases result from nuclear reactions between energetic nuclear primary and secondary particles with the nuclei of meteoritic target material. These primary particles,

mainly protons and α-particles come from galactic sources (galactic cosmic rays) or from the Sun (solar cosmic rays) and are able to penetrate meteoritic material in the range of a few meters (GCR) or millimetres (SCR), respectively. These primary particles can produce secondary reaction products, i. e. protons and neutrons. The irradiation can occur after meter-sized meteorites have been ejected from their parent-body or within the topmost few meters of the surfaces of their atmosphere-less parent-bodies. Reviews about cosmogenic nuclides and irradiation records in meteorites are given by Reedy *et al.* (1983), Caffee *et al.* (1988) and Vogt *et al.* (1990).

Cosmogenic nuclides are normally used to determine exposure ages of their carrier materials, since concentrations of cosmogenic nuclides depend on the residence time of the meteorite in space or at the surface of its parent body (see reviews cited above or e. g. Eugster, 1988 or Marti and Graf, 1992). Cosmogenic contributions mainly affect also those isotopes with low relative abundances in other components. In particular, ^{3}He, ^{21}Ne and ^{38}Ar are prone to be compromised by cosmogenic contributions. However, all isotopes of an element are produced in more or less equal concentrations. **Cosmogenic ^{3}He** is a product of almost all elements abundant in meteorites, ^{21}Ne is predominantly produced from Si, Mg and Al. ^{38}Ar is mainly produced from Ca, Fe and, to a lower extent, from K, Kr and Xe isotopes from Br, Rb, Sr, Y, Zr, I, Ba and some rare earth elements (Caffee *et al.*, 1988; Vogt *et al.*, 1990; Marti and Graf, 1992).

Since these noble gases are produced in situ, they may also be abundant in carrier phases containing other components. High abundances of the efficiently produced **cosmogenic ^{3}He** and ^{21}Ne considerably influence the determination of e. g. trapped primordial noble gases (chapters 1.1.2 and 1.1.3). The heavier cosmogenic noble gases (Ar, Kr, Xe) are less problematic, *since the ratios of target nuclide abundance to trapped noble gas isotope abundance are much lower for the heavier gases than for the light noble gases and, therefore, the relative production is much lower (Eugster, 1988; Sears and Dodd, 1988).*

1.1.1.2   Radiogenic noble gases

Radiogenic noble gases are used to determine gas-retention ages of meteorites. These ages give a measure of the time during which gaseous stable daughter products have been accumulating due to decay and spontaneous or neutron-induced fission of radioactive nuclides. Therefore, radiogenic noble gases often date secondary events such as (thermal) metamorphism or shock reheating which release previously accumulated noble gases (Turner, 1988).

Especially, ^{4}He, ^{40}Ar and ^{129}Xe are very abundant in meteorites, since their mother nuclides ^{235}U, ^{238}U, ^{232}Th, ^{40}K and ^{129}I are or were quite prominent in almost all meteoritic samples. Therefore, the measurement of ^{4}He, ^{40}Ar and ^{129}Xe in e. g. primordial components can be affected by these very abundant radiogenic isotopes. The heavy Kr and Xe isotopes are produced by spontaneous or neutron-induced fission of extinct ^{244}Pu and of $^{235, 238}$U (Wetherill, 1953; Alexander, 1971; Eugster *et al.*, 1983; Michel and Eugster, 1994). These **fissiogenic Kr and Xe isotopes** do not compromise the examinations of primordial gases in this work due to their low abundances, in particular in carbonaceous carrier phases.

1.1.2 Trapped and primordial components

In this chapter, we discuss noble gas components which were either implanted into the meteorites after their formation, the **trapped solar gases** (chapter 1.1.2.2), or were incorporated during the condensation of the meteorite parent bodies during the formation of the solar system. This could happen e. g. by incorporation from a gaseous atmosphere (**trapped primordial gases**, chapter 1.1.3), but the noble gases could also site in already condensed matter, e. g. in **primordial presolar or circumstellar grains** (chapter 1.1.2.4). Table 1.1 summarises the information about noble gas components in meteorites. Most components important for this work are introduced in this and the subsequent chapter. However, the most mysterious trapped component is missing: **Primordial noble gases of phase Q** which dominate the heavier noble gases in primitive chondrites and which are the topic of this thesis. Q-gases will be discussed in detail in chapter 1.1.3.

Table 1.1: Most important noble gas components in meteorites (see text for references).

component	noble gas	carrier	accompanied by	most significant isotopic characteristics	typical release temperature
A	He, Ne, Ar	originally assumed well-defined "planetary" component in meteorites, but clearly a mixture of HL, P3, P6 and Q			
A1	Ne	former synonym for Ne-P3			
A2	Ne	mixture of mostly Ne-HL and Ne-P6			
A3	Ne	oxidisable organic polymer		normal, similar to Ne-HL	
AVCC	Kr, Xe	originally assumed well-defined component in carbonaceous meteorites, but a mixture of HL, P3, P6 and Q			
B	He, Ne, Ar	former synonym for SW			
C	He, Ne, Ar	former synonym for SEP			
CCF	Kr, Xe	former synonym for HL			
D	He, Ne, Ar	existence not confirmed			
E	Ne	divided into sub-components Ne-E(L) and Ne-E(H)			
E(H)	Ne	presolar SiC	^{4}He, Ar, Kr-s, Xe-s	^{20}Ne/^{22}Ne = 0.083 ^{21}Ne/^{22}Ne = 0.00059	1600-1800 °C
E(L)	Ne	oxidisable presolar graphite	Kr-s, Xe-s	^{20}Ne/^{22}Ne ≈ 0 ^{21}Ne/^{22}Ne ≈ 0	two release peaks between 700- 1000 °C
HL	He-Xe	presolar diamond		^{124}Xe/^{132}Xe = 0.0083 ^{126}Xe/^{132}Xe = 0.0056 ^{134}Xe/^{132}Xe = 0.636 ^{136}Xe/^{132}Xe = 0.699	1100-1600 °C
P1	He-Xe	synonym for noble gases of phase Q			
P3	He-Xe	presolar diamond		normal	200-900 °C
P6	He-Xe	presolar diamond		assumed to be normal	slightly higher than HL
Q	He-Xe	oxidisable phase Q		normal	1000-1200 °C
s	Kr	presolar SiC, presolar oxidisable graphite	Ne-E(L), Ne-E(H), Xe-s	^{80}Kr/^{84}Kr = 0.01-0.02 ^{82}Kr/^{84}Kr = 0.42 ^{83}Kr/^{84}Kr = 0.12 ^{86}Kr/^{84}Kr = 0.45-1.17	700-1000 °C, 1600-1800 °C (SiC)
s	Xe	presolar SiC, presolar oxidisable graphite	Ne-E(L), Ne-E(H), Kr-s	^{124}Xe/^{132}Xe ≈ 0 ^{128}Xe/^{132}Xe ≈ 0 ^{128}Xe/^{132}Xe = 0.22 ^{129}Xe/^{132}Xe = 0.12 ^{130}Xe/^{132}Xe = 0.48 ^{131}Xe/^{132}Xe = 0.19 ^{134}Xe/^{132}Xe ≈ 0 ^{136}Xe/^{132}Xe ≈ 0	700-1000 °C, 1600-1800 °C (SiC)
SEP	He-Xe	bulk meteorite		normal	
SF	He-Xe	former synonym for SEP			
SW	He-Xe	bulk meteorite		normal	
U (ureilites)	Ne	diamond, unknown carbonaceous combustible phase, similar to Q			
U ("Ur")	Xe	unknown		normal	
X	Xe	uncommon synonym for Xe-HL			

1.1.2.1 Distinctions of trapped and primordial noble gas components

Elemental compositions...
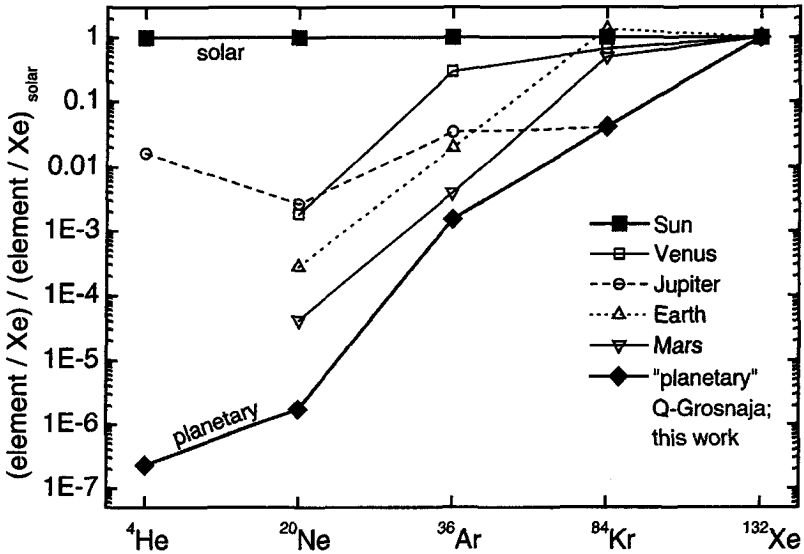
Figure 1.2: Elemental composition of noble gas reservoirs in the solar system normalised to solar abundances (Anders and Grevesse, 1989) and ^{132}Xe. Primordial meteoritic "planetary" noble gases are depleted in the lighter elements by up to 7 orders of magnitude compared to solar abundances. Planetary atmospheres display similar elemental patterns. References: Venus & Mars: Donahue (1986); Jupiter: Niemann *et al.* (1998).

Early examinations revealed that most meteorites contain two dominant noble gas components with distinct *elemental* compositions (Signer and Suess, 1963). One of these components has an elemental composition similar to that in the **Sun** (Anders and Grevesse, 1989) or in the **solar** wind (chapter 1.1.2.2). The other component is heavily depleted in the light noble gases, compared to solar abundances and normalised to Xe which is shown in Figure 1.2. The name **"planetary"** (Signer and Suess, 1963) was introduced for these meteoritic noble gases, since they roughly resemble those of planetary atmospheres as can also be seen in Figure 1.2. These bulk "planetary" gases in meteorites were originally labelled with the letter "A" (He-A and Ne-A; Pepin, 1967; Black and Pepin, 1969). However, today, the

attribute "planetary" appears misleading. "Planetary" noble gas components do not have to originate from either planetary atmospheres or even from our solar system, and most current models of the origin of planetary atmospheres assume that noble gases in planets are not derived from "planetary" noble gases in meteorites (e. g. Zahnle, 1993).
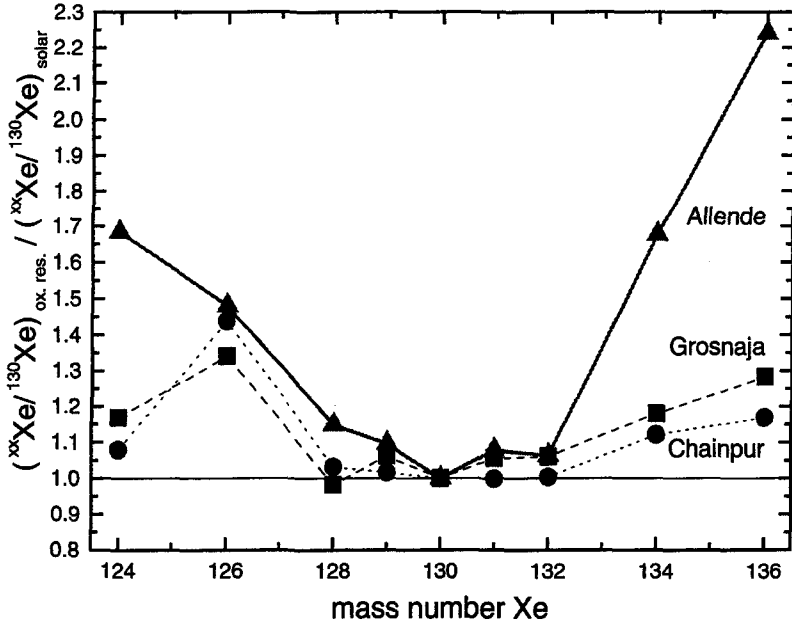
Figure 1.3: Xe isotope ratios in oxidised HF/HCl-resistant residues relative to solar wind abundances, normalised to ^{130}Xe (Eberhardt *et al.*, 1972; Wieler and Baur, 1994). Xe in oxidised residues is dominated by isotopically "exotic" Xe-HL, enriched in the *light* and *heavy* isotopes. The Allende residue (Wieler *et al.*, 1991) shows a pure HL composition. The oxidised residues of Grosnaja and Chainpur (this work) display admixtures of isotopically "normal" gases. The relatively high ^{126}Xe values of Grosnaja and Chainpur are rather due to too high hydrocarbon background than to Xe-L.

"**Subsolar**" noble gases show a mixture of properties of both, solar and "planetary" noble gases. Figure 1.4 shows that Ar, Kr and Xe are elementally less fractionated, i. e. more similar to solar composition than planetary gases. In contrast, the isotopic composition is similar to those of "planetary" components. They are found in various meteorite classes such as E-chondrites, ureilites and carbonaceous chondrites and are not known to be connected to a special carrier phase (Göbel *et al.*, 1978; Alaerts *et al.*, 1979b; Matsuda *et al.*, 1980; Crabb and Anders, 1981).

Isotopic compositions...

Very remarkable differences were also discovered in *isotopic* compositions of meteoritic noble gas components (see chapter 1.1.2.4 for references). Isotopic ratios which can be explained as a result of fractionation mechanisms within the solar system or the parent molecular cloud are called **"normal"**. Noble gases in the Sun are one example of a normal component. These are a mixture of components which are produced by nucleosynthesis in many stellar sources. Some **"exotic"** isotopic compositions do not show these similarities to solar isotopic ratios. They are assumed to have a clearly extra-solar system origin and can be related to *single* processes of stellar nucleosynthesis (chapter 1.1.2.4). Figure 1.3 shows, as an example, the isotopic composition of Xe-HL (chapter 1.1.2.4), a very distinctive exotic noble gas composition, relative to solar abundances and normalised to ^{130}Xe. After these general definitions of solar and "planetary" elemental compositions, as well as normal and exotic isotopic ratios, the components will be now described in more detail.

1.1.2.2   Solar gases

Solar gases are emitted from the solar chromosphere and then implanted into the superficial dust layers of the meteorite parent-bodies/asteroids or the moon which form, well mixed, the *regolith*. These regoliths are well stirred, such that almost every grain has been exposed once at the immediate surface where it trapped solar noble gases. Asteroidal regoliths may get compacted, and upon impact induced ejection, fractions may form gas-rich meteorites. Therefore, these samples provide an important archive of the solar history (Wieler, 1998). Fractionation processes during the transport of particles from inner to outer regions of the Sun are not known in detail (Bochsler *et al.*, 1990), but since the solar wind ^{3}He/^{4}He ratio did not increase by more than 5 %/Ga (Wieler, 1998), it is clear that the amount of He that has been brought to the surface of the Sun must be small (Bochsler, 1992). The composition of the emitted solar gases is not exactly the same as the noble gas composition of the bulk Sun and, hence, the whole solar system, but the isotopic fractionation at the surface is estimated to be only about 1.5 % per amu in the Mg/Ne mass region, favouring the light isotope (Geiss and Gloeckler, 1998; Kallenbach *et al.*, 1998). Xe and Kr are enriched in the solar wind, similar to elements with a first ionisation potential (FIP) < 10 eV. Since Kr and Xe have a somewhat higher FIP, this indicates that the first ionisation time (FIT) is the parameter that actually governs the elemental fractionation in the solar chromosphere (see Wieler, 1998 for references).

Two solar components have been found in all five noble gases: The **solar wind** ("SW", Black, 1972; Wieler, 1998) and the **solar energetic particles** ("SEP", Wieler *et al.*, 1986). The latter have higher kinetic energies and isotopically heavier He, Ne and Ar compositions than the solar wind (Benkert *et al.*, 1993; Wieler, 1998). SEP originally was associated with **solar flare** events ("SF", Black, 1972a; Etique *et al.*, 1981). These noble gases were formerly labelled with the letters „B" and „C". Black (1972a) also identified a third solar component „D" with isotopically lighter Ne and Ar, but heavier He (similar to "planetary" He, see chapter 1.1.2.1), but this component has never been confirmed. Solar gases are extremely enriched in He and Ne relative to Xe compared to "planetary" components, as illustrated in Figure 1.2. Therefore, solar gases in meteoritic regolith breccias can significantly disturb measurements of primordial "planetary" He and Ne.

1.1.2.3   Primordial noble gases in HF/HCl-resistant residues

In 1975, Lewis *et al.* discovered that the primordial noble gas components in chondrites can be enriched by dissolving meteoritic samples in the demineralising acids HF/HCl. Most of the radiogenic, cosmogenic and solar noble gases (chapters 1.1.1 and 1.1.2.2) which reside mostly in the silicate phases of a meteorite, are removed by this procedure. The primordial noble gases remain to a large extent in only about 1 % of the original bulk sample. This HF/HCl-resistant residue was further dissolved in oxidising acids and it turned out that the oxidisable part of an acid-resistant residue carried most of the heavy primordial noble gases. Lewis *et al.* named this almost mass-less carrier *phase Q*. Noble gases of phase Q are the topic of this work and will be further discussed in chapter 1.1.3. The non-oxidisable fraction of the residue also contained presolar grains which were later discovered to be the carrier of Xe-HL (Lewis *et al.*, 1987). These presolar components are described in the subsequent chapter.

1.1.2.4   Noble gas components in presolar grains

Several noble gas components reside in **presolar or circumstellar grains**. These grains have been formed in outflows of earlier star generations and have then been incorporated into the forming solar system or, earlier, into the Sun's parent molecular cloud (reviews: Anders and Zinner, 1993; Zinner, 1995; 1998a; 1998b). Because different stars produce different isotopic compositions, it has become possible to assign certain grain types to certain stars. All presolar

grains were discovered, since they are carriers of substantial isotope anomalies, particularly in the noble gases. These "exotic" isotopic compositions (see chapter 1.1.2.1) can not be explained by processes within the solar system, but only by distinct nucleosynthesis processes in stars and subsequent mixing processes.

The basic nucleosynthesis processes, e. g. r-, s-, p-processes, which produce the elements in stars, are known since 1957. *R- and s-process* stand for rapid and slow neutron capture reactions, compared to β-decay life times, the *p-process* designates proton capture reactions (p,γ) and photodisintegration reactions (γ,n) (Burbidge *et al.*, 1957; Wallerstein *et al.*, 1997). It was believed that the products of several stellar sources contributed to a well-mixed hot solar nebula (Cameron, 1962) and that all presolar material was completely homogenised, since the isotopic abundances of all elements, except the noble gases, in all reservoirs such as e. g. Earth or primitive meteorites have been found to be essentially the same (Reynolds, 1967). However, it was discovered that inhomogeneities existed not only for Xe (Reynolds and Turner, 1964), but in the isotopic compositions of e. g. oxygen (Clayton *et al.*, 1973; Begemann, 1980; Thiemens, 1988). Furthermore, some presolar grains evidently survived the formation of the solar system and kept their isotopic compositions (Lewis *et al.*, 1987). Since the discovery of these presolar grains, it is possible to test astrophysical predictions of the nucleosynthesis under certain stellar conditions in different stars (Zinner, 1998a) by comparing isotopic and elemental abundances.

Table 1.2: Presolar grains and their origins (see e. g. Zinner, 1998a; 1998b for references).

presolar grain	*main* stellar sources	noble gases	identification
diamond $(C_\delta, C_\zeta)^{1)}$	supernovae	yes	Lewis *et al.*, (1987)
SiC $(C_\beta \equiv C_\epsilon)$	AGB stars[2], supernovae	yes	Bernatowicz *et al.* (1987) Tang and Anders (1988a)
graphite (C_α)	supernovae, AGB stars	yes	Amari *et al.* (1990a)
TiC[3]	AGB stars		Bernatowicz *et al.* (1991)
ZrC[3]	AGB stars		Bernatowicz *et al.* (1996)
MoC[3]	AGB stars		Bernatowicz *et al.* (1996)
Al_2O_3 (corundum)	AGB stars	no[4]	Huss *et al.* (1992)
Si_3N_4	supernovae	no[4]	Nittler *et al.* (1995)
$MgAl_2O_4$ (spinel)	AGB stars	no[4]	Nittler *et al.* (1994)

[1] former nomenclature; [2] asymptotic giant branch stars, low-mass stars at the end of their evolution [3] minor minerals found as inclusions in presolar graphite and SiC (only TiC); [4] probably not detectable due to too low grain abundances.

Presolar grains exist in all chondritic groups and their abundances correlate inversely with the meteorites' petrographic type (Huss, 1990). The abundances of some of these grains are also correlated with each other. Both observations indicate that the presolar grains in meteorites

were sampled from the same homogeneously mixed reservoir (Huss *et al.*, 1997). Table 1.2 shows a list of the identified interstellar grain types. It was suggested that these tiny grains must originate from at least 35-40 stellar sources (Alexander, 1997). The first three grain types listed in Table 1.2 are of importance for this work because of their occurrence in all chondrite samples, their noble gas contents and their resistance to HF-HCl treatment (references in: Anders and Zinner, 1993; Zinner, 1995; 1998a; 1998b).

Below, presolar noble gas components are discussed in more detail in order of relevance to this work. Table 1.1 summarises the most important information and gives characteristic isotopic compositions which help to identify the components.

Noble gases in graphite and SiC...

The first group of presolar noble gas components occurs in μm-sized graphite and SiC grains. Most relevant to this work are Ne-E(L) and its -less abundant- companions Kr-s and Xe-s, since their carrier graphite is only weakly resistant to oxidising acids and therefore releases significant amounts of ^{22}Ne-E(L) on HNO_3-etching (Tang *et al.*, 1988; Nichols *et al.*, 1991).

Ne-E was discovered due to its very exotic composition: It consists of almost pure ^{22}Ne (Black and Pepin, 1969). Two subcomponents of Ne-E can be separated due to their different gas release temperatures and carrier densities (Eberhardt *et al.*, 1981): **Ne-E(L)** resides exclusively and in high concentrations in graphite and is released at *low* temperatures of between 700 and 900 °C (Amari *et al.*, 1990b). Ne from presolar graphite consists of at least three fractions: Strongly dominating pure ^{22}Ne from the decay of trapped ^{22}Na, Ne with dominating ^{22}Ne originating - among other sources - from AGB-stars, and normal composed Ne (Amari *et al.*, 1995). Ne-E(L) is accompanied by smaller amounts of Kr-s and Xe-s (Amari *et al.*, 1995). Helium has not been discovered in graphite (Nichols *et al.*, 1992; Kehm *et al.* 1996). **Ne-E(H)** resides in a small fraction of ~4 % (Nichols *et al.*, 1992) of very stable interstellar silicon carbide (SiC) grains, and is released at *high* temperatures of more than 1000 °C, depending on the experimental procedures (Eberhardt *et al.*, 1981; Bernatowicz *et al.*, 1987; Tang and Anders, 1988a). Ne-E(H) originates clearly not from the decay of ^{22}Na, since in addition to dominant ^{22}Ne also ^{20}Ne and ^{21}Ne have been found (Lewis *et al.*, 1994). Presolar SiC grains, containing Ne-E(H), originate from low mass AGB stars (Gallino *et al.*, 1990). The Ne-E(H) is accompanied by Kr-s and Xe-s, but also, unlike Ne-E(L), by ^{4}He and Ar (Lewis *et al.*, 1990; Nichols *et al.*, 1992).

Kr-s resides in graphite and in SiC. It is of variable composition and is the product of nuclear *s-process* reactions in different stars (Srinivasan and Anders, 1978; Lewis *et al.*, 1994). The ratios $^{80}Kr/^{84}Kr$ and $^{86}Kr/^{84}Kr$ are variable, depending on the stellar conditions in which Kr-s was produced, but $^{82}Kr/^{84}Kr$ and $^{83}Kr/^{84}Kr$ are quite uniform (Ott *et al.*, 1988).

Xe-s is also found in graphite and in SiC. It has high and constant abundances of the even isotopes ^{128}Xe, ^{130}Xe, and ^{132}Xe and but is essentially devoid of ^{134}Xe and ^{136}Xe (Srinivasan and Anders, 1978; Lewis *et al.*, 1994). This composition agrees strikingly well with the predicted *s-process* Xe production in some stars (Clayton and Ward, 1978; Ott *et al.*, 1988).

Noble gases in diamonds...

The following components reside in very refractory presolar diamonds (Lewis *et al.*, 1987). These *nano*diamonds have sizes of only about 2nm and are not destroyed upon etching. They are also important for this work, since He-HL and Ne-HL in diamonds dominate the light noble gases in acid-resistant residues of primitive chondrites. Furthermore, He-HL is isotopically very similar to He-Q, the most important component of this work.

Xe-HL was the first observed presolar gas component (Reynolds and Turner, 1964; Lewis *et al.*, 1987). It is highly enriched in the *low* mass (^{124}Xe, ^{126}Xe) and *high* mass isotopes (^{134}Xe, ^{136}Xe) which is shown in Figure 1.3. First, this exotic component got the name **carbonaceous chondrite fission (CCF)** Xe, since the observed abundances of the *heavy* isotopes were explained by a fissiogenic origin (Lewis *et al.*, 1975; Srinivasan *et al.*, 1977). Now, it is widely accepted that this component originates in the r-process (Xe-H) and p-process (Xe-L) in stellar sources, although it is problematic two find stellar environments which provide conditions suitable for both processes and the formation of the diamond carriers (see e. g. Ott, 1993).

Since the discovery of Xe-HL, huge efforts were made to find possible different carrier phases of **Xe-H** and **Xe-L** which would make it easier to separately explain the observed enrichments. However, the first separation succeeded only recently (Meshik *et al.*, 1998). The isotopically most spectacular Xe-HL is accompanied by characteristic components in all other noble gases which by analogy have been labelled **He-HL** to **Kr-HL** (Huss and Lewis, 1994a). HL gases are released at temperatures between 1100 and 1600 °C.

He-HL and **Ne-HL** dominate the trapped He and Ne in unequilibrated chondrites (Huss and Lewis, 1994a). In contrast to Xe-HL, which is of exotic composition, He-HL and Ne-HL are isotopically "normal", according to the definitions given in chapter 1.1.2.1. Originally, **He-A**

and **Ne-A** were assumed to be the well-defined trapped components in primitive meteorites (Pepin, 1967; Black and Pepin, 1969). Now, it is clear that these He-A and Ne-A are mixtures of Q-gases (see chapter 1.1.3) and presolar components, such as HL/A2 or P3/A1 (Alaerts *et al.*, 1980; Huss and Lewis, 1994a).

Alaerts *et al.* (1980) observed two sub-components of Ne-A, **Ne-A1** and **Ne-A2**. Since Ne-A2 is released together with the already known Xe-HL, it is now labelled **Ne-HL** (see also comment on Dhajala in chapter 2.1.1), whereas Ne-A1 is now called **Ne-P3** (Huss and Lewis, 1994a). The original composition of Ne-A2 (Alaerts *et al.*, 1980) included also minor contributions of **Ne-P6** (Huss and Lewis, 1994a).

Xe-P3 and related other P3 gases (**He-P3** to **Kr-P3**) also reside in diamonds and are released at low temperatures of 200-900 °C (Tang and Anders, 1988b; Huss and Lewis, 1994a). Thus, they are probably located near the surfaces of diamonds (Huss and Lewis, 1994a). Significant amounts of P3 gases only reside in unmetamorphosed presolar diamonds (Huss and Lewis, 1994b). Apart from the light elements **He-P3** and **Ne-P3**, there are no large isotopic or elemental differences compared to the major heavy noble gas component **Q** in primitive meteorites (chapter 1.1.3).

Xe-P6 and related noble gases form a minor component (10-15 % of Xe-HL) which is difficult to enrich and to measure (Huss and Lewis, 1994a; Huss and Lewis, 1994b). P6 gases are also carried by diamonds and released at slightly higher temperatures than HL-gases (1100-1600 °C).

The letter "P" was introduced to describe that the components P3 and P6 have *"planetary"* compositions (chapter 1.1.2.1) (Tang and Anders, 1988b). The isotopic composition of P3 is normal, the composition of P6 is rather ambiguous but is also assumed to be normal (Huss and Lewis, 1994a). This shows that the usage of the terms "planetary" and "normal" is somewhat misleading since both components are of extra-solar origin (chapter 1.1.2.1). In contrast, the solar wind has also "normal" composition, but is of solar system origin.

1.1.2.5   Other noble gas components in meteorites

Ne-A3 resides in an oxidisable fraction of organic polymer in Murchison which remains after demineralisation with HF/HCl (Srinivasan *et al.*, 1977; Wieler *et al.*, 1992). Its existence

is assumed to better explain the release of Ne-P3-like Ne during oxidation of an acid-resistant residue of Murchison with HNO_3. Hence, its composition is different from Ne-Q which is the component normally released upon oxidation (chapter 1.1.3).

U-Xe is a primitive component, whose existence was postulated 20 years ago (Takaoka, 1972; Pepin and Phinney, 1978). U stands for "Ur", the German prefix meaning "prime, original". U-Xe is assumed to be the primordial fission-free (^{244}Pu) and Xe-H-free Xe, incorporated into planetary and meteoritic bodies during the formation of the solar system. This component was observed first in achondrites (Michel and Eugster, 1994; Weigel and Eugster, 1994).

Furthermore, *there is always the possibility that a meteoritic sample (re-)adsorbs* **terrestrial noble gases** or other, freshly released components during weathering on earth or during chemical or even mechanical treatments in the laboratory. This adsorption can be a serious problem, especially for Kr and Xe (Michel and Eugster, 1994).

1.1.3   Noble gases of phase Q

As described already in chapter 1.1.2.3, Lewis *et al.* (1975) discovered, while analysing the carbonaceous chondrite Allende, that the primordial noble gas components in chondrites are almost completely retained upon dissolving meteoritic samples with HF/HCl. The primordial noble gases largely reside in only about 1 % of the original bulk sample (e. g. Huss and Lewis, 1995). In addition, Lewis *et al.* showed that most of the heavier primordial noble gases but only minor parts of the lighter He and Ne are removed by oxidising these HF/HCl-resistant residues with e. g. HNO_3 or $HClO_4$. For this oxidisable and rather mysterious phase of only minor mass (about 5 % of the acid-resistant residue is dissolved in concentrated HNO_3, see Table 2.5), they introduced the name "**phase Q**", for "*Quintessence*". Another name, **P1** (P ≡ "planetary") is used by Huss *et al.* (1996).

Noble gases...

Noble gases contained in phase Q have proven to be a major primordial component probably present at the formation of the solar nebula, since they were found in different classes of primitive undifferentiated as well as differentiated meteorites, e. g. ureilites (Alaerts *et al.*,

1979a; 1979b; Moniot, 1980; Ott *et al.*, 1985a; Schelhaas *et al.*, 1990; Wieler *et al.*, 1991; 1992; Huss *et al.*, 1996). Their parent bodies condensed at different distances from the Sun, indicating that "Q-gases" must have been widely distributed in the asteroid-forming regions or in the protosolar molecular cloud. If this suggestion can be confirmed by measuring Q-gases in further meteorite classes, it would appear quite probable that Q-gases would also have been incorporated, possibly besides other components, into Earth and the other planets during their formation.
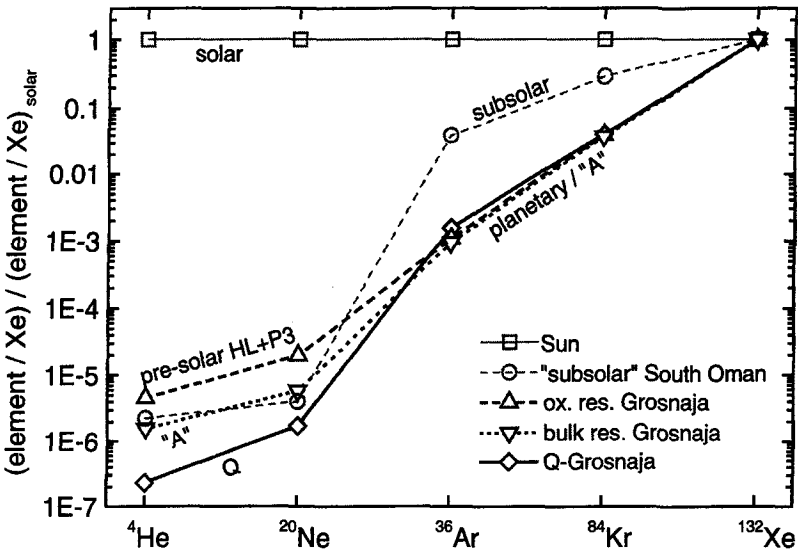
Figure 1.4: *The same plot as Figure 1.2, but with elemental compositions of meteoritic noble gas reservoirs. Subsolar noble gases (chapter 1.1.2.1) are less depleted in Ar and Kr relative to solar abundances and Xe. The curve labelled "A" represents noble gases in bulk HF/HCl-resistant residues. Noble gases from phase Q dominate the heavier gases Ar-Xe, whereas He and Ne in bulk residues are dominated by presolar components (HL, P3,…) that resides in non-oxidisable presolar grains. Presolar He and Ne contribute much more to the noble gases in acid-resistant residues than He-Q and Ne-Q. References: Crabb and Anders, 1981 (South Oman); this work (Grosnaja).*

The assumption of a common origin for the Q-noble gases in all meteorite classes, incorporated from a well-defined, widely distributed and homogeneously mixed reservoir, is based on the characteristic depletion of the light noble gases, relative to Xe and solar composition (Figure 1.4), that was found in all samples examined. While $(^4He/^{132}Xe)_Q$ is, as we will see, constant within a factor of 5, it is 7 orders of magnitude smaller than $(^4He/^{132}Xe)_{solar}$. It

is very unlikely that metamorphic processes on several different parent bodies can account for such similar depletions.

The origin of these Q-gases is subject to debate, in contrast to that of most of the other noble gas components mentioned above. One model proposes that Q-gases were incorporated into their carrier phase(s) at the formation of our solar system (Ozima *et al.*, 1998). In this model, Q-gases are derived by mass-fractionation from noble gases of solar composition. Q-gases are viewed as a *local* component derived from noble gases in the solar nebula. The young Sun can not change the composition of noble gases incorporated from the solar nebula by stellar nucleosynthesis, with one exception: He. All deuterium will be converted to ^{3}He. In the model of Ozima *et al.*, the present-day value of $(^3He/^4He)_{SW}$ is more suitable as initial component than a proto-solar $^3He/^4He$ value. Therefore, this model suggests that *post-D-burning He* was incorporated into carrier phase Q. Another model, proposed by Huss and Alexander (1987), suggests that Q-gases have been brought into the solar system in solids that carried the noble gases from the Sun's parent molecular cloud. This *presolar* origin implies that He in phase Q has been derived from *pre-D-burning* composition.

Similar to Figure 1.2, Figure 1.4 shows the elemental noble gas compositions of phase Q and the presolar components in acid-resistant residues, relative to solar system composition and ^{132}Xe. The depletion of the light noble gases in phase Q, compared to HL and P3 compositions illustrates the difficulty to obtain data for He and Ne in phase Q with sufficient precision.

First, the "planetary" and normal (chapter 1.1.2.1) noble gases in meteorites were precisely characterised by determining Kr and Xe. Due to their prevailing abundances in unequilibrated carbonaceous chondrites (Figure 1.4), Kr and Xe could be measured in unprepared bulk samples. This led to a composition called **AVCC-Kr** and **AVCC-Xe** - *Average Carbonaceous Chondrites* (Eugster *et al.*, 1967b). Although these gases are in fact a mixture of mainly Q (up to 90%) and other primordial presolar components such as HL-gases, AVCC-Kr and AVCC-Xe are well-established as components. They are used to correct for primordial noble gases when calculating the concentrations of cosmogenic Kr and Xe abundances.

Carrier "phase Q"

Despite of many efforts, the structure of phase Q is not yet known. Therefore, we use the "operational" definition that phase Q is *the oxidisable part of an HF/HCl-resistant residue* that carries primordial noble gases dominating the trapped Ar, Kr and Xe in meteorites (Lewis *et al.*, 1975). We will see later that this definition has to be modified.

After its discovery, it was assumed that phase Q is a "double sulfide with a Fe/Cr ratio between 1 and 2" (Lewis *et al.*, 1975). However, soon a carbonaceous phase was assumed for phase Q (Phinney *et al.*, 1976; Reynolds *et al.*, 1978). Finally, chromite and metal sulfides were eliminated as important noble gas carriers (Frick and Chang, 1978). Yang *et al.* (1982) and Ott *et al.* (1984) proved the carbonaceous character of phase Q. In contrast to presolar components which reside within the volume of presolar carrier grains, Wacker *et al.* (1985) assumed that Q noble gases reside somehow on grain surfaces as indicated by the complete gas loss on oxidation with only little mass loss. In view of this, it seems mysterious that theses gases are so strongly bound that the release temperatures during pyrolysis lie between 1000-1200 °C (Huss *et al.*, 1996). Sorption experiments of noble gases on carbonaceous matter suggested "physisorption" within a "labyrinth of micropores at or near the surfaces of amorphous carbon" as the mechanism to trap the Q-gases (Wacker *et al.*, 1985).

More recent experiments succeeded for the first time in enriching Q-gases solely by physical separation techniques (Amari and Matsuda, 1998; Matsuda *et al.*, 1999). Freeze-thaw disaggregation was used to produce a residue from Allende with noble gas concentrations almost as high as those of HF/HCl-resistant residues. However, this does not necessarily mean that phase Q is indeed an original, discrete, separable phase. Nakamura *et al.* (1998) found that primordial gases including Q and presolar components are enriched by two orders of magnitude and homogeneously distributed in chondrule rims. This would indicate that phase Q possibly was homogeneously distributed in nebular regions where the chondrules acquired the dust rims and also that the noble gas carrier phase(s) together with mineral dust have accreted and formed the rims on the chondrules in the early solar system *prior* to the formation of the parent bodies.

1.2 Objectives

The aim of this work is to contribute to a better characterisation of phase Q and its noble gases. A major step is to extend the existing small database by measuring all five Q noble gases in samples from different meteorite classes of different petrographic types. This is essential to study some of the following questions:

- Can we find Q-gases in residues of meteorites from a large variety of classes?
- Is this component Q isotopically and elementally the same in meteorites that condensed in different regions of the solar system? If so, the *noble* gases should have been homogeneously distributed in large parts of the nebula at the beginning of the solar system, at least in the meteorite-forming regions, a scenario which would be consistent

with the idea that the noble gases were well-mixed and largely in the gas phase prior to incorporation. On the other hand, if systematic differences in the elemental or isotopic composition of the noble gases can be found in different meteorite classes, this would point to an inhomogeneous distribution of the noble gases, e. g. because they were condensed on ice-grains. This would, presumably, require lower temperatures in the nebula than for the first case.

- Can more than one noble gas component be attributed to the poorly characterised phase Q, indicating that possibly different carrier phases with similar properties exist?

- Do metamorphic processes on the parent bodies influence the Q-noble gas compositions?

- Are Q-noble gases possibly related to a common primordial noble gas reservoir from which terrestrial and other planetary noble gases can be deduced?

- Can we obtain some evidence for the genetic origin of Q-gases and, thereby support one of the suggested models (chapter 1.1.3)?

- Can we, finally, explain the already observed differences in the measured Ne-Q composition (Table 1.3)?

Table 1.3: Examples for $(^{20}Ne/^{22}Ne)_Q$ in literature.

sample	petrographic type	$(^{20}Ne/^{22}Ne)_Q$	source
Allende[1]	CV3	10.4 ± 1.0	Smith et al. (1977)
Hamlet[2]	LL4	11.0 ± 1.5	Alaerts et al. (1979a)
Bishunpur[2]	LL3.1	11.6 ± 2.0	Alaerts et al. (1979a)
Chainpur[2]	LL3.4	10.6 ± 1.1	Alaerts et al. (1979a)
Kainsaz[2]	CO3.1	12.4 ± 1.8	Alaerts et al. (1979a; 1979b)
Ornans[2]	CO3.3	9.8 ± 0.6	Alaerts et al. (1979a; 1979b)
Dhajala[3]	H3.8	10.11 ± 0.16	Schelhaas et al. (1990)
Allende[4]	CV3	**10.70 ± 0.15**	Wieler et al. (1991)
Murchison[4]	CM2	**10.70 ± 0.20**	Wieler et al. (1992)

[1] bulk analysis; [2] pyrolysis of acid-resistant residues; [3] stepwise combustion; [4] CSSE.

Originally, noble gases of phase Q were determined either as the difference of conventionally measured gas concentrations in oxidised and non-oxidised HF/HCl-resistant residues, respectively, or by stepwise pyrolysis experiments (e. g. Lewis et al., 1975; Alaerts et al., 1979a; 1979b; Huss et al., 1996). These techniques are sufficient to precisely measure the heavier Q-gases which dominate the inventory in non-oxidised residues. However, these techniques are not suitable to determine He-Q and Ne-Q, since they are only minor fractions of the total (see Figure 1.4) and subtraction of two similar numbers results in large errors. Therefore, no isotopic ratios for He-Q and only a few and rather unprecise ratios for Ne-Q had

been obtained with those techniques (Table 1.3). This was unsatisfactory, because He and Ne in Q are of particular importance:

- The existence of He and Ne within Q was doubted altogether by Sabu and Manuel (1980). Only a simultaneous measurement of *all* 5 noble gases released unquestionably from phase Q could prove the existence of He-Q and Ne-Q.

- He-Q *is potentially important for cosmology to test predictions of the standard Big-Bang nucleosynthesis theory, because* $(^3He/^4He)_Q$ *might be used to deduce the presolar, and therefore interstellar, D/H ratio.*

- He isotopes have a larger relative mass difference than the other noble gases. The $^3He/^4He$ ratio is therefore more sensitive to mass-dependent processes, e. g. *diffusion due to* metamorphic losses or fractionation during incorporation.

- $(^{20}Ne/^{22}Ne)_Q$ data available prior to this work point to differences in the composition of Q in different meteorite classes (Table 1.3).

- If Q plays a major role in the understanding of the evolution of the noble gases in the interiors and atmospheres of the Earth and the other planets, the complete set of noble gas abundances, including He and Ne, is required to have this possible "starting composition" completely defined.

In 1991, the stepped on-line etch technique (*Closed System Stepped Etching* - CSSE) was applied for the first time to acid-resistant residues (Wieler *et al.*, 1991). This technique originally was used to examine lunar samples to resolve SW and SEP particles residing at different depths, (Wieler *et al.*, 1986; Benkert *et al.*, 1993). In this new application of CSSE, the carrier phase Q was oxidised in-vacuo by HNO_3 and only the noble gases released upon etching were measured. According to the operational definition of phase Q, given in chapter 1.1.3, this technique was predestined to be most suitable to measure Q-gases in almost pure form and, especially, to measure the lighter gases He-Q and Ne-Q with sufficient precision almost without interference from He-HL and Ne-HL.

Although CSSE is very suitable, it is not perfect: Ne-E from oxidisable graphite grains, solar Ne and especially cosmogenic Ne can harm the analysis of the Q-gases which is implied by the "operational definition" of phase Q. However, CSSE provides the advantage to measure several steps which allows the resolution of these simultaneously released components. Since gas release occurs at low temperatures by chemical destruction of the carrier(s), no isotopic fractionation in the laboratory, e. g. due to diffusive fractionation, has to be expected.

This method requires large amounts of bulk meteorite to yield a sufficient amount of residue after demineralisation. Thus, until now, only a few measurements were carried out on the

particularly large and gas-rich carbonaceous chondrites CV3 Allende and CM2 Murchison (Wieler *et al.*, 1991; 1992). Their elemental Q-noble gas compositions have shown the expected large "planetary" depletion in the light noble gases, relative to the solar composition (Figure 1.4). The isotopic composition of Ar, Kr, and Xe was also rather similar to all previous results. These experiments yielded the first isotopic ratios for He-Q and new data for Ne-Q which were not in complete agreement with previously published results (Table 1.3). To measure He-Q and Ne-Q in less gas-rich unequilibrated ordinary chondrites, thus, represents a great challenge. Experiments on five meteorites of different classes, among them two ordinary chondrites, performed with CSSE, their results and their discussion are the topic of this thesis and are described in the following.

2 Experimental

In this chapter, the criteria that led to the selection of the meteorites used for this study and their preparation to obtain samples enriched in phase Q are described. Methods to release and purify noble gases from phase Q and bulk residues are introduced. Finally, noble gas measurements made with our two mass spectrometers are discussed.

2.1 Sample treatment

2.1.1 Sample selection and origin

As described in chapter 1.2, the aim of this work is to analyse the noble gases in phase Q in a variety of different meteorite classes. For the determination of all five noble gases, but mostly of He and Ne, the sample selection is a very important factor to obtain pure Q-data, i. e. the samples should contain as little as possible of interfering solar, presolar and cosmogenic noble gas components (chapter 1.1). The sample selection criteria are discussed in the following.

Most importantly, the set of chosen meteorites should cover a wide range of unequilibrated chondrites of different petrographic types. We attempt to find similarities and/or differences, especially in the light noble gases He and Ne, between different meteorite classes and between samples having experienced different metamorphic histories (chapter 1.2).

Measurements of noble gases on oxidised and non-oxidised HF/HCl-resistant residues (chapter 1.1.3) or, if unavailable, on bulk samples should reveal meteorites with significant Q-gas abundances. These data should also allow us to exclude meteorites with large concentrations of solar-type noble gases ("gas-rich" meteorites). It turns out that solar gas bearing phases can not completely be removed with our sample preparation technique (chapter 3.1.1). Therefore, regolith breccias, as collectors of solar wind gases should be excluded from our selection. To minimise contributions of cosmogenic noble gases on ^{3}He and ^{21}Ne, cosmic-ray exposure ages should be as small as possible. However, this criterion can not always be met. In fact, as can be seen in Table 2.1, ^{21}Ne concentrations in some bulk samples are high, indicating long cosmic-ray exposure of up to 25 Ma. Meteorite sample amounts of 5-25 g have to be available to provide a sufficient yield after demineralisation with HF/HCl (chapters 1.1.3 and 2.1.2).

The lack of noble gas data in the literature and the rather small number of easily available samples set limits on these goals. In the following, the meteorites selected for preparation of HF/HCl-resistant residues (Table 2.1) and CSSE measurements, are discussed in more detail in chronological order:

Lancé CO3.4: Lancé is the first in a planned series of three CO chondrites that includes also CO3.3 Ornans and CO3.7 Isna. The major aim of studying this series is to find a possible dependency of the Q-gas composition on the petrographic type within one chondrite class which reflects metamorphism on the CO parent body (McSween, 1977). The difference between noble gas concentrations in oxidised and non-oxidised HF/HCl-resistant residues (Alaerts *et al.*, 1979b) showed that Lancé contains Q-gases, including Ne. The measurement of Lancé with CSSE extends earlier examinations of the heavier noble gases with conventional techniques (Alaerts *et al.*, 1979b) to the light gases He and Ne.

Table 2.1: Sample selection for the study of Q-gases with CSSE. Exposure ages are determined with $(^{22}Ne/^{21}Ne)_{cosm} = 1.11$ (average chondritic value) and $^{21}Ne_{bulk} = ^{21}Ne_{cosm}$ according to Eugster (1988). The Allende and Murchison samples have already been analysed by CSSE by Wieler *et al.* (1991; 1992).

sample	classification	$^{21}Ne_{bulk}$ [$10^{-8}cm^3/g$]	$(^{20}Ne/^{22}Ne)_{bulk}$	exposure age [Ma]	reference
Lancé	CO3.4	1.59 ± 0.01	2.55 ± 0.02	5.0	1)
Vigarano	CV3 (red.)	1.88 ± 0.19	5.28 ± 0.04	5.9	2)
Dimmitt	H 3.7	1.50 ± 0.04	6.58 ± 0.07	4.9	3)
Grosnaja	CV3 (ox.)	0.66 ± 0.07	5.01 ± 0.06	2.1	2)
		0.60 ± 0.01	5.10 ± 0.04	1.9	this work
Chainpur	LL3.4	8.18 ± 0.80	1.06 ± 0.04	24.6	4)
Cold Bokkeveld	CM2	0.11 ± 0.01	7.61 ± 0.09	0.4	1)
Ornans	CO3.3	4.76 ± 0.02	1.07 ± 0.01	14.9	1)
Isna	CO3.7	0.04 ± 0.01	5.65 ± 0.11	0.13	5)
Abee	EH4	2.06 ± 0.21	1.46 ± 0.02	8.0	6)
Brownfield	H3.7	4.77 ± 0.18	0.91 ± 0.02	15.4	3)
	H3.7	12.1 ± 0.6	0.93 ± 0.07	39.2	7)
Dhajala	H3.8	2.48 ± 0.18	0.94 ± 0.01	8.0	8)
Kainsaz	CO3.1	8.16 ± 1.64	1.70 ± 0.01	25.6	9)
Krymka	LL3.1	9.23 ± 1.76	1.01 ± 0.01	27.8	10)
Allende	*CV3 (ox.)*	*2.18 ± 0.12*	*2.27 ± 0.01*	*6.8*	*11)*
Murchison	*CM2*	*0.62 ± 0.01*	*10.04 ± 0.10*	*2.4*	*12)*

1) Mazor *et al.* (1970); 2) Matsuda *et al.* (1980); 3) Moniot (1980); 4) Eugster (1988); 5) Englert *et al.* (1983); 6) Wacker and Marti (1983); 7) Müller *et al.* (1981); 8) Schelhaas *et al.* (1990); 9) Alaerts *et al.* (1979b); 10) Alaerts *et al.* (1979a); 11) Smith *et al.* (1977); 12) Smith *et al.* (1978).

Vigarano CV3 (reduced): This meteorite is examined to detect possible differences or similarities in the Q-composition between reduced and oxidised members of the CV3 group (Allende, Wieler *et al.*, 1991; and Grosnaja, this work).

Matsuda *et al.* (1980) found heavy Q-gases in residues of this brecciated CV3 chondrite of the reduced subgroup. This group consists of only a few meteorites: Arch, Efremovka, Leoville, Vigarano and small Antarctic samples (e. g. Weisberg *et al.*, 1997). On the other hand, Matsuda *et al.* suggested only minor contributions of Ne-Q in Vigarano. The cosmic-ray exposure age of Vigarano (5.9 Ma) is the minimum age of the available CV3 chondrites of the reduced subgroup, but is relatively high, compared with that of CV3 Grosnaja (2.0 Ma).

Dimmitt H3.7: This meteorite is the first ordinary chondrite that has been measured by CSSE, with the aim to extend this technique to meteorite classes other than carbonaceous chondrites. Dimmitt was chosen mainly because large sample amounts were available which offsets the disadvantage of its relatively high exposure age of 4.9 Ma (Table 2.1). At the time of sample selection, it had been overlooked that Dimmitt is a solar gas-rich regolith breccia (Rubin *et al.*, 1983), containing large amounts of solar He and Ne. However, the CSSE technique eventually proved that it is able to resolve different major noble gas components, since we were able to determine He-Q and Ne-Q in Dimmitt.

Grosnaja CV3 (oxidised): The 5.8 g of Grosnaja were kindly provided by Yu. A. Shukolyukov, Russian Academy of Science, Moscow. This sample is especially important for this work, since it allowed us to measure He-Q and Ne-Q in particularly pure form. This meteorite has a very low exposure age of 2.0 Ma (see Table 2.1). Therefore, cosmogenic ^{3}He and ^{21}Ne are expected to affect the determination of Q noble gases less than in most other examinations. Matsuda *et al.* (1980) measured already all heavier Q-gases by a conventional technique, but nominally negative concentrations of Ne-Q had been derived. This is in clear contrast to our results (chapter 3.1.1) and Grosnaja is therefore a prime example that CSSE is the preferred technique for the measurement of He-Q and Ne-Q.

Chainpur LL3.4: The largest part (4.3 g) of the measured sample has been kindly provided by U. Herpers, University of Cologne. Chainpur was the first unequilibrated ordinary chondrite (UOC) of the LL class to be analysed by CSSE. It was selected since Alaerts *et al.* (1979a) had already measured Ne-Q in Chainpur conventionally, though with a large error (Table 1.3). Chainpur contains large amounts of cosmogenic ^{21}Ne (Table 2.1) yielding an exposure age of 25 Ma (Eugster, 1988) which complicated the separation of cosmogenic and Q components.

Cold Bokkeveld CM2: A sample of 27.7 g was kindly provided by M. Grady, National History Museum, London, of which we used 9.3 g for our CSSE analysis. This CM2 meteorite

has been selected in particular to verify the new $(^3He/^4He)_Q$ value from Grosnaja determined in this work. It also offered a comparison with the CSSE data from CM2 Murchison (Wieler *et al.*, 1992). Cold Bokkeveld is a large meteorite with an extraordinarily short cosmic exposure age of less than 0.5 Ma (Mazor *et al.*, 1970; Eugster, 1988) and shows few signs (Macdougall and Phinney, 1977) of solar gases which are common in this meteorite class. CM2 chondrites are particularly suitable to examine Q-gases, since they exhibit characteristically short exposure ages. Cold Bokkeveld turned out to provide the most important results obtained in this work.

Ornans CO3.3: This sample ("No. 581", 4.6 g) was kindly provided by C. Perron, Muséum National d'Histoire Naturelle, Paris. Interestingly, Ornans (CO3.3) has a *lower* volatile content than Lancé (CO3.4), including carbon and the Q-noble gases, although it has a lower petrographic type (the "Ornans Paradox"; McSween, 1977; Alaerts *et al.*, 1979b). These observations suggest that the volatile concentrations were *not* determined by metamorphism but were established in the solar nebula (Alaerts *et al.*, 1979b), contrary to the suggestions of Huss *et al.* (1996). The examination of especially He-Q and Ne-Q in Ornans by CSSE tests these assumptions. Unfortunately, this meteorite has a rather high exposure age of 15 Ma (Table 2.1).

Isna CO3.7: Specimens were kindly provided by U. Herpers, University Cologne (2.0 g), G. MacPherson, National Museum of Natural History, Smithsonian Institution, Washington ("USNM 5890", 5.5 g) and J. Zipfel, Max-Planck-Institute for Chemistry, Dept. of Cosmochemistry, Mainz (2.5 g).

Isna is an especially interesting meteorite for analysis with CSSE, because of it's low cosmic ray exposure age of 0.13 Ma (Table 2.1). It completes our series of experiments on Q-gases in CO chondrites and their dependency on the metamorphic sequence (McSween, 1977). The elemental concentrations and ratios of He, Ar and Xe in the *bulk sample* are similar to those in other CO chondrites. However, the Ne content is unusually low by a factor of ~10 which possibly indicates losses. The isotopic composition of He in the bulk resembles pure He-A $(^3He/^4He = 1.4 \times 10^{-4})$, and thus does not show any influences of cosmogenic, radiogenic or solar He (Kirsten *et al.*, 1980; Englert *et al.*, 1983).

In addition, residues of several other meteorites (see Table 2.3) have been prepared, e. g. Abee (EH4), Krymka (LL3.1) and Dhajala (H3.8). Schelhaas *et al.* (1990) did not find Xe-HL in the acid-resistant residue of Dhajala. Thus, Dhajala probably contains no Ne-HL which can also be deduced from the Ne data of the oxidised and non-oxidised samples (Schelhaas *et al.*, 1990). Therefore, the sample should be especially suitable for the examination of Q-noble

gases. These results further confirm that Xe-HL and Ne-HL reside in the *same* diamonds and thus justify the usage of the name "Ne-HL" (Huss and Lewis, 1994a).

Of our entire sample collection, samples from Lancé (CO3.4), Dimmitt (H3.7), Grosnaja (CV3 ox.), Chainpur (LL3.4), and Cold Bokkeveld (CM2) have been measured successfully. This set covers different meteorite classes and several petrographic types which enables us to discuss differences in the incorporated reservoir(s) or metamorphic losses. The isotopic composition, in particular of the light noble gases He and Ne of phase Q, can be analysed particularly well with Grosnaja and Cold Bokkeveld which have very short cosmic ray exposure ages.

The first two attempts on Lancé and Vigarano failed due to too small noble gas yield, leaks in the extraction system and insufficient gas cleaning procedures. Fortunately, the second analysis of a residue of Lancé succeeded. Ornans and Isna, as well as the other prepared residues, are not part of this work and will be studied in a future project.

2.1.2 Chemical sample preparation and yields

The procedure used in this work to obtain the HF-HCl-resistant residues, follows that given in the original paper of Lewis *et al.* (1975) and subsequent publications of the Chicago group (e. g. Alaerts *et al.*, 1979a; Amari *et al.*, 1994). Table 2.2 shows the sequence of demineralisation steps by 10.4 molar HF, 6.0 molar HCl, 1.0 molar HCl, and 0.6 molar $AlCl_3$. Each step requires at least 8h.

Table 2.2: Chemical procedure to produce the HF/HCl-resistant residues.

step	at room temperature:	step	at 55-65°C:	step	cleaning:
1	10 M HF/1 M HCl	23	10 M HF/1 M HCl	36-39	0.1 M HCl
2	10 M HF/1 M HCl	24	6 M HCl		(several times)
3	10 M HF/1 M HCl	25	10 M HF/1 M HCl		
4	6 M HCl	26	10 M HF/1 M HCl	40	acetone
5	10 M HF/1 M HCl	27	6 M HCl	41	propanole
	8 cycles of:	28	6 M HCl	42	CS_2
		29	10 M HF/1 M HCl	43	CS_2
		30	10 M HF/1 M HCl	44	acetone
6-21	10 M HF/1 M HCl	31	6 M HCl	45	propanole
	6 M HCl	32	6 M HCl	46	acetone
	....	33	0.3 M $AlCl_3$	47	propanole
		34	10 M HF/1 M HCl	48	acetone
22	0.3 M $AlCl_3$	35	0.3 M $AlCl_3$		

The treatment with hydrochloric and hydrofluoric acid removes the bulk mass (silicates, metals, troilite) carrying the major part of cosmogenic and solar gases. The 6 M HCl removes precipitated fluorides and most sulfides (Johnson and Maxwell, 1981). $AlCl_3$ is then used to complex residual fluoride ions (Johnson and Maxwell, 1981). Elemental sulphur which is especially abundant in the residue of Cold Bokkeveld, can be removed by solution in CS_2 and acetone. This meteorite indeed contains the highest sulphur concentration of all samples selected for demineralisation (Dreibus *et al.*, 1995). However, Reynolds *et al.* (1978) observed even *higher* sulphur contents in samples treated with CS_2 which was applied in order to *remove* sulphur. In addition, we therefore used acetone which is probably more suitable for this purpose. Experiments to demineralise Allende with H_3BO_3 instead of $AlCl_3$, and KOH instead of CS_2, respectively, did not succeed, because the solutions formed white precipitation. This problem disappeared upon using the standard solutions of $AlCl_3$ and CS_2.

The remaining residue is a grey or black, sticky and fluffy carbonaceous substance. It consists of several minerals including presolar minerals. Of these, presolar nanodiamonds, graphite, and SiC are important carriers of noble gases (chapter 1.1.2.4). Other, more abundant constituents, which probably do not contain noble gases (Frick and Chang, 1978), are: Polymer/kerogen (macromolecular material containing C, H, O, N, S), chromite ($FeCr_2O_4$), spinel ($MgAl_2O_4$), hibonite ($Ca(Al, Ti)_{12}O_{19}$), corundum (Al_2O_3), osbornite (TiN) or metal sulfides as daubréelite ($FeCr_2S_4$) (Lewis *et al.*, 1975; Alaerts *et al.*, 1980; Crabb and Anders, 1982; Ott *et al.*, 1984; Amari *et al.*, 1994; Huss and Lewis, 1995; Huss *et al.*, 1996).

In the first experiments the acids used simply were poured off which possibly resulted in minor losses of the lowest density parts of the sample. Therefore, beginning with Vigarano II, a centrifuge has been used for the residue preparation, with which acids can be removed by syringes.

Pyrolysis measurements of a residue of Lancé were corrupted by huge amounts of background gases, with large peaks, for example, at masses 31, 50, 51, 69, 100, and 101. This points to a Teflon contamination. The Teflon most likely was introduced during the chemical preparation of the residues. The demineralisation has been aided by magnetic, Teflon-coated stirring bars and has been carried out, in the first experiments, in Teflon beakers. All other materials in contact to samples and acids (beakers, disposable syringes, bottles, centrifuge tubes, etc.) were made of polypropylene or polyethylene, and should, thus, not have caused the Teflon contamination. A similar pollution of samples had already been observed in stepwise pyrolysis of acid-resistant residues (Reynolds *et al.*, 1978). The CSSE etch runs with HNO_3 were not affected by these tiny inseparable Teflon particles, since the acid does not etch Teflon.

The Teflon-like molecules may also have been produced by an insufficient removal of residual fluorides during chemical processing and subsequent recombination of these fluorides with always available carbon.

Table 2.3: Sample weights and yields of the HF/HCl-resistant residues.

sample	petrographic type	weight [g]	yield [mg]	yield [%]
Allende	CV3 (ox.)	1.78 ± 0.01	73.9 ± 0.1	4.2[1]
Lancé I	CO3.4	5.98 ± 0.01	86.3 ± 0.1	1.4
Brownfield I	H3.7	13.57 ± 0.01	74.6 ± 0.5	0.5
Brownfield II	H3.7	7.52 ± 0.01	27.1 ± 0.5	0.4
Vigarano I	CV3 (red.)	11.35 ± 0.01	104.6 ± 0.1	0.9
Lancé II	CO3.4	6.78 ± 0.01	68.5 ± 0.5	1.0
Dhajala I	H3.8	6.95 ± 0.01	15.23 ± 0.05[2]	0.2
Dimmitt	H3.7	25.84 ± 0.01	482.1 ± 0.2	1.9
Vigarano II	CV3 (red.)	11.42 ± 0.01	270.7 ± 0.5	2.4
Grosnaja	CV3 (ox.)	5.68 ± 0.01	68.3 ± 0.5	1.2
Chainpur	LL3.4	6.05 ± 0.02	279.9 ± 0.2	4.6
Dhajala II	H3.8	4.89 ± 0.02	93.3 ± 0.5	1.9
Abee	EH4	9.151 ± 0.005	77.2 ± 0.5	0.8
Cold Bokkeveld	CM2	9.299 ± 0.005	276.7 ± 1.0	3.0
Krymka	LL3.1	6.038 ± 0.005	98.1 ± 0.5	1.6
Ornans	CO3.3	4.588 ± 0.005	127.7 ± 0.5	2.8
Isna	CO3.7	9.871 ± 0.005	104.8 ± 0.5	1.1
Allende	CV3 (ox.)	13.106 ± 0.001	134.9 ± 0.5	1.0

[1] probably accidental pollution during chemical preparation; [2] almost completely dissolved and removed, residue grey and fluffy, probably Teflon or not readily removed fluorides.

Reynolds *et al.* (1978) determined release patterns and temperatures for some dominant background gases (CO_2, diethyl phthalate, SO_2, Teflon, SiF_4,...). Since these gases are mainly released at temperatures below 600 °C, a two step pyrolysis (~600 °C and ~1800 °C)[1] is performed here to measure bulk oxidised and non-oxidised residues. High gas pressures of more than 1 mbar are measured, in particular, in the two heavy gas phases (Ar, Kr+Xe) of the 600 °C steps. Therefore, the 600 °C steps of these phases normally are pumped off to protect the spectrometer. Less than 10 % of the total heavy gases should have been lost this way, as estimated from the measurements of ^4He and ^{20}Ne in both, the 600 °C and 1800 °C steps (chapter 7).

Yields of the demineralisation procedures are given in Table 2.3 and Figure 2.1. Of the starting mass 0.2-4.6 % remained after all acid and cleaning steps. The rather simple chemical

---

[1] The oven temperature is estimated by heating the oven until red-hot and observing the melting of aluminium at 660 °C.

processing can not avoid small sample losses. Despite this uncertainty, a rough systematic trend can be seen in Figure 2.1: Meteorites of higher petrographic type seem to contain lower abundances of HF/HCl-resistant minerals. This observation is in accordance with Huss and Lewis (1995). They found a correlation between petrographic type and abundances of presolar diamonds, graphite, and SiC grains.
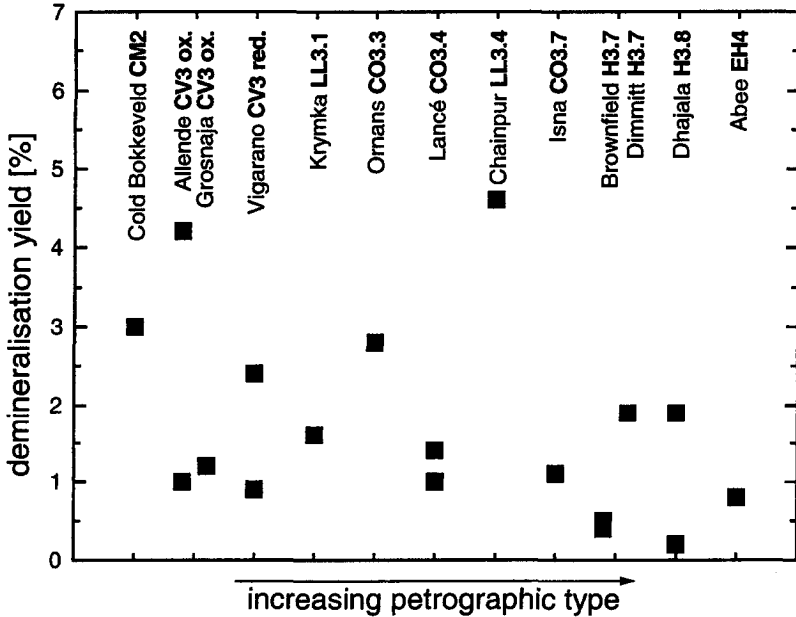
Figure 2.1: Mass yields in percent after complete demineralisation. A rough trend between petrographic type and demineralisation yield can be seen.

2.2 Noble gas processing

2.2.1 Gas extraction by CSSE

Phase Q is lost per definition during treatment of HF/HCl-resistant residues with oxidising acids, e.g. nitric acid (HNO_3) (chapter 1.1.3). Only very small mass fractions are lost upon this etching (Table 2.4), indicating that the noble gas concentrations per gram of phase Q are exceedingly high (e. g. 6.5×10^{-3} cm^3 STP/g ^{4}He in phase Q of Cold Bokkeveld). Other abundant minerals in HF/HCl-resistant residues, as chromite or diamonds, are HNO_3-insoluble.

Construction details of the CSSE apparatus are given by Signer *et al.* (1993). Concentrated nitric acid (65 %, 14.4 molar) is filled into an acid "finger" made of massive gold (total volume 0.64 ml, filling at least 0.3 ml HNO_3). The HF/HCl-resistant residue is located in a similar gold finger (volume 3.82ml). Acid and sample are separated by valve "G2", whose acid exposed parts also consist of either pure gold or pure platinum (Figure 2.2). The acid is degassed before each etching run by several cycles of heating (up to 50 °C) and freezing (-25 °C). Typically, 16 % of the acid are lost upon this degassing. The acid vapour/gas mixture is pumped through a special vacuum line with a cold trap (-80 °C, defrosted after each run) and an acid-resistant turbo molecular pump equipped with nitrogen countercurrent to protect the ball-bearing. However, degassing usually was not complete. Since the solubility of Kr and Xe in water (and therefore probably also in acid) are considerably higher than those of the lighter noble gases, Kr and Xe are often affected by atmospheric contributions from the acid which results in nearly atmospheric Xe isotopic compositions in the first steps (chapter 3.1.5). Elemental abundances of these steps have to be corrected for relatively large amounts of Kr and Xe (chapter 3.2). Fortunately, these atmospheric contributions are negligible in most steps.
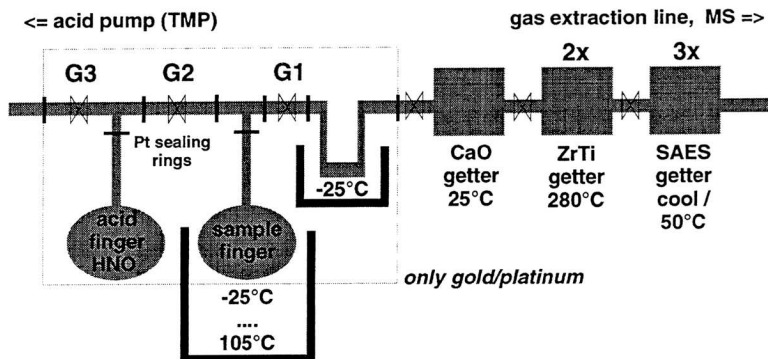
Figure 2.2: Closed system stepped etching (CSSE) apparatus. The sample resides in the right gold finger, the acid in the left one. Valve "G1" separates the etch volume from the gas extraction line including the cleaning devices. Valve "G3" leads to a special turbo-molecular pump (TMP). The etching is regulated with valve "G2". All parts in contact with acid consist of pure gold or platinum. Several further noble gas cleaning steps follow to protect gas extraction line and mass spectrometer (MS) from acid and reactive background gases.

Valves G1-G3 are directly in contact with the acids and are therefore made of pure gold and platinum. They survive a limited number of closings (normally 100 to 150 closings, the record being 353). All other parts of the CSSE apparatus, which are in contact with acid, are also made

of gold and platinum. The sealing rings used to connect two pieces of gold tube consist of pure platinum. At the beginning, palladium instead of platinum seals were tried, but these react with HNO_3 and form red $Pd(NO_3)_2$.

The released gases pass valve "G1" and a golden cold trap (about -25 °C, Figure 2.2) which is intended to freeze out gaseous HNO_3. Nonetheless, the subsequent steel vessel and copper seals of the CaO getter become strongly oxidised and tarnished.

Table 2.4: Weights of etched samples and yields.

sample	petrographic type	sample mass before etching [mg]	recovered mass after etching [mg]	Losses on etching [%]
Lancé I	CO3.4	81.3 ± 0.1	78.2 ± 0.1	3.8
Vigarano I	CV3 (red.)	97.7 ± 0.1	[1]	..
Lancé II	CO3.4	67.2 ± 0.5	58.9 ± 0.1	12.4
Dimmitt	H3.7	$470.1 \pm 0.2^{2)}$	$471.8 \pm 0.5^{2)}$	..
Grosnaja	CV3 (ox.)	68.3 ± 0.5	66.9 ± 0.2	2.0
Chainpur	LL3.4	279.9 ± 0.2	$238.9^{1)}$	..
C. Bokkeveld	CM2	276.7 ± 0.1	273.9 ± 0.2	1.0
Allende I[3]	CV3	24.9 ± 0.5	13.0 ± 0.5	47.8
Allende II[4]	CV3	10.6 ± 0.5	3.6 ± 0.5	66.0
Allende III[5]	CV3	22.3 ± 0.5	10.3 ± 0.5	53.8

[1] inadvertently lost; [2] weighing error probably due to remaining solvents or acid; [3] etched off-line with H_2O_2; [4] etched off-line with concentrated HNO_3 (14.4 molar); [5] etched off-line with diluted HNO_3 (0.04 molar).

To remove possible atmospheric contamination or rests of solvents, the sample finger is heated before etching for several hours or days to up to 90 °C. At the beginning of an etching run, the sample is etched with acid vapour which is expanded from the acid finger at room temperature through valve "G2" onto the sample. To achieve this, the separating valve "G2" is opened for a variable period of time (1 to 100 hours). When enough gas is presumed to have been released from the sample, the acid in the acid finger is cooled (-15 °C to -25 °C) for several hours. Valve "G2" is closed, and the Q-gases are expanded onto the CaO by opening valve "G1". After a number of vapour steps, the amount of gas released is no longer sufficient to be measured accurately. Next, the acid is heated to about 100 °C and distilled on the sample which is kept at -25 °C. The etching procedure can continue at acid/sample temperatures of 25 °C to 130 °C until no further significant amounts of Q-gases are released. During the heating of the sample, the upper parts of the gold apparatus are heated to a temperature 10 °C higher than that of the acid to keep the acid near the sample. The sample finger is cooled to -25 °C for some hours before gas extraction to minimise the amount of acid expanded into the clean-up line.

To prevent extraction line and mass spectrometer from acid and reactive gases, several cleaning steps are inserted (Figure 2.2). At the beginning of the cleaning procedure, the released gases are cleaned with dried CaO at room temperature to absorb H_2O and HNO_3. Two getters, filled with commercial Zr/Ti pellets and heated to 280 °C, follow to remove reactive gases. Finally, the gases are exposed to three commercial Zr/Al getters (SAES) to remove especially H_2 (getter at room temperature) and CH_4 (getter at 250 °C or higher). After the discovery of neonhydride (NeH) in particular on mass 21 (see chapters 2.3.3 and 7.8.1), the getter near the spectrometer has been operated at room temperature, instead of the previously used 400 °C which eliminated the problem. The prior measurements (Lancé II, Dimmitt) are corrected for NeH as described in chapter 7.8.2. During the first two runs on Lancé and Vigarano, the two getters closest to the sample were filled by a Zr/Ti alloy at 700 °C. It seems that the guttering capacity of this material had been insufficient which resulted in a too high background in the mass spectrometer.

Table 2.5: Weight losses upon etching with oxidising acids.

sample (#)	acid		loss [%]	source
CV3 Allende	conc. HNO_3	3.5h, 80 °C	5	Anders *et al.* (1975)
CV3 Allende (2)	fuming HNO_3	26h, 80 °C	24-45	Anders *et al.* (1975)
CM2 Murchison	fuming HNO_3	16h, 60 °C	44	Srinivasan *et al.* (1977)
LL (14)	fuming HNO_3	overnight, 60 °C	2-13	Alaerts *et al.* (1979a)
CO3 (3)	fuming HNO_3	overnight, 60 °C	6-42	Alaerts *et al.* (1979b)
CV3 (4)	fuming HNO_3	overnight, 60 °C	1-54	Matsuda *et al.* (1980)
OC (3)	30 % H_2O_2	few days, 60 °C	63-95	Moniot (1980)
CV3 Allende (2)	conc. HNO_3	4/17h, 80 °C	14/19	Ott *et al.* (1981)
CV3 Allende	fuming HNO_3	1h, 80 °C	41	Ott *et al.* (1981)
CV3 Allende	conc. $HClO_4$	1.5h, 139 °C	84	Ott *et al.* (1981)
OC (8)	conc. HNO_3	17h, 80 °C	13-63	Schelhaas *et al.* (1990)
all classes (14)	$Cr_2O_7^=/H_2SO_4$	11h, 75 °C	9-75	Huss and Lewis (1995)

The masses of the oxidised samples, which were recovered after the etch experiments, are given in Table 2.4. Astonishingly, oxidation with concentrated HNO_3, which removes some 95 % of the total primordial Xe in acid-resistant residues, leads to a mass loss of only about 5 % (Anders *et al.*, 1975). Losses on that order of magnitude are observed also for Lancé, Grosnaja and Cold Bokkeveld. However, these loss fractions are upper limits, because some samples may not have been completely recovered. Due to the uncertainty in sample recovery, we can not detect a possible correlation between meteorite type and resistance to etching (Huss *et al.*, 1996). Furthermore, larger losses can be seen for the Allende samples. These samples were etched off-line for future examinations with atomic force microscopy. Moniot (1980) noticed that etching with H_2O_2 generally yields larger losses. A possible reason might be the

formation of solid chemical products upon etching with HNO_3. Table 2.5 also shows that our results are in the expected range of etch yields, which largely vary, probably dependent on the acid applied and the etching time. In view of these strongly varying results, it seems unreasonable to calculate noble gas concentrations per gram of phase Q.

A problem can arise after opening gold valve "G1" which separates sample volume and gas clean-up line. Light particles in the residue can move out of the sample volume and lead to a leaking valve. This happened during etching of Cold Bokkeveld, but most of the leaked gas was collected at a following valve. Maximum losses per step were: 2.4 % ^{3}He, 1.5 % ^{22}Ne, 0.9 % ^{36}Ar[2], 1.4 % ^{84}Kr, 1.1 % ^{132}Xe. Since the first three steps, for which leaked gases were not collected, produced less than 1.5 % of the total gas amounts, no systematic errors, neither in the concentrations nor in the isotopic ratios, should have occurred in this run. After three runs, a mere 0.05 mg of these light particles could be washed out from gold tubes and valves. Noble gas contamination from such minute amounts of samples from earlier runs should therefore be negligible.

2.2.2 Gas extraction with the furnace

Comparing gas concentrations in non-oxidised and CSSE-oxidised residues allows one to check whether the CSSE experiments have released all noble gases of phase Q from the samples (chapter 3.3). This information is needed to compare absolute abundances of Q-gases in the samples. Aliquots of non-oxidised HF/HCl-resistant and on-line oxidised residues are measured conventionally by pyrolysis. The molybdenum crucible is heated by electron impact to about 1800 °C. To collect reactive gases (chapter 2.1.2), and to check for absorbed atmospheric gases, a 600 °C step is taken prior to the main step. These first steps often contain too much background gas and have to be pumped off. Cleaning procedures resemble those of the CSSE experiments (chapter 2.2.1).

2.2.3 Gas separation

The released gases are separated into three fractions (He/Ne, Ar, Kr/Xe) to avoid interference of ^{40}Ar^{++} on ^{20}Ne and Ar_2 on ^{80}Kr and not to provoke large *memory effects*. This release of noble gases within the mass spectrometer due to ion-impact can increase due to long

---

[2] Since the leaked Ar was dominated by an atmospherically composed blank, as discernible by the high ^{40}Ar/^{36}Ar ratio, probably from outgassing of CaO, the leaked Ar has not been added.

gas residence times in the mass spectrometer. Furthermore, large amounts of e. g. ^{40}Ar especially compromises the measurement of isotopes with smaller abundances, e. g. ^{124}Xe.

Table 2.6: Typical losses due to gas separation in dependence of the charcoal temperature.

run	sample	temperature	Ar [%]	Kr [%]	Xe [%]
HB03	Lancé	-100 °C	1.4	20.5	0.2
HB04	Dimmitt	-105 °C	1.7	6.4	0.001
HB05	Grosnaja	-110 °C	2.0	8.7	0.3
HB06	Chainpur	-115 °C	3.0	6.1	0.4
HB07	oven	-115 °C	2.0	4.4	0.4
HB08	Cold Bokkeveld	-115 °C	4.4	7.1	0.7
HB09	oven	-115 °C	3.1	6.3	0.3
HB10	oven	-115 °C	2.6	7.7	0.3

First, the heavier gases (Ar, Kr, Xe) are trapped completely in a stainless steel finger filled with activated charcoal at liquid nitrogen temperature (−196 °C), while He and Ne are expanded into the mass spectrometer and measured. Next, He, Ne and all gases which remained in the gas phase upon the cold charcoal are briefly pumped off. Then, Ar is released at −100-125 °C, and trapped in another coal-filled steel finger, while Kr and Xe remain adsorbed on the first coal. No fractionation occurs during this procedure (Marti, 1967). To correct for incomplete separation, ^{84}Kr and ^{132}Xe are also measured in the Ar fraction, as well as ^{40}Ar in the Kr/Xe fraction. Table 2.6 shows typical losses as a function of the coal temperature. Only Xe losses exceeding 0.5 % are corrected.

2.3 Noble gas measurement

2.3.1 Mass spectrometry

Most measurements in this work are carried out in the new mass spectrometer *"Albatros"* which is especially constructed to measure low noble gas abundances. The old mass spectrometers *"Minneapolis-Down/Upstream"* are not suitable to measure such small He and Ne amounts as released by CSSE (chapter 2.2.1) due to higher memory and interference of HD on ^{3}He due to an insufficient mass resolution.

"Albatros"...

The new non-commercial mass spectrometer *"Albatros"* (60°, 21cm radius) has a mass resolution M/ΔM of about 550. This is sufficient to resolve ^{3}He and HD as well as benzene and ^{78}Kr, respectively. Gas is ionised by electrons with an energy of only 45 eV to reduce double ionisation of ^{40}Ar and CO_2 and thus, the interference on ^{20}Ne and ^{22}Ne. To reach a similar electron emission current as with a standard voltage of 100 eV, the low electron acceleration voltage would have to be compensated by a higher filament current which would lead to a lower lifetime of the filament. We therefore prefer to use a lower electron emission current to protect the filament, in spite of the resulting lower ion yield.

A higher mass resolution requires a higher precision in the magnetic field settings. This causes problems especially for jumps to lower masses, because remnant magnetism of the deflecting magnets harms the correct peak adjustment. This can be avoided by extended demagnetising operations prior to all measurements. *"Albatros"* is equipped with two collectors: A multiplier operated in counting mode allowing an upper limit of 500 000 Hz corresponding to 2 x 10^{-8} cm^3 STP ^{22}Ne and a Faraday cup to measure higher ion currents.

"Upstream"...

The old mass spectrometers *"Minneapolis-Downstream"* (for He and Ne) and *"Minneapolis-Upstream"* (Ar-Xe), were used in this study only to measure noble gases released by CSSE from Lancé I and Vigarano. These spectrometers are operated with electron energies of 40 eV and 100 eV and resolutions of M/ΔM = 93 and 97, respectively. These resolutions are not sufficient to resolve the interference mentioned above. For later runs, only "Upstream" was used to measure noble gases extracted from bulk residue samples in the oven (chapter 2.2.2). CO_2^{++} and Ar^{++} corrections applied in these experiments are described in chapter 2.3.4. These old, original *Nier spectrometers*, built in the sixties but strongly modified, have each a Faraday cup for higher ion currents and a multiplier in analogue mode (upper limit: 5 x 10^{-9}A ≈ 20 x 10^{-8} cm^3 STP ^{22}Ne).

2.3.2 Blanks

Blank corrections were made by subtraction of "procedure" blanks (CSSE measurements *without* sample volume) and "hot" blanks (oven measurements with pure aluminium), respectively. These blanks were measured prior to almost every sample steps.

Typical **procedure blanks** for each etch experiment are given in Table 2.7. Also shown are maximum blank corrections observed in any step of a given run. However, most corrections are considerably lower than these maximum values and are, in fact negligible. Ar in runs HB05-8 (Grosnaja, Chainpur, Cold Bokkeveld) can not be corrected by a simple subtraction because of the dilutions applied to these steps. The applied Ar-blank corrections are described in chapter 3.1.4.

Table 2.7: *Typical* "procedure" blanks for CSSE experiments. Also given (in brackets) are the *maximum* blank corrections for any step in the given run.

run	^{4}He [10^{-10} cm^3]	^{20}Ne [10^{-13} cm^3]	^{36}Ar [10^{-12} cm^3]	^{40}Ar [10^{-10} cm^3]	^{84}Kr [10^{-15} cm^3]	^{132}Xe [10^{-15} cm^3]
Lancé	5.3	20.8	6.4	46.3	12.2	4.1
(HB03)	*(18.4%)[1]*	*(3.4%)[1]*	*(0.1%)[1]*	*(6.0%)[1]*	*(0.04%)*	*(0.01%)*
Dimmitt	3.7	5.5	7.2	21.3	7.0	3.7
(HB04)	*(2.7%)*	*(0.7%)*	*(1.3%)*	*(17.9%)*	*(0.1%)*	*(0.01%)*
Grosnaja	3.8	5.0	10.8	32.6	28.7	9.8
(HB05)	*(0.7%)*	*(0.1%)*	*(0.2%)*	*(17.5%)[2]*	*(0.1%)*	*(0.02%)*
Chainpur	3.6	10.0	2.6	7.2	65.3	41.7
(HB06)	*(2.0%)[3]*	*(0.5%)[3]*	*..*	*(3.2%)[2] [3]*	*(0.2)[3]*	*(0.04%)[3]*
Cold Bokkeveld	3.2	5.3	12.5	32.1	52.4	50.5
(HB08/I)	*(0.3%)*	*(0.1%)*	*(0.2%)*	*(0.1%)[2]*	*(0.1%)*	*(0.1%)*
Cold Bokkeveld	3.2	5.0	16.7	38.2	32.5	29.1
(HB08/II)	*(2.4%)*	*(0.7%)*	*(0.8%)*	*(8.5%)[2]*	*(0.2%)*	*(0.1%)*
bulk residues, oven	8.4	505	256	775	5540	2780
(HB07)	*(0.1%)*	*(9.1%)*	*(8.0%)*	*(9.1%)*	*(12.4%)*	*(3.3%)*
bulk residues, oven	329	1950	1550	150	17800	26700
(HB09)	*(32.6%)*	*(21.6%)*	*(37.9%)*	*(38.6%)*	*(36.0%)*	*(40.7%)*
bulk residues, oven	26.9	2050	3530	168	35900	59500
(HB10)	*(7.6%)*	*(9.8%)*	*(4.3%)*	*(71.4%)*	*(4.3%)*	*(3.3%)*

[1] without almost gas-less step 9; [2] see chapter 3.1.4 for Ar-blank correction; [3] without step 19 which contains almost no gas.

In addition, 1-4 complete CSSE **"gold blanks"** were determined before each etch run, after the sample had been loaded. These gold blanks include the sample volume but not the acid volume, and were measured after closure duration of the sample volume of between 21 hours and 49 days. These blanks were treated and analysed as "normal" steps. Results of the main isotopes are given in Table 7.49. "Gold blanks" depend highly on duration and the time within an etch run, at which they are measured, as is discernible best from the data for Dimmitt and Grosnaja and from the decreasing influence of adsorbed Kr and Xe (see subsequent paragraph about Kr and Xe). It is not possible to measure a truly adequate gold blank for every step, because this would be too time consuming, and, in particular, blank measurements including the sample volume are no longer possible, once valve "G2" has been opened. Therefore, we

compare available gold blank data with those of the corresponding procedure blanks (Table 2.7 and Table 7.49):

He and Ne amounts of these gold blanks are mostly of the same order of magnitude as average procedure blanks and, thus, do not cause any problems.

Ar abundances vary strongly, but the isotopic composition is clearly close to atmospheric ($^{36}Ar/^{40}Ar > 200$ in most cases; Table 7.49). Thus, large contributions of blank Ar from the gold line during the sample runs would be recognised by high $^{40}Ar/^{36}Ar$ ratios. Since this was never observed in any major release fraction, essentially all measured ^{36}Ar and ^{38}Ar is from phase Q and blank corrections on these isotopes are negligible. On the other hand, ^{40}Ar in all steps is most probably only a upper limit due to radiogenic admixtures.

Kr and Xe in gold blanks are much more abundant than in procedure blanks. Gold surfaces seem to easily absorb the heavier noble gases Kr and Xe, similar to liquids (chapter 2.2.1). In fact, the first few steps of each run contain significant amounts of atmospheric admixtures, recognised by Xe isotopic ratios close to atmospheric composition (chapter 3.1.5). This is not observed in later steps, and the gold blanks should not be important anymore. Steps influenced by these atmospheric contributions are not used for the determination of isotopic compositions of Kr and Xe in Q (chapters 3.1.6 and 3.1.5). Elemental abundances of these steps are corrected for atmospheric Kr and Xe (see chapter 3.2). Therefore, it is justified to use procedure blanks to correct for all blank contributions including those from the sample volume.

The high abundances of all noble gases in the third gold blank for Cold Bokkeveld (Table 7.49) can be explained by droplets of acid in the gold apparatus remaining from earlier experiments. The sample was heated for 50 h to 100 °C to remove absorbed gases prior to the gold blank measurement. This old acid then had already begun to etch phase Q which is clearly seen by the isotopic composition of the gases released in this nominal blank step. This blank is analysed as a first step. He, Ne and Ar in this step amount to about 1 % of the total gas released upon etching. Kr and Xe contain higher contributions of the total amounts, but are atmospherically affected.

2.3.3   Calibrations and standards

Mass discrimination and sensitivity of the spectrometers are obtained by measuring exactly known amounts of pure calibration noble gases. The experiments are calibrated separately with at least three calibration measurements (**"slow-calibration"**) for He-Ne, Ar and Kr-Xe each. Thus, "long-term" variations, e. g. caused by the change of gas extraction procedures or volumes are taken into account. Calibration gases are measured under exactly the same

conditions and by expanding them into the same volume (except the negligible sample volume, << 1 %) as the sample gas. Table 2.8 and Table 2.9 show roughly calculated sensitivities for single etch runs, as simply determined from the averaged ratio of measured ion current or count rate and standard gas amount. No blank or interference corrections are applied for this simple estimate, though all these corrections are included in the final data analysis. Note, however, that blank-signals always came to less than 0.12 % of the standard amount, except for Ar where this contribution was up to 4 %.

Table 2.8: Estimated sensitivities for counter ("Albatros") and multiplier ("Upstream").

		^{3}He	^{22}Ne	^{36}Ar	^{84}Kr	^{132}Xe
Counter [10^{-14} cm^3 STP/Hz]	HB03[1]	3.83	2.90	0.16	0.11	0.10
	HB04	6.02	4.52	0.22	0.18	0.16
	HB05	6.08	4.61	0.29	0.22	0.17
	HB06	6.57	4.94	0.30	0.28	0.24
	HB08/I	5.36	3.97	0.23	0.16	0.13
	HB08/II	6.27	4.75	0.29	0.28	0.24
Multiplier [cm^3 STP/A]	HB07[2]	29.1	18.3	4.74	6.39	7.16
	HB09	85.3	43.7	14.0	18.1	18.5
	HB10	83.8	44.3	14.0	16.9	18.4

[1] old multiplier and filament, replaced between runs HB03 and HB04; [2] old filament, replaced between runs HB07 and HB09.

Table 2.9: Estimated sensitivities for the Faraday cups.

		^{4}He	^{20}Ne	^{40}Ar	^{84}Kr	^{132}Xe
		[10^5 cm^3/A]				
(CSSE/"Albatros")	HB03[1]	1.84	1.41	0.07	0.04	0.04
	HB04	3.53	2.70	0.12	0.05	0.10
	HB05	3.46	2.62	0.15		
	HB06	3.53	2.62	0.14		
	HB08/I	3.19	2.38	0.13		
	HB08/II	3.31	2.45	0.13		
(Oven/"Upstream")	HB07[2]	0.78	0.44	0.08		
	HB09	1.95	1.13	0.22		
	HB10	1.94	1.07	0.21		

[1] old filament, replaced between runs HB03 and HB04; [2] old filament, replaced between runs HB07 and HB09.

One single etch experiment lasts up to 5 months. The spectrometer sensitivity varies considerably within such a period, since it can even change discernibly within hours. To take into account these "short-term variations", each sample measurement is also accompanied by relative standard gas measurements (**"fast-calibration"**). Residual gas determinations within the spectrometer volume are also considered here. These variations can e. g. be caused by decreasing ion to electron conversion efficiencies on the first multiplier dynode because of a

too high integrated ion current. Differences in % between maximum and minimum of these "fast-calibration" standard amount determinations are given in Table 2.10.

Table 2.10: Sensitivity variations ("Fast-Calibration") within one experiment. First number: mean variations from fast-calibration to fast-calibration [%]; second number: Max./min. [%].

	^{3}He(C/M)	^{4}He(F)	^{20}Ne(F)	^{22}Ne(C/M)	^{36}Ar(C/M)	^{40}Ar(F)	^{84}Kr(C/M)	^{132}Xe(C/M)
HB03	1/3	0/1	2/6	0/2	1/4	0/1	1/1	1/2
HB04	1/7	1/7	3/14	1/10	1/14	1/10	2/16	3/19
HB05	1/4	1/4	2/10	1/4	1/8	1/5	1/17	2/20
HB06[1]	5/37	5/39	6/40	5/39	3/27	3/29	5/31	5/30
HB07	3/9	1/5	1/5	3/8	2/7	1/6	3/27	4/12
HB08/I[2]	1/10	0/2	2/8	1/12	1/23	0/1	2/32	2/36
HB08/II	1/4	1/5	2/9	1/5	1/6	1/4	1/14	2/15
HB09	5/19	1/2	1/2	4/16	3/14	1/1	4/17	3/12
HB10	2/5	0/1	0/1	2/6	3/6	0/0	3/6	2/4

[1] The largest variations followed those steps with the largest background gas amounts which corrupted the ionisation efficiency of the ion source; [2] The counter sensitivity for Ar, Kr and Xe decreased continuously, indicating a considerable decrease of conversion efficiency on the first multiplier dynode.

Table 2.11: Calibration gas amounts [10^{-8} cm^3 STP].

	reservoir	HB03-5	reservoir	HB06-9	reservoir	HB07+9+10
^{3}He	7 old	34.2	7 new	1.70	17	54.2
^{4}He	I	726	I	28.1	I	56.7
^{20}Ne	I	21.1	I	1.15	I	26.4
^{22}Ne	I	2.18	I	0.118	I	2.72
^{36}Ar	I	1.07	8	0.071		
^{40}Ar	I	316	I	20.9		
^{84}Kr	6	0.0057	6	0.0057		
^{132}Xe	I	0.0030	I	0.0030		

Due to a leakage of one calibration gas reservoir, absolute **gas standards** from different reservoirs were used (Table 2.11): The combined He-Ne-Ar reservoir was used for the experiments HB03-5. Since it contained too much gas to be measurable with the counter, the calibration steps have been diluted by a factor of about 0.04. The experiments on Chainpur, Cold Bokkeveld and the oven measurements (HB06-10) were calibrated without dilution with separate standard reservoirs for He plus Ne and Ar. Two reservoirs with different gas amounts of He and Ne (one suitable to measure all isotopes with the Faraday cup and one with lower abundances) were used. Except for He, the gas standards are of atmospheric isotope composition.

For each element and each collector, the absolute amount of one *reference isotope* is determined by peak height comparison between calibration and sample gas. Isotopic ratios are then determined relative to these reference isotopes. Thereby, the variable sensitivities of the

spectrometers for the different isotopes of an element have to be corrected for. These sensitivity variations (**mass discrimination**[3]) are determined from all calibration analyses with the equation:

$$\Delta m\left[\% / amu\right] = \frac{1 - \dfrac{ratio_{std}}{ratio_{msr}}}{\left(m_i - m_{ref}\right)} \times 100$$

where

$$ratio_{std / msr} = \frac{isotope\ x}{reference\ isotope} (standard / measured)$$
$$m_{i / ref} = mass\ of\ isotope\ i / reference\ isotope\ [amu]$$

Mass discriminations are determined for each run separately. They vary little from run to run (Table 7.54). Most of the values are lower than 1 %/amu. However, the mass discrimination determined from $^{21}Ne/^{22}Ne$ is significantly higher in all experiments than that obtained from $^{20}Ne/^{22}Ne$. The latter is adopted for both isotopic Ne ratios.

The ^{20}NeH interference on ^{21}Ne (chapter 2.2.1) has been discovered due to this higher mass discrimination for $^{21}Ne/^{22}Ne$. It is the result of too high H_2-background during the first two experiments with the new mass spectrometer (Lancé II, Dimmitt). ^{20}Ne-hydride influences the measurement of low ^{21}Ne abundances. Reducing this H-background eliminates this problem for subsequent experiments (see chapter 7.8.2 for details and corrections). But, even after elimination of the contributions from this interference, the mass discrimination remains too high. I suspect that this is probably due to an incorrect standard ratio (Eberhardt *et al.*, 1965).

2.3.4 Uncertainties

The uncertainties (chapter 7) for the reference isotope concentrations include 1σ statistical errors[4], the uncertainties of sample weight (Table 2.4), dilution (chapter 2.3.3), blank (chapter 2.3.2) and interference corrections (chapter 2.3.5). Not included are errors of the standard gas

---

[3] *Multiplier* sensitivities are mass-dependent, since the incoming isotopes have different momenta, and therefore, different conversion electron yields. This dependence is assumed to be roughly linear within the isotopes of one element.

[4] All isotopes were measured 5-8 times and the signals were extrapolated to the time of gas inlet. The data were extrapolated linearly for He, Ne and Ar, but exponential fits were applied to most of the Kr and Xe data. The uncertainties of these extrapolations give the statistical errors.

amounts which are estimated to be about 1 %. The errors of the isotopic ratios include statistical errors, errors of the mass discrimination (chapter 2.3.3), blank (chapter 2.3.2) and interference errors (chapter 2.3.5).

2.3.5 Interference

Interference disturbs the noble gas measurements, as already mentioned above. The most important interfering ions and the corrections applied are presented in this chapter.

The **heavy hydrogen molecule HD** interferes with ^{3}He. This is eliminated for the CSSE measurements by increasing the resolution of mass spectrometer *"Albatros"*. Besides this, the H_2-background in this spectrometer is quite constant. Therefore, possible residual HD-contributions to ^{3}He are corrected by the routine blank subtraction.

In contrast, ^{3}He data from the oven samples measured in *"Upstream"* are strongly affected by HD. It is possible to determine the effective HD/H_2 ratio by assuming ^{3}He = 0 for residual and blank measurements which is justified by the sufficiently low ^{4}He amounts. This implicitly also should correct for the mass discrimination between H_2 and HD which may well exceed 10 % (Table 7.54). However, runs HB07 and HB09 give $HD/H_2 = (2.2 \pm 0.2) \times 10^{-4}$ and $(1.1 \pm 0.2) \times 10^{-4}$, respectively, much lower than the mean terrestrial value of 3.0×10^{-4}. Direct measurements of HD/H_2 in *"Albatros"* without mass discrimination correction give ratios of $(3.4 \pm 0.3, 3.2 \pm 0.3, 3.2 \pm 0.4,$ and $3.3 \pm 0.9) \times 10^{-4}$ in agreement with the terrestrial value. Therefore, for *"Upstream"* data I correct for HD assuming $HD/H_2 = (3.0 \pm 1.5) \times 10^{-4}$. The large error accounts for the unknown mass discrimination. The corrections vary between 0-16 % of the total signal on mass 3.

Another interference occurs on ^{20}Ne due to $H_2^{18}O$. This contribution can be estimated from the monitored H_2O amounts and the natural value for $H_2^{18}O/H_2^{16}O = 0.002$. It is in most cases smaller than 0.5 % and never exceeds 2.5 %. An explicit correction is not necessary, since H_2O is quite constant in sample and blank measurements, and hence, the correction is done implicitly by the blank correction.

Fluorine forms **hydrofluoric acid HF** of mass 20 in the mass spectrometer with unknown efficiency and, therefore, can also affect ^{20}Ne. However, *"Albatros"* shows negligible ^{19}F abundances, and ^{19}F amounts in *"Upstream"* are extremely constant. As with $H_2^{18}O$, the correction is thus performed by the blank subtraction.

Table 2.12: Cross sections for 45 eV electron-impact single and double ionisation of Ar.

reference	$\sigma(^{40}Ar^+)$ [10^{-16} cm^2] (max. uncertainty)	$\sigma(^{40}Ar^{++})$ [10^{-16} cm^2] (max. uncertainty)	$\sigma(^{40}Ar^{++})/\sigma(^{40}Ar^+)$
Wetzel et al. (1987)	2.56 (± 15%)	0.003 (± 15%)	0.0012 ± 0.0003
Ma et al. (1991)	2.42 (± 15%)	0.002 (± 15%)	0.0008 ± 0.0002
Syage (1992)	2.49[1]	0.0065 (± 12%)	0.0026 ± 0.0004
Straub et al. (1995)	2.66 (± 3.5%)	0.00048 (± 4.5%)	0.00018 ± 0.00001
adopted value	2.53	0.0030	**0.0012 ± 0.0006**

[1] data compilation.

Interfering **doubly ionised** $^{40}Ar^{++}$ on ^{20}Ne can be roughly estimated as the product of the measured ^{40}Ar in the He-Ne fraction and the electron-impact ionisation cross section ratio of double to single ionisation, $\sigma(^{40}Ar^{++})/\sigma(^{40}Ar^+)$. Unfortunately, literature values are not perfectly consistent (Table 2.12 and Table 2.13). The electron energy of 45 eV used in *"Albatros"* is only slightly above the threshold for double ionisation of Ar. In this region, the excitation function is rather steep and error-prone. The value $\sigma(^{40}Ar^{++})/\sigma(^{40}Ar^+)_{45eV} = 0.12$ % (with 50% error) is adopted here. Cross sections for an electron acceleration of 100 eV (for *"Upstream"*) are higher and better known. The adopted ratio $\sigma(^{40}Ar^{++})/\sigma(^{40}Ar^+)_{100eV}$ is 7.2 % with 25 % error. A correction of Ar^{++} in CSSE measurements is not necessary, since these contributions mostly amount to less than 0.1 % of the measured ^{20}Ne and never exceed 0.7 %. The same holds for oven run HB07 and HB10. Only some measurements of HB09 show higher possible $^{40}Ar^{++}$ contributions of up to 11% of ^{20}Ne.

Table 2.13: Cross sections for 100 eV electron-impact single and double ionisation of Ar.

reference	$\sigma(^{40}Ar^+)$ [10^{-16} cm^2] (max. uncertainty)	$\sigma(^{40}Ar^{++})$ [10^{-16} cm^2] (max. uncertainty)	$\sigma(^{40}Ar^{++})/\sigma(^{40}Ar^+)$
Wetzel et al. (1987)	2.68 (± 15%)	0.177 (± 15%)	0.066 ± 0.014
Ma et al. (1991)	2.47 (± 15%)	0.215 (± 15%)	0.087 ± 0.018
Syage (1992)	2.53[1]	0.158 (± 12%)	0.063 ± 0.011
Straub et al. (1995)	2.64 (± 3.5%)	0.189 (± 4.5%)	0.072 ± 0.004
adopted value	2.58	0.185	**0.072 ± 0.018**

[1] data compilation.

Finally, **doubly ionised** CO_2^{++} admixtures to ^{22}Ne are discussed. *"Albatros"* shows very small and very constant CO_2 abundances, corresponding to typically $(6-10) \times 10^{-12}$ cm^3 STP-equivalent. Thus, CO_2^{++} contributions to ^{22}Ne can be neglected. *"Upstream"* shows a much higher CO_2 background. A correction factor CO_2^{++}/CO_2^+ can be estimated by using air-Ne corrected residual measurements. The long-term mean ratio is 0.02 ± 0.01. This value is used for the corrections which can reach 13 %, but are less than 5 % in most cases.

Interference from **ions hitting the flight tube** occurred after replacing the multiplier of the mass-spectrometer *"Albatros"* prior to the measurement of Dimmitt for ions directed to the **Faraday cup** with a magnetic field ratio $B_{interference}/B_{peak} = 1.028 \pm 0.001$. For this reason, ^{38}Ar ions can not properly be measured with the Faraday cup due to interfering ^{36}Ar ions. Unfortunately, the Ar data of Dimmitt were obtained almost exclusively with the Faraday cup. Subsequent measurements are obtained in such a way that, if necessary, the Ar fraction is diluted to measure ^{36}Ar/^{38}Ar with the counter (see Ar-chapter 3.1.4). This problem does not affect the other isotopes.

3 Noble gas results

Noble gas data on five HF/HCl-resistant residues of Lancé (II), Dimmitt, Grosnaja, Chainpur and Cold Bokkeveld are presented in this chapter. The first part considers the isotopic ratios of the Q-gases. Contributions from simultaneously released components are also discussed. The second part then deals with elemental ratios and release patterns of the noble gases released in the etch experiments. Finally, total Q-noble gas abundances for our samples are determined.

3.1 Isotopic ratios

The isotopic compositions of all noble gases released during the five etch runs are presented here in order to reveal the possible release of interfering components, to give isotopic ratios for "pure" Q-gases in the various samples and to compare the values obtained with other results.

3.1.1 Neon

Few isotopic ratios of Ne-Q have been published to date (Table 3.2). Most of these values have large errors, since they were deduced as the small differences between Ne present in similar abundances in oxidised and non-oxidised residues, respectively, or from stepwise heating experiments, where the components released interfere due to overlapping release temperatures (see also chapter 1.1.3).

Table 3.1: Isotopic composition of Ne in different reservoirs.

component	$^{20}Ne/^{22}Ne$	$^{21}Ne/^{22}Ne$	source
air	9.80 ± 0.08	0.0290 ± 0.0003	Eberhardt et al. (1965)
SW	13.8 ± 0.1	0.0328 ± 0.0005	Benkert et al. (1993)
SEP	11.2 ± 0.2	0.0295 ± 0.0005	Benkert et al. (1993)
A ($\equiv$ Q+A2+P3)	8.2 ± 0.4	0.025 ± 0.003	Pepin (1967)
A2 ($\equiv$ HL+P6)	8.50 ± 0.06	0.036 ± 0.001	Huss and Lewis (1994a)
P3 ($\equiv$ A1)	8.91 ± 0.06	0.029 ± 0.001	Huss and Lewis (1994a)
E(L)	≈ 0	≈ 0	Amari et al. (1995)
E(H)	0.08	0.0006	Lewis et al. (1994)
cosmogenic "GCR"	≈ 0.85	≈ 0.92	typical chondritic value

In the following, I discuss new data obtained in this work which enhance the existing small number of reliable measurements of Ne-Q. We will see that other components, like solar Ne or Ne-E, are in some experiments released simultaneously with Ne-Q (and traces of cosmogenic Ne). Although this leads to certain problems, it also proves the impressive capability of CSSE to separate different noble gas components. All Ne results of this work are given in Table 3.2 and Table 3.4. The determination of these results begins with Ne in Lancé that consists only of Ne-Q and some cosmogenic Ne contributions.

Table 3.2: $(^{20}Ne/^{22}Ne)_Q$ obtained in this work and in literature.

sample	petrographic type	$(^{20}Ne/^{22}Ne)_Q$	source
Lancé	CO3.4	10.17 ± 0.03	this work
Dimmitt	H3.7	10.6 ± 0.2	this work
Grosnaja	CV3 (ox.)	10.66 ± 0.04	this work
Chainpur	LL3.4	10.60 ± 0.06	this work
Cold Bokkeveld	CM 2	10.05 ± 0.05	this work
Allende[1]	CV3	11.0 ± 2.0	Lewis *et al.* (1975)
Allende[1]	CV3	10.4 ± 1.0	Smith *et al.* (1977)
Allende[1]	CV3	10.5 ± 1.9	Srinivasan *et al.* (1977)
Murchison[1]	CM2	6.78 ± 0.06[5]	Srinivasan *et al.* (1977)
Allende[1]	CV3	10.4 ± 0.5	Srinivasan *et al.* (1978)
Murchison[1]	CM2	6.8[5]	Smith *et al.* (1978)
Hamlet[1]	LL4	11.0 ± 1.5	Alaerts *et al.* (1979a)
Bishunpur[1]	LL3.1	11.6 ± 2.0	Alaerts *et al.* (1979a)
Chainpur[1]	LL3.4	10.6 ± 1.1	Alaerts *et al.* (1979a)
"averaged Q"[1]	LL	10.9 ± 0.8	Alaerts *et al.* (1979a)
Kainsaz[1]	CO3.1	12.4 ± 1.8	Alaerts *et al.* (1979a)
Ornans[1]	CO3.3	9.8 ± 0.6	Alaerts *et al.* (1979a)
"averaged Q"[1]	CO	10.3 ± 0.4[3]	Alaerts *et al.* (1979b)
Hajmah "Ne-U"[2]	Ureilite	10.4 ± 0.3	Ott *et al.* (1985a)
Dhajala[2]	H3.8	10.11 ± 0.16	Schelhaas *et al.* (1990)
Allende[4]	CV3	10.70 ± 0.15	Wieler *et al.* (1991)
Murchison[4]	CM2	10.70 ± 0.20	Wieler *et al.* (1992)
Abee[1]	EH4	10.1[6]	Huss *et al.* (1996)
Julesburg[1]	L3.6	9.7[6]	Huss *et al.* (1996)

[1] Bulk pyrolysis and stepwise heating; [2] stepwise combustion; Ne-U is included into this table, since the primordial noble gases from ureilites are closely related to Q-noble gases (Ott *et al.*, 1985b); [3] uncertainties of the single measurements (Kainsaz, Ornans) are much larger (Alaerts *et al.*, 1979a); [4] obtained with CSSE; [5] mixture of Ne-E and Q; [6] "modified P1", re-calculated from given regression lines (Huss *et al.*, 1996), assuming $^{21}Ne/^{22}Ne = 0.0294$.

CO3.4 Lancé...

Figure 3.1 shows the Ne data for Lancé (Table 7.1). In such 3-isotope plots, data points representing two-component mixtures lie on a straight line between the two points which define the pure components. The data points of all steps form a relatively well defined mixing line,

pointing towards the cosmogenic end member on the lower right (off scale in main panel, in inset) and the Q-component near the left ordinate.
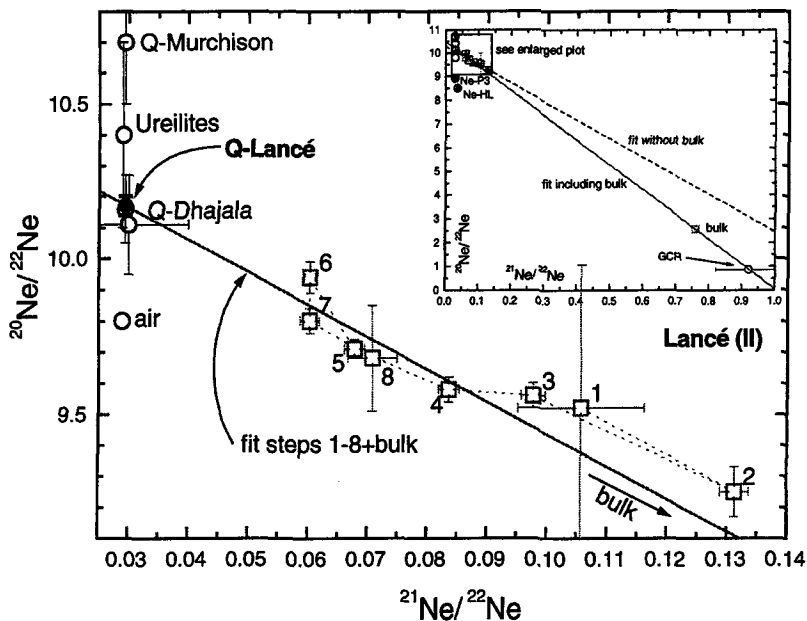
Figure 3.1: Ne released from Lancé. The data form a mixing line between a Q-like and a cosmogenic component. The data point for Q-Lancé ($^{20}Ne/^{22}Ne = 10.17 \pm 0.03$) is determined by the extrapolation of the regression line (including bulk value) to $(^{21}Ne/^{22}Ne)_Q = 0.0294$. References for bulk data: Mazor *et al.* (1970); other data see Table 3.1 and Table 3.2.

The inset in Figure 3.1 shows that the enrichment of Q-gases in the acid-resistant residue succeeded very well, because all CSSE data points fall much closer to the Q data point than to the bulk sample point, indicating much reduced proportions of cosmogenic Ne which are in all steps ≤ 1 % for ^{20}Ne. This allows one to deduce a precise value for $(^{20}Ne/^{22}Ne)_Q$.

The extrapolation[5] of the data of steps 1-8 to an assumed $(^{21}Ne/^{22}Ne)_Q$ ratio of 0.0294, as determined for Murchison (Wieler *et al.*, 1992), results in $^{20}Ne/^{22}Ne = 10.05 \pm 0.10$. However, the inset in Figure 3.1 shows that this best fit line clearly misses the point for any reasonable GCR-Ne composition. Therefore, the regression line forced through the bulk data point (Mazor *et al.*, 1970) has been calculated, since bulk Lancé is dominated by cosmogenic Ne. This

---

[5] To allow a re-calculation of the $(^{20}Ne/^{22}Ne)_Q$ ratios for other choices of $(^{21}Ne/^{22}Ne)_Q$, all regression lines used in this chapter are given in Table 3.3.

extrapolation leads to $(^{20}Ne/^{22}Ne)_Q = \mathbf{10.17 \pm 0.03}$ which is very similar to the value deduced for Q-Dhajala $(^{20}Ne/^{22}Ne = 10.11 \pm 0.16)$ by a stepped combustion experiment (Schelhaas *et al.*, 1990). Dhajala was in particular suitable for combustion, because it did not contain diamonds, the carriers of most disturbing Ne-HL and Xe-HL (Schelhaas *et al.*, 1990). Even in steps 6 and 7 with the lowest $^{21}Ne/^{22}Ne$ ratios, ~50 % of the ^{21}Ne is cosmogenic (Figure 3.1). Therefore, an upper limit for $(^{21}Ne/^{22}Ne)_Q$ in Lancé can not be given.

Table 3.3: Regression lines $(^{20}Ne/^{22}Ne)_Q = a + b * (^{21}Ne/^{22}Ne)_Q$.

experiment	steps	a	b
Lancé	1-8	10.28 ± 0.10	-7.83 ± 1.29
Lancé	1-8+bulk[1]	10.48 ± 0.03	-10.43 ± 0.06
Dimmitt	5-9	10.59 ± 0.14	-5.79 ± 1.28
Dimmitt	7+8+"GCR"[2]	11.10 ± 0.02	-11.14 ± 0.07
Grosnaja	1-15+bulk[3]	11.07 ± 0.02	-13.23 ± 0.20
Chainpur	1-3+14+bulk[4]	10.93 ± 0.06	-11.45 ± 0.10
Cold Bokkeveld	4-22	-0.80 ± 0.32	372.50 ± 17.91
Cold Bokkeveld	1-3,23-30+"GCR"[2]	10.35 ± 0.05	-10.32 ± 0.18

[1] Mazor *et al.* (1970); [2] Table 3.1; [3] Table 7.15; [4] Eugster (1988).

CV3 (ox.) Grosnaja...

A second meteorite, which shows only contributions of Ne-Q and cosmogenic Ne, is Grosnaja (Table 7.14). It provides the best and purest Ne-Q data of all CSSE experiments carried out in this work (Figure 3.2): Cosmogenic contributions are so small (in all steps ≤ 0.17 % of ^{20}Ne) that a best fit line through the data points is almost horizontal. The concentration-weighted mean of $(^{20}Ne/^{22}Ne)_Q$ from steps 2-14, which all have $^{21}Ne/^{22}Ne$ ratios lower than 0.04, would lead to $(^{20}Ne/^{22}Ne)_Q = 10.60 \pm 0.02$ for Grosnaja. Similar to the other experiments, a regression line (Table 3.3) through all data points of steps 1-15 and the bulk value for Grosnaja (Table 7.15), has been determined and extrapolated to the "Q-standard" value of $^{21}Ne/^{22}Ne = 0.0294$. This yields $(^{20}Ne/^{22}Ne)_Q = 10.68 \pm 0.02$ which is slightly higher than the value determined above.

The smallest $^{21}Ne/^{22}Ne$ ratio, measured in step 11, $(^{21}Ne/^{22}Ne)_Q = \mathbf{0.0314 \pm 0.0004}$, is adopted as the best estimate for $(^{21}Ne/^{22}Ne)_Q$ in Grosnaja. However, this value is still an upper limit, because it can not be ruled out that even this step released cosmogenic Ne, as was also suggested for the lowest known value of 0.0294 for Q-Murchison (Wieler *et al.*, 1992). Using the value of $(^{21}Ne/^{22}Ne)_Q$ and the regression line given above, the value $(^{20}Ne/^{22}Ne)_Q = \mathbf{10.66 \pm 0.04}$ is finally adopted for Grosnaja.
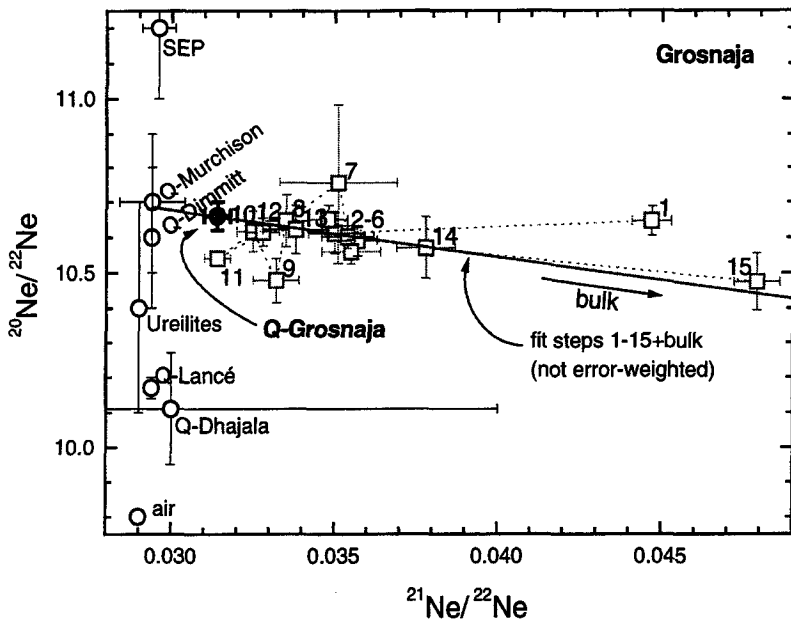
Figure 3.2: The experiment on Grosnaja provides the data set with the smallest non-Q contributions achieved with the CSSE technique in this work: Only minor cosmogenic admixtures are observable. The regression of the data points of all steps including that of the bulk sample (Table 7.15) reveals $(^{20}Ne/^{22}Ne)_Q = 10.66 \pm 0.02$ for $(^{21}Ne/^{22}Ne)_Q = 0.0314$ and $(^{20}Ne/^{22}Ne)_Q = 10.68 \pm 0.02$ for $(^{21}Ne/^{22}Ne)_Q = 0.0294$. References: Table 3.1 and Table 3.2.

LL3.4 Chainpur...

The Ne three-isotope-plot for Chainpur (Table 7.24) in Figure 3.3 displays a quite complex release pattern with admixtures of cosmogenic Ne as well as of Ne-E, a presolar component (see chapter 1.1.2.4 for details) not found in the meteorites discussed above. Ne-E in our oxidisation experiments will be discussed in chapter 3.1.2. While the data points of the first three steps are located in the region between typical Q and cosmogenic values, the following steps are increasingly affected by Ne-E (up to 16 % of ^{22}Ne in step 9). Beginning with step 12, the influence of Ne-E decreases again. Of these latter steps, step 14 is least influenced by Ne-E, since its data point falls close to the Q-bulk mixing line. Chainpur bulk has by far the largest cosmic-ray exposure age among the meteorites investigated here (Table 2.1). Despite this, the $^{21}Ne/^{22}Ne$ ratios measured in the residue are only slightly higher than those of Lancé and Grosnaja. This indicates that the removal of cosmogenic Ne bearing silicates during demineralisation has been very effective.

A linear fit (Table 3.3) through the least Ne-E affected steps (1-3, 14) and the bulk value (Eugster, 1988) leads to $(^{20}Ne/^{22}Ne)_Q = 10.60 \pm 0.06$ for Chainpur, if $(^{21}Ne/^{22}Ne)_Q = 0.0294$ is adopted. One might object that this value deduced above is only a lower limit for Ne-Q in Chainpur, since steps 1-3 and 14 could contain significant amounts of Ne-E. However, steps 1-3 cluster on the Q-bulk mixing line rather than forming a trend towards Ne-E like steps 4-10. It is unlikely that Ne-E and Ne-Q are released in such similar proportions in several consecutive steps. In addition, $(^{20}Ne/^{22}Ne)_Q$ for Chainpur is in the same range as observed for Allende, Murchison and Grosnaja (Table 3.2). It is therefore reasonable to adopt $(^{20}Ne/^{22}Ne)_Q =$ **10.60 ± 0.06** for Chainpur.
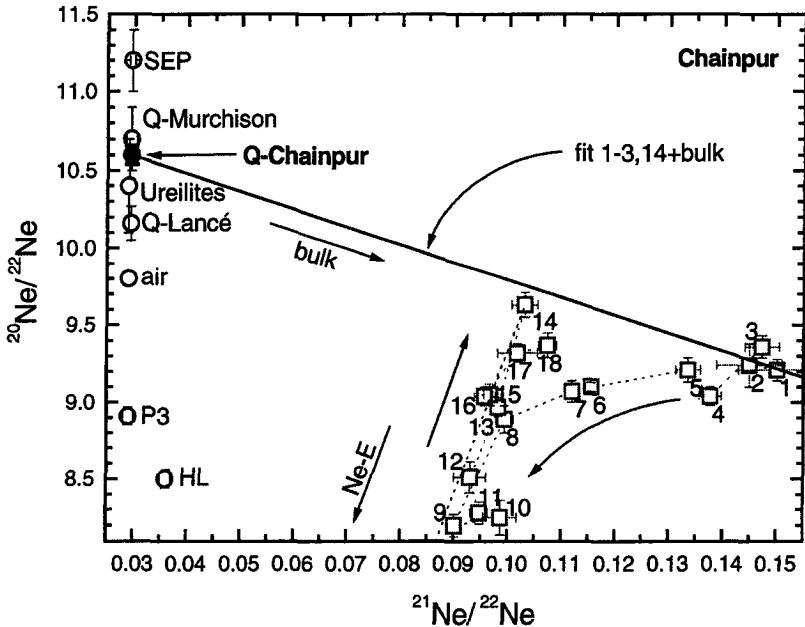
Figure 3.3: Ne from the Chainpur residue shows influences of three components: Cosmogenic Ne, which is released especially in the first steps, Ne-E, affecting only the intermediate steps and Ne-Q. Steps 1-3, 14 and the Chainpur bulk value (Eugster, 1988) are used to determine Ne-Q in Chainpur $(^{20}Ne/^{22}Ne)_Q = 10.60 \pm 0.06$.

Assuming a three-composition mixing with the end members Ne-Q (as deduced above), cosmogenic Ne of typical chondritic composition (Table 3.1) and Ne-E (see chapter 3.1.2), each contribution can be calculated. Ne_{cosm} amounts to no more than 1.3 % of the total ^{20}Ne, but to 74-83 % of the measured ^{21}Ne. Therefore, $(^{21}Ne/^{22}Ne)_Q$ for Chainpur can not be given. The fact

that Ne-E and cosmogenic Ne are not released in constant proportions shows that the carriers of these two components are not the same. While most of the cosmogenic Ne has been removed by the HF/HCl demineralisation, as can be seen e. g. in Figure 3.1, and remaining cosmogenic Ne most likely has been released from incompletely dissolved bulk material, the carrier of Ne-E(L) probably survived the demineralisation procedure completely (chapter 4.5).
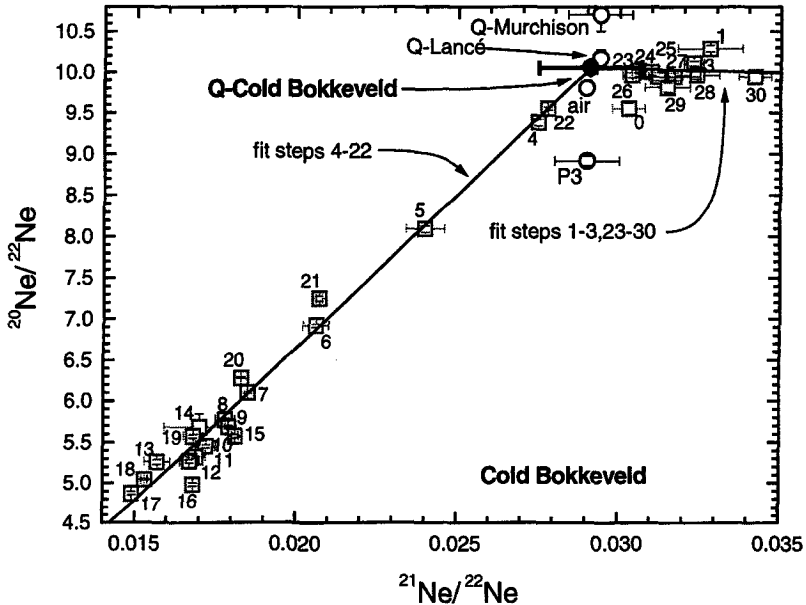
Figure 3.4: Ne released from Cold Bokkeveld consists almost exclusively of two Ne components. Steps 4-22 form a perfect mixing line of presolar Ne-E and Ne-Q. Steps 0-3 and 23-30 are dominated by Ne-Q with minor cosmogenic admixtures.

CM2 Cold Bokkeveld...

A "Ne-E problem" (Ne-E will be discussed separately more detailed in chapter 3.1.2.) has also been encountered upon etching of Cold Bokkeveld (Table 7.33) as can be seen in Figure 3.4: The first steps (0-3) reveal the expected Q-like trapped component. The next steps 4-22, however, form a "textbook mixing line" between Ne-E and Ne-Q. The remaining steps 23-30 seem to be dominated by Ne-Q again, solely affected by cosmogenic Ne. An extrapolation of the Ne-Q/Ne-E data points (steps 4-22) to $^{21}Ne/^{22}Ne = 0.0294$ (assumed to be error-free) leads to $(^{20}Ne/^{22}Ne)_Q = 10.15 \pm 0.32$. This rather large error is easily explained by the steep slope of

this regression line (Table 3.3). A second extrapolation (Table 3.3) of the remaining data points (steps 1-3, 23-30), which are not affected by Ne-E, including the chondritic cosmogenic Ne data point (Table 3.1) provides $(^{20}Ne/^{22}Ne)_Q = 10.05 \pm 0.05$. The weighted mean of both values $(^{20}Ne/^{22}Ne)_Q = \mathbf{10.05 \pm 0.05}$ is adopted for Cold Bokkeveld.

Step 26 displays the lowest $^{21}Ne/^{22}Ne$ ratio (0.0304 ± 0.0003) of those steps (23-30) that are clearly not Ne-E affected. This value is, thus, an *upper limit* for Q in Cold Bokkeveld, and approaches the value deduced from Murchison (0.0294). In contrast, the data point of step 22 lies exactly on the calculated Ne-E to Q mixing line. This implies that cosmogenic Ne does not affect this step. Thus, thanks to its Ne-E component, Cold Bokkeveld offers the unique possibility to determine also a *lower limit* for $(^{21}Ne/^{22}Ne)_Q$ of 0.0278 ± 0.0002 which is the measured value of step 22. Therefore, the ratio $(^{21}Ne/^{22}Ne)_Q$ for Cold Bokkeveld lies in the interval 0.0278 - 0.0304. Another way to determine the isotopic ratios for Ne-Q of Cold Bokkeveld is to calculate the intersection of both regression lines. This gives $(^{20}Ne/^{22}Ne)_Q = 10.05 \pm 0.05$ and $(^{21}Ne/^{22}Ne)_Q = \mathbf{0.0291 \pm 0.0016}$, in perfect agreement with the limits deduced above.

Table 3.4: Isotopic composition of Ne-Q determined in this work.

meteorite	petrographic type	$^{20}Ne/^{22}Ne$	$^{21}Ne/^{22}Ne$
Lancé	CO 3.4	10.17 ± 0.03	$(0.0294)^{[1]}$
Dimmitt	H 3.7	10.6 ± 0.2	$(0.0294)^{[1]}$
Grosnaja	CV 3 ox.	10.66 ± 0.04	$\leq 0.0314 \pm 0.0004$
Chainpur	LL 3.4	10.60 ± 0.06	$(0.0294)^{[1]}$
Cold Bokkeveld	CM 2	10.05 ± 0.05	0.0291 ± 0.0016

[1] from Murchison (Wieler *et al.*, 1992), used for regression.

H3.7 Dimmitt...

The solar-gas-rich chondrite Dimmitt (chapter 2.1.1) demonstrates the impressive capabilities of the CSSE technique to selectively analyse the different Ne components released upon etching. Figure 3.5 shows the complex Ne data released from Dimmitt (Table 7.5). $^{20}Ne/^{22}Ne$ values of steps 1 and 2 are quite high, indicating a mixture of cosmogenic Ne with solar SW/SEP-Ne (Table 3.1) rather than with Ne-Q. The abundant solar wind gases in Dimmitt (Srinivasan, 1977) have been incompletely removed by the demineralisation procedure with HF/HCl. In the next steps, the influence of solar Ne decreases progressively, while Ne-Q dominates increasingly. The data points of steps 6-9 cluster on a mixing line between Q-like and cosmogenic Ne, indicating that they are not compromised by large amounts of solar Ne.

Finally, steps 10 and 11 contain again a Q-poor mixture of cosmogenic and solar Ne. A similar trend can also be observed in the $^3He/^{21}Ne$ vs. $^{22}Ne/^{21}Ne$ plot (Figure 3.8).
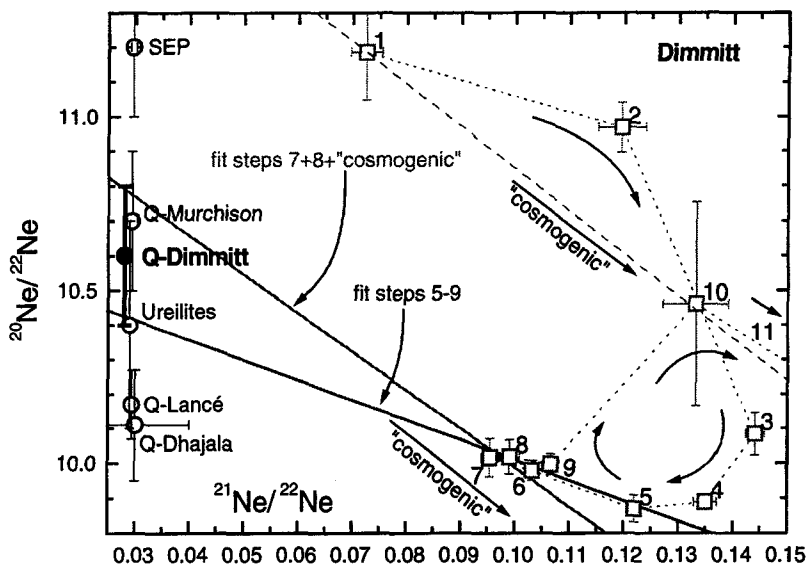
Figure 3.5: Isotopic composition of Ne released from Dimmitt. The first steps are clearly dominated by solar wind Ne (SEP/SW). The next steps are less affected by solar wind Ne and show increasing Ne-Q influences. The mixing line of steps 5-9 provides a lower limit for Ne-Q in Dimmitt, the mixing line of steps 7 and 8 including a cosmogenic value an upper limit. From these limits, $^{20}Ne/^{22}Ne = 10.6 \pm 0.2$ is adopted for Q in Dimmitt. References for Q and other data: See Table 3.2 and Table 3.1.

As in the case of Lancé (see inset of Figure 3.1), the acid demineralisation has successfully removed most of the cosmogenic Ne, since all Ne data points fall much closer to the Q-point than to the bulk-point. Nevertheless, all steps still contain traces of cosmogenic Ne, indicated by the $^{21}Ne/^{22}Ne$ values greater than typical Q-values. A fit through the data of steps 5-9 provides a very conservative lower limit for Ne-Q, since the slope of this fit is too flat to reach the cosmogenic Ne data point. Small admixtures of solar gases still seem to exist in step 5 that dominates the slope of this fit. To set an upper limit, I extrapolate the presumably most Q-like data points, 7 and 8. As cosmogenic end member, I have adopted the standard chondritic value (Table 3.1), since bulk data for Dimmitt (Srinivasan, 1977; Moniot, 1980; Wieler and Signer, 1989) are compromised by solar wind Ne. Assuming $(^{21}Ne/^{22}Ne)_Q$ to be 0.0294, the upper limit is estimated to be 10.78 ± 0.02, the lower one is 10.42 ± 0.14. The regression lines are given in Table 3.3. From these values, $(^{20}Ne/^{22}Ne)_Q = \mathbf{10.6 \pm 0.2}$ is adopted for Dimmitt.

3.1.2 Neon-E

As we have seen above, two of the residues examined in this work, Chainpur (LL3.4) and Cold Bokkeveld (CM2), released considerable amounts of Ne-E during etching (chapter 3.1.1). The same occurred also during the CSSE-experiment on CM2 Murchison (Wieler *et al.*, 1992). While Ne-Q resides in an unknown phase, possibly formed in the solar system, Ne-E originates definitely from grains of presolar origin. In this chapter, I discuss the observations of Ne-E in our experiments.

Ne-E and Phase Q...

These observations question the "operational" definition of phase Q given in chapter 1.1.3. Even mild oxidation with HNO_3 vapour already attacks the carrier of Ne-E (see steps 4-6 of Chainpur in Table 7.24 and steps 4-12 of Cold Bokkeveld in Table 7.33 for etch conditions). Of the two known presolar Ne-E carriers, graphite is more likely to be dissolved by HNO_3 than the more refractory SiC. Therefore, Ne-E observed here most likely is the subcomponent Ne-E(L) (see chapter 1.1.2.4). Both carriers survive the harsh demineralisation procedure, but slow or even complete destruction was observed only on graphite ("C_α") after treatment of HF/HCl-resistant residues with oxidising acids like HNO_3, $Cr_2O_7^-$ and $HClO_4$ (Srinivasan, 1977; Tang *et al.*, 1988; Nichols *et al.*, 1991). According to the "operational" definition of phase Q, the presolar carrier of Ne-E(L), graphite, actually would be a part of phase Q. The definition is thus not reasonable, since graphite grains can be separated and analysed without any hints of Q-gases. Similarly, solar gases released upon CSSE would also be part of the Q-gases (see Dimmitt, chapter 3.1.1). Therefore, it seems reasonable to limit phase Q to be the host phase of the *"planetary"* noble gas component(s) released on etching of HF/HCl-resistant residues of primitive chondrites.

^{22}Ne-E(L) concentrations...

Concentrations of ^{22}Ne-E(L) in meteorites depend on their petrographic types, and thus, on the metamorphic history of the parent bodies (Huss, 1997). I obtained the total amounts of ^{22}Ne-E(L) released from Chainpur and Cold Bokkeveld by CSSE by applying a three-component decomposition of Ne-Q, cosmogenic Ne and Ne-E. The end member isotopic compositions and the revealed ^{22}Ne-E(L) concentrations are given in Table 3.5. The ^{22}Ne-E

contributions amount to 6 % in Chainpur and 30 % in Cold Bokkeveld, respectively, of the released total ^{22}Ne. The concentrations of Ne-E(L) will be compared in chapter 4.5 with results of other meteorites in order to confirm the trend suggested by Huss (1997).

Table 3.5: Ne compositions used to determine Ne-E(L) concentrations.

component	Chainpur (steps 4-18)	Cold Bokkeveld (steps 4-22)
$(^{20}Ne/^{22}Ne)_Q$	10.60	10.05
$(^{20}Ne/^{22}Ne)_{cosm}$	0.85	0.85
$(^{20}Ne/^{22}Ne)_E$	0	0
$(^{21}Ne/^{22}Ne)_Q$	0.0294	0.0291
$(^{21}Ne/^{22}Ne)_{cosm}$	0.92	0.92
$(^{21}Ne/^{22}Ne)_E$	0	0
total ^{22}Ne [10^{-10}cm^3 STP/g residue]	49. 6	567.1
^{22}Ne-E(L) [10^{-10}cm^3 STP/g residue]	3.16	172.1
^{22}Ne-E(L) [10^{-10}cm^3 STP/g meteorite]	**0.15**	**5.12**

Missing Ne-E in Dimmitt...

Here, I discuss why we detected Ne-E with CSSE in some meteorites (CM2 Murchison, LL3.4 Chainpur, CM2 Cold Bokkeveld), while we found no evidence for Ne-E in the H3.7 chondrite Dimmitt (Figure 3.5), even though Ne-E has been released by stepwise pyrolysis of an acid-resistant (HF/H$_2$SO$_4$) residue of Dimmitt (Niederer and Eberhardt, 1977) (hereafter: Dimmitt$_{Bem}$). The most Ne-E-like gas fraction for Dimmitt$_{Bem}$ with $^{20}Ne/^{22}Ne = 1.25$ and $^{21}Ne/^{22}Ne = 0.0016$ was observed at relatively low temperatures of 800 °C (Niederer, 1978). This might indicate Ne-E(L) from graphite (see chapter 1.1.2.4). However, so far, no Ne-E(L) has been clearly identified in meteorites other than CM2, CI and primitive LL-chondrites (e. g. Eberhardt. 1978; Amari et al., 1990a; Huss and Lewis, 1995). This may suggest that Ne-E(H) from SiC was released from Dimmitt$_{Bem}$. This would also explain why no Ne-E was seen in our etch experiment and why the carrier of Ne-E in Dimmitt$_{Bem}$ was not destroyed by preparing the acid resisting residue with HF/H$_2$SO$_4$. Note that the carrier of Ne-E(H), SiC, is even resistant to boiling HClO$_4$ (Tang et al., 1988). If Ne-E(H) from SiC was released, it would question the release temperatures given for Ne-E in general (chapter 1.1.2.4) or for the specific Dimmitt$_{Bem}$ experiment. However, a general shift of the release temperatures for Ne-E seems rather unlikely.

Graphite is recovered from acid-resistant residues by density separation (Huss and Lewis, 1995). During our Dimmitt residue preparation or loading of the sample, graphite might thus unintentionally have been largely lost. However, this seems an unlikely explanation for the missing Ne-E in our experiment, especially, since Chainpur and Cold Bokkeveld did not

undergo such a "selective" treatment, and since graphite grains are fairly large (up to 8μm; chapter 1.1.2.4).
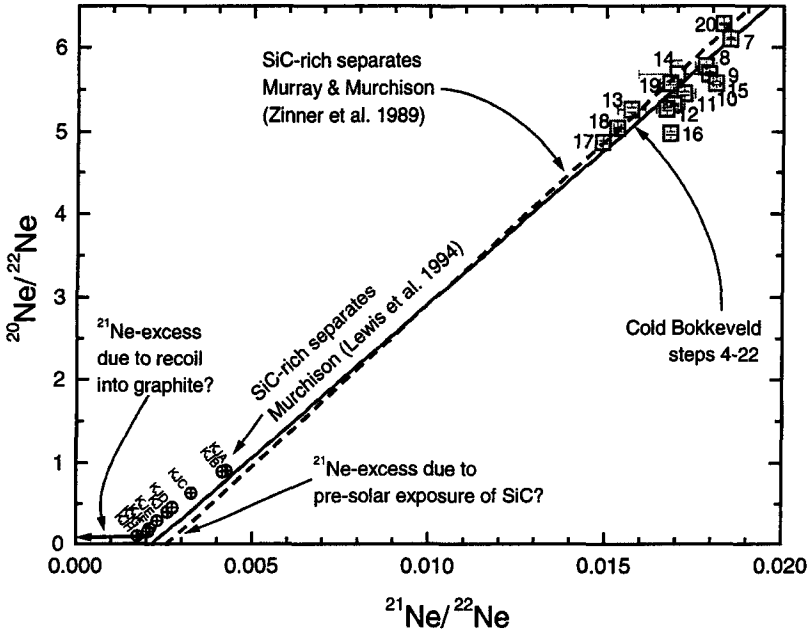
Figure 3.6: The Ne-E(L)/Ne-Q mixing line from steps 4-22 of Cold Bokkeveld (CM2), an extrapolation from SiC-rich separates from CM2 chondrites Murray and Murchison (Zinner *et al.*, 1989) and Murchison (Lewis *et al.*, 1994).

Huss and Lewis (1995) did not find Ne-E in Dimmitt (H3.7), confirming an earlier analysis of Moniot (1980). Their explanation of this result was that Niederer *et al.* had measured graphite, brought in by CI or CM2 xenoliths in the Dimmitt regolith breccia. Indeed, carbonaceous chondritic clasts were found in this meteorite (Rubin *et al.*, 1983). Huss and Lewis (1995) measured a concentration of $(0.011 \pm 0.022) \times 10^{-10} \, cm^3$ STP/g meteorite of Ne-E(L) in the comparable H3.6 chondrite Tieschitz. This is less than 10 % of the amount found in Chainpur. It seems unlikely that such a small amount of Ne-E would have been detectable in the CSSE experiment on Dimmitt (compare Figure 3.5 with Figure 3.3). However, it is also questionable whether comparably small amounts could have been detected by stepwise heating experiments.

In summary, the variable resistance of the two Ne-E carriers strongly suggest that Ne-E(L) from graphite was released during the etch experiments on Chainpur and Cold Bokkeveld, but it

is not entirely clear, why no Ne-E was found in our analysis of Dimmitt. I believe that the answer is to be found in the work of Niederer and Eberhardt (1977; 1978). Most probably, Ne-E in Dimmitt$_{Bern}$ originates from carbonaceous xenoliths and resides in graphite.

^{21}Ne in Ne-E of Cold Bokkeveld...

Figure 3.6 shows again the regression line defined by steps 4-22 of Cold Bokkeveld which contain essentially only Ne-E and Ne-Q (Figure 3.4, Table 3.3). For comparison, a regression line from stepwise heating measurements obtained from *SiC*-rich grain size separates of the CM2 chondrites Murray and Murchison (Zinner *et al.*, 1989) and data points of SiC-enriched separates from Lewis *et al.* (1994) are also shown. The offset of ^{21}Ne/^{22}Ne at the intercept with the x-axis has been explained as due to the presolar exposure of these SiC grains to GCR for 26-58 Ma (Zinner *et al.*, 1989). Lewis *et al.* (1994) calculated a presolar cosmic-ray irradiation of SiC grains from Murchison of at least 13-133 Ma. These nominal ages could even be an order of magnitude larger, since most of the ^{21}Ne resides in only a small fraction of less than 10 % of the SiC grains. Surprisingly, a very similar excess is also observed in Figure 3.6 for Ne-E(L) from graphite in Cold Bokkeveld, although cosmogenic Ne can not be produced from graphite. Therefore, *this* ^{21}Ne either must be an intrinsic part of Ne-E(L) or has been incorporated into graphite by recoil.

Ott and Begemann (1997) determined retention factors of spallation ^{21}Ne in *SiC* by irradiating SiC grains in suspension in paraffin wax. These factors were much smaller than those assumed by Lewis *et al.* (1994). Taking these recoil losses and also the dilution with gas-poor SiC grains into account, Ott *et al.* re-calculated the presolar exposure ages of SiC grains from Lewis *et al.* (1994) and obtained new presolar exposure ages which would even exceed the age of the universe. Therefore, Ott and Begemann (1997) concluded that a determination of presolar exposure ages for SiC from a ^{21}Ne excess is not possible. In view of these results, they suggested to search for an explanation of this "excess" ^{21}Ne within in the SiC source, He-shells of AGB stars, e. g. due to neutron exposure effects. Our data might suggest a similar conclusion for Ne-E(L) from graphite. However, the ^{21}Ne-excess observed in Ne-E(L) from CM2 Cold Bokkeveld is probably not an intrinsic part of Ne-E in graphite, since pure graphite separates from CM2 Murchison, analysed by Amari *et al.* (1995), contain Ne with ^{21}Ne/^{22}Ne ratios <0.0004. Otherwise, ^{21}Ne incorporated into graphite by recoil should be also visible in the pure separates of Amari *et al.* Therefore, this ^{21}Ne excess might be due to cosmogenic Ne in a phase closely related to graphite or phase Q, since the observed nearly perfect mixing line points to a two-component mixing. The cosmogenic Ne might be in-situ produced or recoiled into this

unknown phase. In any case, this requires a rather homogeneous mixing of the $^{21}Ne_{cosm}$ or $^{21}Ne_{recoil}$ residing in this unknown phase and the primordial ^{21}Ne.

It is possible to roughly estimate the amount of ^{21}Ne needed to produce the ^{21}Ne excess in the residue of Cold Bokkeveld, assuming that it consists completely of HF/HCl-resistant phases. The $^{21}Ne_{cosm}$ concentration in the bulk is 7×10^{-10} cm^3 STP/g meteorite (Pedroni, 1993), if one corrects for primordial Ne with $(^{21}Ne/^{20}Ne)_{prim} = 0.0035$. Assuming that for Ne_{recoil} $(^{20}Ne/^{22}Ne)_{cosm} \approx (^{21}Ne/^{22}Ne)_{cosm}$, then some 5 % of the $^{21}Ne_{cosm}$ bulk concentration can cause the ^{21}Ne excess. In conclusion, it is possible that this ^{21}Ne observed in Cold Bokkeveld is due to recoil into a phase closely related to graphite or phase Q and not an intrinsic part of Ne-E(L) from graphite. The $^{21}Ne/^{22}Ne$ ratio of Ne-E in Chainpur can not be determined precisely from the extrapolation of the data points towards $^{20}Ne \approx 0$ because of the scattering of these data points (Figure 3.3).

3.1.3 Helium

Table 3.6: Isotopic composition of He in different reservoirs.

component	^{3}He/^{4}He [10^{-4}]	remarks	source
Q-Allende	1.59 ± 0.04		Wieler et al. (1991)
Q-Murchison	1.53	upper limit	Wieler et al. (1992)
SW	4.56 ± 0.08		Benkert et al. (1993)
SEP	2.17 ± 0.05		Benkert et al. (1993)
He-A	1.35 – 1.55	Q + HL + P3 in "original residues"	e. g. Black (1972b); Eberhardt (1978)
He-A	1.42 ± 0.02[1]	Q + HL + P3	Reynolds et al. (1978)
He-HL	1.70 ± 0.10[2]		Huss and Lewis (1994a)
He-P3	1.35 ± 0.10	upper limit	Huss and Lewis (1994a)
cosmogenic He	≈ 0.2	adopted value from iron meteorites	

[1] Murray, Murchison and Cold Bokkeveld (all CM2), Allende (CV3); [2] probably too high, see text.

Helium consists of only the two isotopes, ^{3}He and ^{4}He, which makes it difficult to distinguish Q and non-Q components. As described in chapter 1, primordial He in phase Q is largely depleted relative to the heavier noble gases and other reservoirs, such as solar abundances (Figure 1.2). Therefore, the contributions from presolar, solar and cosmogenic components can easily affect results for He-Q. Thus, a determination of He-Q with conventional (stepwise) pyrolysis or combustion experiments has not been possible. A major goal of this work is to increase the small number of only two values determined for $(^3$He/^{4}He)$_Q$ previously with CSSE on CV3 Allende and CM2 Murchison (Table 3.6). We will see that we succeeded in determining $(^3$He/^{4}He)$_Q$ ratios for Grosnaja and Cold Bokkeveld. It is evident that

admixtures of cosmogenic or solar He would raise the measured ratios above the Q values, whereas additional radiogenic ^{4}He would lower this ratio. Contributions of cosmogenic He in the analyses of Lancé, Dimmitt and Chainpur (Figure 3.7) were too large to determine He-Q precisely. It is much more difficult to correct for cosmogenic He than for cosmogenic Ne, because He consists of only two stable isotopes. Therefore, it is most important to analyse meteorites with short exposure ages, such as Grosnaja or Cold Bokkeveld ($\leq$ 2 Ma; Table 2.1), to minimise these influences.

The "bulk" trapped "planetary" He-A (e. g. Black, 1972b) is assumed to have a ratio of about 1.42 x 10^{-4} (Table 3.6), but this He "component" is actually a mixture of He-HL and He-P3 from presolar diamonds (Huss and Lewis, 1994a) and He-Q (Table 3.6). Huss and Lewis (1994a) reported a value of (1.70 $\pm$ 0.10) x 10^{-4} for $(^3He/^4He)_{HL}$. This value can not be correct. Assuming that $^{132}Xe_Q/^{132}Xe_{HL}$ = 48, calculated from 17 HF/HCl-resistant residues (Huss and Lewis, 1995), $(^4He/^{132}Xe)_Q$ = 359 (Table 3.14), $(^4He/^{132}Xe)_{HL}$ = 120000 (Huss and Lewis, 1994b) and assuming that P3 and P6 are negligible relative to HL, we can conclude that $^4He_Q/^4He_{HL}$ = 0.14. Thus, $(^3He/^4He)_A$ is mainly composed of $(^3He/^4He)_{HL}$ and, considering the only slightly smaller values for He$_Q$ (see below), the values for He$_A$ and He$_{HL}$ should be rather similar.

CV3 (ox.) Grosnaja...

Figure 3.7 shows the ^{3}He/^{4}He ratios measured in all etch runs. Helium in Grosnaja (Table 7.14) shows extraordinarily constant ^{3}He/^{4}He ratios. This allows us to exclude a possible release of substantial amounts of radiogenic or cosmogenic He in most steps. The data therefore permit us to determine $(^3He/^4He)_Q$ with high precision. The concentration-weighted mean of the He released in steps 8-12, which have the lowest $^{21}Ne/^{22}Ne$ ratios (Figure 3.2), is used to define $(^3He/^4He)_Q$ = (1.45 $\pm$ 0.01) x 10^{-4} for Grosnaja. Only the last two steps (14, 15) are compromised by significant cosmogenic contributions which can also be seen in the increased $^{21}Ne/^{22}Ne$ ratios of these steps (Figure 3.2).

CM2 Cold Bokkeveld...

Cold Bokkeveld (Table 7.33) was exposed to cosmic rays for only some 0.4 Ma (Table 2.1). Therefore, it is the most suitable sample to determine $(^3He/^4He)_Q$ in our series of CSSE

analyses. This run consists of an especially large number, 31, of steps[6] with low and very constant $^3He/^4He$ ratios. Only the last steps (23-30) show somewhat increased values up to $1.70-1.73 \times 10^{-4}$ (steps 27-29). The concentration-weighted mean of He released in steps 4-22 determines $(^3He/^4He)_Q = (1.41 \pm 0.01) \times 10^{-4}$ for Cold Bokkeveld.
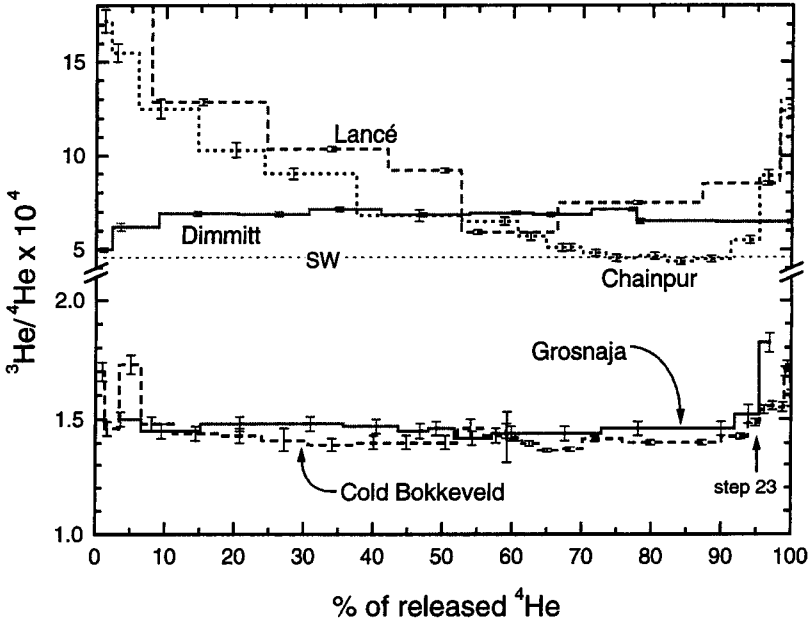
Figure 3.7: $^3He/^4He$ release patterns of all etch runs of this work.

Therefore, one might think that we simply measured the well-known "He-A" instead of a distinct He component released from phase Q, since $(^3He/^4He)_A$ is about 1.42×10^{-4} (Table 3.6). However, the release of He with extraordinarily constant $^3He/^4He$ and the parallel elemental release patterns with e. g. typical Q-like $^4He/^{20}Ne$ ratios observed in all experiments (chapter 3.2) indicate that all five noble gases were clearly released from *one* carrier, phase Q. The $(^3He/^4He)_Q$ ratio determined for Cold Bokkeveld is similar to the value deduced above for the CV3 chondrite Grosnaja but distinct from the values for Allende (CV3) and Murchison (CM2). In view of the new results presented here (Table 3.7), it is likely that the older values for

---

[6] including step "0"; see comment on Table 7.33.

Allende and Murchison, which are based on only 2 or 3 steps, have been slightly compromised by cosmogenic He.

Table 3.7: Isotopic composition of He-Q.

	petrographic type	^{3}He/^{4}He [10^{-4}]	source
Q-Allende	CV3	1.59 ± 0.04	Wieler *et al.* (1991)
Q-Murchison	CM2	< 1.53	Wieler *et al.* (1992)
Q-Grosnaja	CV3	1.45 ± 0.01	this work
Q-Cold Bokkeveld	CM2	1.41 ± 0.01	this work

CO3.4 Lancé...

Lancé, as well as Dimmitt and Chainpur discussed below, have considerably higher exposure ages (Table 2.1) and smaller Q-gas concentrations (chapter 3.3) compared to Grosnaja and Cold Bokkeveld. Due to this the He data of the following analyses are corrupted by cosmogenic He and can not be used to determine $(^3$He/^{4}He$)_Q$. The release pattern of Lancé (Table 7.1) shows considerable contributions of cosmogenic ^{3}He (Figure 3.7): The first steps, which have probably etched easily dissolvable silicate remnants, and the last steps, when He-Q has already been released completely, are most strongly dominated by cosmogenic He. Even the lowest ratio, measured in step 5 (^{3}He/^{4}He = 5.92 x 10^{-4}), is much too high to be pure He-Q: It is even higher than the solar wind values (Table 3.6). Conservatively estimated, cosmogenic ^{4}He amounts to less than 0.5 % of the measured ^{4}He. Therefore, cosmogenic ^{4}He does not need to be further considered for the calculation of elemental ratios and concentrations for Q from Lancé (chapters 3.2 and 3.3).

LL3.4 Chainpur...

Chainpur He (Table 7.24) shows a release pattern very similar to Lancé (Figure 3.7): The first and last steps are especially high certainly due to cosmogenic ^{3}He. The lowest ^{3}He/^{4}He ratios (steps 9-15) are relatively constant which usually might be interpreted to indicate the release of a well-defined component. However, even these ratios are much higher than all known values deduced for Q-gases or presolar components. A solar wind origin (Table 3.6) can also be ruled out, since the Ne-3-isotope-plot (Figure 3.3) provides no hints for a release of SW gases in steps 9-15. Assuming that we did not discover a new component, the remaining explanation is the release of a rather constant mixture of cosmogenic He and He-Q. Surprisingly, ^{3}He/^{4}He *and* ^{21}Ne/^{22}Ne are quite constant for the main steps 8-15, although the spallogenic Ne must have been incorporated, either by recoil or during chemical preparation,

since the carrier of Q is assumed to be carbonaceous. Assuming $(^3He/^4He)_{cosm} = 0.2$ and $^3He_{cosm}$ $\gg$ ^3He_Q yields cosmogenic ^4He fractions of only 0.2-0.9 %. A correction of the ^4He abundances is, thus, not necessary.
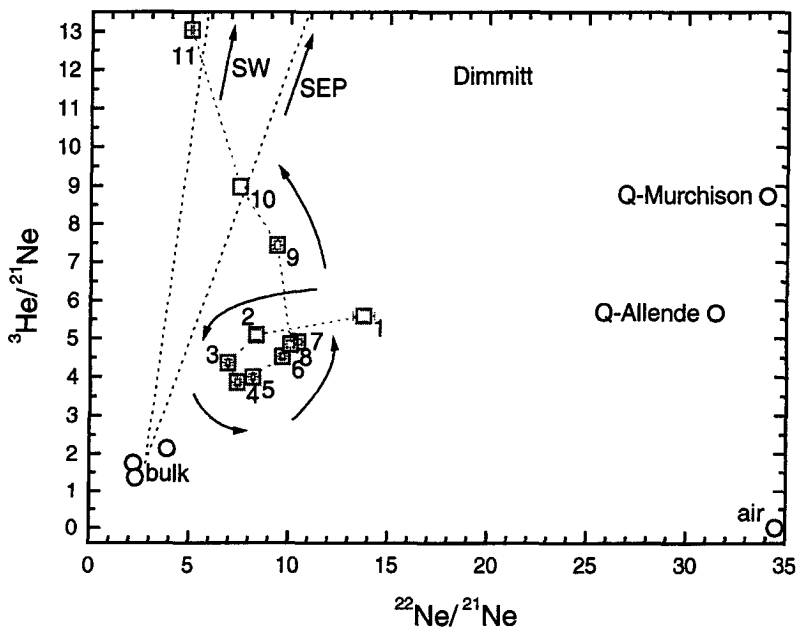
Figure 3.8: $^3He/^{21}Ne$ vs. $^{22}Ne/^{21}Ne$ for Dimmitt. The released gases are a mixture of mainly cosmogenic ("bulk") and Q-gases. The last steps contain larger amounts of solar gas with $(^3He/^{21}Ne)_{SW} = 125$ and $(^3He/^{21}Ne)_{SEP} = 53$. References for bulk data: Srinivasan (1977); Moniot (1980); Wieler and Signer (1989). Solar wind values are calculated from Benkert et al. (1993) with $^4He/^{20}Ne = 650$ (Murer et al., 1997); Q data: Wieler et al. (1991; 1992). See also footnote [7].

H3.7 Dimmitt...

Finally, I want to discuss the data from Dimmitt (Table 7.5). Dimmitt released He with constant, but incomprehensibly high $^3He/^4He$ ratios with a mean $^3He/^4He = (6.85 \pm 0.08) \times 10^{-4}$ in steps 3-11 (Figure 3.7). As with Chainpur, the only reasonable way to explain such high values seems to be by an admixture of cosmogenic He, because all other known reservoirs have lower $^3He/^4He$ ratios (Table 3.6). Assuming $(^3He/^4He)_Q = 1.43 \times 10^{-4}$ and that no cosmogenic and no solar ^4He has been released, 78-80 % of the released ^3He in each step (3-11) is cosmogenic. Thus, the $^3He_Q/^3He_{cosm}$ ratio is surprisingly constant, considering that the ^3He

amounts released per step vary by a factor of 20. Helium is certainly released from the same phase as the other Q-gases as can be seen from the almost parallel release of all noble gases during this run (Figure 3.18).

It may seem surprising that cosmogenic gases were incorporated homogeneously into phase Q by recoil or during the chemical preparation. On the other hand, the $(^3He/^{21}Ne)_{cosm}$ ratios are also very similar in steps 3-8. Since $^{21}Ne_{cosm}$ can not have been produced in situ in the carbonaceous phase Q, this indicates that cosmogenic He could also have been trapped. Assuming a three-component-mixing of Ne-Q, solar wind Ne and cosmogenic Ne, 71-81 % of the measured ^{21}Ne in steps 3-8 is cosmogenic. The $(^3He/^{21}Ne)_{cosm}$ ratios are 3.8-5.5 which is in the expected range for H chondrites (e. g. Eugster, 1988). However, a final solution of the question on the origin of the constant $^3He/^4He$ in steps 3-11 can not be given, since Q-gases have $^3He/^{21}Ne$ ratios in the same range, and "locally" produced gas in SiC grains, which are also abundant in HF/HCl-resistant residues, has also a $^3He/^{21}Ne$ ratio of 7.4 (Reedy, 1989).

Dimmitt is a regolith breccia containing large amounts of solar wind gases (chapter 2.1.1). Actually, the Ne isotopic data (Figure 3.5), the $^3He/^{21}Ne$ vs. $^{22}Ne/^{21}Ne$ plot (Figure 3.8)[7], and the elemental release pattern (Figure 3.18) show that solar wind gases partly survived the demineralisation by HF/HCl and were released in steps 1, 2 and 9-11. In view of these solar contributions, it is even more mysterious, why $^3He/^4He$ is almost constant in steps 3-*11*.

3.1.4 Argon

Ar has three stable isotopes, but ^{40}Ar in phase Q can most probably not be determined, since it will always be dominated by re-trapped radiogenic or adsorbed atmospheric ^{40}Ar. Hence, ^{40}Ar can be used to indicate the degree of atmospheric contamination; steps with the lowest $^{40}Ar/^{36}Ar$ ratios will contain the purest Ar-Q.

On the other hand, ^{36}Ar and ^{38}Ar in Q are usually easier to determine than He-Q and Ne-Q, because Ar-Q is the dominant Ar component in acid-resistant residues (Figure 1.4). Unlike for He and Ne, no problems should arise from other Ar components released simultaneously with Ar-Q. In situ produced cosmogenic ^{36}Ar and ^{38}Ar should be completely negligible, since

---

[7] This $^3He/^{21}Ne$ vs. $^{22}Ne/^{21}Ne$ plot is usually used to show the dependency of $(^3He/^{21}Ne)_{cosm}$ and $(^{22}Ne/^{21}Ne)_{cosm}$ from shielding depths of chondritic bulk samples. Diffusive ^3He losses are recognisable by data points located below a standard correlation line ("Bern-line"; Eberhardt *et al.*, 1966; Nishiizumi *et al.*, 1980). The Bern-line is based on several chondrites and is defined only for typical ratios 1.06 $\leq$ $(^{22}Ne/^{21}Ne)_{cosm} \leq 1.30$.

possible target elements in phase Q are rare (chapters 1.1.1 and 1.1.3). Cosmogenic Ar, incorporated into phase Q by recoil does not compromise the determination of Ar-Q: Assuming $(^{21}Ne/^{38}Ar)_Q = 0.0008$ (Grosnaja and Cold Bokkeveld), a mean chondritic $(^{21}Ne/^{38}Ar)_{cosm} = 6.7$ (Eugster, 1988), and a maximum $^{21}Ne_{cosm}/^{21}Ne_{measured}$ of 87 % (Dimmitt), the maximum contribution of $^{38}Ar_{cosm}$ to the measured ^{38}Ar should not exceed 0.01 %. Furthermore, no other abundant presolar components, comparable to Ne-E, have been found in our samples. This is easy to understand, since P3-Ar is too similar to Ar-Q to be discovered easily (see Table 3.8), and HL-Ar which is isotopically considerably heavier resides in unetchable presolar diamonds (Table 3.8). Therefore, besides atmospheric Ar, the solar wind Ar components SW and SEP are the only sources that might compromise the analysis of Ar-Q (Table 3.8). However, the He and Ne data indicate that solar wind Ar should occur only in Dimmitt.

Table 3.8: Isotopic composition of Ar in different reservoirs.

component	$^{36}Ar/^{38}Ar$	source
Q-Allende	5.29 ± 0.02	Wieler et al. (1991)
Q-Murchison	5.29 ± 0.02	Wieler et al. (1992)
P1 (≡Q)	5.33 ± 0.03	Huss et al. (1996)
air	5.32 ± 0.01	Nier (Nier, 1950a)
SW	5.48 ± 0.05	Benkert et al. (1993)
SEP	4.87 ± 0.05	Benkert et al. (1993)
A	5.3 ± 0.1	Reynolds et al. (1978)
HL	4.41 ± 0.06	Huss and Lewis (1994a)
P3	5.26 ± 0.03	Huss and Lewis (1994a)
cosmogenic (in residues)	0.65 ± 0.05	Alaerts et al. (1979a)

The Ar compositions of several noble gas reservoirs are listed in Table 3.8, in which "P1", as used by Huss et al. (1996), is an synonym for the noble gases of phase Q. As described in chapter 1.1.3, Ar-Q, as well as Kr-Q and Xe-Q, dominates the noble gases in bulk samples of primitive chondrites. Therefore, the composition of Ar-Q can, in contrast to He-Q and Ne-Q, be deduced also with conventional stepwise heating experiments (Huss et al., 1996).

CO3.4 Lancé...

Figure 3.9 shows data obtained for Lancé (Table 7.1). $(^{36}Ar/^{38}Ar)_Q$ is determined with steps 5-7, because these steps show the lowest $^{40}Ar/^{36}Ar$ ratios (< 2.2) and also the lowest admixture of cosmogenic Ar, as indicated by the low $^{21}Ne/^{22}Ne$ ratios (see Figure 3.1). The concentration-weighted mean gives $(^{36}Ar/^{38}Ar)_Q = \mathbf{5.34 \pm 0.04}$ for Lancé.
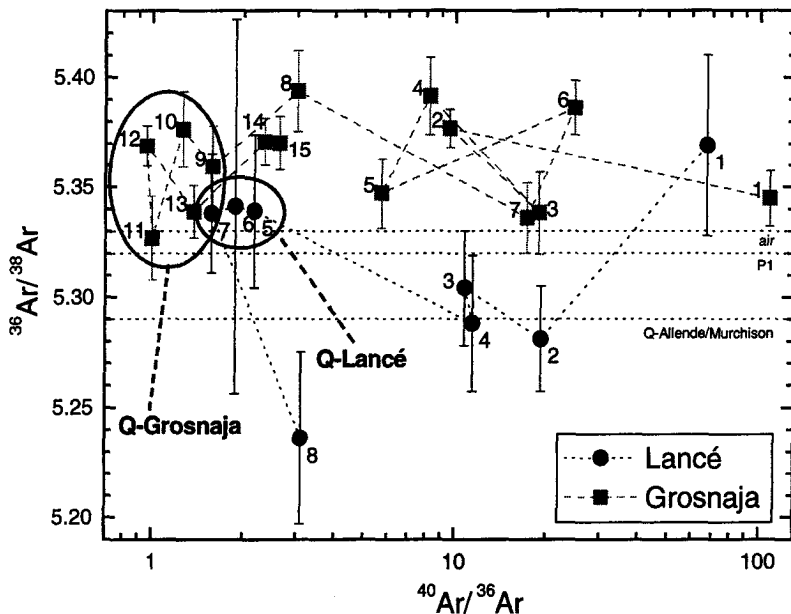
Figure 3.9: This 3-isotope-plot shows Ar released during etching of Lancé and Grosnaja. The steps with the lowest contributions of cosmogenic, radiogenic and atmospheric Ar (Lancé: 5-7; Grosnaja: 9-13) are used to determine Ar-Q. References are given in Table 3.8.

CV3 (ox.) Grosnaja...

Huge amounts of Ar-Q were also released from the acid-resistant residue of Grosnaja (Table 7.14). Therefore, small splits of 2-19 % were separately re-measured on the multiplier after a first analysis on the Faraday cup. The concentration-weighted mean of Ar released from steps 9-13 with the lowest $^{40}Ar/^{36}Ar$ ratios (< 1.31) are used to calculate $(^{36}Ar/^{38}Ar)_Q = 5.36 \pm 0.01$ for Grosnaja (Figure 3.9). The choice of data points is not critical, since the mean value of 5.37 ± 0.01 for all steps is identical to the adopted value within the error limits.

LL3.4 Chainpur...

A quite similar Ar release pattern was also be observed for Chainpur (Table 7.24; data are not shown here). Similar to Grosnaja, separated gas splits of 1-7 % were measured on the multiplier. The mean of steps 5, 6 and 14 with the lowest $^{40}Ar/^{36}Ar$ ratios determines

$(^{36}Ar/^{38}Ar)_Q = 5.37 \pm 0.01$ which does not differ from the mean of all steps, indicating the uniformity of the Ar released from Chainpur.
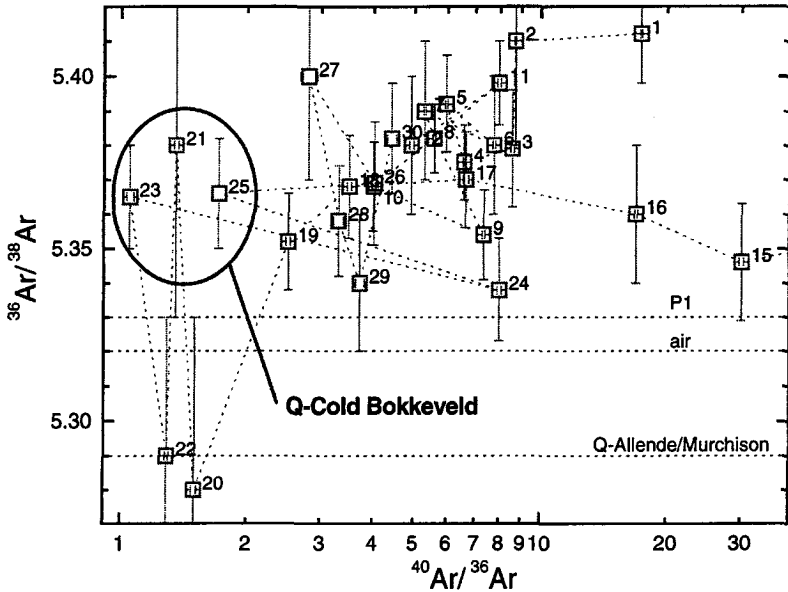
Figure 3.10: Ar data points of the 30 steps of Cold Bokkeveld are shown in this plot. Steps 21, 23, and 25 determine $^{36}Ar/^{38}Ar$. Steps 20 and 22 are too low and, thus, excluded, see footnote [8].

CM2 Cold Bokkeveld...

Figure 3.10 displays the release pattern of Cold Bokkeveld (Table 7.33). We adopt the weighted mean of steps 21, 23 and 25 which are the three steps with the lowest $^{40}Ar/^{36}Ar$ ratios (<1.9). This yields $(^{36}Ar/^{38}Ar)_Q = 5.37 \pm 0.04$. Again, this value is essentially identical to the mean for all steps (excluding rejected steps 20 and 22[8]) of $^{36}Ar/^{38}Ar = 5.36 \pm 0.01$.

---

[8] The non-diluted steps 20 and 22, measured prior to the main measurement with the less precise Faraday cup, do not show significant differences from the deduced value for Ar-Q ($^{36}Ar/^{38}Ar = 5.35 \pm 0.03$ and 5.36 ± 0.03 respectively). This suggests that the low ratios of the diluted steps 20 and 22 are the result of fractionating losses due to incompletely closed valves.

H3.7 Dimmitt...

Ar released from Dimmitt (Table 7.5) was almost exclusively measured with the Faraday cup, not being aware at this time of the broad peak of scattered ^{36}Ar which interferes with ^{38}Ar and its baseline measurement (chapter 2.3.5). Therefore, unfortunately, no dilution was applied, and no reliable $(^{36}Ar/^{38}Ar)_Q$ value can be given for Dimmitt.

The new values for Ar-Q are summarised in Table 3.9. Remarkably, $(^{36}Ar/^{38}Ar)_Q$ of Lancé, Grosnaja, Chainpur, and Cold Bokkeveld are identical within the error limits and slightly higher than older values for Ar-Q determined by CSSE (Wieler *et al.*, 1991; 1992) as well as by stepwise heating measurements on HF/HCl-resistant residues of 14 chondrites ("P1"; Huss *et al.*, 1996). However, Huss *et al.* pointed out that their value probably has an asymmetric uncertainty, with a lower value being unlikely, but a higher value being a distinct possibility. The differences of at most 1.5 % can not be explained with cosmogenic contributions, as outlined above. The lowest measured $^{40}Ar/^{36}Ar$ values determined for each sample are also given in Table 3.9. However, these data are only a measure of contamination by atmospheric or radiogenic Ar and certainly do not reflect the correct primordial ^{40}Ar concentrations.

Table 3.9: Isotopic composition of Ar-Q[1].

	$(^{36}Ar/^{38}Ar)_Q$	$(^{40}Ar/^{36}Ar)_{upper\ limit}$	source
Lancé	5.34 ± 0.04	1.570 ± 0.007	this work
Grosnaja	5.36 ± 0.01	0.90 ± 0.02	this work
Chainpur	5.37 ± 0.01	3.182 ± 0.012	this work
Cold Bokkeveld	5.37 ± 0.04	1.05 ± 0.02	this work
Allende	*5.29 ± 0.02*		*Wieler et al. (1991)*
Murchison	*5.29 ± 0.02*		*Wieler et al. (1992)*
P1(≡Q)	*5.33 ± 0.03*		*Huss et al. (1996)*

[1] As described in detail in chapter 2.3.5, interference corrupted the measurement of Dimmitt with the Faraday cup. Therefore, the results obtained by this etch run are rejected.

3.1.5 Xenon

Due to its large number of nine stable isotopes, Xe is especially suitable to resolve distinct simultaneously released components. Xe-Q is, in general, easy to determine, since this component dominates, similar to Ar-Q and Kr-Q, the noble gases in HF/HCl-resistant residues as well as in bulk primitive meteorites. Indeed, for most isotopes, the determination of Xe-Q in our five acid-resistant residues is straightforward and confirms the results of older examinations (Table 3.10). The isotopic composition of Kr and Xe in chondrites is generally quite uniform,

and the mean values from bulk samples of carbonaceous chondrites are known by the acronym AVCC (chapter 1.1.3; Eugster *et al.*, 1967b). However, these are not "true" components, due to admixtures of presolar components (chapter 1.1.2.4). In particular, AVCC is not identical to Q; only the latter should be regarded as "component" in a more fundamental sense.

Table 3.10: Isotopic composition of Xe in different reservoirs ($^{132}Xe \equiv 100$). For references, see second part of this table.

component	$^{124}Xe/^{132}Xe$	$^{126}Xe/^{132}Xe$	$^{128}Xe/^{132}Xe$	$^{129}Xe/^{132}Xe$	$^{130}Xe/^{132}Xe$
Q-Allende	0.465 ± 0.003	0.406 ± 0.003	8.26 ± 0.04	≤ 107	16.27 ± 0.06
Q-Murchison	0.459 ± 0.006	0.409 ± 0.004	8.26 ± 0.03	103.6 ± 0.5	16.22 ± 0.08
P1≡Q[1]	0.462 ± 0.006	0.410 ± 0.005	8.30 ± 0.03	104.0 ± 0.2	16.28 ± 0.04
P3[1]	0.446 ± 0.006	0.400 ± 0.004	8.06 ± 0.02	104.2 ± 0.4	15.89 ± 0.02
HL[1]	0.833 ± 0.009	0.564 ± 0.008	9.05 ± 0.06	105.6 ± 0.2	15.42 ± 0.03
Xe-s	..	..	24 ± 2	2 ± 6	53 ± 3
U-Xe	0.4873	0.4201	8.412	104.0	16.535
air	0.354 ± 0.001	0.330 ± 0.002	7.14 ± 0.09	98.32 ± 0.1	15.14 ± 0.01
AVCC-Xe[1]	0.454 ± 0.010	0.406 ± 0.004	8.20 ± 0.04	..	16.06 ± 0.11

[1] re-calculated according to atmospheric composition (Basford *et al.*, 1973), see chapter 7.8.3.

Table 3.10: Isotopic composition of Xe in different reservoirs ($^{132}Xe \equiv 100$).

component	$^{131}Xe/^{132}Xe$	$^{134}Xe/^{132}Xe$	$^{136}Xe/^{132}Xe$	source
Q-Allende	82.1 ± 0.4	38.07 ± 0.10	31.84 ± 0.11	Wieler *et al.* (1991)
Q-Murchison	81.9 ± 0.3	37.99 ± 0.14	31.77 ± 0.15	Wieler *et al.* (1992)
P1≡Q[1]	82.30 ± 0.12	37.77 ± 0.11	31.61 ± 0.10	Huss *et al.* (1996)
P3[1]	82.47 ± 0.10	37.67 ± 0.10	30.96	Huss and Lewis (1994a)
HL[1]	84.57 ± 0.13	63.56 ± 0.13	69.91	Huss and Lewis (1994a)
Xe-s	12 ± 5	-2 ± 3	≡ 0	Ott *et al.* (1988)
U-Xe	82.60	35.20	27.50	Pepin and Phinney (1978)
air	78.90 ± 0.11	38.79 ± 0.06	32.94 ± 0.04	Basford *et al.* (1973)
AVCC-Xe[1]	81.8 ± 0.3	38.2 ± 0.2	32.1 ± 0.2	Eugster *et al.* (1967b)

[1] re-calculated according to atmospheric composition (Basford *et al.*, 1973), see chapter 7.8.3.

Of all possible additional Xe components, only two have to be taken into consideration in this work: Radiogenic ^{129}Xe and adsorbed atmospheric Xe. Radiogenic ^{129}Xe in HF/HCl-resistant residues is recognisable by $^{129}Xe/^{132}Xe$ ratios which decrease with increasing etch step numbers (Figure 3.11). Probably, $^{129}Xe_{rad}$ has been incorporated into phase Q by recoil after the decay of ^{129}I within the matrix. Matrix-related excess-$^{129}Xe_{rad}$ can also be re-trapped during *demineralisation, simultaneously with the adsorption of atmospheric Xe*. As described in chapter 1.1.2.5, possible adsorption of terrestrial atmospheric noble gases and gases dissolved in the acid (chapter 2.2.1) especially concern the heavier elements. Fortunately, first steps with significant portions of air can be easily recognised in 3-isotope-plots of Xe from low, air-like $^{124, 126, 128}Xe/^{132}Xe$ ratios (Figure 3.12 and Figure 3.13), and by high Kr/Xe ratios. These steps are excluded from the determination of Xe-Q.
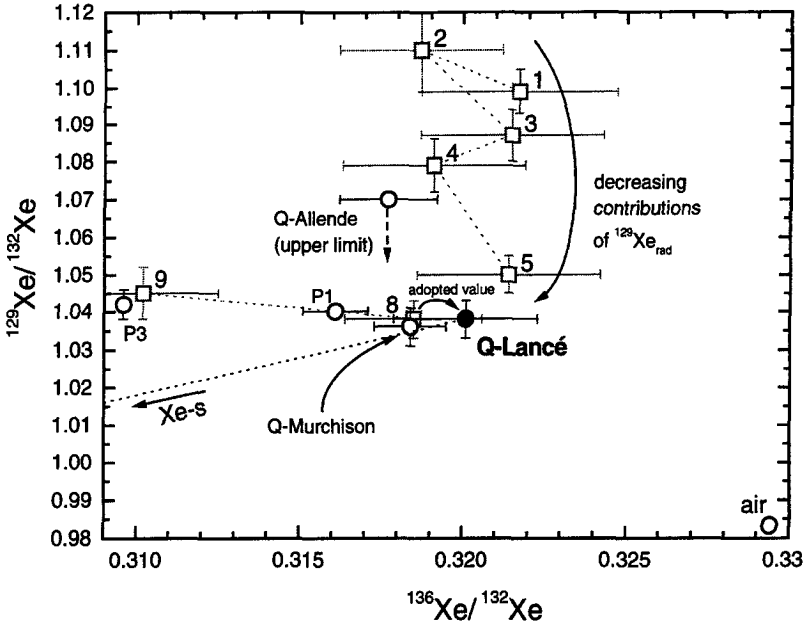
Figure 3.11: The 3-isotope plot $^{129}Xe/^{132}Xe$ vs. $^{136}Xe/^{132}Xe$ for Lancé shows the decreasing influence of re-trapped $^{129}Xe_{rad}$ which is simultaneously released. The lowest value (step 8) is adopted as the pure Q-value. See **Table 3.10** for references.

No hints of presolar Xe-HL, affecting the light (^{124}Xe, ^{126}Xe) and the heavy isotopes (^{134}Xe or ^{136}Xe), have been found. Similar to Ar, no cosmogenic (chapter 1.1.1.1) or solar (chapter 1.1.2.2) admixtures should affect the measurements, since for most steps these components are insignificantly small, relative to Q-gases in carbonaceous residues. Xe_{cosm}, incorporated into phase Q by recoil should not significantly compromise the determination of Xe-Q: Assuming $(^{21}Ne/^{126}Xe)_Q = 3.2$ (from Grosnaja and Cold Bokkeveld), a mean chondritic $(^{21}Ne/^{126}Xe)_{cosm} = 4.6 \times 10^5$ (Eugster, 1988), and a maximum $^{21}Ne_{cosm}/^{21}Ne_{measured}$ of 87 % (Dimmitt), the maximum contribution of $^{126}Xe_{cosm}$ to the measured ^{126}Xe should never exceed 0.001 %. Such low contributions are certainly not observable. In view of $(^{132}Xe/^4He)_{sw} \approx 2 \times 10^{-9}$ (Wieler and Baur, 1995; Murer et al., 1997), it is clear that SW Xe can not be observed, not even in the most SW-like step of Dimmitt with $^4He_{sw}/^4He_{measured} = 88$ % and $(^4He/^{132}Xe)_Q = 155$. No indication of fissiogenic Xe (chapter 1.1.1.2) can be found in any of the $^{134}Xe/^{132}Xe$ vs. $^{136}Xe/^{132}Xe$ plots. These ratios are most indicative, since fissiogenic Xe consists of the heavy isotopes $^{131-136}Xe$.

Table 3.10 lists the isotopic compositions of several Xe components that can be found in meteorites.
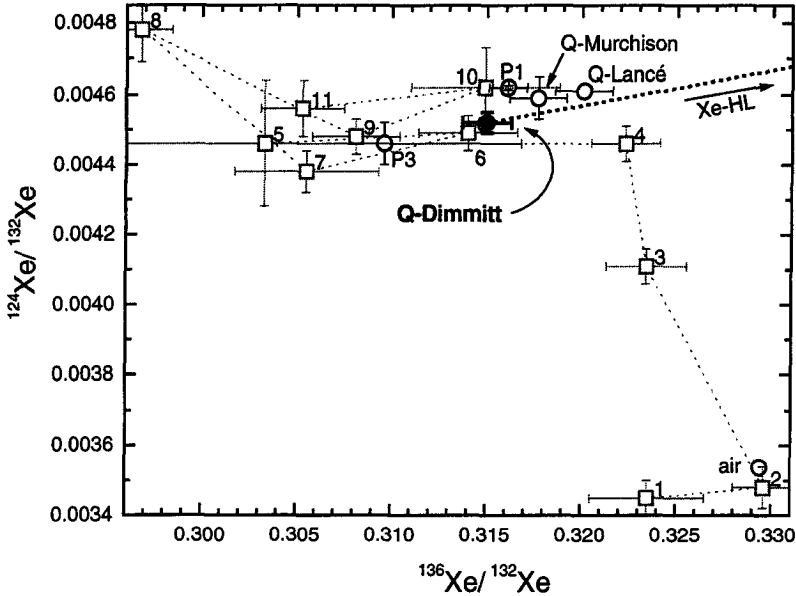
Figure 3.12: This plot displays the influence of atmospheric Xe on the first 3 steps of the experiment on Dimmitt. Therefore, these steps are not considered to determine Xe-Q. Step 8 differs from the other steps and is not used to determine $^{124}Xe/^{132}Xe$ and $^{136}Xe/^{132}Xe$. The data show no evidence for the release of Xe-HL. References are given in Table 3.10.

CO3.4 Lancé...

Only minor problems arose during the measurements of Xe-Q in Lancé (Table 7.4). I used steps 2-5 and 8 for the determination of Xe-Q. Step 1 was slightly air-affected (evident by low $^{124}Xe/^{132}Xe = 0.0042$, $^{126}Xe/^{132}Xe = 0.0037$ and high $^{84}Kr/^{132}Xe = 1.98$), step 9 contained hardly any gas and steps 6 and 7 contained too much gas to measure the most abundant isotopes ^{129}Xe and ^{132}Xe with the multiplier. Figure 3.11 shows the $^{129}Xe/^{132}Xe$ and $^{136}Xe/^{132}Xe$ ratios for Lancé. A trend of decreasing contributions of radiogenic ^{129}Xe with step number is evident. The lowest value (step 8) gives an upper limit for Xe-Q in Lancé. However, since this value of $^{129}Xe/^{132}Xe = 1.038 \pm 0.005$ is in agreement with data for P1 $\equiv$ Q (Huss *et al.*, 1996) and Q in Murchison (Wieler *et al.*, 1992) and since step 9 displays a similar value, I think that no significant admixtures of $^{129}Xe_{rad}$, re-trapped from the bulk during demineralisation, has

compromised this value. Therefore, this value is adopted as pure Xe-Q. All results for Xe-Q in Lancé are listed in Table 3.11.
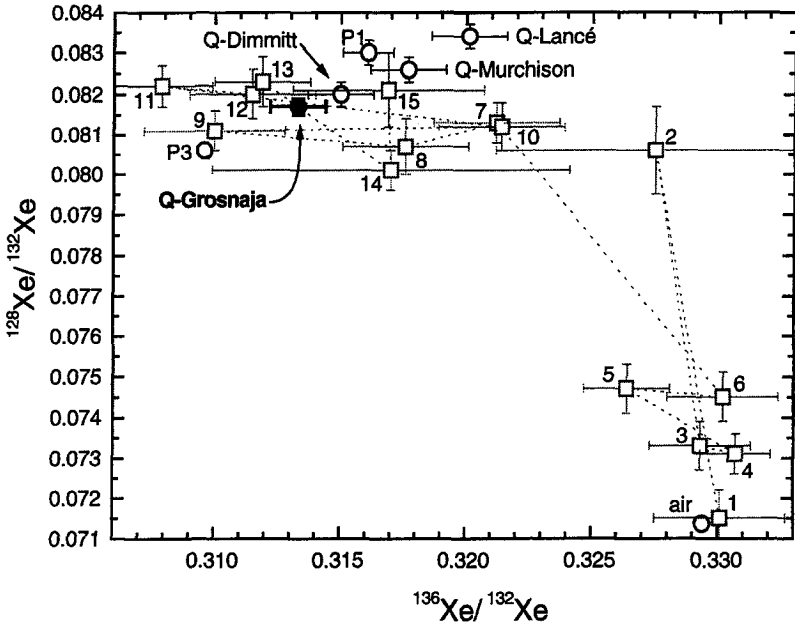
Figure 3.13: This figure plots the ratios $^{128}Xe/^{132}Xe$ and $^{136}Xe/^{132}Xe$ released from Grosnaja. The first 6 steps, except step 2, consist of almost pure atmospheric Xe. The following steps 7-15 show typical Q-composition. References are listed in Table 3.10.

H3.7 Dimmitt...

Xe from Dimmitt (Table 7.11) shows significant admixtures of adsorbed or re-trapped atmospheric Xe. The first 3 steps consist of almost pure terrestrial Xe is evident from all Xe isotopic ratios but especially from $^{124}Xe/^{132}Xe$ (Figure 3.12). Besides steps 1-3, I also discard step 5, because of its large errors which are the result of large amounts of reactive gases in the mass spectrometer and subsequent difficulties to extrapolate the measured data. The average value of the remaining steps 4 and 6-11 has been used to determine the $(^{129}Xe/^{132}Xe)_Q$ ratio, since the ratio $^{129}Xe/^{132}Xe$ is almost constant (between 104.3 and 106).

CV3 (ox.) Grosnaja...

Xe released from Grosnaja (Table 7.21) has a bimodal release pattern (Figure 3.13). While the first 6 steps are dominated by atmospheric contributions, all other steps are quite uniform and, hence, determine Xe-Q in Grosnaja well. The terrestrial gases originate from the acid. One piece of evidence for this is that the acid was distilled on the sample after step 6. Concurrently, the acid was degassed completely. Furthermore, step 2 is Q-dominated and not atmospheric, and in this step, valve "G2", which separates sample and acid volumes, remained closed during etching. The weighted mean of all other steps (7-15) has been used as Xe-Q for Grosnaja, shown in Table 3.11, to take into account the statistical spread of some of the isotopic ratios. The $^{129}Xe/^{132}Xe$ ratios of steps 7-15 lie between 102.2 and 106.3. Therefore, radiogenic ^{129}Xe can not be very abundant and this ratio was calculated from the weighted average of steps 7-15.

Table 3.11: Isotopic composition of Xe-Q determined with CSSE ($^{132}Xe \equiv 100$).

	steps	$^{124}Xe/^{132}Xe$	$^{126}Xe/^{132}Xe$	$^{128}Xe/^{132}Xe$
Lancé	2-5, 8	0.461 ± 0.002	0.406 ± 0.002	8.34 ± 0.03
Dimmitt	4, 6-11[1]	0.452 ± 0.003	0.411 ± 0.002	8.20 ± 0.03
Grosnaja	7-15	0.454 ± 0.002	0.407 ± 0.002	8.17 ± 0.02
Chainpur	3-6, 9-12, 14, 15, 17, 18[2]	0.451 ± 0.002	0.408 ± 0.002	8.18 ± 0.02
Cold Bokkeveld	4-12, 15-30	0.443 ± 0.001	0.394 ± 0.001	8.19 ± 0.02
Allende[3]		*0.465 ± 0.003*	*0.406 ± 0.003*	*8.26 ± 0.04*
Murchison[4]		*0.459 ± 0.006*	*0.409 ± 0.004*	*8.26 ± 0.03*

[1] without step 8 for $^{124}Xe/^{132}Xe$ and $^{136}Xe/^{132}Xe$; [2] without steps 3-6 for $^{126}Xe/^{132}Xe$ and step 3 for $^{128}Xe/^{132}Xe$ and $^{129}Xe/^{132}Xe$; [3] Wieler *et al.* (1991); [4] Wieler *et al.* (1992).

Table 3.11: Isotopic composition of Xe-Q determined with CSSE ($^{132}Xe \equiv 100$).

	$^{129}Xe/^{132}Xe$	$^{130}Xe/^{132}Xe$	$^{131}Xe/^{132}Xe$	$^{134}Xe/^{132}Xe$	$^{136}Xe/^{132}Xe$
Lancé	103.8 ± 0.5	16.40 ± 0.06	82.3 ± 0.3	38.32 ± 0.13	32.01 ± 0.15
Dimmitt	104.7 ± 0.4	16.16 ± 0.05	81.6 ± 0.3	37.73 ± 0.14	31.50 ± 0.13
Grosnaja	104.3 ± 0.2	16.15 ± 0.04	81.5 ± 0.2	37.59 ± 0.11	31.33 ± 0.11
Chainpur	104.5 ± 0.3	16.11 ± 0.04	82.0 ± 0.2	37.58 ± 0.12	31.73 ± 0.08
Cold Bokkeveld	103.9 ± 0.2	16.11 ± 0.03	81.8 ± 0.2	37.39 ± 0.08	31.47 ± 0.07
Allende	*107[5]*	*16.27 ± 0.06*	*82.1 ± 0.4*	*38.07 ± 0.10*	*31.84 ± 0.11*
Murchison	*103.6 ± 0.5*	*16.22 ± 0.08*	*81.9 ± 0.3*	*37.99 ± 0.14*	*31.77 ± 0.15*

[5] upper limit.

LL3.4 Chainpur...

The measurement of Xe in Chainpur (Table 7.30) was corrupted by large amounts of reactive gases which prevented that steps 7, 8, 13 and 16 could be measured. Steps 1 and 2 in general contain atmospheric admixtures and were excluded from the determination of Xe-Q.

Step 19 contains no significant amount of gas. The steps 3-18 lead to the composition of Xe-Q in Chainpur. The results for Xe-Q in Chainpur can be found in Table 3.11.

The portion of simultaneously released Xe-s can be calculated, assuming that the carrier of Ne-E is SiC and ^{22}Ne(H)/^{132}Xe-s = 1665 (SiC-rich sample "KJ"; Lewis *et al.*, 1994). The highest ^{132}Xe-s contribution (step 10) would then not exceed 0.01 % is within the typical errors and thus would be undetectable.
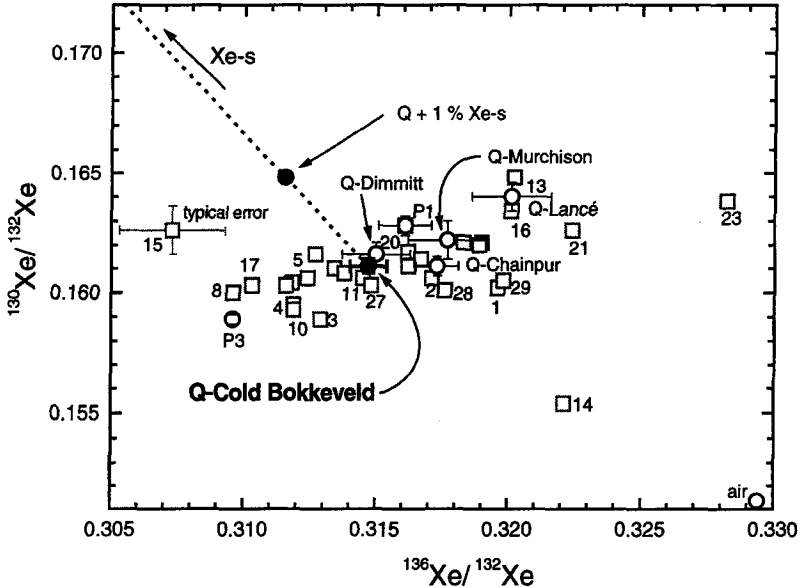
Figure 3.14: The possible release of Xe-s would lead to a contribution of at most 0.04 % of Xe-s (step 20) in the case where the related Ne-E (chapter 3.1.2) originates from SiC. The calculated mixture of Xe-Q (Table 3.11) and 1 % Xe-s (Table 3.10) would lead to the data point shown in the figure. Thus, possible admixtures of Xe-s can not be resolved. For references, see Table 3.10.

CM2 Cold Bokkeveld...

Finally, I present the Xe data of Cold Bokkeveld (Table 7.39). Step 13 was not measured due to problems with reactive gases, step 14 shows air admixtures (indicated by low ^{126}Xe/^{132}Xe = 0.00389 and ^{128}Xe/^{132}Xe = 0.0811), and the remaining steps are summed up to deduce Xe-Q for Cold Bokkeveld (Table 3.11). A possible release of Xe-s can be estimated similar to Chainpur. At most 0.036 % (step 20) of Xe-s would contribute to the measured Xe amounts,

assuming that SiC is the origin of released Ne-E (chapter 3.1.2) and ^{22}Ne(H)/^{132}Xe-s = 1665 (SiC-rich sample "KJ"; Lewis et al., 1994). From the data in Table 3.10 and Table 3.11, resulting Xe-Q-s mixing ratios can be calculated. However, these small admixtures of Xe-s are not resolvable within the typical uncertainties (Figure 3.14).

3.1.6 Krypton

As for $^{36,\,38}$Ar and Xe, Kr abundances in primitive chondrites are dominated by primordial gases from phase Q. Hence, bulk measurements of these meteorites normally represent a fairly good approximation to Q-gases. However, Kr-Q is not *identical* to these gases, as described above (chapter 3.1.5). Due to their low abundances, cosmogenic and solar Kr do not influence Q measurements in carbonaceous acid-resistant residues and are, therefore, not given in Table 3.12 which lists all relevant Kr-reservoirs. The assumptions of an incorporation of ^{80}Kr$_{cosm}$ due to recoil, similar to ^{21}Ne with $(^{21}$Ne/^{80}Kr$)_Q$ = 0.5 and $(^{21}$Ne/^{80}Xe$)_{cosm}$ = 5.4 x 10^4 (Alexander *et al.*, 1971; Eugster, 1988), reveals a limit of 0.001 % ^{80}Kr$_{cosm}$ for steps with maximum contributions of ^{21}Ne$_{cosm}$ of 87 %. Therefore, contributions of Kr$_{cosm}$ are not recognisable. Since $(^{84}$Kr/^{4}He$)_{solar}$ ≈ 1.8 x 10^{-8} (Wieler and Baur, 1995; Murer *et al.*, 1997), it is, similar to Xe, impossible to observe SW-Kr. No hints of presolar Kr-HL or Kr-s can be found in any of our samples, not even in the Ne-E-bearing Chainpur and Cold Bokkeveld (chapter 3.1.2). Kr-Q and atmospheric Kr are rather similar and, therefore, not easy to resolve from one another (Table 3.12).

Table 3.12: Isotopic composition of Kr in different reservoirs (^{84}Kr ≡ 100).

component	^{78}Kr/^{84}Kr	^{80}Kr/^{84}Kr	^{82}Kr/^{84}Kr	^{83}Kr/^{84}Kr	^{86}Kr/^{84}Kr
Q-Allende[1]	0.621 ± 0.007	3.952 ± 0.016	20.15 ± 0.10	20.17 ± 0.09	30.99 ± 0.12
Q-Murchison[2]	0.611 ± 0.007	3.928 ± 0.011	20.13 ± 0.05	20.19 ± 0.04	31.03 ± 0.04
P1[3][4]	0.66 ± 0.06	3.965 ± 0.033	20.24 ± 0.03	20.21 ± 0.05	30.91 ± 0.09
P3[4][5]	0.64 ± 0.10	3.95 ± 0.04	20.23	20.32 ± 0.05	31.28 ± 0.06
HL[4][5]	0.42 ± 0.10	3.05 ± 0.10	15.90	19.89 ± 0.10	36.23 ± 0.18
Kr-s[6]		3.1 ± 3.5	34.8 ± 0.7	12.1 ± 1.8	40.9 ± 23.0
air[7]	0.609 ± 0.002	3.960 ± 0.002	20.217 ± 0.004	20.14 ± 0.02	30.52 ± 0.03
AVCC-Kr[4][8]	0.588 ± 0.005	3.87 ± 0.03	19.87 ± 0.10	19.86 ± 0.10	30.52 ± 0.11

[1] Wieler *et al.* (1991); [2] Wieler *et al.* (1992); [3] Huss *et al.* (1996); [4] re-calculated according to atmospheric composition (Basford *et al.*, 1973), see chapter 7.8.3; [5] Huss and Lewis (1994a); [6] ^{80}Kr-s and ^{86}Kr-s are highly variable, since they were affected by branching in the s-process, according to different stellar neutron environments (Ott *et al.*, 1988; Lewis *et al.*, 1994). The calculated values are averages of measured temperature steps (Ott *et al.*, 1988). The errors cover the lowest and highest values; [7] Basford *et al.* (1973); [8] Eugster *et al.* (1967b).

Due to the large number of Kr isotopes, only some of the results of this work are discussed in detail. Since the composition of Kr-Q and Xe-Q is very well known (Wieler *et al.*, 1991; 1992; Huss *et al.*, 1996), the Kr and Xe data presented here should serve mainly as a consistency check which finally further confirms the hypothesis of a uniform Q component in all meteorites. As shown in Table 3.12 and Table 3.13, our results agree well with existing data. Only the ^{78}Kr/^{84}Kr ratio deserves some further attention, since ^{78}Kr is influenced in many measurements by interfering benzene. The new spectrometer used here resolves this interference (chapter 2.3.1). All isotopic ratios of Q are deduced by the concentration-weighted mean of several steps to take into account the large differences in the amounts of released gas.

CO3.4 Lancé...

For the determination of Kr-Q in Lancé, steps 2-8 were used (Table 7.3). Step 1 shows some atmospheric admixtures (chapter 3.1.5), and both steps 1 and 9 released only small amounts of gas (< 2% of the total ^{84}Kr). The results deduced for Q-Lancé are presented in Table 3.13.

Table 3.13: Isotopic composition of Kr-Q determined in this work. ^{84}Kr ≡ 100.

	steps	^{78}Kr/^{84}Kr	^{80}Kr/^{84}Kr	^{82}Kr/^{84}Kr	^{83}Kr/^{84}Kr	^{86}Kr/^{84}Kr
Lancé	2-8	0.595 ± 0.003	3.939 ± 0.013	20.26 ± 0.05	20.32 ± 0.06	31.22 ± 0.08
Dimmitt	4-11	>0.59 ± 0.04[1]	3.923 ± 0.008	20.24 ± 0.04	20.19 ± 0.04	30.96 ± 0.06[2]
Grosnaja	7-15	0.600 ± 0.003	3.940 ± 0.011	20.16 ± 0.06	20.15 ± 0.05[3]	30.92 ± 0.09
Chainpur	2-5, 9-12, 14-15, 17-18	0.611 ± 0.004	3.964 ± 0.014	20.23 ± 0.05	20.19 ± 0.05	30.92 ± 0.07
Cold Bokkeveld	4-12, 15-30	0.595 ± 0.002	3.901 ± 0.007	20.10 ± 0.04	20.10 ± 0.11	30.81 ± 0.05
Allende[4]		*0.621 ± 0.007*	*3.952 ± 0.016*	*20.15 ± 0.10*	*20.17 ± 0.09*	*30.99 ± 0.12*
Murchison[5]		*0.611 ± 0.007*	*3.928 ± 0.011*	*20.13 ± 0.05*	*20.19 ± 0.04*	*31.03 ± 0.04*

[1] ^{78}Kr was not measured accurately due to problems with peak centring: The highest value (step 10) is probably a lower limit for Kr-Q in Dimmitt; [2] without step 6 and 10; [3] without step 11; [4] Wieler *et al.* (1991); [5] Wieler *et al.* (1992).

H3.7 Dimmitt...

The first 3 steps from Dimmitt (Table 7.8) are strongly compromised by adsorbed Xe (see chapter 3.1.5). Therefore, Kr is deduced from steps 4-11. In order to measure all isotopes with the multiplier, some steps had to be diluted by a factor of about 3. In general, no significant deviations in the isotopic ratios of the diluted steps could be discovered, indicating that non-linear effects did not disturb the measurements. The values for Q-Dimmitt are given in Table 3.13.

CV3 (ox.) Grosnaja...

The first 6 steps of Grosnaja (up to acid distillation) are clearly dominated by adsorbed Xe (chapter 3.1.5), as can been seen in Figure 3.13 and other 3-isotope-plots. The $^{84}Kr/^{132}Xe$ ratios are higher than typical Q values (4.64-6.79), also indicating air admixtures. Therefore, these steps were not taken into account to determine the Kr isotopic composition in Grosnaja (Table 7.18). Large amounts of Kr required the dilution by factors of 3-68. The resulting ratios for Q-Grosnaja are listed in Table 3.13.
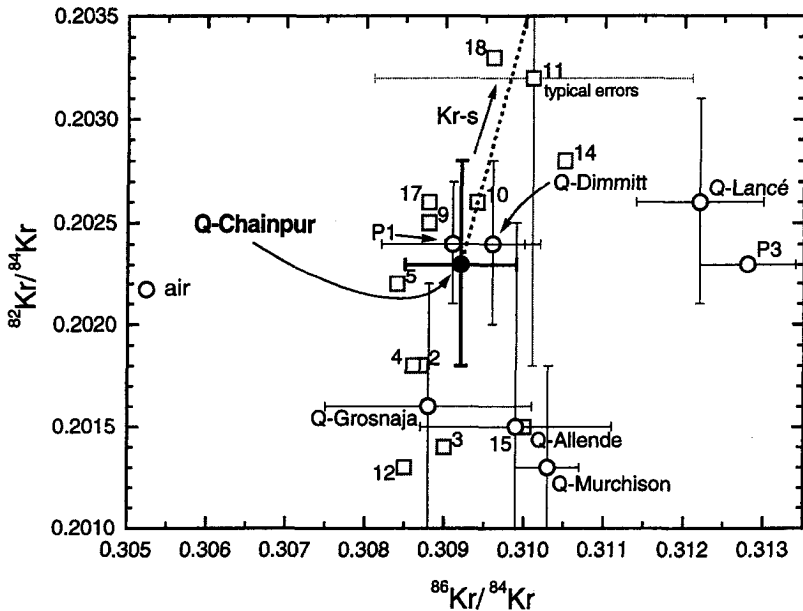
Figure 3.15: 3-isotope-plot of $^{82}Kr/^{84}Kr$ vs. $^{86}Kr/^{84}Kr$ released from Chainpur. Even the most Ne-E-bearing steps 9-12 do not show admixtures of Kr-s which is assumed to have the following composition: $^{82}Kr/^{84}Kr = 0.348$ and $^{86}Kr/^{84}Kr = 0.409$ (Ott *et al.*, 1988). For references, see Table 3.12.

LL3.4 Chainpur...

Kr in Chainpur could be measured without any dilution (Table 7.27). Steps 1, 7, 8, 13, 16 and 19 were excluded (see chapter 3.1.5), as well as step 6 which shows too large deviations due to too large amounts of reactive gases; the other steps are used to determine Kr-Q (Table

3.13). Steps 9-12 in Chainpur contain up to 16 % Ne-E (chapter 3.1.2). Since Ne-E(H) from SiC should be accompanied by Kr-s (chapter 1.1.2.4), it is interesting to ask whether such a Kr-s contribution might be detectable. The answer is no, since no Kr-s can be found in these steps (Figure 3.15). Assuming a ratio of ^{22}Ne-E(H)/^{82}Kr-s = 8589 (SiC-rich sample "KJ"; Lewis *et al.*, 1994), at most 0.006% (step 10) of ^{82}Kr should be s-process ^{82}Kr. This admixture can not be resolved since average typical errors are about 0.7%. The absence of detectable amounts of Kr-s in any etch step of Chainpur can therefore not be used to decide whether Ne-E(L) or Ne-E(H) was released during this experiment (chapter 3.1.2).
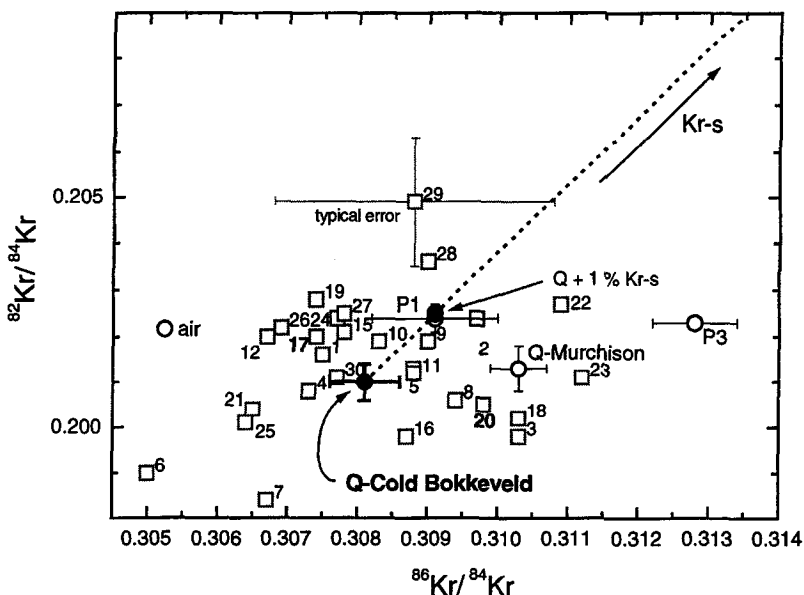
Figure 3.16: ^{82}Kr/^{84}Kr vs. ^{86}Kr/^{84}Kr plot for Cold Bokkeveld. Assuming that the released Ne-E is from SiC, step 20 should display the largest (0.06 %) admixtures of ^{82}Kr-s. Shown is the point corresponding to an Kr-s admixture of 1 %. Obviously, an admixture of 0.06 % is negligible, considering the uncertainties of the data points. For references and Kr-s composition, see Table 3.12.

CM2 Cold Bokkeveld...

The data from most of the 31 steps of the Cold Bokkeveld run (Table 7.36) can be used to determine the composition of Kr-Q (see chapter 3.1.5 on Xe for step selection). Steps 20-22 had to be diluted by a factor of 3. The results are given in Table 3.13. Cold Bokkeveld released large amounts of Ne-E (chapter 3.1.2). Similar as for Chainpur, the amount of expected ^{82}Kr-s

can be calculated, assuming that SiC is the carrier phase of the released Ne-E. If so, up to 0.06 % of the measured ^{82}Kr has to be ^{82}Kr-s. Such a small Kr-s contribution is not resolvable. Typical uncertainties of the measured ^{82}Kr/^{84}Kr ratios amount to some 0.6 % (Figure 3.16). Hints of Kr-s can not be seen in any isotope ratio.

3.2 Elemental ratios

In this chapter elemental ratios for Q-noble gases in the five samples examined are derived. These ratios are important for the detection of differences among meteorite classes or possible metamorphic losses as function of the petrographic type. Relative mass differences between elements are larger than between isotopes and, therefore, possible physical fractionation effects are larger and easier to uncover with elemental than with isotopic compositions. Physical processes, such as adsorption or solubility are observed to depend rather on elements than on isotopes (Ozima and Podosek, 1983).

In order to obtain representative values and to compensate outliers, as many steps as possible are used to calculate these ratios. To take into account the largely different gas amounts released by the different steps, element concentrations from the selected steps are added up. As can be seen in Figure 3.17-Figure 3.21, the various noble gases are released rather simultaneously, indicating that one homogeneously mixed single noble gas component is released from phase Q. However, due to admixtures of solar or atmospheric noble gases, some of the steps have to be rejected or to be corrected to allow for the determination of elemental ratios and, in particular, element concentrations for Q. The corrections are listed in Table 3.15, details are given in chapter 7.

CO.3.4 Lancé...

For the determination of the Q elemental ratios in Lancé, steps 2-8 are used, since steps 1 and 9 contain only insignificant gas amounts of together less than 2 % of the total. Step 5 shows significantly lower Ne (33 % lower than expected by comparison with ^{36}Ar concentrations) and especially lower He abundances (66 % lower) relative to Ar, Kr and Xe (Figure 3.17). This *points to fractionating losses due to a leakage through a valve during gas separation or etching.* Therefore, He and Ne of step 5 were corrected (Table 7.1). Surprisingly, no fractionation could be seen in the Ne isotopic ratios (Figure 3.1), although these losses should be recognisable in a shift towards smaller ^{20}Ne/^{22}Ne and ^{21}Ne/^{22}Ne ratios in the Ne three-isotope-plot. Assuming that

the loss is in proportion to mass$^{-1/2}$, the ^{20}Ne/^{22}Ne ratio should decrease by about 4 %. The elemental ratios obtained for Q-Lancé and all other samples are listed in Table 3.14.
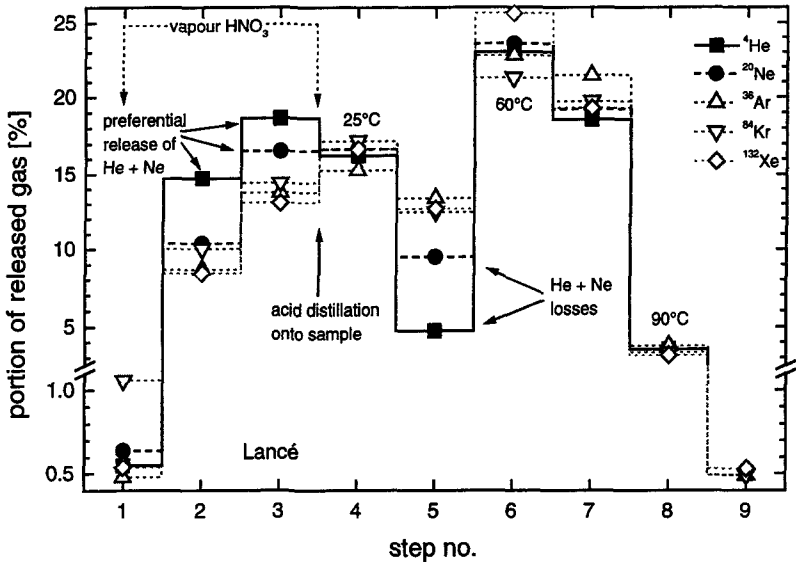
Figure 3.17: Noble gas release pattern of Lancé. All abundances are normalised to the total gas amounts released upon etching. He and Ne of step 5 show losses. Except for this step, gases are released in relatively uniform proportions.

H3.7 Dimmitt...

As shown by the isotopic compositions in chapter 3.1.5, the first three steps of Dimmitt clearly contain admixtures of atmospheric Xe. Non-Q admixtures of Kr and Xe in steps 1-4 can be observed also in the elemental release pattern (Figure 3.18 and Figure 7.1). These adsorbed, *isotopically* atmospheric Kr and Xe contributions are corrected by assuming two-component-mixing of Q (elemental composition taken from step 5) and adsorbed noble gases (see Figure 7.1). Since the Kr/Xe ratio of the adsorbed air is not atmospheric, the end member is determined by extrapolation of the first steps to (^{36}Ar/^{132}Xe)$_{adsorbed}$ = 0, assuming that no Ar has been adsorbed. This is described in Table 7.8 of the appendix.

The discussion of the Ne isotopic ratios in chapter 3.1.1 revealed that solar Ne is abundant in steps 1, 2, 10 and 11. This is also indicated by very high ^{4}He/^{36}Ar (8.3-31.3) and ^{20}Ne/^{36}Ar ratios (0.09-0.45) of steps 1-3. Furthermore, the very high amounts of ^{4}He in the last steps 9-11 most likely are due to the presence of solar He. Another possibility might be that these steps

released fractionated (He-enriched) presolar noble gases, since the sample temperature of the last step (130 °C) was rather high. However, the $^4He/^{20}Ne$ ratio of step 11 is 407 and thus 5 times higher than the value finally deduced for Q-Dimmitt (Table 3.14). This value is considerably higher than that of 183 for presolar diamonds (Wieler *et al.*, 1991) and close to the solar wind value $^4He/^{20}Ne = 650$ (Murer *et al.*, 1997). Therefore, a solar wind origin seems more likely. These contributions can not be corrected accurately enough to certainly exclude influences on the elemental ratios. Therefore, steps 5-8 are used to deduce the elemental composition of Q-Dimmitt (Table 3.14).
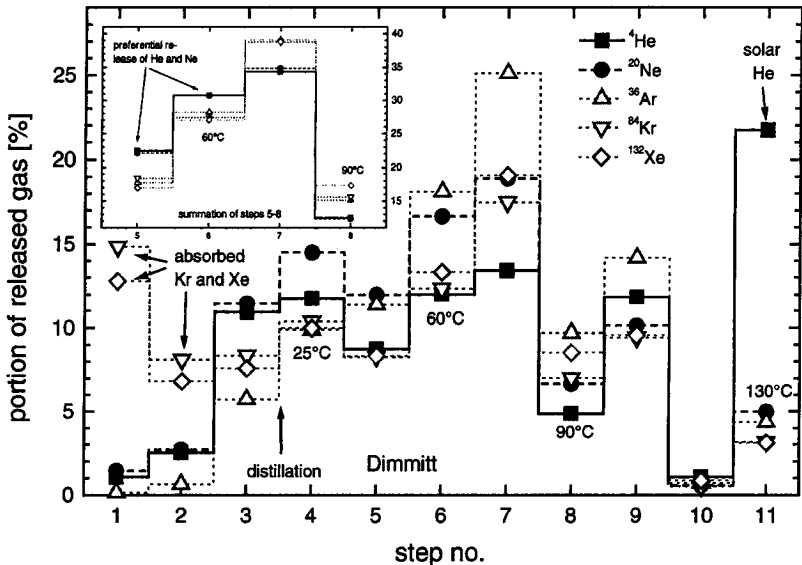
Figure 3.18: The noble gas release from Dimmitt is less uniform than that from Lancé. The increased Kr and Xe amounts of steps 1 and 2 are clearly due to adsorbed atmospheric contributions (see also chapter 3.1.5). The large He amounts in the last steps are most likely due to the release of solar He. Steps 5-8 (inset) without contributions from solar wind noble gases are used to determine Q-Dimmitt. As expected, these steps show a release of all noble gases in similar proportions.

Grosnaja...

Steps 1 and 3-6 of the etch experiment on Grosnaja contain large amounts of isotopically atmospheric Kr and Xe (chapter 3.1.5). Adsorbed Kr and Xe are also observable in the elemental release pattern (inset in Figure 3.19). These are the steps obtained before the acid

was distilled onto the sample. An exception to this is step 2 shows a Q-like composition similar to steps 7-15. Notably, in this step, valve "G2", which separates sample and acid, remained closed during etching. Therefore, Kr and Xe abundances of steps 1 and 3-6 are corrected in the same way as those of Dimmitt (Table 7.18). After correction, the release pattern is again quite uniform (Figure 3.19). Taking the corrections into account, the elemental composition of Q-Grosnaja is determined as the weighted mean of *all* steps (Table 3.14).
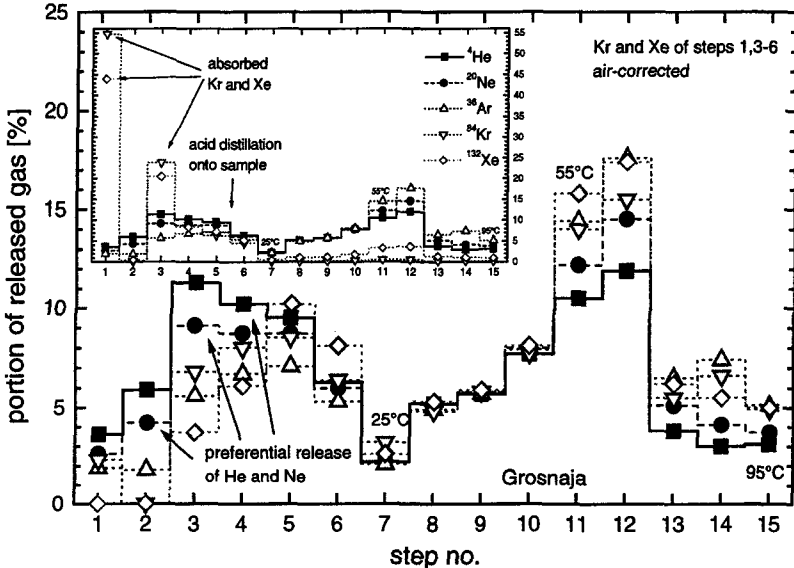
Figure 3.19: Elemental release pattern of Grosnaja. Except for steps 1 and 3-6, which are influenced by atmospheric contributions (evident by steps 1 and 3 in inset), the release of Q noble gases is quite uniform.

Chainpur...

The elemental composition of Q-gases from Chainpur (Table 3.14) is determined straightforwardly including steps 1 and 2 which show very slight admixtures of adsorbed atmospheric Kr and Xe (chapter 3.1.5). These contributions are neglected since they amount to less than 0.8 % of the total released Kr and Xe and therefore do not affect the elemental ratios significantly. Ar, Kr and Xe of steps 8, 13 and 16 could not be measured due to too high background. The remaining steps are shown in Figure 3.20. As in the other experiments, the noble gases are released in similar proportions in each etch step.
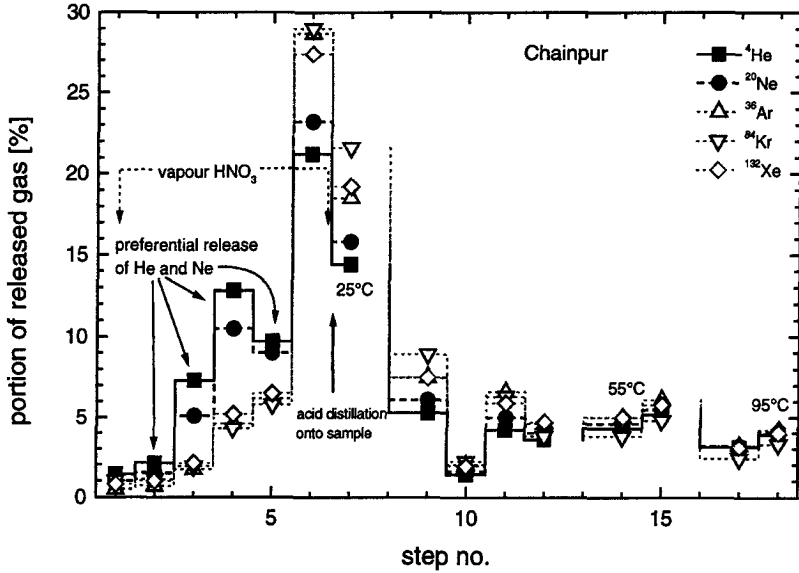
Figure 3.20: The uniform elemental release pattern for Chainpur. Steps 8, 13 and 16 could not be measured due to reactive gas problems.

Cold Bokkeveld...

The Cold Bokkeveld analysis (Figure 3.21) was not affected by atmospheric contributions except for the very gas-poor step 14. Ar, Kr and Xe could not be measured in step 13 due to large amounts of reactive gases in the mass spectrometer. All other steps are used to determine the elemental composition of Q-Cold Bokkeveld (Table 3.14).

Gas release systematics...

As described above, the almost parallel release of the elements during all 5 experiments appears to justify the view that these gases released from phase Q represent *one* single rather uniform and homogeneously mixed component. However, a closer look at the plots and the elemental ratios of single steps reveals a more complex situation: The lighter elements He and Ne are released earlier than Kr and Xe. Ar shows some evidence for a slightly "delayed" release compared to He and Ne. These trends hold for all experiments, but are partly masked by solar and atmospheric admixtures for Dimmitt and Grosnaja. The preferential release of He and Ne in the first steps was also observed during the CSSE experiments on Allende and Murchison

(Wieler *et al.*, 1992). To better illustrate this trend, the elemental ratios are re-calculated in Table 3.14 for the first and the second part of each run, separately. The parts for all runs except for Cold Bokkeveld are defined in such a way that both parts contain almost the same amounts of ^{4}He and ^{20}Ne. The first part of the Cold Bokkeveld run ends with step 17, the second starts with step 23, since this division takes into account two well-defined sub-components, as we will see below. The ratios are plotted, normalised to the ratios calculated from *all* steps, in Figure 3.22.
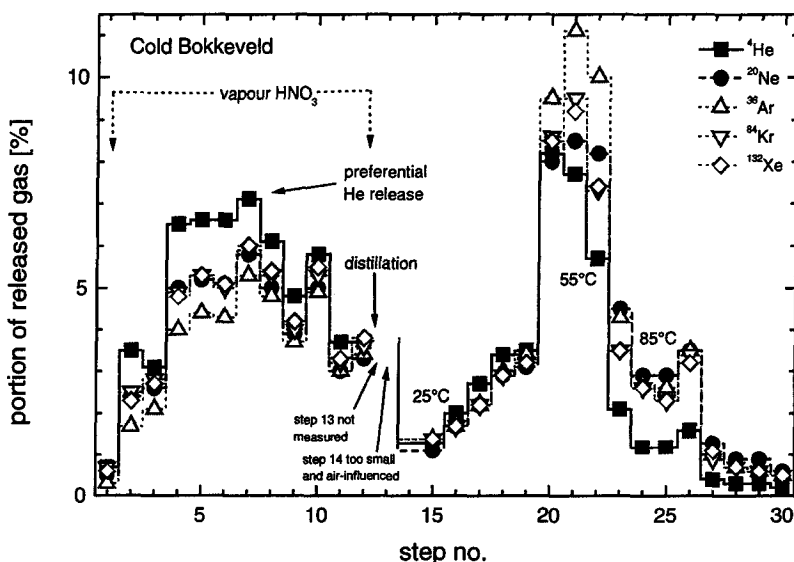
Figure 3.21: Noble gases released from Cold Bokkeveld. All elements are released in similar proportions during the etch experiment.

The ratios ^{4}He/^{20}Ne, ^{4}He/^{36}Ar, ^{4}He/^{132}Xe, ^{20}Ne/^{36}Ar and ^{20}Ne/^{132}Xe (except for Cold Bokkeveld) of the second half of all experiments are significantly lower than those of the first part, while most ^{36}Ar/^{84}Kr and ^{36}Ar/^{132}Xe ratios show the reverse trend. Later steps with a higher relative Ar abundance (e. g. steps 20-23 in Figure 3.21) are generally those with the smallest ^{40}Ar/^{36}Ar ratios and are therefore used for the determination of the isotopic composition of Ar-Q in chapter 3.1.4. In contrast, relative Kr and Xe abundances are almost constant in both groups of steps in all experiments (Figure 3.22).
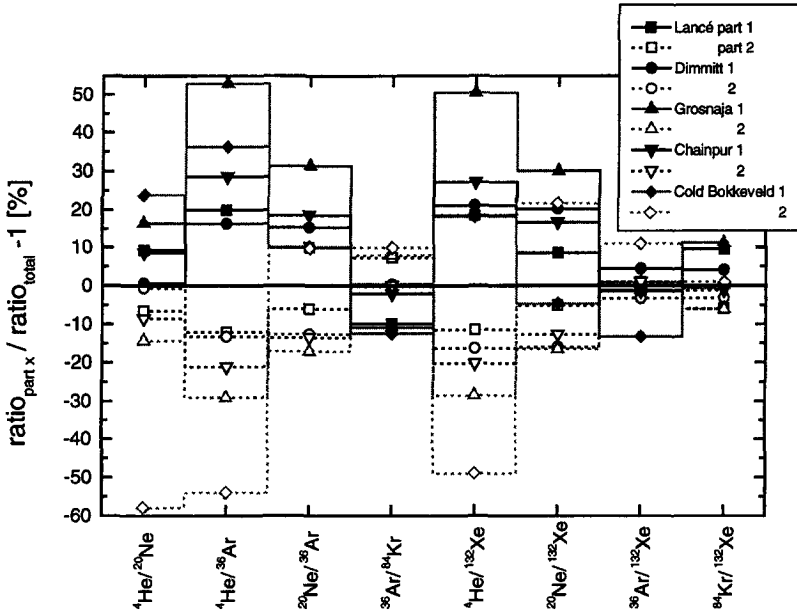
Figure 3.22: This plot shows elemental ratios, determined separately for the first and the second part of each run (Table 3.14), normalised to the ratios deduced from all steps. Filled symbols are used for the first parts of released gases, open symbols for the second parts.

Sub-components in Q from Cold Bokkeveld...

The experiment on Cold Bokkeveld with 30 steps allows for a more precise examination of this phenomenon. Figure 3.23 shows elemental ratios for all steps normalised to the ratios of step 30. All ratios are well defined and further support the observation clarified above: Ratios with He in the numerator are higher in the first 22 steps compared to later steps. Plateaux with rather constant ratios are observed between steps 4-17. This points to the release of two distinct He-Q components rather than to a continuously decreasing portion of released He. A continuous change would indicate different physical release properties for He compared to the other noble gases. The $^{20}Ne/^{132}Xe$ ratio is quite constant during the Cold Bokkeveld run, in contrast to the other experiments which show larger differences of this ratio between first and second part of the run (Figure 3.22 and Table 3.14). Similar to the other meteorites (see Figure 3.17-Figure 3.20), Ar is released in higher proportion relative to ^{132}Xe in the later steps 21-23 which are those with the lowest $^{40}Ar/^{36}Ar$ ratios (Figure 3.10). This ratio is used as an indicator of the purest Ar-Q fractions. The binary elemental release pattern of Cold Bokkeveld can not be

explained by contributions from other components. Assuming that steps 4-17 contain "true" Q, atmospheric contamination would indeed lower the ratios $^4He/^{20}Ne$, $^4He/^{36}Ar$ and $^4He/^{132}Xe$ of the following steps 18-30. However, it is not possible to find corresponding proportions of atmospheric ^4He, ^{20}Ne and ^{36}Ar admixtures from the $^4He/^{36}Ar$ and $^{20}Ne/^{36}Ar$ ratios, under the assumption that the data points of step 17 and air are pure end members. Based on the $^4He/^{36}Ar$ ratio, $^4He_{atm}$ contributions in steps 18-30 would not exceed 2.2 %, while up to 66 % of ^{36}Ar would be atmospheric. In contrast, based on the $^{20}Ne/^{36}Ar$ ratio, $^{36}Ar_{atm}$ would amount to only 7 %. Adding of 7 % $^{36}Ar_{atm}$ would *raise* the ratio $(^{40}Ar/^{36}Ar)_Q$ from a value of 6.6 in step 17 to values of about 26 for steps 18-30 which is not observed. Almost all steps have *lower* $^{40}Ar/^{36}Ar$ ratios; steps 20-23 and 25 have even the lowest isotopic $^{40}Ar/^{36}Ar$ ratios (<2) of all steps released from Cold Bokkeveld. Similar arguments also exclude noble gases from diamonds, which are the most gas-rich carriers along with phase Q, to be the components that compromise steps 23-30: $^4He/^{20}Ne$, $^4He/^{36}Ar$ and $^4He/^{132}Xe$, measured in presolar diamonds (Wieler *et al.*, 1991), are *larger than in phase Q*, and, thus, *can not lower these ratios as shown in Figure 3.23*.

Table 3.14: Elemental compositions of Q deduced in this work.

	steps	$^4He/^{20}Ne$	$^4He/^{36}Ar$	$^{20}Ne/^{36}Ar$	$^{36}Ar/^{84}Kr$	$^4He/^{132}Xe$	$^{20}Ne/^{132}Xe$	$^{36}Ar/^{132}Xe$	$^{84}Kr/^{132}Xe$
Lancé[1]	2-8	74.6	1.96	0.0262	90.0	175.5	2.35	89.7	0.996
		0.8	0.03	0.0004	1.4	1.6	0.02	1.5	0.008
	2-4	81.5	2.35	0.0288	81.0	207.8	2.55	88.4	1.091
	5-8	69.7	1.72	0.0246	96.6	155.2	2.23	90.5	0.936
Dimmitt	5-8	67.2	2.63	0.0392	97.3	142.9	2.13	54.2	0.557
		0.5	0.04	0.0006	1.4	1.7	0.03	1.0	0.007
	5-6	67.6	3.06	0.0452	97.6	173	2.56	56.6	0.580
	7-8	66.7	2.28	0.0342	97.1	119.4	1.79	52.4	0.540
Grosnaja[2]	1-15	128.9	6.30	0.0489	119	663	5.15	105.2	0.881
		0.7	0.05	0.0004	2	10	0.08	1.7	0.019
	1-8	150.0	9.64	0.0642	106	998	6.7	104	0.98
	9-15	110.4	4.47	0.0405	128.4	474	4.30	106.1	0.827
Chainpur[3]	1-18	112.5	3.46	0.0308	72	202	1.80	58.4	0.82
		1.2	0.04	0.0004	3	4	0.03	1.1	0.03
	1-6	122.1	4.45	0.0365	70.5	257	2.10	57.6	0.817
	7-18	102.8	2.73	0.0266	72	161	1.57	59.0	0.81
Cold Bokkeveld[4]	1-30	162.0	11.51	0.0710	84.1	611	3.77	53.1	0.631
		0.7	0.06	0.0004	0.5	4	0.02	0.4	0.004
	1-17	200.8	15.68	0.0781	73.5	722	3.60	46.1	0.627
	23-30	68.0	5.29	0.0779	92.4	312	4.58	58.9	0.637

[1] He and Ne of step 5 corrected, see Table 7.1; [2] Steps 1 and 3-6 corrected for Kr and Xe air contributions, see Table 7.18; [3] without steps 8, 13 and 16 (Ar, Kr, Xe not measured); [4] without step 13 (Ar, Kr, Xe not measured) and step 14 (small step with significant atmospheric contributions).

Figure 3.22 and, in particular, Figure 3.23 suggest that two noble gas components exist. One possibility is the release of one sub-component (Q_2) which contains all noble gases and the additional release of He and (possibly Ne) from a sub-component Q_1 which resides in a phase slightly easier to etch. The other possibility is that both components contain all noble gases, but with different relative abundances. He and Ne are enriched in phase Q_1, which is etched first, and Ar is more abundant in the second phase Q_2.
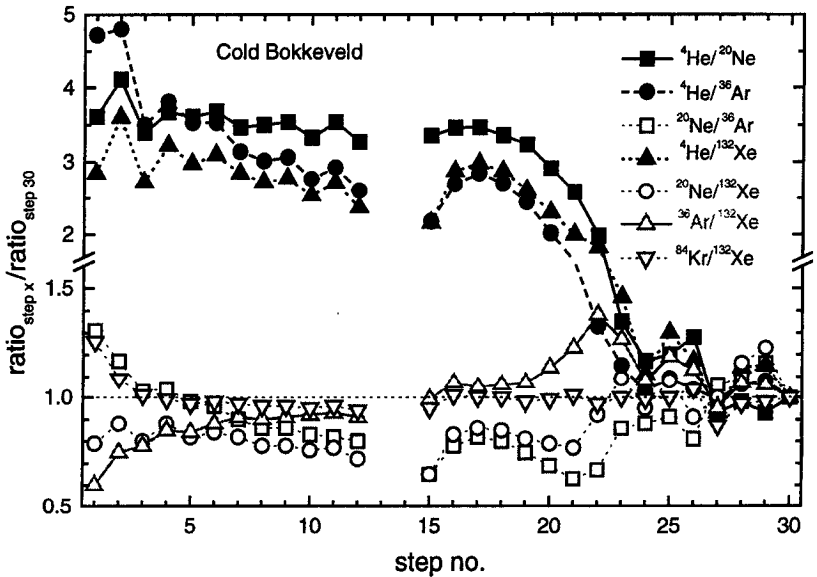
Figure 3.23: Elemental ratios of all steps released from Cold Bokkeveld, normalised with ratios of step 30. Steps 13 and 14, which were compromised by background and atmospheric gases, are not included. The steps clearly show a binary release pattern, rather indicating two Q sub-components than a physically explainable earlier release of He relative to the other noble gases from a single reservoir.

The hypothesis of two sub-components of Q is supported, in addition to the elemental variations demonstrated above, by the isotopic compositions of He and Ne. These change between step 22 and step 23. $^3He/^4He$ is rather constant for steps 4-22 (phase Q_1), but is slightly increased for steps 23-30 which are dominated by Q_2 noble gases (Table 7.33 and Figure 3.7). Furthermore, Ne-E(L) from graphite (Figure 3.4) is released in steps 4-22, where $^4He/^{20}Ne$ is rather constant (Figure 3.23), while data points of steps 23-30 do not show any Ne-E contribution and lower $^4He/^{20}Ne$ ratios. This points to a connection between phase Q_1 and graphite which is illustrated in Figure 3.24.
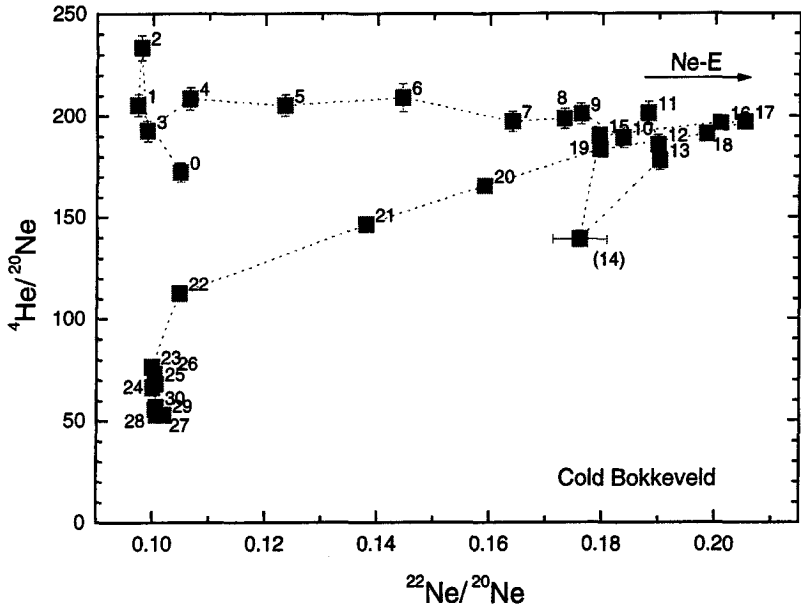
Figure 3.24: This ^{4}He/^{20}Ne vs. ^{22}Ne/^{20}Ne plot for the data of Cold Bokkeveld suggests that Ne-E is connected with component Q_1 which is released first. Steps 4-22, which contains Ne-E, also have higher and at least for steps 4-18 quite constant ^{4}He/^{20}Ne ratios, while steps 23-30 cluster in a region with lower ^{4}He/^{20}Ne ratios.

3.3 Absolute abundances

In this chapter, I want to determine the absolute concentrations of the Q-noble gases in HF/HCl-resistant residues. If metamorphic processes on the meteorite parent bodies have influenced the gas content of our samples, this should not only be seen in the elemental ratios (chapter 3.2), but also in the absolute abundances of Q-gases. Before I discuss the data, three problems have to be considered to allow for quantitative comparison of the results: Some components, which were additionally released, have to be subtracted, the residues should not contain significant amounts of undissolved silicates and it must be verified that the samples have lost all noble gases on etching by CSSE.

Corrections...

Corrections for the various components released besides Q, discussed in chapter 3.2, lead to somewhat inaccurate absolute abundances. However, because the differences of Q-gas concentrations in the different samples are so large, the general trend displayed in Figure 3.25 is not severely disturbed. Table 3.15 lists the corrections for leakage, adsorbed atmospheric and solar gases. Cosmogenic contributions that considerably compromised some of the He and Ne isotope analyses (chapters 3.1.1 and 3.1.3) can be neglected here: He_{cosm} and Ne_{cosm} do not affect the isotopes ^4He and ^{20}Ne most abundant in Q. This is conservatively estimated by assuming ^3He and ^{21}Ne to be exclusively cosmogenic and by using $(^3He/^4He)_{cosm} \approx 0.2$ and $(^{21}Ne/^{20}Ne)_{cosm} = 1$. $^4He_{cosm}$ and $^{20}Ne_{cosm}$ would amount to some 0.01% and 1.2 %, respectively, of the measured concentrations.

Table 3.15: Corrections of absolute Q-gas abundances in %.

sample	correction for...	steps	^4He	^{20}Ne	^{36}Ar	^{84}Kr	^{132}Xe	for details, see...
Lancé	leakage	5	9.1	4.7				Table 7.1
Dimmitt	adsorbed air	1-4				28.8	24.6	Table 7.8, Table 7.11
	solar gases[1]	1-3, 9-11	34.9	11.2				Table 7.5
Grosnaja	adsorbed air	1-6				96.7	79.4	Table 7.18, Table 7.21
Chainpur	missing Ar, Kr, Xe[2]	8, 13, 16			18.6	18.6	18.6	
Cold Bokkeveld	missing Ar, Kr, Xe[2]	13			1.5	1.5	1.5	

[1] To account for solar He and Ne in the first and last steps of Dimmitt (see Figure 3.18), simple corrections were applied; [2] Ar, Kr and Xe were not measured due to background problems and are calculated from He and Ne abundances.

Sample mass...

It is not clear if the samples were completely demineralised (chapter 2.1.2). If not, remaining silicates would influence the weights and, thus, also the concentrations. A future analysis of the major elements in aliquots of the residues will allow to answer this question. However, other minerals such as spinel or chromite generally contribute to the residues in different and unknown amounts. Alaerts *et al.* (1979a) determined chromite abundances of 35-100 % in HF/HCl-resistant residues of LL-chondrites.

Etching efficiency...

To allow for a quantitative comparison, phase Q has to be removed completely by the oxidising acid. The elemental release patterns (Figure 3.17-Figure 3.21) do not indicate that

significant amounts of Q-gases remained in the oxidised residues: Although the last steps of all runs were measured after harshest and longest oxidation, they did not contain more than 5 % of the total gas amounts. Complete removal of phase Q can be checked with the analysis of the oxidised residues. Especially, the isotopic compositions of Ar and Xe should indicate remaining Q-noble gases. Xe in HF/HCl-resistant residues consists mainly of Xe-Q (> 96 %; Huss *et al.*, 1996) and only minor portions from presolar components. Therefore, even small remaining admixtures of phase Q strongly influence the measurement of oxidised residues. Completely oxidised and Q-depleted residues can be recognised by $^{36}Ar/^{38}Ar \approx 4.8$ (Wieler *et al.*, 1991) and by the typical Xe-HL isotopic composition (Figure 1.3). On the other hand, from He and Ne isotopic compositions of the oxidised samples, generally, no conclusions can be drawn, since contributions of He-Q and Ne-Q are rather small, even without any oxidation (Figure 1.3). Therefore, data points of oxidised and non-oxidised samples in Ne three-isotope-plots are located too close to each other to allow for a statement about remaining Ne-Q. The $^4He/^{20}Ne$ ratios in oxidised and non-oxidised residues are also too similar to be diagnostic.

CV3 (ox.) Grosnaja...

Data of the bulk measurements on non-oxidised and oxidised residues of Grosnaja are given in Table 7.16, Table 7.17, Table 7.20 and Table 7.23. To avoid problems with too much reactive gases possibly from Teflon, the Ar and Kr/Xe phases of all 600 °C and most 1800 °C steps were not measured but pumped off. The errors of the total gas concentrations because of these gas losses should be less than 10 %, as estimated from He and Ne in some of the residues of Dimmitt, Grosnaja and Chainpur. He and Ne of the 600 °C steps amount on average to 7 % and at maximum to 17 % of the respective gas amounts in the 1800°C steps.

In a $^4He/^{36}Ar$ vs. $^{20}Ne/^{36}Ar$ plot not shown[9], the data point of the oxidised residue lies exactly on a mixing line between Q and the value of the oxidised residue "B" (Matsuda *et al.*, 1980). From this, the amount of Ar-Q, which remained in the oxidised residue, is calculated to be 66 % of the total Ar in the etched residue. The $^{36}Ar/^{38}Ar$ ratio of 5.4 ± 0.2 also indicates that Ar in the residue is dominated by Ar-Q. Assuming that the mass of the removed phase Q can be neglected, the He-Q, Ne-Q and Ar-Q fraction, which remained in the oxidised residue

[9] In this plot, the data point of our non-oxidised bulk HF/HCl-resistant residue lies very close to that of the residue "A" of Matsuda *et al.* (1980) and exactly on the Q-oxidised residue-mixing line. This indicates that our demineralisation procedure yielded residues comparable to those of other groups.

corresponds, each to about **27 %** of the He-Q, Ne-Q and Ar-Q, respectively, measured by CSSE.

The Ne isotopic composition of the oxidised residue might suggest that most of the Ne-Q has been released, since the respective data point is very close to the Ne-HL data point. However, as outlined above, since Ne-Q is only a minor part of the Ne in HF/HCl-resistant residues, the data do not allow for a reliable quantitative estimate.

The Xe isotope composition of the oxidised residue of Grosnaja displays an isotope pattern *similar to that of presolar Xe-HL (Figure 1.3). However, the pure HL composition has not been* reached. Assuming that all Xe in the residue is Xe-HL plus Xe-Q and that mass loss due to etching is negligible (Table 2.5) and comparing the isotope concentrations of ^{132}Xe, ^{134}Xe and ^{136}Xe, we can conclude that **41 %** of the ^{132}Xe in phase Q has not been removed by our CSSE experiment. Under the assumption that *all* ^{36}Ar and ^{132}Xe in the oxidised residue originate from phase Q, these gases would amount to **36 %** and **45 %**, respectively, of the total Q-gases in Grosnaja.

LL3.4 Chainpur...

He and Ne data of the oxidised residue of Chainpur (Table 7.25, Table 7.26, Table 7.28, Table 7.29, Table 7.31 and Table 7.32) can not be used to determine the degree of dissolving of phase Q during the etch experiment. The $^{36}Ar/^{38}Ar$ ratio of 5.45 ± 0.03 in the oxidised residue is even larger than the value 5.37 ± 0.01 for Ar-Q (Table 3.9). This is difficult to understand but in any case indicates that Ar-Q is more abundant than Ar-A in our oxidised residue. The $^{4}He/^{36}Ar$ ratio is 101.9 for our oxidised residue which is relatively close to the value of 143 reported by Alaerts *et al.* (1979a) for their residue "1C1a". Since the $(^{4}He/^{36}Ar)_Q$ ratio for Chainpur is 3.46, this suggests that phase Q was largely removed during the CSSE experiment. Similar to Grosnaja, the amount of Ar-Q, which remained in the oxidised residue, can be estimated from the $^{4}He/^{36}Ar$ and $^{20}Ne/^{36}Ar$ ratios of our oxidised residue by assuming the end member compositions from Q-Chainpur (chapter 3.2) and an conventionally oxidised residue "1C5" (Alaerts *et al.*, 1979a), respectively. It turns out that only **2 %** of the total He-Q, Ne-Q and Ar-Q in Chainpur were not released by CSSE. Using the elemental ratios of ^{36}Ar, ^{84}Kr and ^{132}Xe instead, the remaining ^{36}Ar, ^{84}Kr and ^{132}Xe amount to **3 %**, **6 %** and **5 %**, respectively. Such small proportions are also suggested by the isotopic Xe composition of the oxidised residue. In a $^{134}Xe/^{132}Xe$ vs. $^{136}Xe/^{132}Xe$ three isotope plot its data point lies close to the mixing line between the end member data points for Q and Xe-HL. The decomposition of this mixture reveals that only **5 %** of Xe-Q has remained in the residue oxidised by CSSE. Figure 1.3

displays the Xe-HL-like pattern for Chainpur. Even this minor fraction of the Xe-Q in Chainpur still dominates the Xe composition of the oxidised residue[10].

H3.7 Dimmitt…

Bulk data for the original and the oxidised residues of Dimmitt (Table 7.6, Table 7.7, Table 7.9, Table 7.10, Table 7.12 and Table 7.13) were obtained for all 5 noble gases. The He, Ne, Ar and Kr isotopic ratios in both residues are identical within the errors. The ratios $(^3He/^4He)_{res.} = 4.05 \times 10^{-4}$, $(^3He/^4He)_{ox. res.} = 4.03 \times 10^{-4}$ and $(^{20}Ne/^{22}Ne)_{res.} = 11.6$ and $(^{20}Ne/^{22}Ne)_{ox. res.} = 11.4$ resemble the SEP composition with $(^3He/^4He)_{SEP} = 4.56 \times 10^{-4}$ and $(^{20}Ne/^{22}Ne)_{SEP} = 11.2$ (Benkert et $al.$, 1993), respectively. This indicates that solar noble gases dominate even He and Ne in the oxidised residue. The oxidised residue contains Ar with $^{36}Ar/^{38}Ar = 5.4 \pm 0.3$. Since admixtures of Ar_{SEP} with $^{36}Ar/^{38}Ar_{SEP} = 4.87$ can only lower this value, it points to abundant amounts of Ar-Q. Similar to the He and Ne isotopic ratios, the elemental ratios of He, Ne and Ar are also solar-like. Evidently, the demineralisation procedure with HF/HCl did not completely remove an important carrier of the incorporated solar gases in the regolith breccia Dimmitt, as we have seen in chapter 3.1.1. Fortunately, this carrier is not oxidisable by HNO_3 to a larger extent and, thus, has allowed a determination of the isotopic composition of Ne-Q. However, a determination of fraction of He-Q, Ne-Q and Ar-Q in the oxidised residue is not possible.

Most Xe isotope ratios are also similar in the oxidised and non-oxidised residues which means that Xe-Q has not been completely released. Only the ratios $^{124}Xe/^{132}Xe$ and $^{126}Xe/^{132}Xe$ in the oxidised residue are higher, but this enrichment in "Xe-L" must be due to insufficient hydrocarbon background correction, since no enrichment in the heavier Xe isotopes can be found. The oxidised residue contained less than 40 % of the Xe of the original residue and was therefore more easily affected by the hydrocarbon interference on masses 124 and 126. Assuming that ^{36}Ar and ^{132}Xe released from the oxidised residue originate completely from phase Q and that etching caused no significant mass losses (see Table 2.4), about **38 %** and **36 %**, respectively, of ^{36}Ar-Q and ^{132}Xe-Q were not released from Dimmitt upon etching with CSSE.

---

[10] The ^{84}Kr and ^{132}Xe concentrations measured in the non-oxidised bulk residue (Table 7.28 and Table 7.31) are much smaller than the concentrations released by CSSE (Table 7.27 and Table 7.30). This can be the result of inhomogeneities or a weighing error, but does not harm the estimations above which are based only on elemental and isotopic ratios.

CM2 Cold Bokkeveld...

Two original and two oxidised (bulk) residues of Cold Bokkeveld (Table 7.34, Table 7.35, Table 7.37, Table 7.38, Table 7.40 and Table 7.41) have been measured. Unfortunately, Kr and Xe could be determined only for one aliquot each. The results show that CSSE has oxidised the original residue incompletely and rather inhomogeneously. A comparison of the $^{134}Xe/^{132}Xe$ and $^{136}Xe/^{132}Xe$ ratios in the oxidised residue (a) with the composition of Xe-Q and Xe-HL yielded that 51 % of Xe-Q has not been removed by CSSE. A similar fraction of 49 % Ar-Q, Kr-Q and Xe-Q can be derived from the $^{36}Ar/^{132}Xe$ vs. $^{84}Kr/^{132}Xe$ plot, assuming that the oxidised residue KB1/II from CM2 Murchison (Wieler *et al.*, 1992) has a composition similar to a completely oxidised residue of CM2 Cold Bokkeveld[11]. As deduced from the $^{4}He/^{36}Ar$ vs. $^{20}Ne/^{36}Ar$ plot, the oxidised residues (a) and (b) still contain 55 % and 32 %, respectively of He-Q, Ne-Q and Ar-Q.
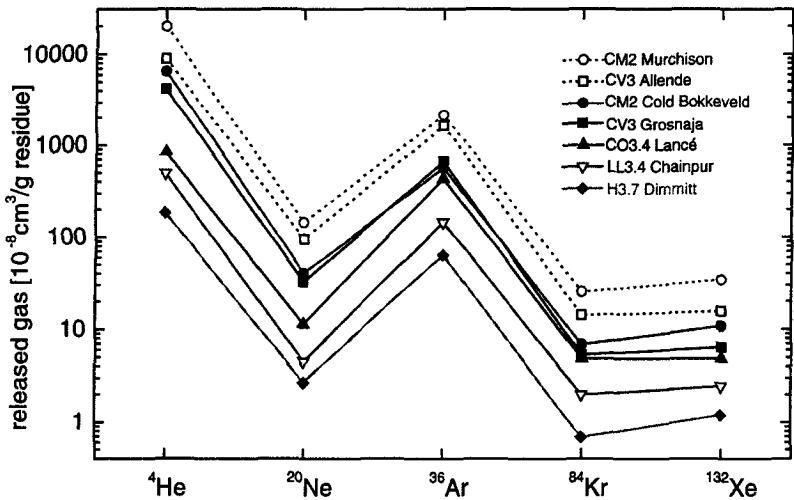
Figure 3.25: Total Q-gas concentrations in residues for all meteorites examined with CSSE experiments. References: Allende (average of runs BA I+II; Wieler *et al.*, 1991); Murchison (average of runs 2C1a/III and KB1/I+II; Wieler *et al.*, 1992).

---

[11] This assumption seems to be justified, since all data points for Q and the residues of Murchison and Cold Bokkeveld in three-element-plots lie exactly on mixing-lines between Q and the most-oxidised residue of Murchison (KB1/II).

CO3.4 Lancé...

For the oxidised residue of Lancé, only He and Ne (Table 7.2) could be measured due to Teflon contamination (chapter 2.1.2). The data point of our oxidised residue in the Ne-three-isotope-plot is, within the large uncertainties of all data, similar to the oxidised ("1C5") as well as to the untreated original residue ("1C1"; Alaerts *et al.*, 1979b). Therefore, the amounts of Q that remained in the residue upon etching can not be determined.

Table 3.16: Absolute abundances for noble gases of phase Q deduced in this work by CSSE.

[10^{-8} cm^3/g residue]		^{4}He	^{20}Ne	^{36}Ar	^{84}Kr	^{132}Xe
Lancé	CO3.4	839	11.25	431	4.81	4.81
		5	0.09	7	0.02	0.03
Dimmitt	H3.7	177	2.60	63.6	0.653	1.148
		6	0.08	0.6	0.008	0.016
Grosnaja	CV3	4147	32.18	658	5.51	6.25
		15	0.12	4	0.08	0.10
Chainpur	LL3.4	492	4.46	143.6	2.01	2.46
		4	0.03	1.7	0.08	0.04
Cold Bokkeveld	CM2	6497	40.03	563	6.85	10.79
		20	0.12	3	0.03	0.07

Absolute Q gas concentrations...

The amounts of Q-noble gases, which remained in the residue after CSSE, vary, as shown above, largely between less than 5 % for Chainpur and about 40-50 % for Dimmitt, Grosnaja or Cold Bokkeveld. However, these numbers must be seen as upper limits, since contributions of presolar P3 gases (chapter 1.1.2.4) can significantly affect the gas concentrations in the oxidised residues of at least the less metamorphosed sample Grosnaja. Huss and Lewis (1994b) calculated that 70 % of the Xe from the oxidised residue of the CI chondrite Orgueil is Xe-P3. On the other hand, P3 is released at temperatures of 200-800 °C which makes it likely that some of the P3 in *our* residues has been lost in the pumped-off pyrolysis steps at 600 °C. For more altered ordinary chondrites of petrographic type 3.5-3.6, Huss *et al.* gave an insignificant P3-fraction of only 4 % in the residues. Fortunately, even using the upper limits for the remaining concentrations of Q-gases in the oxidised residues does not affect the general trend displayed in Figure 3.25 and Figure 3.26. Therefore, I do not correct the total Q-gas concentrations for these roughly estimated gas amounts.

The absolute abundances of noble gases in Q are calculated as the sums of the contributions of all steps. These values are shown in Table 3.16 and Figure 3.25. For comparison, data for Allende and Murchison are also shown in the figure (Wieler *et al.*, 1991; 1992). The highly

metamorphosed meteorites CO3.4 Lancé, LL3.4 Chainpur and H3.7 Dimmitt contain significantly smaller amounts of Q-gases than the more primitive CM2 and CV3 chondrites. The similarity in the abundance patterns of all samples within seven orders of magnitude relative to solar and Xe abundances is striking (Figure 3.26) and supports the hypothesis that all five noble gases have been incorporated simultaneously from the same uniform reservoir into the meteorites' parent bodies or into the carrier phase(s) Q.
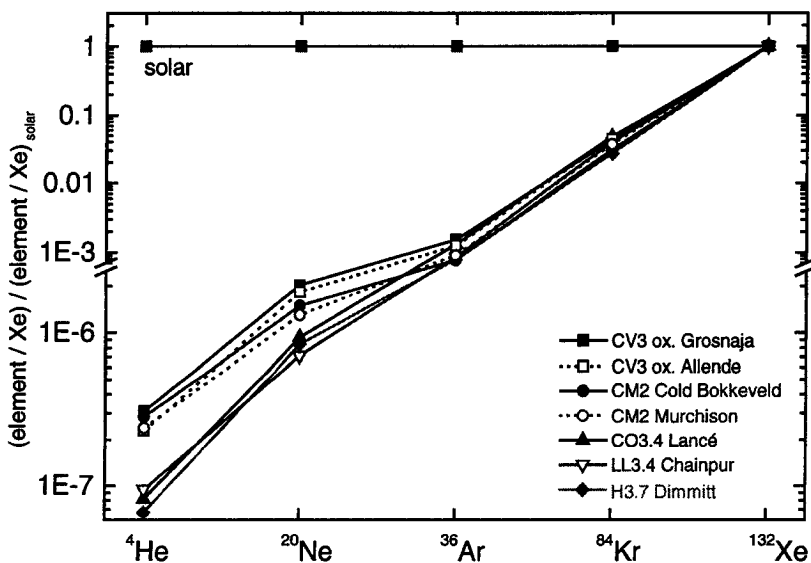
Figure 3.26: Elemental composition of Q noble gases normalised to solar abundances (Anders and Grevesse, 1989) and ^{132}Xe. He-Q and Ne-Q in all meteorites are similarly depleted by up to 7 orders of magnitude compared to cosmic abundances. The highly metamorphosed meteorites Lancé, Chainpur and Dimmitt have lost He and Ne. Allende and Murchison data are from Wieler *et al.* (1991; 1992).

4 Discussion

The CSSE analyses of this work have proven that noble gases of phase Q exist in the meteorites CO3.4 Lancé, H3.7 Dimmitt, CV3 (ox.) Grosnaja, LL3.4 Chainpur and CM2 Cold Bokkeveld and have further confirmed that Q-gases in different meteorite classes generally have very similar elemental and isotopic compositions, despite of the depletion of the light noble gases of many orders of magnitude relative e. g. to solar noble gases. However, our new data also provide insights into a "fine-structure" of phase Q and its noble gases (chapter 3.2). The composition is not identical for all samples nor for all etch steps, and the conclusion of Wieler (1994) and Huss et al. (1996) that Q is one single component has to be reconsidered.
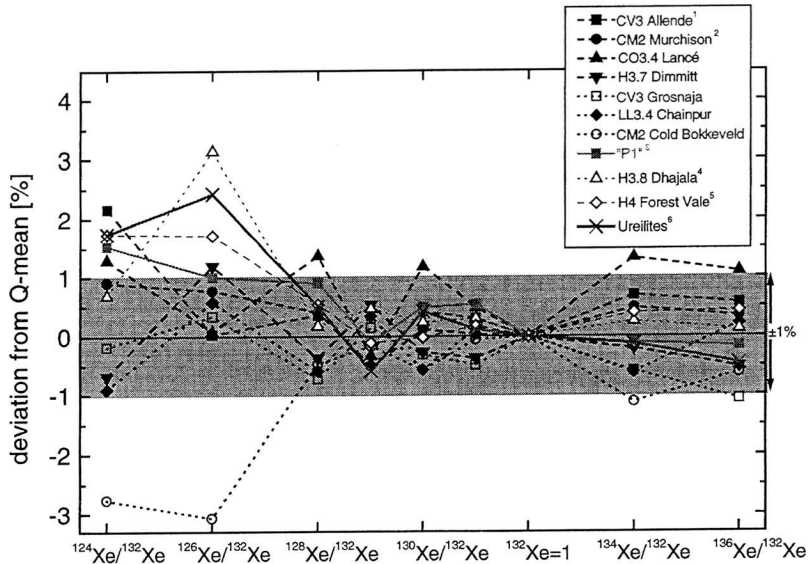
Figure 4.1: Xe isotopic ratios in different primordial reservoirs. Deviations from mean Xe-Q, obtained by all CSSE experiments on 7 chondrites of different classes, are mostly <1 %. References: [1] Wieler et al. (1991); [2] Wieler et al. (1992); [3] Huss et al. (1996); [4] Schelhaas et al. (1990); [5] Lavielle and Marti (1992); [6] Göbel et al. (1978).

4.1 Noble gas component Q in chondrites and ureilites

In this work, the assumption that only one, widely distributed, primordial component has been incorporated into all meteorite parent bodies at their formation is confirmed to be correct

for Ar, Kr and Xe. Table 4.1 lists the mean Xe-Q/Xe-P1 isotopic ratios, obtained by CSSE and by stepwise heating experiments, as well as "OC-Xe" from H3.8 Dhajala, H4 Forest Vale and mean ratios from 7 ureilites (Göbel et al., 1978; Schelhaas et al., 1990; Wieler et al., 1991; 1992; Lavielle and Marti, 1992; Huss et al., 1996). The ratios agree almost perfectly within their uncertainties, indicating that Xe-Q has been incorporated homogeneously and did not change its isotopic composition due to metamorphism or aqueous alteration. Even Xe from ureilites, which resides in diamonds and/or amorphous carbon that might have been formed in the solar nebula (Fukunaga et al., 1987; Fukunaga and Matsuda, 1997) is similarly composed, as can be seen in Figure 4.1. Ureilites contain noble gases with a "planetary" pattern similar to the Q-noble gases (Figure 4.10), and "normal" isotopic ratios almost identical with those of Q. Therefore, Ott et al. (1985a; 1985b) suggested that these ureilitic noble gases must be closely related to the primordial phase Q noble gases, although they reside in achondritic, heavily differentiated and partly shocked meteorites (Goodrich, 1992).

Table 4.1: Xe isotopic composition of primordial Q reservoirs. $^{132}Xe \equiv 100$.

	Q[1]	P1[3]	OC-Xe[4]	FVC/OC-Xe[5]	ureilites[6]
$^{124}Xe/^{132}Xe$	**0.455 ± 0.003**	0.462 ± 0.006	0.458 ± 0.009	0.463 ± 0.005	0.463 ± 0.006
$^{126}Xe/^{132}Xe$	**0.406 ± 0.002**	0.410 ± 0.005	0.419 ± 0.012	0.413 ± 0.003	0.416 ± 0.004
$^{128}Xe/^{132}Xe$	**8.23 ± 0.02**	8.30 ± 0.03	8.24 ± 0.07	8.27 ± 0.04	8.27 ± 0.05
$^{129}Xe/^{132}Xe$	**104.1 ± 0.02**[2]	104.0 ± 0.2	104.6 ± 0.6	104.0 ± 0.3	103.5 ± 0.5
$^{130}Xe/^{132}Xe$	**16.20 ± 0.04**	16.28 ± 0.04	16.24 ± 0.12	16.20 ± 0.05	16.27 ± 0.05
$^{131}Xe/^{132}Xe$	**81.86 ± 0.11**	82.30 ± 0.12	82.1 ± 0.7	82.0 ± 0.2	81.95 ± 0.13
$^{134}Xe/^{132}Xe$	**37.81 ± 0.12**	37.77 ± 0.11	37.9 ± 0.3	37.96 ± 0.11	37.76 ± 0.12
$^{136}Xe/^{132}Xe$	**31.67 ± 0.09**	31.61 ± 0.10	31.7 ± 0.2	31.80 ± 0.06	31.52 ± 0.19

[1] mean ratios for Q, obtained from all 7 CSSE experiments; [2] without Murchison; [3] mean of 14 CI, LL, L, H, EH, CV and CO chondrites, obtained by stepwise heating (Huss et al., 1996); [4] HF/HCl-resistant residue "R10" from H3.8 Dhajala which does not contain diamonds (Schelhaas et al., 1990); [5] H4 Forest Vale (Lavielle and Marti, 1992); [6] mean ratios from 7 ureilites, obtained by stepwise heating of carbon-rich separates (Göbel et al., 1978).

Few data are available for Kr-Q and related components. As for Xe, all data are similar to each other. Kr in ureilites shows no deviations from Kr-Q (Table 4.2). Slight differences can be found between the $^{36}Ar/^{38}Ar$ ratio in Q and in ureilites (Table 4.2). Ar in ureilites tends to have somewhat lower $^{36}Ar/^{38}Ar$ ratios than Ar-Q. However, considering the uncertainties, it is justified to assume that Ar-Q is uniform in chondrites and ureilites. Both measurements for Allende and Murchison gave values of $(^{36}Ar/^{38}Ar)_Q = 5.29 \pm 0.02$, while the newer CSSE examinations of Q and data for P1 (Huss et al., 1996) revealed ratios between 5.33 and 5.37 (Table 3.9). The extraordinarily low $^{40}Ar/^{36}Ar$ ratios of as low as $(2.9 \pm 1.7) \times 10^{-4}$ found in ureilites (Göbel et al., 1978) indicate that ^{40}Ar in etch steps with $^{40}Ar/^{36}Ar$ ratios of ~1 (Table 3.9) is mainly radiogenic. The isotopic compositions of Ar, Kr and Xe in phase Q and ureilites

are thus, except for $^{40}Ar/^{36}Ar$, identical. Not considering the trapping mechanisms, their carrier phases and their origin, these noble gases should be seen as one single component.

Table 4.2: Ar and Kr isotopic compositions of primordial Q reservoirs. $^{84}Kr \equiv 100$.

	Q[1]	P1[3]	"OC"-Ar/Kr[5]	ureilites[6]
$^{36}Ar/^{38}Ar$	5.34 ± 0.02	5.33 ± 0.03	5.29 ± 0.13	5.26 ± 0.06
$^{78}Kr/^{84}Kr$	0.602 ± 0.004[2]	0.66 ± 0.06[4]	0.62 ± 0.01	0.601 ± 0.008[7]
$^{80}Kr/^{84}Kr$	3.935 ± 0.008	3.97 ± 0.03	4.03 ± 0.07	3.99 ± 0.05
$^{82}Kr/^{84}Kr$	20.18 ± 0.02	20.24 ± 0.03	20.23 ± 0.19	20.37 ± 0.18
$^{83}Kr/^{84}Kr$	20.19 ± 0.02	20.21 ± 0.05	20.32 ± 0.18	20.26 ± 0.15
$^{86}Kr/^{84}Kr$	30.98 ± 0.05	30.91 ± 0.09	31.0 ± 0.3	30.91 ± 0.12

[1] mean ratios for Q, obtained from all 7 CSSE experiments; [2] without Allende (Wieler *et al.*, 1991) and Dimmitt; [3] mean of 14 CI, LL, L, H, EH, CV and CO chondrites, obtained by stepwise heating (Huss *et al.*, 1996); [4] probably too high due to benzene background; [5] HF/HCl-resistant residue "R10" from H3.8 Dhajala which does not contain diamonds (Schelhaas, 1987); [6] mean ratios from 7 ureilites, obtained by stepwise heating (Göbel *et al.*, 1978); [7] from ureilite Kenna, obtained by stepwise heating (Wilkening and Marti, 1976).

We can not report such a perfect agreement for Ne. The reliable $(^{20}Ne/^{22}Ne)_Q$ ratios lie in a range between 10.05 ± 0.05 and 10.7 ± 0.2 (Table 3.2) and show a binary distribution. This is not explainable with experimental uncertainties. We will see in chapter 4.2.2 that these differences are also not the result of metamorphic processes. $^{20}Ne/^{22}Ne$ ratios in ureilites fall also in the interval, inferred by the chondritic data (Table 4.3). Due to the relatively large uncertainties of the ureilitic values, it is not clear, whether they fill the gap between the chondrite groups with high and low $(^{20}Ne/^{22}Ne)_Q$ ratios. He data from other non-chondritic meteorite gas components possibly related to Q are not available. We can conclude that the Ne, Ar, Kr and Xe isotopic ratios in the chondritic phase Q and in ureilites are identical, although the elemental compositions of both noble gas components are distinct (Figure 4.10).

Table 4.3: Ne isotopic ratios in ureilites.

sample	$^{20}Ne/^{22}Ne$	$^{21}Ne/^{22}Ne$	source
deduced from 7 ureilites[1]	10.70 ± 0.25	*0.03-0.05*	Göbel *et al.* (1978)
Hajmah "Ne-U"	10.4 ± 0.3	0.027 ± 0.003	Ott *et al.* (1985a)
ALHA 78019	10.5 ± 0.7	0.032 ± 0.003	Wacker (1986)
weighted mean	**10.57 ± 0.19**	0.030 ± 0.003	

[1] Dingo Pup Donga, Dyalpur, Goalpara, Havaroe, Kenna, North Haig, Novo Urei

4.2 Alteration processes and phase Q

In this section, I want to discuss the possible influence of metamorphic events on the meteorite parent bodies on the compositions of noble gases of phase Q. In the first part, the

elemental ratios obtained in this work are compared with other ratios and with total abundances. However, the information to be derived from the analysis of Q-gas concentrations is rather limited, as we will see. In the second part, the Ne isotopic composition is discussed, since Ne is the only noble gas from phase Q that shows significant differences between the meteorites.

4.2.1   Alteration processes and Q elemental ratios

Undoubtedly, thermal metamorphism alters the elemental abundances of primordial noble gases in chondrites. Concentrations of primordial ^{36}Ar and ^{132}Xe are two of several (mostly petrographic) parameters which are used to determine the petrographic type and subtype of ordinary chondrites (van Schmus, 1967; Sears et al., 1980; Anders and Zadnik, 1985). A well-established correlation between the abundances of the heavier Q-noble gases (as well as the abundances of presolar grains) and the metamorphic history has been described by Huss et al. (1996), assuming that all chondrites have sampled gases of the same composition. However, He and Ne data were not considered or yielded inconsistent results. In addition to *thermal processes* that may have modified phase Q, Browning et al. (1996) suggested that *aqueous alteration* also destroys the primary carrier phase of the trapped noble gases. This is to be addressed below.

Ar, Kr and Xe...

Petrographic observations of the effect of thermal metamorphism and aqueous alteration on chondrites are displayed in Figure 4.2. Originally, it was assumed that chondrites of petrographic type 1, as classified according to Van Schmus (1967), are the least altered meteorites and especially type 4-6 chondrites have suffered increasing thermal metamorphism. However, since it turned out that CM and, especially, CI chondrites are aqueously altered, type 3 carbonaceous chondrites might better represent unaltered nebular matter (McSween, 1979). Sears et al. (1980) introduced a petrologic subclassification for type 3 unequilibrated ordinary chondrites (Figure 4.2 below) with subtypes 3.0-3.9 which has later been applied also on CO chondrites (Scott and Jones, 1990). The subclassification is based, among other properties, on thermoluminescence (TL). A higher classification should, similar to the main petrographic classification, be correlated with a more severe metamorphic history. However, aqueous alteration has been observed for those meteorites which have first been classified as most unequilibrated, e. g. LL3.0 Semarkona, LL3.1 Bishunpur or CO3.0 Colony (Hutchison et al.,

1987; Keck and Sears, 1987). The low thermoluminescence of these samples is attributed to aqueous processes which have changed the original petrographic type to lower values (Guimon *et al.*, 1988). Therefore, samples of petrographic type *3.2* and *3.3* of both, the CO3 and LL chondrites, as well as the CV3 chondrites are the least altered meteorites. We will see now that the heavy noble gases of phase Q reflect this alteration classification.
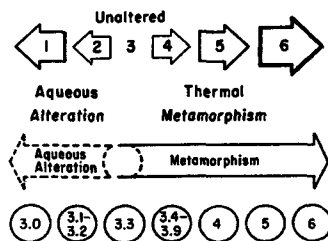
Figure 4.2: Thermal metamorphism and *aqueous alteration processes affect carbonaceous chondrites (above) and unequilibrated ordinary chondrites (below).* Figure from Sears and Dodd (1988).

Figure 4.3 shows a three-element-plot of the heavier Q-noble gases Ar, Kr and Xe in HF/HCl-resistant residues. The filled squares symbolise the direct Q-measurements by CSSE and stepwise combustion data of H3.8 Dhajala (Schelhaas *et al.*, 1990). The other data which were obtained conventionally are also considered to be reliable due to the predominant abundances of phase Q in the residues. $(^{36}Ar/^{132}Xe)_Q$ is clearly correlated with $(^{84}Kr/^{132}Xe)_Q$ and the chemical class or the petrographic (sub)type, respectively, of the meteorites. Indicated by the highest ratios, the CV3 and CO3 chondrites seem to be the least metamorphosed meteorites, while the ordinary and CM2 chondrites show lower values and thus more alteration, in accordance with the petrographic results outlined above. This is reflected e. g. by lower $(^{36}Ar/^{132}Xe)_Q$ and $(^{84}Kr/^{132}Xe)_Q$ ratios in CI Orgueil compared to CV3 Leoville, Vigarano and CO3 Kainsaz (Figure 4.3). These data were obtained by Huss *et al.* (1996), who have chosen in particular CI Orgueil and the LL3.0/3.1 chondrites to be most suitable to study the *thermally* least processed primary characteristics of P1. However, Figure 4.3 shows that obviously also *aqueous alteration* changes the elemental abundances of the Q-noble gases. Different grades of alteration within chondritic classes, which have been deduced by petrographic observations, can be confirmed with the Q-noble gases:

- The CSSE data for Ar, Kr and Xe confirm the aqueous alteration sequence that was found for **CM chondrites** by Browning *et al.* (1996). They stated that Cold Bokkeveld

is the most heavily aqueously altered CM chondrite. This can be seen in the noble gas data in Figure 4.3, since Cold Bokkeveld contains Q with $(^{36}Ar/^{132}Xe)_Q$ and $(^{84}Kr/^{132}Xe)_Q$ ratios lower than for CM2 Murchison and as low as the more thermally metamorphosed H3.7/8 chondrites Dimmitt and Dhajala.

- As described above, ordinary chondrites of petrographic types 3.2-3.0 are affected by increasing aqueous alteration rather than by thermal metamorphism. Therefore, **LL chondrites** of petrographic type *3.0* and *3.1*, e. g. Semarkona and Krymka, are more altered than LL3.4 Chainpur which indeed shows higher $(^{36}Ar/^{132}Xe)_Q$ and $(^{84}Kr/^{132}Xe)_Q$ ratios and, thus, supports the TL data.

- Guimon *et al.* (1995) found differences among **CV3 chondrites** due to low-temperature parent body metamorphism and introduced a petrologic subdivision similar to CO3 chondrites and UOCs. This subdivision has been taken into account in Figure 4.3. Guimon *et al.* could not find a correlation of the TL sensitivity with the noble gas abundances of ^{4}He, ^{20}Ne and ^{36}Ar. They used *bulk* concentrations which, especially for the light noble gases He and Ne, can not lead to reasonable results without correcting for the more abundant radiogenic ^{4}He and cosmogenic ^{20}Ne. The data points in Figure 4.3, however, show that the *reduced* CV3 chondrites suffered higher losses of Q-gases then the *oxidised* CV3 chondrites and, in general, samples of lower subtype show higher ratios.

- **H and L chondrites** of subtype $\geq$ 3.6 clearly cluster in the lower left of Figure 4.3 with the lowest elemental ratios. Thus, the heavier noble gases in unequilibrated ordinary chondrites do show a trend depending on the metamorphic history, in contrast to observations by Huss *et al.* (1996).

- Finally, Figure 4.3 suggests that the **CO3.1 chondrite** Kainsaz suffered more severe aqueous alteration than CO3.3 Ornans and CO3.4 Lancé. Aqueous alteration has been suggested for Kainsaz only by analogy considerations (Rubin, 1998).

We can conclude that aqueous alteration *and* thermal metamorphism on the parent bodies affect the carrier phase Q of the *heavier* primordial noble gases and deplete Ar and Kr relative to Xe. Ar/Xe and Kr/Xe ratios are suitable to detect influences of both kinds of processing of the original parent body material. However, the fractionation mechanism that led to a stronger depletion of the lighter noble gas elements relative to the heavier ones remains unclear. A "wholesale destruction" of the primary noble gas carrier, as proposed by Browning *et al.* (1996), would release all noble gases completely. The clear dependence of the Ar/Xe and Kr/Xe ratios on the thermal metamorphic/aqueous alteration history suggests that Ar, Kr and

Xe have been homogeneously incorporated into all chondrite classes with a composition similar to that in CV3 and CO3 chondrites. Generally, meteorites of subtypes 3.2-3.4 of all meteorite classes show the highest Ar/Xe and Kr/Xe ratios.

Figure 4.3: $(^{36}Ar/^{132}Xe)_Q$ vs. $(^{84}Kr/^{132}Xe)_Q$ plot. CSSE and stepwise combustion data are labelled with filled squares. References: [1] Alaerts et al. (1979b); [2] Alaerts et al. (1979a); [3] Schelhaas et al. (1990); [4] Srinivasan et al. (1977); [5] Wieler et al. (1991); [6] Wieler et al. (1992); [7] Moniot (1980); [8] Matsuda et al. (1980); [9] Huss et al. (1996); [10] this work, data from a bulk non-oxidised residue (chapter 7.6) applicable since Dhajala does not contain diamonds (Schelhaas et al., 1990).

Huss et al. (1996) observed that Ar/Xe and Kr/Xe ratios in CV and CO chondrites are higher, in accordance with Figure 4.3, but also that the Ne/Xe ratios are *lower* than in CI and LL3.0/1 chondrites. They attributed this observation to nebular processing of phase Q in CV chondrites prior to accretion and a mixture of two components for CO3.2 Kainsaz. This inference is not warranted if one assumes that aqueous alteration has lowered the Ar/Xe and Kr/Xe ratios of the CI and LL3.0/3.1 chondrites. However, the observations by Huss et al. give us a hint that He and Ne might behave somehow differently from Ar, Kr and Xe.

He, Ne and Ar...

A plot (Figure 4.4) similar to Figure 4.3 shows the lighter elemental ratios $(^4He/^{36}Ar)_Q$ and $(^{20}Ne/^{36}Ar)_Q$. The database for He and Ne is much smaller than for the heavier noble gases due to the difficulty to exactly determine He-Q and Ne-Q by conventional pyrolysis techniques. Nevertheless, the conventionally deduced data possibly suggest a rough trend. However, large differences between data obtained by the "difference method" and by CSSE for Chainpur, Murchison, and Allende indicate that they are useable for our comparison only very carefully. Our new CSSE data alone indicate a more clear-cut correlation and we will use mostly these data.
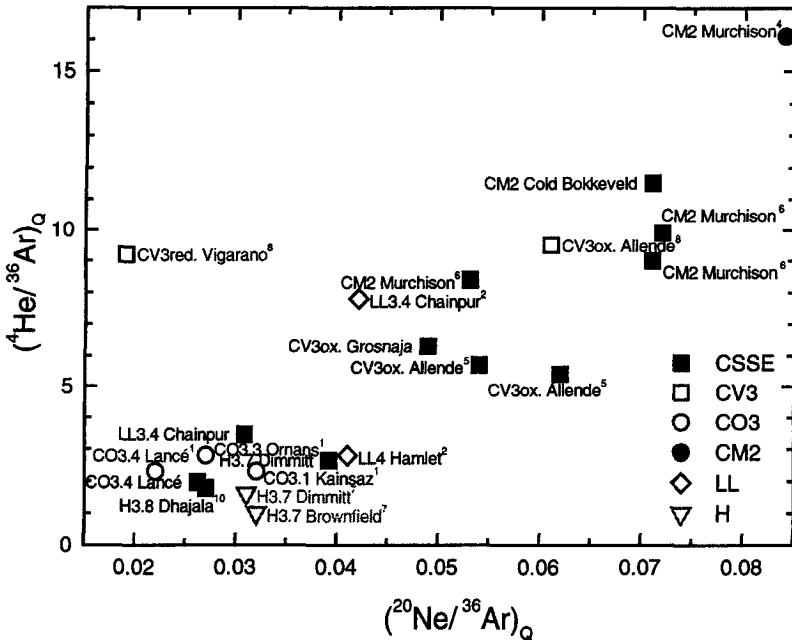
Figure 4.4: $(^4He/^{36}Ar)_Q$ vs. $(^{20}Ne/^{36}Ar)_Q$ plot. CSSE and stepwise combustion data are labelled with filled squares. The regression line is obtained from these data. See Figure 4.3 for references.

$(^4He/^{36}Ar)_Q$ correlates with $(^{20}Ne/^{36}Ar)_Q$, similar to the correlation observed above for Ar/Xe and Kr/Xe. In contrast to the elemental ratios of the heavier noble gases which clearly reflect thermal metamorphism *and* aqueous alteration, respectively, experienced on the parent bodies, the $(^4He/^{36}Ar)_Q$ and $(^{20}Ne/^{36}Ar)_Q$ ratios show a distinct trend: CM2 chondrites show the highest

ratios while the less aqueously altered CO chondrites reveal very low $(^4He/^{36}Ar)_Q$ and $(^{20}Ne/^{36}Ar)_Q$ ratios. The noble gases of CO3.4 Lancé are similarly composed as the unequilibrated chondrites LL3.4 Chainpur and H3.7 Dimmitt. All these meteorites experienced thermal alteration, as indicated by the petrographic classification $\geq$ 3.4. However, *if* one assumes one carrier phase for all noble gases, thermal metamorphism can not be the reason for the low He/Ar and Ne/Ar ratios of the CO chondrites, since the heavier elemental Ar/Xe and Kr/Xe ratios do not indicate any depletion of Ar and Kr relative to Xe compared to other chondrite classes (see Figure 4.3).

Light vs. heavy Q-noble gases...

A comparison of Figure 4.3 with Figure 4.4 suggests that metamorphism and aqueous alteration affect the lighter and heavier noble gases of phase Q *differently*. This is also indicated by a rather uncorrelated pattern of the data points in a $^{20}Ne/^{132}Xe$ vs. $^{84}Kr/^{132}Xe$ plot (not shown). This could point to two scenarios. Either there is one carrier phase Q that preferentially loses He and Ne upon *thermal processes*, but Ar and Kr upon *aqueous alteration*. This seems very unlikely. Or the observations could point to the existence of two carrier phases Q_1 and Q_2 which are differently resistant to both kinds of alteration process and contain distinct amounts of He and Ne. Two subcomponents have been already suggested in chapter 3.2 and will be further discussed in chapter 4.4. Note that these possible subphases must be closely related, since the most significant characteristic of the Q-noble gases, the "planetary" depletion of He-Q relative to Xe-Q and solar abundances has been observed in all samples (Figure 3.26). However, this plot also point to slightly different He abundances for the CV3 and CM2 chondrites with high $(He/Xe)_Q$ ratios and the other chondrites with lower $(He/Xe)_Q$ ratios.

Ar, Kr and Xe elemental ratios are in general suitable to trace alteration on the parent bodies. Primordial differences in the composition of the Q reservoir prior to incorporation into the parent bodies seem unlikely in view of the good correlation of the $(^{36}Ar/^{132}Xe)_Q$ and $(^{84}Kr/^{132}Xe)_Q$ ratios with the degree of parent body alteration (Figure 4.3). Ne, and in particular He, seem to monitor the abundance of the possible phase Q_1. This phase Q_1 seems easier to etch (chapter 3.2). Possible is also that He and Ne are released more easily from Q_1 due to mild thermal metamorphism but not due to aqueous alteration. Q_1 appears to be more abundant in CM2 and CV3 (ox.) chondrites than in all other meteorite classes (Figure 3.26 and Figure 4.3).

Browning *et al.* (1996) found a negative correlation between the primordial ^{36}Ar concentrations and a "mineralogical alteration index", describing the degree of aqueous alteration suffered by CM chondrites. They deduced that in CM chondrites the carrier phase of

the primordial noble gases is susceptible to aqueous alteration. The more altered CM2 Cold Bokkeveld indeed contains less ^{36}Ar than CM2 Murchison (chapter 3.3 and Figure 4.5). In addition, as demonstrated above, the (Ar/Xe)$_Q$ and (Kr/Xe)$_Q$ ratios confirm this suggestion for CM chondrites but also suggest a similar susceptibility to aqueous alteration for meteorites of different classes. This has been deduced without having considered the absolute gas-concentrations.

While aqueous alteration clearly affect the elemental (Ar/Xe)$_Q$ and (Kr/Xe)$_Q$ ratios, a correlation between the ^{36}Ar concentration and the degree of aqueous alteration can not be deduced (Figure 4.5). This, and also the absolute ^{132}Xe abundances for P1, deduced by Huss *et al.* (1996) and plotted in Figure 4.6, show that the concentrations of the heavier Q-gases are more affected by thermal metamorphism. However, in the next section, we will discuss that the absolute Q-gas abundances are only roughly correlated with the alteration history.

Ratios vs. abundances...

In 1979 Alaerts *et al.* reported that the (^{20}Ne/^{36}Ar)$_Q$ ratios in nine LL-chondrites *decrease* with petrographic type and increasing ^{36}Ar concentrations per gram dissolved "mineral" Q. They suggested from this that the trapped noble gas abundances have been established at the time of condensation of the LL-parent body from a cooling solar nebula. According to their condensation model, samples that condensed first at higher temperatures had been less volatile-rich than meteorites that condensed later but with predominant Ne, since Ne has a smaller temperature dependence of its solubility. Since the first condensates had been located closer to the centre of the asteroid, they suffered more severe metamorphism and represent now the meteorites of higher petrographic type. In contrast, if the parent body would have sampled more or less homogeneously Q-noble gases in similar elemental proportions, subsequent metamorphic losses would lead to *increasing* (^{20}Ne/^{36}Ar)$_Q$ ratios with increasing ^{36}Ar content and decreasing petrographic type.

The trend observed by Alaerts *et al.* has not been found by other groups. The analyses of three CO3-chondrites (Alaerts *et al.*, 1979b) confirmed, according to the authors, this LL-chondrite trend of decreasing (^{20}Ne/^{36}Ar)$_Q$ with increasing ^{36}Ar content. However, considering the data points of these three CO3-chondrites separately yields an opposite trend. In addition, Moniot (1980) analysed three H chondrites and did not find this inverse correlation between (^{20}Ne/^{36}Ar)$_Q$ and trapped ^{36}Ar. Ott *et al.* (1981) doubted the usefulness of the (^{20}Ne/^{36}Ar)$_Q$ ratio as a "condensation cosmothermometer" that should indicate different condensation temperatures, because of the insufficient abundances of Ne in Q relative to other

primordial Ne components in acid-resistant residues and because of different weight losses upon etching.
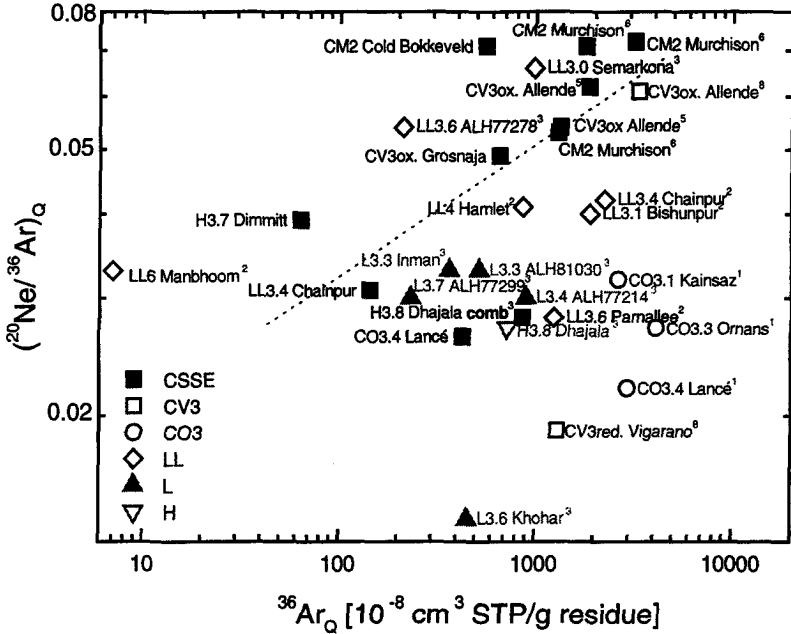
Figure 4.5: $(^{20}Ne/^{36}Ar)_Q$ vs. $^{36}Ar_Q$ concentration of HF/HCl-resistant residues. The ^{36}Ar concentrations are calculated per gram residue. Filled squares indicate Q data obtained by CSSE or stepwise combustion. The regression line is obtained from these data. All other data points are calculated from concentrations of oxidised and non-oxidised residues. See caption of Figure 4.3 for references.

At that time, all Ne-Q concentrations were calculated by difference. However, our new data obtained by CSSE should be able to definitely prove or contradict the hypothesis of Alaerts *et al.* (1979a). Figure 4.5 shows $(^{20}Ne/^{36}Ar)_Q$ ratios vs. ^{36}Ar contents. The concentrations have been calculated per gram *residue* in order to allow a comparison of residues produced by different demineralisation procedures. The direct Q-gas measurements by CSSE and stepwise combustion of H3.8 Dhajala do not show any trend of a decreasing $(^{20}Ne/^{36}Ar)_Q$ ratio with increasing ^{36}Ar concentration. In contrast, the regression line obtained by these data points rather indicates the opposite trend. Furthermore, the data obtained as differences between non-oxidised and oxidised residues also do not support a scenario as suggested by Alaerts *et al.* Probably, their correlation was an artefact due to errors in the weight determination of

"mineral" Q. As stated already in chapter 2.2.1, weight losses upon etching strongly vary (between 1-95 %, Table 2.4 and Table 2.5). For example, Alaerts et al. (1979a) determined for Chainpur a $^{36}Ar_Q$ concentration of 2.5 x 10^{-4} cm^3 STP/g mineral. Assuming an etch loss of 1 %, we would obtain at maximum 1.5 x 10^{-4} cm^3 STP/g phase Q, but assuming a more typical loss of 5 % (Table 2.5), we would obtain only 3 x 10^{-5} cm^3 STP/g phase Q which is one order of magnitude lower than the concentration given by Alaerts et al.
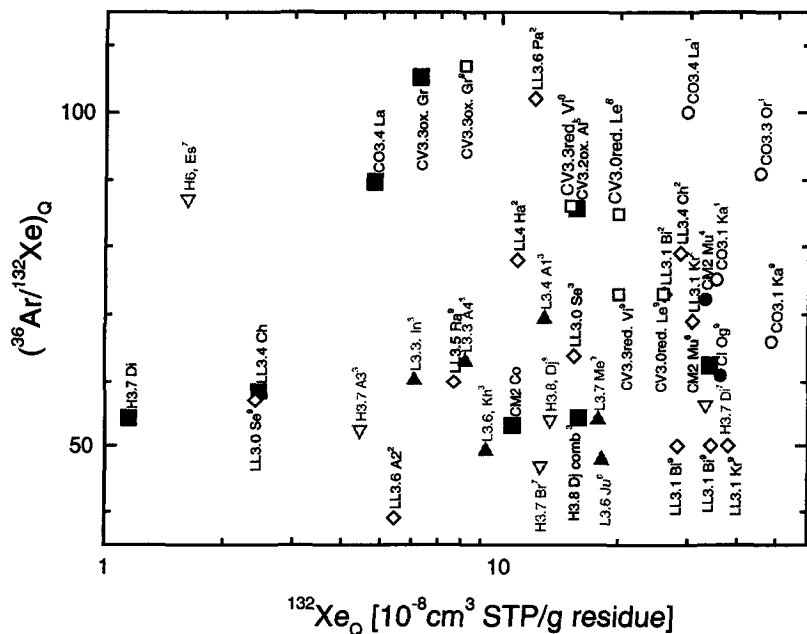
Figure 4.6: The ratio $(^{36}Ar/^{132}Xe)_Q$ vs. the $^{132}Xe_Q$ concentration does not show any correlation, although this would be expected for losses due to parent body alteration. Filled squares indicate Q analysis with CSSE or stepwise combustion. See caption of Figure 4.3 for references.

A plot similar to Figure 4.5 for heavier noble gases, showing the element ratio $^{36}Ar/^{132}Xe$ vs. ^{132}Xe abundance (Figure 4.6), does not reveal any correlation. However, losses due to alteration processes should lead to both lower ^{132}Xe *concentrations* and lower $^{36}Ar/^{132}Xe$ *elemental ratios* and both should thus correlate. In contrast, the elemental ratios $^4He/^{36}Ar$ and $^{20}Ne/^{36}Ar$ as well as $^{36}Ar/^{132}Xe$ and $^{84}Kr/^{132}Xe$, respectively, do correlate to some degree with each other, as outlined above. This leads to the question whether the total Q-gas concentrations in meteorites are determined by different mechanisms prior to any alteration process. This could mean that the primordial concentrations are not similar in all chondrites, in contradiction to the suggestion

of Huss *et al.* (1996). On the other hand, it could also simply be the result of the largely varying demineralisation procedures and yields. Since the CSSE data, which are less dependent on sample weights, vary in a similar way as the conventional obtained data, the first option seems to be more realistic.

4.2.2 Alteration processes and Q isotopic ratios

The effect of alteration of the Q-carrier on the isotopic ratios of a putative original Q-composition are more difficult to detect than those on elemental ratios, since mass differences between different isotopes of an element are much smaller than those between different noble gas elements. Ar, Kr and Xe isotopic ratios for all 7 CSSE experiments (Table 3.9, Table 3.11 and Table 3.13) do not show any deviation from each other and thus no correlation with the petrographic classification of the samples. Huss *et al.* (1996), however, could detect small differences between the Xe isotopic compositions of relatively unmetamorphosed (Xe-P1) and strongly metamorphosed meteorites, respectively. The latter are diamond-poor and diamond-free meteorites. Small contributions of Xe-HL seem to have been retrapped by phase Q upon dissolution or destruction of the less refractory part of these presolar diamonds. This process could have happened during metamorphism or might have occurred during sample preparation.

Of all Q-noble gases, Ne shows the largest variations in the isotopic composition between the different meteorites studied. The $(^{20}Ne/^{22}Ne)_Q$ ratios vary between 10.0 and 10.7. The $(^{20}Ne/^{22}Ne)_Q$ vs. $(^4He/^{20}Ne)_Q$ and $(^{20}Ne/^{22}Ne)_Q$ vs. $(^{36}Ar/^{132}Xe)_Q$ plots in Figure 4.7 and Figure 4.8, respectively, provide a test of whether the different Ne isotopic ratios can be explained by alteration processes, similar to the elemental ratios. No correlation is visible in the two figures, *wherein only the CSSE and combustion data are precise enough to prove or exclude any trend.* The three samples Dhajala, Lancé and Cold Bokkeveld with low $(^{20}Ne/^{22}Ne)_Q$ ratios of about 10.1 have largely varying elemental ratios. These meteorites do not have a similar chemical classification and they have not suffered similar alteration. The $(^{20}Ne/^{22}Ne)_Q$ ratios for Allende, Murchison, Dimmitt, Grosnaja and Chainpur are identical within the uncertainties and give a mean value of $(^{20}Ne/^{22}Ne)_Q = 10.65 \pm 0.02$. *The values obtained from ureilites are very similar* to this mean value, though with large errors, and lead to a weighted mean of $(^{20}Ne/^{22}Ne)_{Ureilites} = 10.57 \pm 0.19$ (Table 4.3). This agreement between chondrites and achondrites points to a primordial $(^{20}Ne/^{22}Ne)_Q$ ratio in the range of 10.6-10.7. However, an unknown mechanism must be responsible for the lower values for Dhajala, Lancé and Cold Bokkeveld. Further examinations should answer whether the mean value of 10.11 ± 0.04 has been matched

accidentally by these three samples or if this match might be the result of another sub-structure of the noble gases in phase Q.
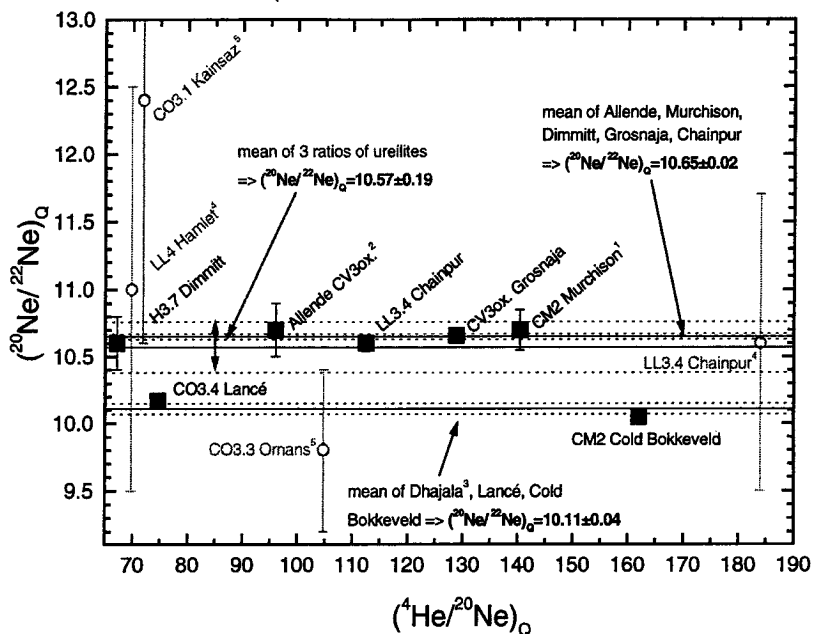
Figure 4.7: The $(^{20}Ne/^{22}Ne)_Q$ vs. $(^4He/^{20}Ne)_Q$ plot does not show any correlation which could point to alteration-depending Ne isotopic ratios. Filled squares symbolise CSSE. The combustion experiment on Dhajala did not yield He data (Schelhaas et al., 1990). Open symbols label pyrolysis data. References: [1] average of 3 runs (Wieler et al., 1992); [2] average of 2 runs (Wieler et al., 1991); [3] stepwise combustion (Schelhaas et al., 1990); [4] Alaerts et al. (1979a); [5] Alaerts et al. (1979b).

A possible mechanism for lowering the $(^{20}Ne/^{22}Ne)_Q$ ratios might be the retrapping of Ne-HL with a low $^{20}Ne/^{22}Ne$ of 8.50 (Table 3.1) upon metamorphic destruction of the diamonds, as proposed for Xe-HL and Xe-Q (Huss et al., 1996) or retrapping of Ne-E. Huss et al. determined similarly low $(^{20}Ne/^{22}Ne)_Q$ ratios of 9.7 and 10.1[12] (Table 3.2) for EH4 Abee and L3.6 Julesburg, respectively. Julesburg, Abee and H3.8 Dhajala are indeed (essentially) presolar

---

[12] Huss et al. determined regression lines, assuming that the Ne, released from Abee and Julesburg by stepwise heating, is a mixture of cosmogenic and "modified P1", without significant contributions of presolar Ne. I recalculate both $^{20}Ne/^{22}Ne$ ratios for $(^{21}Ne/^{22}Ne)_Q = 0.0294$, instead of 0.035, used by Huss et al. Estimated from the original plots, the errors for the $^{20}Ne/^{22}Ne$ ratios amount to about ±0.7.

diamond-free (Schelhaas *et al.*, 1990; Huss, 1997). On the other hand, H3.7 Dimmitt also contains only traces of presolar diamonds but showed a high $(^{20}Ne/^{22}Ne)_Q$ value, while Cold Bokkeveld and Lancé have high abundances of diamonds and a low Ne isotopic ratio (Huss, 1997). Hence, not all results can be explained with the addition of Ne-HL from diamonds. Therefore, a correlation between the abundance of diamonds, and thus the metamorphic history, and the $(^{20}Ne/^{22}Ne)_Q$ ratios is not generally applicable to explain the observed variations.
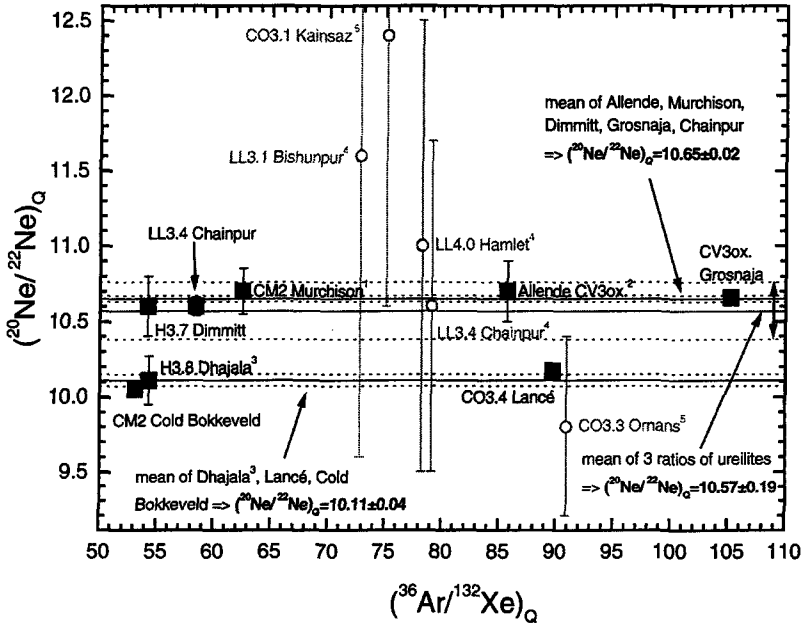
Figure 4.8: The same plot as Figure 4.7, but with the elemental ratio $(^{36}Ar/^{132}Xe)_Q$, also does not indicate any correlation. For references see Figure 4.7.

4.3 The primordial Q composition

Even if the noble gas data suggest two carrier phases Q reacting differently upon aqueous alteration and thermal metamorphism, it is still likely that the composition of the Q-gases, which have originally been incorporated, are identical. The elemental composition of the heavier elements seems to be best preserved in CV3 Grosnaja and in CO3.4 Lancé. However, it can not be ruled out that these ratios are still lower limits to the "true" primordial Q, especially in view of the much higher elemental Ar/Xe and Kr/Xe ratios found in carbon-rich separates of ureilites (Figure 4.10). For He, Ne and Ar ratios, *the noble gas composition in CM2 chondrites*

is the best choice to determine a primordial Q elemental composition. The isotopic compositions of all elements except for Ne are unaffected by these fractionation processes, as shown above, and the isotopic ratios should therefore be identical to the originally incorporated Q-gases. As demonstrated e. g. in Figure 4.6, it is very doubtful if one can give reliable concentrations that could be regarded as a general primordial Q-gas concentration, as has been suggested by Huss *et al.* (1996).

4.4 The nature of phase Q

After the discovery of phase Q Lewis *et al.* (1975) assumed a hypothetical Fe/Ni/Cr-sulfide as the carrier mineral, but it soon turned out that the Q-noble gases must reside in a carbonaceous compound while sulfides and chromite could be excluded (Phinney *et al.*, 1976; Frick and Chang, 1977; 1978; Frick and Pepin, 1981; Ott *et al.*, 1981). However, the nature of this carbonaceous carrier has still not been identified. Wacker *et al.* (1985) and Wacker (1989) suggested that Q-noble gases are located at or near grain surfaces in a layer of amorphous carbon, trapped by adsorption on interior surfaces in a sheltered labyrinth of micropores at temperatures of 300-400 K in the solar nebula. Heymann (1998) proposed so called nanotubes with caps that are removable by HNO_3 to be the carbonaceous carrier phase of the Q-gases. He retreated his earlier proposal that fullerenes may be phase Q (Heymann, 1986).

A new approach by Sandford *et al.* (1997; 1998) tries to simulate the conditions in a typical interstellar dense molecular cloud with temperatures of 10-25 K. These authors exposed a metal foil to an assumed "realistic" composition of ices, noble gases, organic material and UV photons which produces more refractory organic structures. The samples were warmed after the deposition of 10-20 layers which resulted in an organic residue. They succeeded in enriching Xe relative to Kr and also reached concentrations in these residues as high as those of Q-gases observed in carbonaceous chondrites. However, the gas retentivity of the organic matter is still not sufficient to regard the residues as a proper analogue of phase Q, since Kr and Xe are completely released already at 250 °C, far lower than the main release temperatures of more than 1000 °C observed for phase Q (Huss *et al.*, 1996). On the other hand, this could also point to a subsequent mechanism that has fixed the noble gases in phase Q. It would be interesting to see if Sandford and co-workers could also succeed in reproducing the strong depletion for Ne observed in phase Q.

Another group succeeded for the first time in enriching Q-gases solely by physical separation techniques (Amari and Matsuda, 1998; Matsuda *et al.*, 1999). These authors applied a freeze-thaw disaggregation technique to yield residues from Allende with noble gas

concentrations almost as high as those of HF/HCl-resistant residues. However, this does not necessarily mean that phase Q is an original, discrete, separable phase. A residue will be also analysed with CSSE to better characterise especially the lighter noble gases and allow for a better comparison of freeze-thaw disaggregation and HF/HCl-resistant residues.
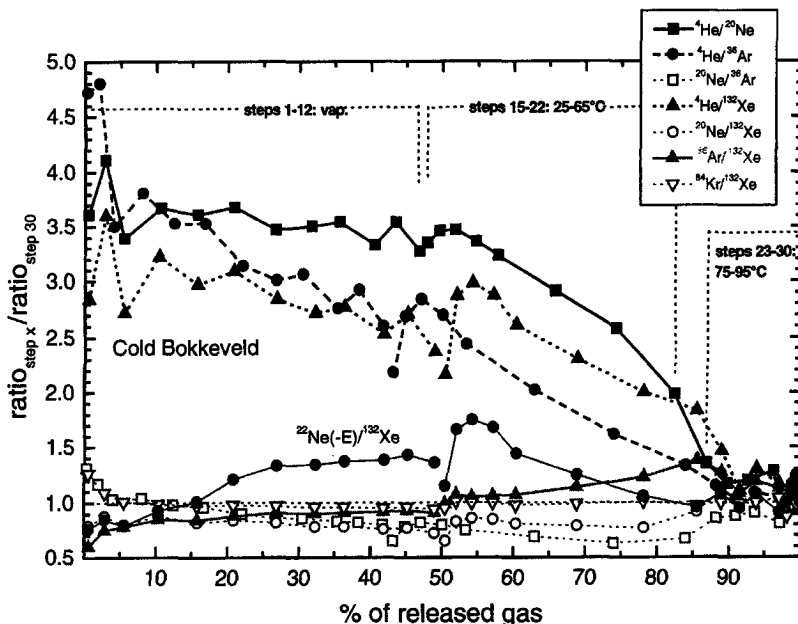
Figure 4.9: Elemental ratios of all steps released from Cold Bokkeveld, normalised with ratios of step 30, similar to Figure 3.23, but the ratios are referred to the released gas amounts of the respective denominators. The ratio $^{22}Ne/^{132}Xe$ was added in order to demonstrate the possibly related release of Ne-E and Q_1-gases.

Our new CSSE data provide evidence for the existence of at least two "sub-components" of the carrier phase Q. This is particularly obvious from Figure 3.23 which shows higher $^4He/^{20}Ne$, $^4He/^{36}Ar$ and $^4He/^{132}Xe$ ratios in steps 1-22 than in the last steps 23-30 of the experiment on CM2 Cold Bokkeveld. The other meteorites also support this suggestion since the elemental ratios obtained from the first and second part of each run vary similarly to Cold Bokkeveld (Figure 3.22). Few hints on a complex character of phase Q have been published so far. Gros and Anders (1977) carried out a stepwise etching experiment with HNO_3 on an HF/HCl-resistant residue of Allende. They suggested two sub-phases[13]: Q_1, soluble in cold diluted

---

[13] Q_1 and Q_2 from Gros and Anders (1977) are underlined in order to distinct these subcomponents from those suggested in chapter 3.2.

HNO$_3$, with a Fe/Cr ratio of >20 which should contain most of the heavy noble gases and Q$_2$, slowly soluble in hot concentrated HNO$_3$ with a Fe/Cr ratio of ~0.5. Q$_2$ was roughly estimated to be at least one order of magnitude poorer in the heavy noble gases than Q$_1$. Gros and Anders suggested that Q$_1$ consists of a sulfide with composition (Fe$_{84}$Ni$_{12}$Cr$_4$,)S$_x$ while Q$_2$ maybe is daubréelite (FeCr$_2$S$_4$) or a variety of chromite (FeCr$_2$O$_4$), but later work has shown that the Q-noble gas carriers must be carbonaceous (Frick and Chang, 1978; Ott *et al.*, 1981). *Our subcomponents* Q$_1$ *and* Q$_2$ *seem to be similarly susceptible to* HNO$_3$ *dissolution as* Q$_1$ *and* Q$_2$, respectively, and contain also similar fractions of Q-noble gases as the subcomponents of Gros and Anders. This can be seen in Figure 4.9[14]. While He-Q$_1$ and Ne-Q$_1$ dominate the first ~20 steps at moderate etch conditions and represent the major part of the released noble gases, Q$_2$ releases its noble gases at acid temperatures higher than 35 °C. Unfortunately, Gros and Anders could not measure any noble gases in their etched fractions. It seems well possible that their sub-phases are related to ours in such a way that carbonaceous carriers contain the noble gases while their minerals determine the weight and element analysis.

A scenario with a more easily etchable carrier phase Q$_1$ containing a significant part of the light noble gases and a more refractory phase Q$_2$ would have important implications. It would explain why the noble gases are completely lost upon relatively slight etching with HNO$_3$, compared to a "total dissolution" of a residue that is, as discernible by the weight losses, strongly acid and time dependent, as outlined in chapter 2.2.1. Huss *et al.* (1996) observed two P1 release peaks on stepwise pyrolysis of CI Orgueil and EH4 Abee and possibly other meteorites. However, ordinary chondrites as well as CV and CO chondrites generally did not show the second peak. The authors attributed the two peaks to reactions of phase Q with chromite and spinel, respectively, but the peaks could also point to different carrier phases. In addition, Huss *et al.* observed slightly increasing release temperatures with increasing metamorphic grade which could indicate that the less refractory subcomponent Q$_1$ has been lost. Ott *et al.* (1985a; 1985b) suggested two different carrier phases for the trapped noble gases in ureilites. While one carrier phase, which carries a component with a high ^{36}Ar/^{132}Xe ratio of 360, is assumed to be diamond, the other, more easily combustible phase is unknown and should contain noble gases with low a ^{36}Ar/^{132}Xe ratio (Ott *et al.*, 1985a). Both carbonaceous carriers could be shock- or metamorphically modified Q$_1$ and Q$_2$. The larger depletion of He and Ne in ureilites (Figure 4.10) relative to those from phase Q points to a larger loss of phase Q$_1$.

---

[14] This plot is similar to Figure 3.23 but is referred to the total amounts of released gas rather than step number.
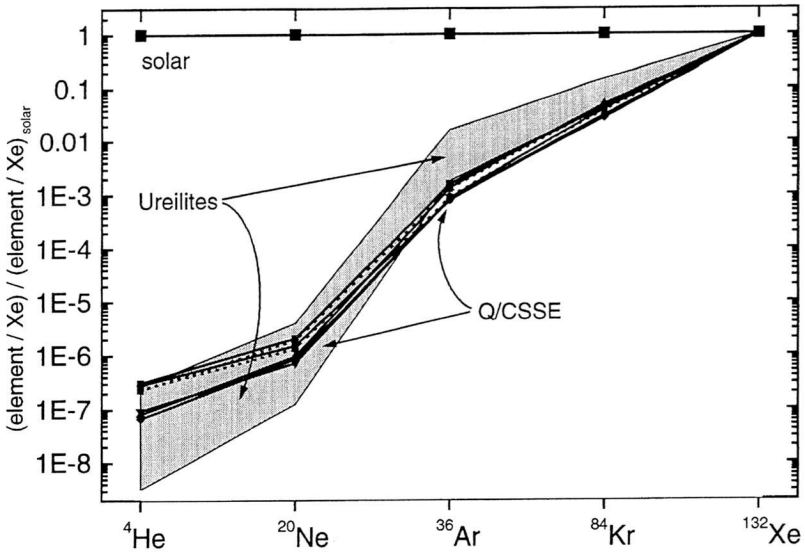
Figure 4.10: Similar to Figure 3.26 but including data from ureilites which contain "planetary" noble gases similar to those in phase Q. He in ureilites is strongly depleted relative to Q, while Ar and Kr are enriched ("subsolar"). Data for ureilites from *"C-rich" separates and HF/HCl-resistant residues* in Göbel *et al.* (1978), Ott *et al.* (1985b) and Wacker *et al.* (1986).

Finally, the fact that the $(^{20}Ne/^{22}Ne)_Q$ ratios between 10.0 and 10.7 do not show any obvious correlation with the metamorphic history might be explained by mixing of Q-subcomponents in different proportions. Unfortunately, due to the release of Ne-E(L), a possible small difference in the Ne isotopic ratios of Q_1 and Q_2 in Cold Bokkeveld was not recognisable. However, the intersection of the Ne-E/Ne-Q mixing line which should determine $(^{20}Ne/^{22}Ne)_{Q1}$ and the Ne-Q/Ne$_{cosm}$ mixing line which should point to $(^{20}Ne/^{22}Ne)_{Q2}$ yield almost identical values which seems to speak against the hypothesis that Ne in Cold Bokkeveld is a mixture of isotopically *differently composed* subcomponents Q_1 and Q_2.

Figure 3.24 and Figure 4.9 suggest that phase Q_1 may somehow be connected with Ne-E(L) and its carrier graphite. This suggests that parts of the Q-gases were trapped on graphite grain surfaces. This could have happened either within the solar system, as suggested by Wacker *et al.* (1985) and Wacker (1989) by adsorption in a labyrinth of micropores. On the other hand, Q-noble gases sited on surfaces of presolar graphite grains could also be related to trapping mechanisms simulated by Sandford *et al.* (1997; 1998) and postulated by Huss and Alexander (1987) to have happened in the presolar molecular cloud. If an exposure of cold presolar grains

to noble gases have indeed led to the trapping of the Q-noble gases, carriers other than graphite, e. g. diamonds or SiC grains, need to be considered as well. Since Q-gases have been found also in more metamorphosed meteorites, but Ne-E(L) and presolar grains are abundant only in the least metamorphosed samples (Huss, 1997), Q-gases can not be related solely to graphite. Other more refractory carriers are necessary. This would require the existence of subcomponents of Q, and the correlation of presolar noble gas carriers and phase Q, respectively, with the metamorphic history as deduced by Huss (1997) can be explained straightforwardly. However, serious arguments contradict the idea of graphite as an important part of phase Q. The release temperature of the Q-gases between 1200-1600 °C is higher than the release temperatures of Ne-E(L) from graphite of 700 °C and 900 °C (Amari *et al.*, 1990b; Huss *et al.*, 1996). It seems unlikely that the volume correlated Ne-E(L) is released prior to the surface-correlated Q-gases. No Q-gas has been found in pure graphite separates. However, possibly, organic coatings, may have been formed similarly to the procedures of Sandford *et al.* (1997; 1998) and may have been lost completely upon preparing the graphite residues. The enrichment of He and Ne in the easier etchable phase Q_1 and the somehow "delayed" Ar from phase Q_2 (chapter 3.2) would then be only due to distinct trapping efficiencies of different carbonaceous carrier materials upon noble gas exposure. Isotopic fractionations are not expected to occur if one assumes e. g. trapping by plasma implantation (Fukunaga and Matsuda, 1997).

4.5   Ne-E(L) in Chainpur and Cold Bokkeveld

The Ne-E(L) concentrations of Chainpur and Cold Bokkeveld were determined in chapter 3.1.2. Here, I show that these results confirm the trend suggested by Huss (1997) that the Ne-E(L) concentration, and therefore, the abundance of its carrier phase, presolar graphite, strongly depends on the meteorite class and decreases as a function of increasing petrographic type. Huss and Lewis (1995) found highest Ne-E(L) contents in CI and CM2 chondrites. They could not unambiguously detect (i. e. resolve) Ne-E(L) in UOCs of petrographic type > 3.1, since the low abundances of Ne-E(L) could have been compromised by Ne-E(H). Possibly, Ne-E released by stepwise pyrolysis below 1000 °C in the experiment by Huss and Lewis was rather Ne-E(H) which was released in parts. In contrast, we were able to determine an actual value for Ne-E(L) in the LL chondrite Chainpur which is an UOC of petrographic type 3.4.

The new data in Table 4.4 better illustrate that the carrier of Ne-E(L), graphite, is strongly depleted due to the metamorphic history of the meteorites which is indicated by their classification and their petrographic type. The large difference between CI chondrite Orgueil,

CM2 Cold Bokkeveld and the more differentiated meteorites indicate that presolar graphite has been almost completely destroyed or has lost all Ne-E(L) by *thermal metamorphism* which altered the original meteoritic material. This abundance sequence also indicates that the carrier graphite is hardly sensitive to aqueous alteration, similar to phase Q_1 but in contrast to phase Q_2, as shown in chapter 4.2.1.

Table 4.4: Ne-E(L) in non-oxidised acid residues calculated to bulk meteorite mass.

meteorite	petrographic type	Ne-E(L) $[10^{-10}cm^3$ STP/g meteorite]	source
Orgueil	CI	24.4	Huss and Lewis (1995)
Cold Bokkeveld	CM2	5.12	this work
Chainpur	LL3.4	0.15	this work
Ragland	LL3.5	<0.013[1]	Huss and Lewis (1995)
Tieschitz	H/L3.6	<0.011[1]	Huss and Lewis (1995)

[1] more than 100 % uncertainty, must be seen as upper limit due to possible admixtures of Ne-E(H).

I compare the Ne-E(L) concentrations for Cold Bokkeveld and Chainpur found in this work with those reported by Huss and Lewis for non-oxidised acid-resistant residues. Their oxidised residues also contain Ne-E(L) contributions, indicating that their oxidising procedure did not completely destroy presolar graphite. In contrast, the Ne-three-isotope-plots for Chainpur and Cold Bokkeveld (Figure 3.3 and Figure 3.4) indicate that CSSE released Ne-E(L) almost completely, since the last steps of both runs do not contain significant amounts of Ne-E(L). Since the weights of acid-resistant residues depend considerably on the demineralisation procedure (Table 2.5), the Ne-E(L) concentrations in Table 4.4 are given per bulk meteorite mass.

4.6 He in interplanetary dust particles (IDPs)

Interplanetary dust particles (IDPs) are, apart from the most primitive carbonaceous chondrites, another important source for material almost unprocessed since the condensation of matter in the forming solar system. This is indicated e. g. by the nearly CI composition of many IDPs (Brownlee *et al.*, 1977; Arndt *et al.*, 1996). IDPs are assumed to originate from comets, but asteroids also contribute in unknown relative proportions (Bradley *et al.*, 1988).

He in 60 single IDPs and fragments of cluster IDPs, collected in the stratosphere, showed $^3He/^4He$ ratios between $(1.4 \pm 0.5) \times 10^{-4}$ and $(2.0 \pm 0.3) \times 10^{-2}$ (Nier and Schlutter, 1990; 1992; 1993; Pepin and Schlutter, 1998). 3 IDPs from the complete record contained He with a $^3He/^4He$ ratio $<2.0 \times 10^{-4}$. In two of these IDPs the $^{20}Ne/^{22}Ne$ ratios could be measured. The IDP

with the lowest He isotopic ratio contained Ne with 10.0 ± 1.1, the other measurement revealed $^{20}Ne/^{22}Ne = 12.4 \pm 4.2$. Half of the $^{3}He/^{4}He$ ratios were below 4.6×10^{-4} and have been interpreted as a "normal mixture" of primordial He-Q and implanted He of solar origin (Pepin and Schlutter, 1998). Most importantly, no ratio from a set of 60 data fell below the $(^{3}He/^{4}He)_Q$ ratio of $(1.43 \pm 0.03) \times 10^{-4}$ (Table 3.7). This suggests that our new He-Q value is indeed the correct value for pure primordial He incorporated into the meteorites at their formation and is not compromised by cosmogenic He or He from other sources. Small admixtures of solar He, however, might be possible. Unfortunately, the Ne isotopic ratios do not unambiguously exclude this possibility. Comets have probably been formed in the Uranus-Neptune zone and are remnants from a population of unaltered primordial building blocks, the icy planetesimals that formed the outer planets (Greenberg *et al.*, 1984). If the *cometary* origin of those IDPs with low, Q-like $^{3}He/^{4}He$ ratios could be established, the region where Q-like He has existed and has been incorporated into the forming planetesimals would also include the colder outer solar system regions.

Pepin and Schlutter (1998) also found IDPs with anomalous $^{3}He/^{4}He$ ratios that far exceeded $(^{3}He/^{4}He)_{SW}$. They could not explain these ^{3}He excesses by cosmic ray exposure and, thus, proposed a currently unidentified ^{3}He source, perhaps in the presolar molecular cloud. No hints on such a He source with enhanced $^{3}He/^{4}He$ ratios (or of pure ^{3}He?) have been found in meteorites yet. However, one might ask, rather speculatively, if the He released from Dimmitt with its extraordinarily constant $^{3}He/^{4}He$ ratios (Figure 3.7) might have something in common with this hypothetical ^{3}He source. On the other hand, it seems rather unlikely that just Dimmitt, the most severely metamorphosed meteorite of all samples examined with CSSE, should be the one that carries an additional He component similar to the least altered IDPs.

4.7   Q and the Big-Bang nucleosynthesis theory

The Standard Big-Bang nucleosynthesis theory "SBBN" (e. g. Alpher *et al.*, 1948; Peebles, 1966; Wagoner *et al.*, 1967; Schramm and Turner, 1998) predicts the primordial[15] abundances of the light stable nuclei H, D, ^{3}He, ^{4}He and ^{7}Li as plotted in Figure 4.11 (from Schramm and Turner, 1998). These isotopes have been produced at an early stage of the universe (0.01-200 s) dependent on universal parameters, e. g. the baryon density ρ_B[16], the number of light[17] neutrino

---

[15] *primordial* refers here to the universe

[16] The SBBN predictions of the elemental abundances depend on the baryon-to-photon ratio η which is related to the mass baryon density ρ_B with $\rho_B = \eta \cdot n_\gamma \cdot m_N$, where n_γ is the number density of photons

species N_ν[18] and the half life of the neutron (Schramm and Turner, 1998 and references therein). $\Omega_B \cdot h^2$ is the scale of the upper x-axis of Figure 4.11, where $\Omega_B = \rho_B / \rho_c$, i. e. Ω_B is the baryon density ρ_B normalised with the critical density $\rho_c = 1.88 \cdot h^2 \times 10^{-29}$ g cm^{-3}. The parameter h (probably between 0.5 and 1) is a measure for the hubble constant $H_0 = 100 \cdot h$ km s^{-1} Mpc^{-1} (Schramm and Turner, 1998). Thus, $\Omega_B \cdot h^2$ is the contribution of the baryons to the critical density. For values of $\Omega_B \cdot h^2 > 1$, the universe oscillates or is *closed*, a value < 1 means that the universe monotonically expands.

In the noble gas context of this work, we are interested in the *primordial* abundances which are necessary to test the SBBN theory and to deduce upper and lower bounds for the physical parameters ρ_B and N_ν. This is symbolised by the "consistency" interval in Figure 4.11. The inferred primordial abundances for D, ^{3}He, ^{4}He and ^{7}Li allow for baryon densities within this marked interval. While the upper limit is mainly determined by the D abundance, since nucleosynthetic processes which can produce D are not known, the lower, less restricted, limit can be set by the abundance of D + ^{3}He, because D will be burnt only to ^{3}He and a significant amount of ^{3}He survives the stellar nucleosynthesis processes (Copi *et al.*, 1995b). Apparently, D is the best indicator for the baryon density ρ_B, because it decreases most steeply with increasing ρ_B, and therefore it is most suitable as a cosmic "baryometer" (Copi *et al.*, 1995a; 1995b). The limits for ρ_B set by D alone are indicated by the darker area of the consistency interval in Figure 4.11.

There are several possibilities to infer the abundance ratios $(D/H)_{prim}$, $(^3He/H)_{prim}$, $(^4He/H)_{prim}$ and $(^7Li/H)_{prim}$ from observations and laboratory measurements of cosmic material. We will discuss the ratios $(D/H)_{prim}$ and $(^3He/H)_{prim}$ in detail below, since these values have been inferred by meteoritic and planetary data. $(D/H)_{prim}$ has been deduced from ratios measured in the present-day galaxy in clouds which are not affected seriously by subsequent stellar nucleosynthesis, in the local interstellar cloud (LIC), in which the Sun is located, and from the protosolar cloud (PSC), with the aid of meteorites and the examination of the jovian atmosphere (Geiss and Gloeckler, 1998; Linsky, 1998; Mahaffy *et al.*, 1998). $(^3He/H)_{prim}$ is more difficult to determine, nevertheless data have been inferred from H II regions, planetary

---

(411 cm^{-3}; from the cosmic background radiation) and m_N is the baryon mass (1.66 x 10^{-24} g) (Copi *et al.*, 1995b).

[17] $m_\nu \ll 1$MeV

[18] According to SBBN, the *mass* fraction of ^{4}He in the universe ("Y_p") is, among other parameters, a function of the number of very light neutrino species N_ν. ^{4}He limits N_ν, in accordance to particle physics experiments, to be smaller than 4 (Copi *et al.*, 1997).

nebulae and the LIC; PSC ratios have been deduced from solar system sources (Geiss and Gloeckler, 1998; Gloeckler and Geiss, 1998; Linsky, 1998; Mahaffy *et al.*, 1998; Rood *et al.*, 1998). Differences in the abundance ratios in different cosmic matter point to "chemical evolution", i. e. nuclear processes and subsequent mixing in the interstellar medium, that lead to destruction and production of elements, especially D and ^{3}He (Pagel, 1997).
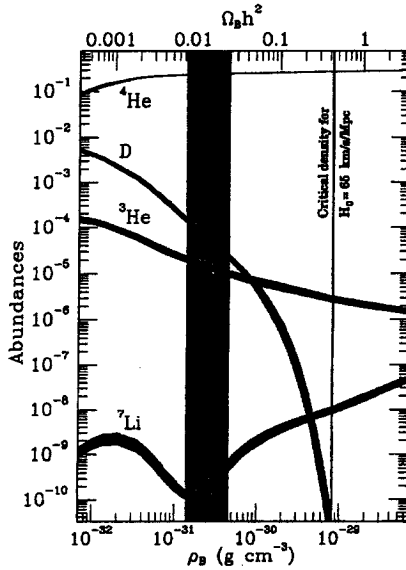
Figure 4.11: Abundances of the primordially produced nuclei H, D, ^{3}He, ^{4}He and ^{7}Li depend on the baryon density ρ_B, as predicted by the standard Big-Bang nucleosynthesis theory. The "consistency" interval, deduced from inferred cosmic abundances, limits the possible values of the baryon density ρ_B. The dark region of this interval is inferred from D alone. (Figure from Schramm and Turner, 1998).

$(D/H)_{prim}$ deduced from meteoritic ^{3}He/^{4}He...

The "classical" way to determine $(D/H)_{prim}$ in the protosolar cloud is to use solar system abundances of ^{3}He and ^{4}He (Geiss and Reeves, 1972; Geiss and Gloeckler, 1998). All primordial D in the Sun should have been converted into ^{3}He within $<1 \times 10^5$ a during the pre-main-sequence phase of the Sun (Ozima *et al.*, 1998). Since there are no nuclear processes known that produce D, $(D/H)_{prim}$ can be calculated in principle with

$(D/H)_{psc/prim} = (^4He/H)_{psc} * [(^3He/^4He)_{Sun} - (^3He/^4He)_{psc}]$

With a $(^4He/H)_{psc}$ ratio of 0.095 ± 0.010 (Copi et al., 1995a), two ratios are needed: $(^3He/^4He)_{Sun}$ and $(^3He/^4He)_{psc}$. $(^3He/^4He)_{Sun}$ has been obtained from solar wind (SW) measurements (Table 4.5), either in gas-rich meteorites, in lunar material or from spacecraft (Black, 1972a; Geiss and Reeves, 1972; Benkert et al., 1993; Bodmer et al., 1995; Gloeckler and Geiss, 1998). The $(^3He/^4He)_{SW}$ ratio from the outer layers of the Sun does not necessarily have to be identical to the $(^3He/^4He)_{Sun}$ ratio. However, the corrections that have to be made because of the isotopic fractionation between the source region and the emitted solar wind and mixing processes between the SW source and deeper layers that have produced additional ^3He, is assumed to be only 8 % (Geiss and Gloeckler, 1998). To obtain $(^3He/^4He)_{psc}$, it has been assumed that He_{psc} was sampled more or less unfractionated in meteorites that accreted during the formation of the solar system (Geiss and Reeves, 1972; Yang et al., 1984; Geiss, 1993). Therefore, these authors adopted values deduced for "planetary" He-A in primitive meteorites $(^3He/^4He)_A = (1.3 \pm 0.6) \times 10^{-4}$ and $(1.5 \pm 0.3) \times 10^{-4}$, respectively, for their calculations. However, He-A, found in several primitive meteorites, is clearly a mixture of He-Q and He trapped in presolar grains and originating from different stars (see chapter 3.1.3). Thus, if primordial "planetary" He, incorporated into meteorites in the solar system, is thought to be useful for the determination of $(D/H)_{psc/prim}$, then one should rather choose He-Q (Copi et al., 1995a) with the new value of $(^3He/^4He)_Q = (1.43 \pm 0.03) \times 10^{-4}$, as deduced in chapter 3.1.3. Fortunately, however, all $^3He/^4He$ ratios for protosolar He that have been derived from meteorite data so far are identical within their errors (Table 4.5). I used this $(^3He/^4He)_Q$ as $(^3He/^4He)_{psc}$, $(^4He/H)_{psc}$ from Copi et al. (1995a) and $(^3He/^4He)_{solar} = (3.8 \pm 0.5) \times 10^{-4}$ from Geiss and Gloeckler (1998) to determine $(D/H)_{psc} = (2.3 \pm 0.5) \times 10^{-5}$ which is in agreement with all other $(D/H)_{psc}$ ratios given in Table 4.6. The protosolar data inferred from different $^3He/^4He$ ratios are listed in the first part of the table, ratios measured directly from different cosmic sources are given in italic letters. Note in particular the very similar $(D/H)_{jovian}$ ratio, measured by the Galileo spacecraft directly in the jovian atmosphere.

Table 4.5: Isotopic composition of He deduced for cosmic reservoirs.

component	^{3}He/^{4}He [10^{-4}]	remarks	source
He-Q	**1.43 ± 0.03**	**meteoritic**	**this work**
He-A	1.50 ± 0.30	meteoritic	Geiss (1993)
He-A	1.42 ± 0.02	meteoritic	Reynolds et al. (1978)
Jupiter	1.66 ± 0.05	Galileo	Mahaffy et al. (1998)
SW	4.56 ± 0.08		Benkert et al. (1993)
SEP	2.17 ± 0.05		Benkert et al. (1993)
slow + fast SW	3.8 ± 0.5	"outer convection zone"	Geiss and Gloeckler (1998)
LISM[1]	1.70 ± 0.10		Linsky et al. (1993)
LIC[2]	2.2 ± 0.8		Gloeckler and Geiss. (1996)
LIC[2]	$2.48^{+0.68}_{-0.62}$		Gloeckler and Geiss. (1998)

[1] local interstellar medium; [2] local interstellar cloud.

According to Ozima et al. (1998), meteoritic noble gas data rather point to a *post*-D-burning origin of the Q-gases and thus He-Q. If so, it is not possible to determine the abundance of primordial D from meteoritic He isotopic ratios.

Table 4.6: Protosolar and other D/H ratios deduced from different cosmic matter.

	D/H [10^{-5}]	^{3}He/^{4}He ratios [10^{-4}] (see also Table 4.5)		source
		solar wind	protosolar	
protosolar	**2.3 ± 0.5**	**3.8 ± 0.5**	**(1.43 ± 0.03)$_Q$**	**this work**
protosolar	2.5 ± 0.5			Geiss and Reeves (1972)
protosolar	2.6 ± 1.0	4.5 ± 0.4	(1.5 ± 0.3)$_{met}$	Geiss (1993)
protosolar	2.1 ± 0.5	3.8 ± 0.5	(1.5 ± 0.2)$_{met+jovian}$	Geiss and Gloeckler (1998)
protosolar	3.01 ± 0.17	4.25 - 4.88[1]	(1.1 ± 0.2)$_{jovian}$[2]	Gautier and Morel (1997)
protosolar	2.7 ± 0.3	4.4 ± 0.4	(1.66 ± 0.05)$_{jovian}$	Mahaffy et al. (1998)
Jupiter (≡protosolar)	2.6 ± 0.7	Galileo probe		Mahaffy et al. (1998)
LIC	1.50 ± 0.10	12 measurements		Linsky (1998)[3]
LISM (without LIC)	1.28 ± 0.36	7 measurements		Linsky (1998)[3]

[1] three space missions; [2] older, uncorrected ^{3}He/^{4}He ratio from Niemann et al.(1996), see Table 4.5; [3] compilation.

Table 4.6 lists several (D/H)$_{psc}$ ratios as determined by the method described above, as well as data for the local interstellar medium (LISM) and Jupiter. (D/H)$_{LISM}$ ratios derived by spectrometric observations at different locations suggest that the D/H ratio does not largely vary in the LISM (Piskunov et al., 1997; Linsky, 1998). These values represent the *present* state and are lower than the protosolar value, which has been established 4.56 Ga ago, due to destruction of D in the galaxy by stellar nucleosynthesis and subsequent mixing. The unaltered (D/H)$_{prim}$ ratio should also be directly observable in very red-shifted extragalactic hydrogen

clouds towards quasars. However, these values, which reach $(D/H)_{prim} = 2 \times 10^{-4}$, vary considerably and probably are spurious (Gloeckler and Geiss, 1996; Linsky, 1998).

A slightly different way to determine $(D/H)_{psc}$ is to adopt the jovian $^3He/^4He$ ratio as $(^3He/^4He)_{psc}$ (Gautier, 1983; Gautier and Morel, 1997; Geiss and Gloeckler, 1998). The giant planets Jupiter and Saturn are assumed to be undisturbed reservoirs, free from production or loss processes (Owen et al., 1986). Their compositions should represent the unaltered protosolar gas, since due to their great masses and low temperatures, no He escape should occur. Niemann et al. (1996) reported a $(^3He/^4He)_{jovian}$ ratio of $(1.1 \pm 0.2) \times 10^{-4}$, measured by the Gallileo probe. Recently, a corrected value of $(1.66 \pm 0.05) \times 10^{-4}$ was published (Mahaffy et al., 1998; Niemann et al., 1998). This new value is higher than the value of $(1.43 \pm 0.03) \times 10^{-4}$ deduced for He-Q in this work (Table 4.5). If the ratio obtained for Jupiter is indeed the correct protosolar value, the value of He-Q must represent another reservoir than the protosolar cloud.

However, Zahn et al. (1998) pointed out that the mass fraction[19] $Y_J = 0.234 \pm 0.005$ measured by Gallileo for Jupiter's atmosphere is lower than the protosolar value of 0.275 ± 0.010 (Bahcall and Pinnsonneault, 1995). Since no escape of H and He should occur, the interior of the planet must contain more He relative to H (Guillot et al., 1997). The depletion is assumed to be the result of downward migration of He-rich droplets and was also observed for Ne (Zahn et al., 1998). At high pressures, H and He separate, and He "rains" downward. This process has been clearly observed at the atmosphere of Venus. I speculate that the enrichment of the heavier species in the interior might also be the mechanism to explain the higher $(^3He/^4He)_{jovian}$ ratio compared to the meteoritic protosolar value $(^3He/^4He)_Q$.

$(^3He/H)_{prim}$ deduced from protosolar $^3He/^4He$...

$(^3He/H)_{prim}$ can similarly be inferred by measurements within the solar system (Yang et al., 1984; Copi et al., 1995a) . Still problematic is the extent of production and destruction of ^3He in stars (Copi et al., 1995b): Bochsler et al. (1990) and Bochsler (1992) expect significant ^3He enhancements within the Sun. ^3He is well observed in galactic HII regions and planetary nebulae. Recently, Rood et al. (1998) suggested that neither stellar production nor destruction of ^3He can be of significance for the galaxy, since they could not observe substantial variations in a great number of HII regions, although planetary nebulae and model calculations show largely (up to 100-fold) evolved $^3He/H$ ratios (Bania et al., 1993; Charbonnel, 1998; Tosi,

---

[19] astrophysical notation for He abundances: $Y = m(He) / [m(H_2) + m(He) + m(heavy\ elements)]$

1998). Thus, Rood *et al.* proposed a primordial ^{3}He/H value of $1.5\,^{+1.0}_{-0.5}\times10^{-5}$ in the galaxy, mostly unaffected from single stellar conditions. Using $(^4\text{He/H})_{psc} = 0.095 \pm 0.010$ (Copi *et al.*, 1995a) and adopting our He-Q value as protosolar, we obtain $(^3\textbf{He/H})_{psc} = (\textbf{1.36} \pm \textbf{0.15}) \times \textbf{10}^{-5}$ in agreement with the value of Rood *et al.* Gloeckler and Geiss (1996) obtained a rather similar $(^3\text{He/H})$ for the LISM of $(2.42 \pm 1.45) \times 10^{-5}$.

If Rood *et al.* (1998) are right, the ^{3}He/^{4}He ratio in the interstellar medium should also not vary as much as the values observed in single stars. This could be the explanation for the remarkable similarity of He-Q and He-A. While the first component has been possibly incorporated at the formation of the well mixed gaseous solar nebula, the second one is dominated by He trapped in interstellar diamonds of a distinct number of stellar sources. A mixture of an ensemble of stellar He reservoirs, as probably represented by the interstellar diamonds, should thus yield a similar ^{3}He/^{4}He ratio as the $(^3\text{He/}^4\text{He})_Q$ which might be also a protosolar mixture of several contributing stellar sources that have contributed to the PSC. This suggestion would clearly require a *pre*-D-burning origin of Q.

5 Summary and conclusions

Five HF/HCl-resistant residues of the meteorites CO3.4 Lancé, H3.7 Dimmitt, CV3 (ox.) Grosnaja, LL3.4 Chainpur and CM2 Cold Bokkeveld have been analysed by the closed system stepped etching (CSSE) technique which is uniquely suitable to measure in particular the light primordial noble gases in the oxidisable phase Q. Stepwise measurements have allowed to resolve Q-noble gases from other simultaneously released components such as solar and cosmogenic noble gases as well as presolar Ne-E. The experiments, lasting up to five months each and consisting of up to 30 etch steps, have shown that the primordial noble gases of phase Q have been sampled by all examined meteorites which are of different chondritic classes. All Q-gases released upon etching with HNO_3 show the characteristic "planetary" elemental release pattern, which is increasingly depleted in the lighter noble gases normalised to Xe and solar abundances, by about seven orders of magnitude in the case of He. The samples contain Q-gas with identical "normal" Ar, Kr and Xe isotopic ratios, in agreement with results from earlier examinations. All these similarities show that Q-gases have been widespread in the meteorite forming regions of the early solar system and were homogeneously incorporated into the accreting planetesimals. The new Ne data confirm a few earlier measurements which have hinted that the Ne-Q isotopic composition is the least uniform of all elements. All reliable $(^{20}Ne/^{22}Ne)_Q$ ratios lie in the range between 10.0 and 10.7 with typical errors in the order of 0.05-0.2. A correlation of $(^{20}Ne/^{22}Ne)_Q$ with the chemical class or alteration history of the meteorites has not been found. However, since the isotopic ratios of all other elements appear to be identical, it can be assumed that Ne has been incorporated homogeneously into all meteorites and another, so far unknown, process must have been responsible for the alteration of the original Ne-Q.

The most important result of this study is the determination of $(^3He/^4He)_Q$ in two meteorites. The values are $(1.45 \pm 0.01) \times 10^{-4}$ for Grosnaja and $(1.41 \pm 0.01) \times 10^{-4}$ for Cold Bokkeveld. Except for older data from the CSSE analyses of Allende and Murchison, which have been slightly compromised by cosmogenic He, these values are the only He isotopic ratios obtained for He-Q. Assuming that Q has been acquired by the meteorites during their formation at the beginning of the solar system, and, in addition, that He-Q represents *pre*-D-burning He, the $(^3He/^4He)_Q$ has been used to determine a protosolar D/H ratio which can be of importance in the framework of standard big-bang nucleosynthesis. The calculated $(D/H)_{protosolar}$ ratio of $(2.3 \pm 0.5) \times 10^{-5}$ is in accordance with values determined from the Jovian atmosphere which is

assumed to have sampled protosolar hydrogen. This indicates that He-Q might indeed contain protosolar He. The new $(^3He/^4He)_Q$ mean value of $(1.43 \pm 0.03) \times 10^{-4}$ is lower than the respective value for the Jovian atmosphere which is $(1.66 \pm 0.05) \times 10^{-4}$. This hints to fractionating processes, since both reservoirs should contain the same, unfractionated He incorporated from the solar nebula.

Relative to solar abundances, all meteorites show a very similar "planetary" elemental composition presumably indicating that phase Q sampled one single component. However, there is evidence, in particular from the etch run of CM2 Cold Bokkeveld, that Q-noble gases reside in at least two distinct carrier phases, "Q_1" and "Q_2", with slightly different properties. Q_1 which contains more He and Ne relative to Xe and Q_2, seems to be related to the carrier of Ne-E, presolar graphite, and is easier to etch than Q_2.

Several petrologic observations on the degree of parent body alteration could be confirmed by the Q-noble gas concentrations. The analysis of the elemental ratios of the Q-noble gases yielded that the heavier noble gases Ar, Kr and Xe reflect both thermal metamorphism and aqueous alteration. Both parent body processes produced larger depletions of Ar and Kr relative to Xe. For He and Ne, the situation is different. Aqueously altered meteorites, such as the CM2 chondrites, do not show depletions of He and Ne relative to Ar. To the contrary, these meteorites contain Q-gases with the highest He/Ar and Ne/Ar ratios. These observations also point towards two Q carrier phases, as suspected above, where the He and Ne enriched carrier phase Q_1 is less susceptible to aqueous alteration.

The determination of the ^{22}Ne-E(L) contents in Chainpur and Cold Bokkeveld has provided further evidence for the assumption that abundances of presolar graphite grains correlate negatively with the grade of metamorphic alteration.

Outlook...

CSSE has proven to be a powerful tool to resolve Q-gases, Ne-E, as well as cosmogenic and solar noble gases from each other. The most important future task will be to identify the carrier phase(s) Q. Noble gas analyses can only help to trace the separation of the subphases Q_1 and Q_2 according to their slightly different He and Ne abundances. The complete deciphering of phase Q would probably help to solve the problem of the origin of the Q-noble gases and answer the question whether they were already trapped in carbonaceous mantles of presolar grains, in the presolar molecular cloud or "locally" within the solar system. The identification of the Q-gas trapping mechanism and its carrier phases might also improve the models of the evolution of planetary noble gas inventories in our solar system.

Several additional HF/HCl-resistant residues have been prepared for this study. First, they should be analysed to complete the series of CSSE analyses of CO chondrites. The comparison of data obtained from members of this single meteorite class then provides a possibility to test whether the carrier phases are differently susceptible to aqueous alteration and thermal metamorphism. The extraordinarily short exposure age of the CO3.7 chondrite Isna should allow for a precise determination of the $(^3He/^4He)_Q$ ratio as well as the $(^{20}Ne/^{22}Ne)_Q$ ratio in a sample that experienced more severe metamorphism than CO3ox. Grosnaja or CM2 Cold Bokkeveld. A further CSSE experiment on a residue of Allende highly enriched in primordial noble gases by purely physical means (i. e., freeze-thaw disaggregation) is planned (Amari and Matsuda, 1998; Matsuda *et al*, 1999). This should test whether Q noble gases are separately releasable equally well as from the HF/HCl-resistant residue of Allende (Wieler *et al.*, 1991). This residue may yield a $(^3He/^4He)_Q$ ratio for Allende possibly less influenced by cosmogenic He than the already known value of 1.59 x 10^{-4} (Wieler *et al.*, 1991).

Another problem that should be addressed is whether graphite and (parts of) phase Q are somehow closely related as indicated by observations discussed in chapter 4.4. Especially interesting is also the question why graphite is, similar to phase Q, very abundant in the CM2 and some LL chondrites, but, in contrast to phase Q, absent in CV and CO chondrites.

6 References

Alaerts L., Lewis R. S. and Anders E. (1979a) Isotopic anomalies of noble gases in meteorites and their origins - III. LL-chondrites. *Geochim. Cosmochim. Acta* **43**, 1399-1415.

Alaerts L., Lewis R. S. and Anders E. (1979b) Isotopic anomalies of noble gases in meteorites and their origins - IV. C3 (Ornans) carbonaceous chondrites. *Geochim. Cosmochim. Acta* **43**, 1421-1432.

Alaerts L., Lewis R. S., Matsuda J.-I. and Anders E. (1980) Isotopic anomalies of noble gases in meteorites and their origins - VI. Presolar components in the Murchison C2 chondrite. *Geochim. Cosmochim. Acta* **44**, 189-209.

Alexander C. M. O. D. (1997) Dust production in the galaxy: the meteorite perspective. *AIP Conf. Proc.* **402**, 567-593.

Alexander Jr. E. C. (1971) Plutonium-244: Confirmation as an extinct radioactivity. *Science* **172**, 837-840.

Alexander Jr. E. C., Lewis R. S., Reynolds J. H. and Michel M. C. (1971) Spallogenic Ne, Kr, and Xe from a depth study of 12002. *Proc. 2nd Lunar Planet. Sci. Conf.* **2**, 1643-1650.

Alpher R. A., Bethe H. and Gamov G. (1948) The origin of chemical elements. *Phys. Rev.* **73**, 803-804.

Amari S., Anders E., Virag A. and Zinner E. (1990a) Interstellar graphite in meteorites. *Nature* **345**, 238-240.

Amari S., Lewis R. S. and Anders E. (1990b) Interstellar graphite in meteorites: growing complexity, implied by its noble-gas components. *Lunar Planet. Sci. Conf.* **XXI**, 19-20.

Amari S., Lewis R. S. and Anders E. (1994) Interstellar grains in meteorites: I. Isolation of SiC, graphite, and diamond; size distribution of SiC and graphite. *Geochim. Cosmochim. Acta* **58**, 459-470.

Amari S., Lewis R. S. and Anders E. (1995) Interstellar grains in meteorites: III. Graphite and its noble gases. *Geochim. Cosmochim. Acta* **59**, 1411-1426.

Amari S. and Matsuda J.-I. (1998) Ion probe analysis of carbonaceous grains in a gas-rich fraction from the Allende meteorite. *Lunar Planet. Sci. Conf.* **XXIX**, #1844.

Anders E. and Grevesse N. (1989) Abundances of the elements: Meteoritic and solar. *Geochim. Cosmochim. Acta* **53**, 197-214.

Anders E., Higuchi H., Gros J., Takahashi H. and Morgan J. W. (1975) Extinct superheavy element in the Allende meteorite. *Science* **190**, 1262-1271.

Anders E. and Zadnik G. (1985) Unequilibrated ordinary chondrites: A tentative subclassification based on volatile-element content. *Geochim. Cosmochim. Acta* **49**, 1281-1291.

Anders E. and Zinner E. (1993) Interstellar grains in primitive meteorites: diamond, silicon carbide, and graphite. *Meteoritics* **28**, 490-514.

Arndt P., Bohsung J., Maetz M. and Jessberger E. K. (1996) The elemental abundances in interplanetary dust particles. *Meteoritics & Planet. Sci.* **31**, 817-833.

Bahcall J. N. and Pinnsonneault M. H. (1995) Solar models with helium and heavy-element diffusion. *Rev. Modern Physics* **67**, 781-808.

Bania T. M., Rood R. T. and Wilson T. L. (1993) The 3-helium abundance in H II regions and planetary nebulae. In *Origin and evolution of the elements* (ed. E. Vangioni-Flam, N. Prantzos and M. Cassé), pp. 107-111. Cambridge University Press, Cambridge.

Basford J. R., Dragon J. C., Pepin R. O., Coscio Jr. M. R. and Murthy V. R. (1973) Krypton and xenon in lunar fines. *Proc. 4th Lunar Sci. Conf.*, 1915-1955.

Begemann F. (1980) Isotopic anomalies in meteorites. *Rep. Progr. Phys.* **43**, 1309-1356.

Benkert J.-P., Baur H., Signer P. and Wieler R. (1993) He, Ne, and Ar from the solar wind and solar energetic particles in lunar ilmenites and pyroxenes. *J. Geophys. Res.* **98(E7)**, 13147-13162.

Bernatowicz T., Fraundorf G., Ming T., Anders E., Wopenka B., Zinner E. and Fraundorf P. (1987) Evidence for interstellar SiC in the Murray carbonaceous meteorite. *Nature* **330**, 728-730.

Bernatowicz T. J., Amari S., Zinner E. K. and Lewis R. S. (1991) Interstellar grains within interstellar grains. *Astrophys. J.* **373**, L73-L76.

Bernatowicz T. J., Cowsik R., Gibbons P. C., Lodders K., Fegley Jr. B., Amari S. and Lewis R. S. (1996) Constraints on stellar grain formation from presolar graphite in the Murchison meteorite. *Astrophys. J.* **472**, 760-782.

Black D. C. (1972a) On the origins of trapped helium, neon and argon isotopic variations in meteorites - I. Gas-rich meteorites, lunar soil and breccia. *Geochim. Cosmochim. Acta* **36**, 347-375.

Black D. C. (1972b) On the origins of trapped helium, neon and argon isotopic variations in meteorites - II. Carbonaceous meteorites. *Geochim. Cosmochim. Acta* **36**, 377-394.

Black D. C. and Pepin R. O. (1969) Trapped neon in meteorites - II. *Earth Planet. Sci. Lett.* **6**, 395-405.

Bochsler P. (1992) Minor ions - tracers for physical processes in the heliosphere. In *Solar Wind Seven* (eds. E. Marsch and R. Schwenn), pp. 323-332. Pergamon Press, Oxford.

Bochsler P., Geiss J. and Maeder A. (1990) The abundance of ^{3}He in the solar wind - A constraint for models of solar evolution. *Solar Physics* **128**, 203-215.

Bodmer R., Bochsler P., Geiss J. and Steiger R. v. (1995) Solar wind helium isotopic composition from SWICS/Ulysses. *Space Sci. Rev.* **72**, 61-64.

Bogard D. D., Nyquist L. E. and Johnson P. (1984) Noble gas contents of shergottites and implications for the martian origin of SNC meteorites. *Geochim. Cosmochim. Acta* **48**, 1723-1739.

Bradley J. P., Sandford S. A. and Walker R. M. (1988) Interplanetary dust particles. In *Meteorites and the early solar system* (eds. J. F. Kerridge and M. S. Matthews), pp. 861-895. The University of Arizona Press, Tuscon.

Browning L. B., McSween Jr. H. Y. and Zolensky M. E. (1996) Correlated alteration effects in CM carbonaceous chondrites. *Geochim. Cosmochim. Acta* **60**, 2621-2633.

Brownlee D. E., Tomandl D. A. and Olszewski E. (1977) Interplanetary dust: A new source of extraterrestrial material for laboratory studies. *Proc. 8th Lunar Planet. Sci. Conf.*, 149-160.

Burbidge E. M., Burbidge G. R., Fowler W. A. and Hoyle F. (1957) Synthesis of the elements in stars. *Rev. Modern Physics* **29**, 547-650.

Caffee M. W., Goswami J. N., Hohenberg C. M., Marti K. and Reedy R. C. (1988) Irradiation records in meteorites. In *Meteorites and the early solar system* (eds. J. F. Kerridge and M. S. Matthews), pp. 205-245. The University of Arizona Press, Tuscon.

Cameron A. G. W. (1962) The formation of the Sun and the planets. *Icarus* **1**, 13-69.

Cassen P. (1994) Utilitarian models of the solar nebula. *Icarus* **112**, 405-429.

Charbonnel C. (1998) Mixing in stars and the evolution of the ^{3}He abundance. In *Space Sciences Series of ISSI* (eds. N. Prantzos, M. Tosi and R. v. Steiger), pp. 199-206. Kluwer Academic Publishers, Dordrecht.

Clayton D. D. and Ward R. A. (1978) s-Process studies: Xenon and krypton isotopic abundances. *Astrophys. J.* **224**, 1000-1006.

Clayton R. N. (1981) Isotopic variations in primitive meteorites. *Phil. Trans. Roy. Soc. London* **A303**, 339-349.

Clayton R. N., Grossman L. and Mayeda T. K. (1973) A component of primitive nuclear composition in carbonaceous meteorites. *Science* **182**, 485-488.

Copi C. J., Schramm D. N. and Turner M. S. (1995a) Big Band nucleosynthesis and a new approach to galactic chemical evolution. *Astrophys. J.* **455**, L95-L98.

Copi C. J., Schramm D. N. and Turner M. S. (1995b) Big-Bang nucleosynthesis and the baryon density of the universe. *Science* **267**, 192-199.

Copi C. J., Schramm D. N. and Turner M. S. (1997) Big-bang nucleosynthesis limit to the number of neutrino species. *Phys. Rev. D* **55**, 3389-3393.

Crabb J. and Anders E. (1981) Noble gases in E-chondrites. *Geochim. Cosmochim. Acta* **45**, 2443-2464.

Crabb J. and Anders E. (1982) On the siting of noble gases in E-chondrites. *Geochim. Cosmochim. Acta* **46**, 2351-2361.

Donahue T. M. (1986) Fractionation of noble gases by thermal escape from accreting planetesimals. *Icarus* **66**, 195-210.

Dreibus G., Palme H., Spettel B., Zipfel J. and Wänke H. (1995) Sulfur and selenium in chondritic meteorites. *Meteoritics* **30**, 439-445.

Eberhardt P. (1978) A neon-E rich phase in Orgueil: Results of stepwise heating experiments. *Proc. 9th Lunar Planet. Sci. Conf.*, 1027-1051.

Eberhardt P., Eugster O., Geiss J. and Marti K. (1966) Rare gas measurements in 30 stone meteorites. *Z. Naturforschung* **21a**, 414-426.

Eberhardt P., Eugster O. and Marti K. (1965) A redetermination of the isotopic composition of atmospheric neon. *Z. Naturforschung* **20a**, 623-624.

Eberhardt P., Geiss J., Graf H., Grögler N., Mendia M. D., Mörgeli M., Schwaller H., Stettler A., Krähenbühl U. and Gunten H. R. v. (1972) Trapped solar wind noble gases in Apollo 12 lunar fines 12001 and Apollo 11 breccia 10046. *Proc. Third Lunar Sci. Conf., Suppl. 3, Geochim. Cosmochim. Acta* **2**, 1821-1856.

Eberhardt P., Jungck M. H. A., Meier F. O. and Niederer F. R. (1981) A neon-E rich phase in Orgueil: results obtained on density separates. *Geochim. Cosmochim. Acta* **45**, 1515-1528.

Englert P., Herpers U., Herr W., Nautiyal C. M., Padia J. T., Rao M. N. and Venkatesan T. R. (1983) Isna, an unusual C3(O) carbonaceous chondrite. *Earth Planet. Sci. Lett.* **65**, 1-6.

Etique P., Signer P. and Wieler R. (1981) An in-depth study of neon and argon in lunar soil plagioclases, revisited: Implanted solar flare noble gases. *Lunar Planet. Sci. Conf.* **XII**, 265-267.

Eugster O. (1988) Cosmic-ray production rates for +He, ^{21}Ne, ^{38}Ar, ^{83}Kr, and ^{126}Xe in chondrites based on ^{81}Kr-Kr exposure ages. *Geochim. Cosmochim. Acta* **52**, 1649-1662.

Eugster O., Eberhardt P. and Geiss J. (1967a) The isotopic composition of krypton in unequilibrated and gas rich chondrites. *Earth Planet. Sci. Lett.* **2**, 385-393.

Eugster O., Eberhardt P. and Geiss J. (1967b) Krypton and xenon isotopic composition in three carbonaceous chondrites. *Earth Planet. Sci. Lett.* **3**, 249-257.

Eugster O., Eberhardt P., Geiss J. and Grögler N. (1983) Neutron-induced fission of uranium: a dating method for lunar surface material. *Science* **219**, 170-172.

Eugster O., Eberhardt P., Thalmann C. and Weigel A. (1998) Neon-E in CM-2 chondrite LEW90500 and collisional history of CM-2 chondrites, Maralinga, and other CK chondrites. *Geochim. Cosmochim. Acta* **62**, 2573-2582.

Eugster O., Weigel A. and Polnau E. (1997) Ejection times of Martian meteorites. *Geochim. Cosmochim. Acta* **61**, 2749-2757.

Frick U. and Chang S. (1977) Ancient carbon and noble gas fractionation. *Proc. 8th Lunar Planet. Sci. Conf.*, 263-272.

Frick U. and Chang S. (1978) Elimination of chromite and novel sulfides as important carriers of noble gases in carbonaceous chondrites. *Meteoritics* **13**, 465-470.

Frick U. and Pepin R. O. (1981) On the distribution of noble gases in Allende: a differential oxidation study. *Earth Planet. Sci. Lett.* **56**, 45-63.

Fukunaga K. and Matsuda J.-I. (1997) Vapour-growth carbon and the origin of carbonaceous material in ureilites. *Geochemical J.*, 263-273.

Fukunaga K., Matsuda J.-I., Nagao K., Miyamoto M. and Ito K. (1987) Noble-gas enrichment in vapour-growth diamonds and the origin of diamonds in ureilites. *Nature* **328**, 141-143.

Gallino R., Busso M., Picchio G. and Raiteri C. M. (1990) On the astrophysical interpretation of isotope anomalies in meteoritic SiC grains. *Nature* **348**, 298-302.

Gautier D. (1983) Helium and deuterium in the outer solar system. *Proc. ESO Workshop "Primordial Helium" Garching, 2-3 Feb. 1983*, 139-161.

Gautier D. and Morel P. (1997) A reestimate of the protosolar $(^2He/^1H)_p$ ratio from $(^3He/^4He)_{sw}$ solar wind measurements. *Astron. Astrophys.* **323**, L9-L12.

Geiss J. (1993) Primordial abundances of hydrogen and helium isotopes. In *Origin and evolution of the elements* (ed. N. Prantzos, E. Vangioni-Flam and M. Cassé). Cambridge University Press, Cambridge.

Geiss J. and Gloeckler G. (1998) Abundances of deuterium and helium-3 in the protosolar cloud. In *Space Sciences Series of ISSI* (eds. N. Prantzos, M. Tosi and R. v. Steiger), pp. 239-250. Kluwer Academic Publishers, Dordrecht.

Geiss J. and Reeves H. (1972) Cosmic and solar system abundances of deuterium and helium-3. *Astron. & Astrophys.* **18**, 126-132.

Gloeckler G. and Geiss G. (1996) Abundance of ^{3}He in the local interstellar cloud. *Nature* **381**, 210-212.

Gloeckler G. and Geiss J. (1998) Measurement of the abundance of helium-3 in the Sun and in the local interstellar cloud with SWICS on Ulysses. In *Space Sciences Series of ISSI* (eds. N. Prantzos, M. Tosi and R. v. Steiger), pp. 275-284. Kluwer Academic Publishers, Dordrecht.

Göbel R., Ott U. and Begemann F. (1978) On trapped noble gases in ureilites. *J. Geophys. Res.* **83**, 855-867.

Goodrich C. A. (1992) Ureilites: A critical review. *Meteoritics* **27**, 327-352.

Graf T., Baur H. and Signer P. (1990) A model for the production of cosmogenic nuclides in chondrites. *Geochim. Cosmochim. Acta* **54**, 2521-2534.

Greenberg R., Weidenschilling S. J., Chapman C. R. and Davis D. R. (1984) From icy planetesimals to outer planets and comets. *Icarus* **59**, 87-113.

Gros J. and Anders E. (1977) Gas-rich minerals in the Allende meteorite: Attempted chemical characterization. *Earth Planet. Sci. Lett.* **33**, 401-406.

Guillot T., Gautier D. and Hubbard W. B. (1997) New constraints on the composition of Jupiter from Galileo measurements and interior models. *Icarus* **130**, 534-539.

Guimon R. K., Lofgren G. E. and Sears D. W. G. (1988) Chemical and physical studies of type 3 chondrites. IX: Thermoluminescence and hydrothermal annealing experiments and their relationship to metamorphism and aqueous alteration in type <3.3 ordinary chondrites. *Geochim. Cosmochim. Acta* **52**, 119-127.

Guimon R. K., Symes S. J. K., Sears D. W. G. and Benoit P. H. (1995) Chemical and physical studies of type 3 chondrites XII: The metamorphic history of CV chondrites and their components. *Meteoritics* **30**, 704-714.

Heymann D. (1986) Buckminsterfullerene, its siblings, and soot: Carriers of trapped inert gases in meteorites? *Proc. 17th Lunar Planet. Sci. Conf., J. Geophys. Res.* **91**, E135-E138.

Heymann D. (1998) A novel idea about the nature of phase Q. *Lunar Planet. Sci. Conf.* **XXIX**, #1098.

Huss G. R. (1990) Ubiquitous interstellar diamond and SiC in primitive chondrites: abundances reflect metamorphism. *Nature* **347**, 159-162.

Huss G. R. (1997) The survival of presolar grains in solar system bodies. *AIP Conf. Proc.* **402**, 721-748.

Huss G. R. and Alexander Jr. E. C. (1987) On the presolar origin of the "planetary" noble gas component in meteorites. *Proc. 7th Lunar Planet. Sci. Conf., J. Geophys. Res.* **92**(B4), E710-E716.

Huss G. R., D.Hutcheon I. and Wasserburg G. J. (1997) Isotopic systematics of presolar silicon carbide from the Orgueil (CI) chondrite: Implications for solar system formation and stellar nucleosynthesis. *Geochim. Cosmochim. Acta* **61**, 5117-5148.

Huss G. R., Hutcheon I. D., Wasserburg G. J. and Stone J. (1992) Presolar (?) corundum in the Orgueil meteorite. *Lunar Planet. Sci. Conf.* **XXIII**, 563-564.

Huss G. R. and Lewis R. S. (1994a) Noble gases in presolar diamonds I: Three distinct components and their implications for diamond origins. *Meteoritics* **29**, 791-810.

Huss G. R. and Lewis R. S. (1994b) Noble gases in presolar diamonds II: Component abundances reflect thermal processing. *Meteoritics* **29**, 811-829.

Huss G. R. and Lewis R. S. (1995) Presolar diamond, SiC, and graphite in primitive chondrites: Abundances as a function of meteorite class and petrologic type. *Geochim. Cosmochim. Acta* **59**, 115-160.

Huss G. R., Lewis R. S. and Hemkin S. (1996) The "normal planetary" noble gas component in primitive chondrites: Compositions, carrier, and metamorphic history. *Geochim. Cosmochim. Acta* **60**, 3311-3340.

Hutchison R., Alexander C. M. O. and Barber D. J. (1987) The Semarkona meteorite: First recorded occurence of smectite in an ordinary chondrite, and its implications. *Geochim. Cosmochim. Acta* **51**, 1875-1882.

Johnson W. M. and Maxwell J. A. (1981) *Rock and mineral analysis*. J. Wiley & Sons, New York.

Kallenbach R., Ipavich F. M., Kucharek H., Bochsler P., Galvin A. B., Geiss J., Gliem F., Gloeckler G., Grünwaldt H., Hefti S., Hilchenbach M. and Hovestadt D. (1998) Fractionation of Si, Ne, and Mg isotopes in the solar wind as measured by SOHO/CELIAS/MTOF. *Space Sci. Rev.* **85**, 357-370.

Keck B. D. and Sears D. W. G. (1987) Chemical and physical studies of type 3 chondrites - VIII: Thermoluminescence and metamorphism in the CO chondrites. *Geochim. Cosmochim. Acta* **51**, 3013-3021.

Kehm K., Amari S., Hohenberg C. M. and Lewis R. S. (1996) ^{22}Ne-E(L) measured in individual KFC1 graphite grains from the Murchison meteorite. *Lunar Planet. Sci. Conf.* **XXVII**, 657-658.

Kerridge J. F. and Matthews M. S. (1988) Meteorites and the early solar system. In *Space science series*. University of Arizona Press, Tuscon.

Kirsten T., Ries D., Englert P. and Herr W. (1980) Cosmogenic nuclides in 13 chondrite finds: Implications for exposure age systematics. *Meteoritics* **15**, 317-318.

Lavielle B. and Marti K. (1992) Trapped xenon in ordinary chondrites. *J. Geophys. Res.* **97**, 20875-20881.

Lewis R. S., Amari S. and Anders E. (1990) Meteoritic silicon carbide: pristine material from carbon stars. *Nature* **348**, 293-298.

Lewis R. S., Amari S. and Anders E. (1994) Interstellar grains in meteorites: II. SiC and its noble gases. *Geochim. Cosmochim. Acta* **58**, 471-494.

Lewis R. S., Ming T., Wacker J. F., Anders E. and Steel E. (1987) Interstellar diamonds in meteorites. *Nature* **326**, 160-162.

Lewis R. S., Srinivasan B. and Anders E. (1975) Host phase of a strange xenon component in Allende. *Science* **190**, 1251-1262.

Linsky J. L. (1998) Deuterium abundance in the local ISM and possible spatial variations. In *Space Sciences Series of ISSI* (eds. N. Prantzos, M. Tosi and R. v. Steiger), pp. 285-296. Kluwer Academic Publishers, Dordrecht.

Linsky J. L., Brown A., Gayley K., Diplas A., Savage B. D., Ayres T. R., Landsman W., Shore S. N. and Heap S. R. (1993) Goddard high-resolution spectrograph observations of the local interstellar medium and the deuterium/hydrogen ratio along the line of sight toward Capella. *Astrophys. J.* **402**, 694-709.

Ma C., Sporleder C. R. and Bonham R. A. (1991) A pulsed electron beam time of flight apparatus for measuring absolute electron impact ionization and dissociative ionization cross sections. *Rev. Sci. Instrum.* **62**, 909-923.

Macdougall J. D. and Phinney D. (1977) Olivine separates from Murchison and Cold Bokkeveld: Particle tracks and noble gases. *Proc. 8th Lunar Sci. Conf.*, 293-311.

Mahaffy P. R., Donahue T. M., Atreya S. K., Owen T. C. and Niemann H. B. (1998) Galileo probe measurements of D/H and ^{3}He/^{4}He in Jupiter's atmosphere. In *Space Sciences Series of ISSI* (eds. N. Prantzos, M. Tosi and R. v. Steiger), pp. 252-263. Kluwer Academic Publishers, Dordrecht.

Marti K. (1967) Isotopic composition of the trapped krypton and xenon in chondrites. *Earth Planet. Sci. Lett.* **3**, 243-248.

Marti K. and Graf T. (1992) Cosmic-ray exposure history of ordinary chondrites. *Ann. Rev. Earth Planet. Sci.* **20**, 221-243.

Matsuda J.-I., Amari S. and Nagao K. (1999) Purely physical separation of a small fraction of the Allende meteorite that is highly enriched in noble gases. *Meteoritics & Planet. Sci.* **34**, 129-136.

Matsuda J.-I., Lewis R. S., Takahashi H. and Anders E. (1980) Isotopic anomalies of noble gases in meteorites and their origins - VII. C3V carbonaceous chondrites. *Geochim. Cosmochim. Acta* **44**, 1861-1874.

Mazor E., Heymann D. and Anders E. (1970) Noble gases in carbonaceous chondrites. *Geochim. Cosmochim. Acta* **34**, 781-824.

McSween Jr. H. Y. (1977) Carbonaceous chondrites of the Ornans type: a metamorphic sequence. *Geochim. Cosmochim. Acta* **41**, 477-491.

McSween Jr. H. Y. (1979) Are carbonaceous chondrites primitive or processed? A review. *Rev. Geophys. Space Sci.* **17**, 1059-1078.

McSween Jr. H. Y. and Sears D. W. G. (1988) Thermal metamorphism. In *Meteorites and the early solar system* (eds. J. F. Kerridge and M. S. Matthews), pp. 102-113. The University of Arizona Press, Tuscon.

Meshik A. P., Pravdivtseva O. P. and Hohenberg C. M. (1998) Selective laser extraction of gases from mineral populations with different optical properties: A first test on Murchison diamonds. *Meteoritics & Planet. Sci.* **33**, A106.

Michel T. and Eugster O. (1994) Primitive xenon in diogenites and plutonium-244-fission xenon ages of a diogenite, a howardite, and eucrites. *Meteoritics* **29**, 593-606.

Moniot R. K. (1980) Noble-gas-rich separates from ordinary chondrites. *Geochim. Cosmochim. Acta* **44**, 253-271.

Müller O., Hampel W., Kirsten T. and Herzog G. F. (1981) Cosmic-ray constancy and cosmogenic production rates in short-lived chondrites. *Geochim. Cosmochim. Acta* **45**, 447-460.

Murer C. A., Baur H., Signer P. and Wieler R. (1997) Helium, neon, and argon abundances in the solar wind: In vacuo etching of meteoritic iron-nickel. *Geochim. Cosmochim. Acta* **61**, 1303-1314.

Nakamura T., Nagao K. and Takaoka N. (1998) Microdistribution of primordial noble gases in CM chondrites determined by in-situ laser microprobe analysis: deciphering of nebular processes. *submitted Geochim. Cosmochim. Acta.*

Nichols Jr. R. H., Hohenberg C. M., Alexander C. M. O. D., Olinger C. T. and Arden J. W. (1991) Xenon and neon from acid-resistant residues of Inman and Tieschitz. *Geochim. Cosmochim. Acta* **55**, 2921-2936.

Nichols Jr. R. H., Hohenberg C. M., Hoppe P., Amari S. and Lewis R. S. (1992) ^{22}Ne-E(H) and ^{4}He in single SiC grains and ^{22}Ne-E(L) in single C_{alpha} grains of known C-isotopic compositions. *Lunar Planet. Sci. Conf.* XXIII, 989-990.

Niederer F. (1978) Edelgasanalysen in getrennten Mineralphasen der Meteoriten Dimmitt und St. Severin. Diss. Universität Bern, Bern.

Niederer F. and Eberhardt P. (1977) A neon-E-rich phase in Dimmitt. *Meteoritics* **12**, 327-331.

Niemann H. B., Atreya S. K., Carignan G. R., Donahue T. M., Haberman J. A., Harpold D. N., Hartle R. E., Hunten D. M., Kasprzak W. T., Mahaffy P. R., Owen T. C., Spencer N. W. and Way S. H. (1996) The Galileo probe mass spectrometer: composition of Jupiter's atmosphere. *Science* **272**, 846-849.

Niemann H. B., Atreya S. K., Carignan G. R., Donahue T. M., Haberman J. A., Harpold D. N., Hartle R. E., Hunten D. M., Kasprzak W. T., Mahaffy P. R., Owen T. C. and Way S. H. (1998) The composition of the Jovian atmosphere as determined by the Gallileo probe mass spectrometer. *J. Geophys. Res.* **103**, 22831-22845.

Nier A. O. (1950a) A redetermination of the relative abundances of the isotopes of carbon, nitrogen, oxygen, argon and potassium. *Phys. Rev.* **77**, 789-793.

Nier A. O. (1950b) A redetermination of the relative abundances of the isotopes of neon, krypton, rubidium, xenon, and mercury. *Phys. Rev.* **79**, 450-454.

Nier A. O. and Schlutter D. J. (1990) Helium and neon isotopes in stratospheric particles. *Meteoritics* **25**, 263-267.

Nier A. O. and Schlutter D. J. (1992) Extraction of helium from individual interplanetary dust particles by step-heating. *Meteoritics* **27**, 166-173.

Nier A. O. and Schlutter D. J. (1993) The thermal history of interplanetary dust particles collected in the Earth's stratosphere. *Meteoritics* **28**, 675-681.

Nishiizumi K., Regnier S. and Marti K. (1980) Cosmic ray exposure ages of chondrites, pre-irradiation and constancy of cosmic ray flux in the past. *Earth Planet. Sci. Lett.* **50**, 156-170.

Nittler L. R., Alexander C. M. O. D., Amari S., Gao X., Walker R. M. and Zinner E. K. (1994) Interstellar oxide grains from the Tieschitz ordinary chondrite. *Nature* **370**, 443-446.

Nittler L. R., Hoppe P., Alexander C. M. O. D., Amari S. and Eberhardt P. (1995) Silicon nitride from supernovae. *Astrophys. J.* **453**, L25-L28.

Ott U. (1993) Interstellar grains in meteorites. *Nature* **364**, 25-33.

Ott U. and Begemann F. (1997) Spallation recoil and the age of presolar meteorite grains. *Meteoritics & Planet. Sci.* **32**, A102-A103.

Ott U., Begemann F., Yang J. and Epstein S. (1988) S-process krypton of variable isotopic composition in the Murchison meteorite. *Nature* **332**, 700-702.

Ott U., Kronenbitter J., Flores J. and Chang S. (1984) Colloidally separated samples from Allende residues: Noble gases, carbon, and an ESCA-study. *Geochim. Cosmochim. Acta* **48**, 267-280.

Ott U., Löhr H. P. and Begemann F. (1985a) Trapped neon in ureilites - a new component. In *Isotopic ratios in the solar system / Rapports isotopiques dans le systeme solaire*, pp. 129-136. Centre National d'Etudes Spatiales, Paris, 19-22 june 84 / 19-22 juin 84.

Ott U., Löhr H. P. and Begemann F. (1985b) Trapped noble gases in 5 more ureilites and the possible role of Q. *Lunar Planet. Sci. Conf.* **XVI**, 639-640.

Ott U., Mack R. and Chang S. (1981) Noble-gas-rich separates from the Allende meteorite. *Geochim. Cosmochim. Acta* **45**, 1751-1788.

Owen T., Lutz B. L. and Bergh C. de (1986) Deuterium in the outer solar system: evidence for two distinct reservoirs. *Nature* **320**, 244-246.

Ozima M. and Nakazawa K. (1980) Origin of rare gases in the Earth. *Nature* **284**, 313-316.

Ozima M. and Podosek F. A. (1983) *Noble gas geochemistry.* Cambridge University Press, Cambridge.

Ozima M., Wieler R., Marty B. and Podosek F. A. (1998) Comparative studies of solar, Q-gases and terrestrial noble gases, and implications on the evolution of the solar nebula. *Geochim. Cosmochim. Acta* **62**, 301-314.

Pagel B. E. (1997) *Nucleosynthesis and chemical evolution of galaxies.* Cambridge University Press, Cambridge.

Pedroni A. (1993) unpublished data, priv. commun. In *Noble gases in meteorites 1998* (ed. L. Schultz), Mainz.

Peebles P. J. E. (1966) Primordial helium abundance and the primordial fireball. II. *Astrophys. J.* **146**, 542-552.

Pepin R. O. (1967) Trapped neon in meteorites. *Earth Planet. Sci. Lett.* **2**, 13-18.

Pepin R. O. (1992) Origin of noble gases in the terrestrial planets. *Ann. Rev. Earth Planet. Sci.* **20**, 389-430.

Pepin R. O. and Phinney D. (1978) Components of xenon in the solar system. *preprint, University of Minnesota.*

Pepin R. P. and Schlutter D. J. (1998) Excess helium-3 in interplanetary dust particles. *Meteoritics & Planet. Sci.* **33**, A121.

Phinney D., Frick U. and Reynolds J. H. (1976) Rare-gas-rich separates from carbonaceous chondrites. *Lunar Planet. Sci. Conf.* **VII**, 691-693.

Piskunov N., Wood N. E., Linsky J. L., Dempsey R. C. and Ayres T. R. (1997) Local interstellar medium properties and deuterium abundances for the lines of sight toward HR 1099, 31 Comae, beta Ceti and beta Cassiopeiae. *Astrophys. J.* **474**, 315-328.

Reedy R. C. (1989) Cosmogenic-nuclide production rates in interstellar grains. *Lunar Planet. Sci. Conf.* **XX**, 888-889.

Reedy R. C., Arnold J. R. and Lal D. (1983) Cosmic-ray record in solar system matter. *Ann. Rev. Nucl. Part. Sci.* **33**, 505-537.

Reynolds J. H. (1967) Isotopic abundance anomalies in the solar system. *Ann. Rev. Nucl. Sci.* **17**, 253-316.

Reynolds J. H., Frick U., Neil J. M. and Phinney D. L. (1978) Rare-gas-rich separates from carbonaceous chondrites. *Geochim. Cosmochim. Acta* **42**, 1775-1797.

Reynolds J. H. and Turner G. (1964) Rare gases in the chondrite Renazzo. *J. Geophys. Res.* **69**, 3263-3281.

Rood R. T., Bania T. M., Balser D. S. and Wilson T. L. (1998) Helium-3: Status and prospects. In *Space Sciences Series of ISSI* (eds. N. Prantzos, M. Tosi and R. v. Steiger), pp. 185-198. Kluwer Academic Publishers, Dordrecht.

Rubin A. E. (1998) Correlated petrologic and geochemical characteristics of CO3 chondrites. *Meteoritics & Planet. Sci.* **33**, 385-391.

Rubin A. E., Scott E. R. D., Taylor G. J., Keil K., Allen J. S. B., Mayeda T. K., Clayton R. N. and Bogard D. D. (1983) Nature of the H chondrite parent body regolith: Evidence from the Dimmitt breccia. *Proc. 13th Lunar Planet. Sci. Conf.*, A741-A754.

Sabu D. D. and Manuel O. K. (1980) Noble gas anomalies and synthesis of the chemical elements. *Meteoritics* **15**, 117-138.

Sandford S. A. (1996) The inventory of interstellar materials available for the formation of the solar system. *Meteoritics & Planet. Sci.* **31**, 449-476.

Sandford S. A., Bernstein M. P. and Swindle T. D. (1997) The trapping of noble gases by the irradiation and warming of interstellar ices. *Lunar Planet. Sci. Conf.* **XXVIII**, 1233-1234.

Sandford S. A., Bernstein M. P. and Swindle T. D. (1998) The trapping of noble gases by the irradiation and warming of interstellar ices. *Meteoritics & Planet. Sci.* **33**, A135.

Schelhaas N. (1987) *Massenspektrometrische Analyse von Edelgasen in gewöhnlichen Chondriten.* Diss. Johannes Gutenberg-Universität Mainz, Mainz.

Schelhaas N., Ott U. and Begemann F. (1990) Trapped noble gases in unequilibrated ordinary chondrites. *Geochim. Cosmochim. Acta* **54**, 2869-2882.

Schramm D. N. and Turner M. S. (1998) Big-bang nucleosynthesis enters the precision era. *Rev. Mod. Phys.* **70**, 303-318.

Scott E. R. D. and Jones R. H. (1990) Disentangling nebular and asteroidal features of CO3 carbonaceous chondrite meteorites. *Geochim. Cosmochim. Acta* **54**, 2485-2502.

Sears D. W., Grossman J. N., Melcher C. L., Ross L. M. and Mills A. A. (1980) Measuring metamorphic history of unequilibrated ordinary chondrites. *Nature* **287**, 791-795.

Sears D. W. G. and Dodd R. T. (1988) Overview and classification of meteorites. In *Meteorites and the early solar system* (eds. J. F. Kerridge and M. S. Matthews), pp. 3-31. The University of Arizona Press, Tuscon.

Signer P., Baur H. and Wieler R. (1993) Closed system stepped etching; an alternative to stepped heating. In *Alfred O. Nier Symp. on Inorganic Mass Spectrometry, May 7-9 1991*, pp. 181-202. Los Alamos National Laboratory, Durango, Colorado.

Signer P. and Suess H. E. (1963) Rare gases in the Sun, in the atmosphere, and in meteorites. In *Earth science and meteorites* (eds. J. Geiss and E. D. Goldberg), pp. 241-272. North Holland Publishing Co., Amsterdam.

Smith S. P., Huneke J. C., Rajan R. S. and Wasserburg G. J. (1977) Neon and argon in the Allende meteorite. *Geochim. Cosmochim. Acta* **41**, 627-647.

Smith S. P., Huneke J. C. and Wasserburg G. J. (1978) Neon in gas-rich samples of the carbonaceous chondrites Mokoia, Murchison, and Cold Bokkeveld. *Earth & Planet. Sci. Lett.* **39**, 1-13.

Srinivasan B. (1977) Noble gases in six ordinary chondrites: comparison of exposure ages from noble gases with Al-26 ages. *Geochim. Cosmochim. Acta* **41**, 977-983.

Srinivasan B. and Anders E. (1978) Noble gases in the Murchison meteorite: possible relics of s-process nucleosynthesis. *Science* **201**, 51-56.

Srinivasan B., Gros J. and Anders E. (1977) Noble gases in separated meteoritic minerals: Murchsion (C2), Ornans (C3), Karoonda (C5), and Abee (E4). *J. Geophys. Res.* **82**, 762-778.

Srinivasan B., Lewis R. S. and Anders E. (1978) Noble gases in the Allende and Abee meteorites and a gas-rich mineral fraction: investigation by stepwise heating. *Geochim. Cosmochim. Acta* **42**, 183-198.

Straub H. C., Renault P., Lindsay B. G., Smith K. A. and Stebbings R. F. (1995) Absolute partial and total cross sections for electron-impact ionization of argon from threshold to 1000eV. *Phys. Rev. A* **52**, 1115-1124.

Swindle T. D. (1988) Trapped noble gases in meteorites. In *Meteorites and the early solar system* (eds. J. F. Kerridge and M. S. Matthews), pp. 535-564. The University of Arizona Press, Tuscon.

Syage J. A. (1992) Electron-impact cross sections for multiple ionization of Kr and Xe. *Phys. Rev. A* **46**, 5666-5679.

Takaoka N. (1972) An interpretation of general anomalies of xenon and the isotopic composition of primitive xenon. *Mass Spectr. (Shitsuryo Bunseki)* **20**, 287-302.

Tang M. and Anders E. (1988a) Isotopic anomalies of Ne, Xe, and C in meteorites. II Interstellar diamond and SiC: Carriers of exotic noble gases. *Geochim. Cosmochim. Acta* **52**, 1235-1244.

Tang M. and Anders E. (1988b) Isotopic anomalies of Ne, Xe, and C in meteorites. III Local and exotic noble gas components and their interrelations. *Geochim. Cosmochim. Acta* **52**, 1245-1254.

Tang M., Lewis R. S., Anders E., Grady M. M., Wright I. P. and Pillinger C. T. (1988) Isotopic anomalies of Ne, Xe, and C in meteorites. I Separation of carriers by density and chemical resistance. *Geochim. Cosmochim. Acta* **52**, 1221-1234.

Thiemens M. H. (1988) Heterogeneity in the nebula: Evidence from stable isotopes. In *Meteorites and the early solar system* (eds. J. F. Kerridge and M. S. Matthews), pp. 899-923. The University of Arizona Press, Tuscon.

Tilton G. R. (1988) Age of the solar system. In *Meteorites and the early solar system* (eds. J. F. Kerridge and M. S. Matthews), pp. 259-275. The University of Arizona Press, Tuscon.

Tosi M. (1998) Galactic evolution of D and ^{3}He. In *Space Sciences Series of ISSI* (eds. N. Prantzos, M. Tosi and R. v. Steiger), pp. 207-218. Kluwer Academic Publishers, Dordrecht.

Turner G. (1988) Dating of secondary events. In *Meteorites and the early solar system* (eds. J. F. Kerridge and M. S. Matthews), pp. 276-288. The University of Arizona Press, Tuscon.

Valkiers S., Aregbe Y., Taylor P. D. P. and De Bièvre P. (1998) A primary xenon isotopic gas standard with SI traceable values for isotopic composition and molar mass. *Int. J. Mass Spectrometry Ion Processes* **173**, 55-63.

Valkiers S., Schaefer F. and De Bièvre P. (1994) Near-absolute gas (isotope) mass spectrometry: isotope abundance (and atomic weight) determinations of neon, krypton, xenon and argon. In *Separation technology* (ed. Vansant E. F.), pp. 965-968.

Van Schmus W. R. and Wood J. A. (1967) A chemical-petrologic classification for the chondritic meteorites. *Geochim. Cosmochim. Acta* **31**, 747-765.

Vogt S., Herzog G. F. and Reedy R. C. (1990) Cosmogenic nuclides in extraterrestrial materials. *Rev. Geophys.* **28**, 253-275.

Wacker J. F. (1989) Laboratory simulation of meteoritic noble gases. III Sorption of neon, argon, krypton, and xenon on carbon: Elemental fractionation. *Geochim. Cosmochim. Acta* **53**, 1421-1433.

Wacker J. F. and Marti K. (1983) Noble gas components in clasts and separates of the Abee meteorite. *Earth Planet. Sci. Lett.* **62**, 147-158.

Wacker J. F., Zadnik M. G. and Anders E. (1985) Laboratory simulation of meteoritic noble gases. I Sorption of xenon on carbon: Trapping experiments. *Geochim. Cosmochim. Acta* **49**, 1035-1048.

Wacker J. K. (1986) Noble gases in the diamond-free ureilite, ALHA 78019: The roles of shock and nebular processes. *Geochim. Cosmochim. Acta* **50**, 633-642.

Wagoner R. V., Fowler W. A. and Hoyle F. (1967) On the synthesis of elements at very high temperatures. *Astrophys. J.* **148**, 3-49.

Wallerstein G., Iben Jr. I., Parker P., Boesgaard A. M., Hale G. M., Champagne A. E., Barnes C. A., Käppeler F., Smith V. V., Hoffman R. D., Timmes F. X., Sneden C., Boyd R. N., Meyer B. S. and Lambert D. L. (1997) Synthesis of the elements in stars: forty years of progress. *Rev. Mod. Phys.* **69**, 995-1084.

Weigel A. and Eugster O. (1994) Primitive trapped Xe in Lodran minerals and further evidence from EET84302 and Gibson for break-up of the lodranite parent asteroid 4 Ma ago. *Lunar Planet. Sci. Conf.* **XXV**, 1479-1480.

Weisberg M. K., Prinz M., Clayton R. N. and Mayeda T. K. (1997) CV3 chondrites: three subgroups, not two. *Meteoritics & Planet. Sci.* **32**, A138-A139.

Wetherill G. W. (1953) Spontaneous fission yields from Uranium and Thorium. *Phys. Rev.* **92**, 907-912.

Wetherill G. W. and Chapman C. R. (1988) Asteroids and meteorites. In *Meteorites and the early solar system* (eds. J. F. Kerridge and M. S. Matthews), pp. 35-72. The University of Arizona Press, Tuscon.

Wetzel R. C., Baiocchi F. A., Hayes T. R. and Freund R. S. (1987) Absolute cross sections for electron-impact ionization of the rare-gas atoms by the fast-neutral-beam method. *Phys. Rev. A* **35**, 559-577.

Wieler R. (1994) "Q-gases" as "local" primordial noble gas component in primitive meteorites. In *Noble Gas Geochemistry and Cosmochemistry* (ed. J. Matsuda), pp. 31-41. Terra Scientific Publishing Company, Tokyo.

Wieler R. (1998) The solar noble gas record in lunar samples and meteorites. *Space Sci. Rev.* **85**, 303-314.

Wieler R., Anders E., Baur H., Lewis R. S. and Signer P. (1991) Noble gases in "phase Q": Closed-system etching of an Allende residue. *Geochim. Cosmochim. Acta* **55**, 1709-1722.

Wieler R., Anders E., Baur H., Lewis R. S. and Signer P. (1992) Characterisation of Q-gases and other noble gas components in the Murchison meteorite. *Geochim. Cosmochim. Acta* **56**, 2907-2921.

Wieler R. and Baur H. (1994) Krypton and xenon from the solar wind and solar energetic particles in two lunar ilmenites of different antiquity. *Meteoritics* **29**, 570-580.

Wieler R. and Baur H. (1995) Fractionation of Xe, Kr, and Ar in the solar corpuscular radiation deduced by closed system etching of lunar soils. *Astrophys. J.* **453**, 987-997.

Wieler R., Baur H. and Signer P. (1986) Noble gases from solar energetic particles revealed by closed system stepwise etching of lunar soil minerals. *Geochim. Cosmochim. Acta* **50**, 1997-2017.

Wieler R. and Signer P. (1989) unpublished data, pers. commun. In *Noble gases in meteorites 1998* (ed. L. Schultz), Mainz.

Wilkening L. L. and Marti K. (1976) Rare gases and fossil particle tracks in the Kenna ureilite. *Geochim. Cosmochim. Acta* **40**, 1265-1473.

Yang J., Lewis R. S. and Anders E. (1982) Sorption of noble gases by solids, with reference to meteorites. I. Magnetite and carbon. *Geochim. Cosmochim. Acta* **46**, 841-860.

Yang J., Turner M. S., Steigman G., Schramm D. N. and Olive K. A. (1984) Primordial nucleosynthesis: A critical comparison of theory and observation. *Astrophys. J.* **281**, 493-511.

Zahn U. v., Hunten D. M. and Lehmacher G. (1998) Helium in Jupiter's atmosphere: Results from the Galileo probe helium interferometer experiment. *J. Geophys. Res.* **103**, 22815-22829.

Zahnle K. (1993) Planetary noble gases. In *Protostars and planets III* (eds. E. H. Levy and J. I. Lunine), pp. 1305-1338. The University of Arizona Press, Tuscon.

Zinner E. (1995) Interstellar grains from primitive meteorites: new constraints on nucleosynthesis theory and stellar evolution models. In *Nuclei in the cosmos III*, pp. 567-579. AIP Press, Assergi, Italy.

Zinner E. (1998a) Stellar nucleosynthesis and the isotopic composition of presolar grains from primitive meteorites. *Annu. Rev. Earth Planet. Sci.* **26**, 147-88.

Zinner E. (1998b) Trends in the study of presolar dust grains from primitive meteorites. *Meteoritics & Planet. Sci.* **33**, 549-564.

Zinner E., Tang M. and Anders E. (1989) Interstellar SiC in the Murchison and Murray meteorites: Isotopic composition of Ne, Xe, Si, C, and N. *Geochim. Cosmochim. Acta* **53**, 3273-3290.

Zolensky M. and McSween Jr. H. Y. (1988) Aqueous alteration. In *Meteorites and the early solar system* (eds. J. F. Kerridge and M. S. Matthews), pp. 114-143. The University of Arizona Press, Tuscon.

7 Appendix

7.1 Noble gases in Lancé

Table 7.1: He, Ne and Ar in the **HF/HCl-resistant residue** of Lancé (**etch** run HB03, 20/05/96-20/07/96).

Step		^{4}He	^{3}He/^{4}He (x 10^4)	^{20}Ne	^{20}Ne/^{22}Ne	^{21}Ne/^{22}Ne[1]	^{36}Ar	^{36}Ar/^{38}Ar	^{40}Ar/^{36}Ar
1	vap. 1h	4.25	181	0.069	9.5	0.108	2.05	5.37	67.3
		0.09	18	0.005	0.5	0.011	0.07	0.04	0.4
2	vap. 120h	113.1	12.85	1.115	9.25	0.134	37.3	5.28	19.27
		0.9	0.16	0.018	0.08	0.002	1.3	0.02	0.07
3	vap. 215h	143.3	10.36	1.78	9.56	0.100	59	5.30	10.76
		1.1	0.14	0.02	0.04	0.002	2	0.03	0.04
4	25°C 112h	124.7	9.17	1.79	9.58	0.0860	66	5.29	11.44
		1.0	0.12	0.02	0.04	0.0017	2	0.03	0.05
5	50°C 20h	36.4	5.92	1.019	9.71	0.0701	58	5.34	2.172
		0.4	0.11	0.07	0.03	0.0016	2	0.04	0.011
5	*corrected*[2]	*107*		*1.53*					
		5		*0.07*					
6	60°C 166h	176.9	7.47	2.53	9.94	0.0627	98	5.34	1.88
		1.3	0.09	0.03	0.05	0.0008	4	0.08	0.02
7	80°C 259h	142.7	8.48	2.07	9.80	0.0627	92	5.34	1.570
		1.1	0.11	0.02	0.04	0.0016	3	0.03	0.007
8	90°C 163h	27.2	12.4	0.378	9.68	0.073	16.2	5.24	3.10
		0.4	0.3	0.009	0.17	0.004	0.6	0.04	0.02
9	60°C 259h	-0.2	5	0.001	11	-0.1	2.09	5.15	8.28
		-0.4	10	0.003	26	0.3	0.08	0.10	0.12
total		768	10.32	10.74	9.68	0.0819	431	5.32	6.43
		3	0.11	0.05	0.06	0.0009	7	0.12	0.17
total	*corrected*[2]	*839*		*11.25*					
		5		*0.09*					

Gas concentrations in 10^{-8} cm^3 STP/g residue; [1] The ^{21}Ne measurements of Lancé as well as of Dimmitt were affected by the neon-hydride interference (chapter 2.2.1). The corrections applied are described in detail in chapter 7.8.1; [2] He and Ne in step 5 suffered losses probably due to leakage (see Figure 3.17). These losses are corrected with the ^{36}Ar abundance of step 5 and mean elemental ratios ^{4}He/^{36}Ar and ^{20}Ne/^{36}Ar of steps 4 and 6. Since these ratios are almost identical, it can be assumed that step 5 is composed similar to steps 4 and 6.

Table 7.2: He and Ne[1] in (26.04 ± 0.05)mg **oxidised HF/HCl-resistant residue** of Lancé (**bulk** measurement HB07, 27/08/97-23/01/98).

Step	^{4}He	^{3}He/^{4}He (x 10^4)	^{20}Ne	^{20}Ne/^{22}Ne	^{21}Ne/^{22}Ne
1800°C[2]	3597	2.22	19.9	8.5	0.056
	22	0.05	0.4	0.2	0.002

Gas concentrations in 10^{-8} cm^3 STP/g residue; [1] Ar, Kr and Xe could not be measured due to too much Teflon-induced background gas (chapter 2.1.2); [2] Total extraction without pre-step at 600°C.

Table 7.3: Kr in the **HF/HCl-resistant residue** of Lancé (**etch run**).

Step	^{84}Kr	^{78}Kr/^{84}Kr x 100	^{80}Kr/^{84}Kr x 100	^{82}Kr/^{84}Kr x 100	^{83}Kr/^{84}Kr x 100	^{86}Kr/^{84}Kr x 100
1	5.11	0.575	3.86	20.19	19.85	31.35
	0.06	0.018	0.02	0.13	0.14	0.15
2	48.2	0.583	3.99	20.30	20.27	30.93
	0.6	0.006	0.03	0.13	0.18	0.19
3	69.4	0.589	3.91	20.06	20.30	30.92
	0.8	0.006	0.02	0.07	0.08	0.13
4	82.6	0.599	3.94	20.25	20.31	31.35
	1.1	0.006	0.04	0.10	0.07	0.14
5	60.0	0.598	3.88	20.14	20.15	30.9
	0.7	0.007	0.03	0.12	0.13	0.2
6	102.3	0.596	3.95	20.32	20.41	31.47
	1.2	0.006	0.03	0.08	0.19	0.14
7	95.0	0.600	3.96	20.36	20.35	31.43
	1.2	0.008	0.03	0.10	0.09	0.18
8	16.1	0.595	3.95	20.39	20.34	31.24
	0.2	0.010	0.03	0.08	0.11	0.18
9	2.36	0.663	3.87	20.57	19.90	30.77
	0.03	0.016	0.09	0.14	0.16	0.16
total	481	0.596	3.94	20.26	20.31	31.2
	2	0.006	0.03	0.17	0.17	0.3

Gas concentrations in 10^{-10} cm^3 STP/g residue.

Table 7.4: Xe in the **HF/HCl-resistant residue** of Lancé (**etch run**).

Step	^{132}Xe	^{124}Xe/^{132}Xe x 100	^{126}Xe/^{132}Xe x 100	^{128}Xe/^{132}Xe x 100	^{129}Xe/^{132}Xe x 100	^{130}Xe/^{132}Xe x 100	^{131}Xe/^{132}Xe x 100	^{134}Xe/^{132}Xe x 100	^{136}Xe/^{132}Xe x 100
1	2.58	0.42	0.37	7.98	109.9	15.72	81.3	37.93	32.2
	0.03	0.02	0.02	0.06	0.6	0.13	0.6	0.17	0.3
2	40.5	0.456	0.406	8.27	111.0	16.40	81.8	38.1	31.9
	0.6	0.006	0.005	0.07	1.1	0.15	0.6	0.3	0.3
3	62.9	0.462	0.414	8.44	108.7	16.45	82.5	38.9	32.1
	0.9	0.004	0.003	0.06	0.7	0.11	0.6	0.3	0.3
4	80.0	0.467	0.404	8.34	107.9	16.44	82.45	38.43	31.9
	1.0	0.003	0.003	0.06	0.7	0.06	0.14	0.09	0.3
5	61.0	0.458	0.402	8.34	105.0	16.31	82.1	37.9	32.1
	0.8	0.003	0.006	0.04	0.5	0.09	0.4	0.3	0.3
6	123[1]	0.446	0.397	8.1	[2]	15.7	81.8	37.1	31.6
	2	0.014	0.013	0.3		0.5	2.7	1.2	1.0
7	92.8	0.488	0.430	8.68	[2]	17.13	85.42	39.67	33.32
	1.2	0.005	0.003	0.03		0.02	0.18	0.19	0.16
8	15.2	0.450	0.407	8.12	103.8	16.30	82.2	37.59	31.8
	0.2	0.008	0.006	0.04	0.5	0.07	0.4	0.16	0.2
9	2.55	0.460	0.395	8.12	104.5	16.69	81.6	38.1	31.0
	0.03	0.006	0.009	0.04	0.7	0.12	0.5	0.2	0.2
total	481	0.462	0.408	8.32	107.3[3]	16.3	82.6	38.2	32.1
	3	0.006	0.005	0.04	1.0	0.2	1.0	0.5	0.4

Gas concentrations in 10^{-10} cm^3 STP/g residue; [1] ^{132}Xe could be measured, although less precisely, with the Faraday cup; [2] not measured; [3] ratio determined without Xe abundances of steps 6 and 7 (including ^{132}Xe of steps 6 and 7: ^{129}Xe/^{132}Xe = 59.1 ± 0.6).

7.2 Noble gases in Dimmitt

Table 7.5: He, Ne and Ar in the **HF/HCl-resistant residue** of Dimmitt (**etch** run HB04, 03/10/96-30/01/97).

Step		^{4}He	^{3}He/^{4}He (x 10^4)	^{20}Ne	^{20}Ne/^{22}Ne	^{21}Ne/^{22}Ne[1]	^{36}Ar	^{36}Ar/^{38}Ar	^{40}Ar/^{36}Ar
1	vap. 3h	2.98	4.98	0.0425	11.18	0.073	0.095	5.4	33
		0.03	0.13	0.0008	0.14	0.003	0.011	0.7	3
1	*corrected[2]*	*0.29*		*0.004*					
		0.15		*0.002*					
2	vap. 17h	6.92	6.2	0.0794	10.97	0.120	0.418	5.42	31.1
		0.05	0.2	0.0010	0.07	0.004	0.015	0.19	0.6
2	*corrected[2]*	*1.3*		*0.021*					
		0.6		*0.011*					
3	vap. 162h	30.2	6.90	0.339	10.08	0.1441	3.65	5.49	10.38
		0.2	0.12	0.004	0.06	0.0017	0.08	0.03	0.05
3	*corrected[2]*	*11*		*0.16*					
		6		*0.08*					
4	25°C 111h	32.4	6.87	0.428	9.89	0.135	6.29	5.52	12.92
		0.2	0.12	0.004	0.02	0.002	0.15	0.06	0.10
5	40°C 88h	24.1	7.13	0.355	9.87	0.1220	7.2	5.51	3.85
		0.2	0.12	0.004	0.04	0.0010	0.2	0.09	0.05
6	60°C 112h	33.1	6.84	0.493	9.98	0.1033	11.5	5.48	1.91
		0.2	0.10	0.005	0.03	0.0011	0.3	0.12	0.03
7	70°C 255h	37.0	6.93	0.559	10.02	0.0955	16.0	5.48	1.667
		0.3	0.10	0.007	0.05	0.0016	0.4	0.03	0.008
8	90°C 211h	13.46	6.86	0.197	10.02	0.0991	6.17	5.40	1.564
		0.10	0.12	0.002	0.05	0.0018	0.14	0.05	0.010
9	100°C 260h	32.7	7.13	0.300	10.00	0.1067	9.0	5.45	1.359
		0.2	0.10	0.003	0.03	0.0015	0.2	0.04	0.008
9	*corrected[2]*	*20*		*0.29*					
		2		*0.03*					
10	115°C 40h	2.98	6.51	0.0173	10.5	0.133	0.46	5.2	2.47
		0.02	0.13	0.0007	0.3	0.006	0.03	0.3	0.09
10	*corrected[2]*	*1.00*		*0.0147*					
		0.11		*0.0017*					
11	130°C 187h	59.9	6.48	0.147	9.78	0.200	2.77	5.46	2.81
		0.4	0.10	0.003	0.11	0.003	0.06	0.05	0.02
11	*corrected[2]*	*6.0*		*0.088*					
		0.6		*0.009*					
total		275.7	6.81	2.957	10.01	0.1186	63.6	5.47	3.82
		0.7	0.04	0.012	0.06	0.0009	0.6	0.08	0.05
total	*corrected[2]*	*222*		*2.63*					
		8		*0.08*					

Gas concentrations in 10^{-8} cm^3 STP/g residue; [1] see footnote [1] of Table 7.1; [2] Steps 1-3 and 9-11 contain large abundances of solar He and Ne (see chapter 3.2, Figure 3.18). Steps 9-11 form a mixing line with Q and SW/SEP data points as end members (Murer *et al.*, 1997). Therefore, these steps can accurately be corrected by calculating two-component mixing ratios. On the other hand, steps 1-3 form also a mixing line, but with an unknown, elementally heavier component. The contributions are corrected with ^{36}Ar abundances of steps 1-3 and elemental ratios ^{4}He/^{36}Ar and ^{20}Ne/^{36}Ar of steps 4-6 with adopted errors of 50 %.

Table 7.6: He, Ne and Ar[1] in (7.63 ± 0.05)mg **HF/HCl-resistant residue** of Dimmitt (**bulk** measurement HB09, 06/05/98-22/05/98).

Step	^{4}He	^{3}He/^{4}He (x 10^4)	^{20}Ne	^{20}Ne/^{22}Ne	^{21}Ne/^{22}Ne	^{36}Ar	^{36}Ar/^{38}Ar	^{40}Ar/^{36}Ar
600°C	2328	5.1	2	10	0.10			
	91	0.5	3	9	0.09			
1800°C	29387	4.0	64	11.7	0.097	100	5.4	16.5
	1170	0.2	2	0.5	0.004	3	0.2	0.6
total	31715	4.05	67	11.6	0.097			
	1173	0.19	4	1.1	0.010			

Gas concentrations in 10^{-8} cm^3 STP/g residue; [1] 600°C step not measured to avoid too much background gas (chapter 2.1.2)..

Table 7.7: He, Ne and Ar[1] in (14.40 ± 0.02)mg **oxidised HF/HCl-resistant residue** of Dimmitt (bulk measurement HB09, 06/05/98-22/05/98).

Step	^{4}He	^{3}He/^{4}He (x 10^4)	^{20}Ne	^{20}Ne/^{22}Ne	^{21}Ne/^{22}Ne	^{36}Ar	^{36}Ar/^{38}Ar	^{40}Ar/^{36}Ar
600°C	1661	4.8	1.9	11	0.18			
	64	0.4	1.9	8	0.13			
1800°C	19757	3.97	41.3	11.5	0.106	38.7	5.4	32.8
	771	0.19	1.2	0.4	0.004	1.2	0.3	1.5
total	21418	4.03	43	11.4	0.110			
	773	3.18	2	0.9	0.011			

Gas concentrations in 10^{-8} cm^3 STP/g residue; [1] 600°C step not measured to avoid too much background gas (chapter 2.1.2).

Table 7.8: Kr in the **HF/HCl-resistant residue** of Dimmitt (etch run).

Step	^{84}Kr	^{78}Kr/^{84}Kr x 100	^{80}Kr/^{84}Kr x 100	^{82}Kr/^{84}Kr x 100	^{83}Kr/^{84}Kr x 100	^{86}Kr/^{84}Kr x 100
1	13.80	0.60	3.71	19.76	19.84	31.3
	0.17	0.02	0.02	0.14	0.13	0.2
1 cor.[1]	*1.75*					
	0.18					
2	7.54	0.51	3.750	19.50	20.03	31.70
	0.09	0.09	0.019	0.08	0.09	0.17
2 cor.[1]	*0.044*					
	0.004					
3	7.78	0.53	3.86	19.84	19.93	30.87
	0.08	0.06	0.02	0.11	0.07	0.10
3 cor.[1]	*3.1*					
	0.3					
4	9.65	0.54	3.91	20.13	20.07	31.07
	0.11	0.06	0.03	0.10	0.05	0.13
4 cor.[1]	*7.1*					
	0.7					
5	7.71	0.532	3.938	20.12	20.12	30.85
	0.08	0.014	0.019	0.09	0.09	0.12
6	11.49	0.56	3.919	20.30	20.16	30.68
	0.13	0.07	0.016	0.07	0.13	0.11
7	16.26	0.54	3.926	20.25	20.25	31.00
	0.18	0.07	0.012	0.07	0.05	0.10
8	6.54	0.540	3.95	20.17	20.23	30.83
	0.07	0.015	0.02	0.17	0.08	0.13

... Table 7.8 continued

Step	^{84}Kr	^{78}Kr/^{84}Kr x 100	^{80}Kr/^{84}Kr x 100	^{82}Kr/^{84}Kr x 100	^{83}Kr/^{84}Kr x 100	^{86}Kr/^{84}Kr x 100
9	8.77	0.57	3.91	20.35	20.30	30.97
	0.10	0.05	0.03	0.08	0.09	0.13
10	0.485	0.59	3.91	20.07	20.12	31.4
	0.006	0.04	0.05	0.13	0.07	0.4
11	2.94	0.50	3.89	20.41	20.13	30.86
	0.03	0.04	0.04	0.09	0.14	0.12
total	93.0	0.55	3.87	20.07	20.10	31.02
	0.4	0.02	0.02	0.12	0.12	0.19
total cor.[1]	*66.2*					
	0.8					

Gas concentrations in 10^{-10} cm^3 STP/g residue; [1] Steps 1-4 contain significant amounts of adsorbed Kr and Xe (see Figure 3.18). Steps 1-5 form a two-component-mixing line with pure Q of step 5 and an adsorbed component (^{36}Ar/^{132}Xe = 0; ^{84}Kr/^{132}Xe = 0.7239) as end members. These components were used with an uncertainty assumed to be 10 % to correct for adsorbed Kr and Xe (Figure 7.1).

Table 7.9: Kr[1] in the **HF/HCl-resistant residue** of Dimmitt (**bulk** measurement).

Step	^{84}Kr	^{78}Kr/^{84}Kr x 100	^{80}Kr/^{84}Kr x 100	^{82}Kr/^{84}Kr x 100	^{83}Kr/^{84}Kr x 100	^{86}Kr/^{84}Kr x 100
1800°C	97	..	4.9	23.3	22.6	..
	5	..	0.3	1.4	1.5	..

Gas concentrations in 10^{-10} cm^3 STP/g residue; [1] 600°C step not measured to avoid too much background gas (chapter 2.1.2).

Table 7.10: Kr[1] in the **oxidised HF/HCl-resistant residue** of Dimmitt (**bulk** measurement).

Step	^{84}Kr	^{78}Kr/^{84}Kr x 100	^{80}Kr/^{84}Kr x 100	^{82}Kr/^{84}Kr x 100	^{83}Kr/^{84}Kr x 100	^{86}Kr/^{84}Kr x 100
1800°C	37	..	4.5	25	24	..
	3	..	0.4	2	2	..

Gas concentrations in 10^{-10} cm^3 STP/g residue; [1] 600°C step not measured to avoid too much background gas (chapter 2.1.2).

Table 7.11: Xe in the **HF/HCl-resistant residue** of Dimmitt (etch run).

Step	^{132}Xe	^{124}Xe/^{132}Xe x 100	^{126}Xe/^{132}Xe x 100	^{128}Xe/^{132}Xe x 100	^{129}Xe/^{132}Xe x 100	^{130}Xe/^{132}Xe x 100	^{131}Xe/^{132}Xe x 100	^{134}Xe/^{132}Xe x 100	^{136}Xe/^{132}Xe x 100
1	19.5	0.345	0.326	6.88	97.3	14.90	77.6	38.7	32.3
	0.3	0.005	0.005	0.06	1.0	0.10	0.5	0.3	0.3
1 cor.[1]	*1.53*								
	0.16								
2	10.43	0.348	0.319	7.18	97.2	15.17	78.0	38.8	32.96
	0.17	0.006	0.002	0.04	0.6	0.06	0.5	0.2	0.16
2 cor.[1]	*0.41*								
	0.04								
3	11.61	0.411	0.365	7.81	104.0	15.70	80.6	38.28	32.3
	0.19	0.005	0.003	0.05	0.4	0.04	0.2	0.13	0.2
cor.[1]	*5.8*								
	0.6								

... Table 7.11 continued

Step	^{132}Xe	^{124}Xe/^{132}Xe x 100	^{126}Xe/^{132}Xe x 100	^{128}Xe/^{132}Xe x 100	^{129}Xe/^{132}Xe x 100	^{130}Xe/^{132}Xe x 100	^{131}Xe/^{132}Xe x 100	^{134}Xe/^{132}Xe x 100	^{136}Xe/^{132}Xe x 100
4	15.3	0.446	0.385	8.04	105.0	16.11	81.2	38.2	32.23
	0.3	0.005	0.003	0.04	0.5	0.06	0.6	0.2	0.18
cor.[1]	11.4								
	1.2								
5	12.8	0.446	0.443	8.9	112	16.6	87	36	30.3
	0.5	0.018	0.021	0.4	4	0.8	3	2	1.4
6	20.4	0.449	0.395	8.29	106	16.19	82.3	37.1	31.4
	0.4	0.005	0.005	0.07	3	0.12	0.6	0.3	0.3
7	29.2	0.456	0.438	8.24	104.8	16.20	81.2	37.5	31.7
	0.5	0.006	0.005	0.07	0.8	0.10	0.6	0.3	0.2
8	13.0	0.478	0.411	8.22	104.3	16.27	82.7	38.2	29.68
	0.2	0.009	0.004	0.05	0.5	0.08	0.4	0.3	0.16
9	14.7	0.448	0.399	8.22	104.7	16.13	81.7	37.8	30.8
	0.2	0.005	0.004	0.06	0.6	0.08	0.4	0.5	0.2
10	1.35	0.462	0.423	8.13	104.4	16.27	81.9	38.4	31.5
	0.02	0.011	0.005	0.07	0.8	0.14	0.8	0.4	0.4
11	4.74	0.456	0.397	8.26	104.4	16.42	82.2	37.6	30.5
	0.08	0.008	0.005	0.08	0.6	0.08	0.6	0.3	0.2
total	153.0	0.429	0.392	7.99	104.0	15.96	81.3	37.8	31.5
	1.0	0.005	0.004	0.09	1.1	0.17	0.8	0.4	0.3
total cor.[1]	115.3								
	1.6								

Gas concentrations in 10^{-10} cm^3 STP/g residue; [1] see footnote [1] of Table 7.8.

Figure 7.1: The ^{36}Ar/^{132}Xe vs. ^{84}Kr/^{132}Xe plot for the CSSE steps of Dimmitt shows (in combination with the Xe three-isotope-plots of chapter 3.1.5) that steps 1-4 contain large amounts of adsorbed atmospheric Kr and Xe. The deduced ^{84}Kr/^{132}Xe ratio of 0.7239 is much smaller than that of air. This might be the result of a higher solubility of Xe in acid. Blank measurements of dissolved air that has been directly released from HNO$_3$ yielded similar ^{84}Kr/^{132}Xe ratios between 0.4 and 1.8.

Table 7.12: Xe[1] in the **HF/HCl-resistant residue** of Dimmitt (**bulk** measurement).

Step	^{132}Xe	^{124}Xe/^{132}Xe x 100	^{126}Xe/^{132}Xe x 100	^{128}Xe/^{132}Xe x 100	^{129}Xe/^{132}Xe x 100	^{130}Xe/^{132}Xe x 100	^{131}Xe/^{132}Xe x 100	^{134}Xe/^{132}Xe x 100	^{136}Xe/^{132}Xe x 100
1800°C	183	0.38	0.38	7.8	108	15.8	83	39.4	33.3
	6	0.04	0.02	0.3	4	0.5	3	1.4	1.1

Gas concentrations in 10^{-10} cm^3 STP/g residue; [1] 600°C step not measured to avoid too much background gas (chapter 2.1.2).

Table 7.13: Xe[1] in the **oxidised HF/HCl-resistant residue** of Dimmitt (**bulk** measurement).

Step	^{132}Xe	^{124}Xe/^{132}Xe x 100	^{126}Xe/^{132}Xe x 100	^{128}Xe/^{132}Xe x 100	^{129}Xe/^{132}Xe x 100	^{130}Xe/^{132}Xe x 100	^{131}Xe/^{132}Xe x 100	^{134}Xe/^{132}Xe x 100	^{136}Xe/^{132}Xe x 100
1800°C	66	0.50	0.45	8.1	109	16.0	81	39	32.1
	3	0.03	0.04	0.4	6	0.8	4	2	1.5

Gas concentrations in 10^{-10} cm^3 STP/g residue; [1] 600°C step not measured to avoid too much background gas (chapter 2.1.2).

7.3 Noble gases in Grosnaja

Table 7.14: He, Ne and Ar in the **HF/HCl-resistant residue** of Grosnaja (etch run HB05, 27/02-12/05/97).

Step		^{4}He	^{3}He/^{4}He (x 10^4)	^{20}Ne	^{20}Ne/^{22}Ne	^{21}Ne/^{22}Ne	^{36}Ar	^{36}Ar/^{38}Ar	^{40}Ar/^{36}Ar
1	vap. 19h	149	1.50	0.852	10.65	0.0447	12.6	5.345	108.9
		2	0.03	0.011	0.04	0.0006	0.3	0.013	0.5
2	vap. 214h[1]	243	1.45	1.34	10.61	0.0350	12.1	5.377	9.56
		3	0.03	0.02	0.06	0.0008	0.2	0.009	0.03
3	vap. 127h	469	1.48	2.91	10.59	0.0357	37.1	5.34	18.71
		6	0.03	0.04	0.04	0.0006	0.8	0.02	0.10
4	vap 113h	423	1.48	2.78	10.56	0.0355	44.0	5.39	8.195
		5	0.03	0.04	0.04	0.0009	0.8	0.02	0.013
5	vap. 43h	394	1.47	2.79	10.65	0.0348	46.7	5.35	5.70
		5	0.03	0.04	0.04	0.0006	1.3	0.02	0.05
6	after dest.	263	1.45	1.94	10.60	0.0354	35.0	5.386	24.62
		3	0.03	0.02	0.03	0.0008	0.7	0.012	0.10
7	25°C 20h	93	1.46	0.72	10.76	0.0351	14.1	5.34	16.90
		1	0.03	0.02	0.23	0.0018	0.3	0.02	0.19
8	25°C 66h	216	1.42	1.67	10.65	0.0335	31.9	5.39	2.68
		3	0.03	0.03	0.07	0.0007	0.6	0.02	0.10
9	35°C 40h	235	1.44	1.86	10.48	0.0332	37.2	5.36	1.31
		3	0.03	0.03	0.06	0.0007	0.7	0.02	0.07
10	45°C 43h	318	1.44	2.57	10.62	0.0325	52.1	5.38	1.07
		4	0.03	0.04	0.06	0.0005	1.2	0.02	0.05
11	55°C 65h	437	1.46	3.93	10.54	0.0314	95	5.33	0.91
		5	0.03	0.05	0.02	0.0004	2	0.02	0.02
12	65°C 68h	495	1.46	4.67	10.62	0.0328	116	5.369	0.90
		6	0.03	0.06	0.04	0.0005	2	0.009	0.02
13	75°C 90h	159	1.52	1.64	10.62	0.0338	42.8	5.339	1.27
		2	0.04	0.02	0.07	0.0010	1.0	0.012	0.03
14	85°C 90h	125	1.82	1.33	10.57	0.0378	48.5	5.371	2.295
		2	0.04	0.02	0.09	0.0009	0.9	0.011	0.014

... Table 7.14 continued

Step		^{4}He	^{3}He/^{4}He (x 10^4)	^{20}Ne	^{20}Ne/^{22}Ne	^{21}Ne/^{22}Ne	^{36}Ar	^{36}Ar/^{38}Ar	^{40}Ar/^{36}Ar
15	95°C 235h	128	2.43	1.19	10.47	0.0479	33.8	5.370	2.58
		2	0.06	0.02	0.08	0.0007	0.7	0.012	0.02
total		4147	1.504	32.18	10.59	0.0348	658	5.36	7.02
		15	0.009	0.12	0.06	0.0003	4	0.05	0.06

Gas concentrations in 10^{-8} cm^3 STP/g residue; [1] Valve G2 (between sample and acid) closed.

Table 7.15: He, Ne and Ar in (107.57 ± 0.05)mg **bulk** Grosnaja (**bulk** measurement HB07, 27/08/97-23/01/98).

Step	^{4}He	^{3}He/^{4}He (x 10^4)	^{20}Ne	^{20}Ne/^{22}Ne	^{21}Ne/^{22}Ne	^{36}Ar	^{36}Ar/^{38}Ar	^{40}Ar/^{36}Ar
1800°C[1]	1587	6.62	6.76	5.10	0.451	29.9	5.43	25.6
	9	0.06	0.07	0.04	0.004	0.7	0.04	0.4

Gas concentrations in 10^{-8} cm^3 STP/g meteorite; [1] Total extraction without pre-step at 600°C.

Table 7.16: He, Ne and Ar[1] in (2.11 ± 0.05)mg **HF/HCl-resistant residue** of Grosnaja (**bulk** measurement HB10, 12/01/99-17/01/99).

Step	^{4}He	^{3}He/^{4}He (x 10^4)	^{20}Ne	^{20}Ne/^{22}Ne	^{21}Ne/^{22}Ne	^{36}Ar	^{36}Ar/^{38}Ar	^{40}Ar/^{36}Ar
1800°C	49319	1.54	267	8.79	0.0373	914	5.3	1.12
	1188	0.09	10	0.19	0.0007	53	0.6	0.06

Gas concentrations in 10^{-8} cm^3 STP/g meteorite; [1] 600°C step and Kr and Xe of the 1800°C step not measured to avoid too much background gas (chapter 2.1.2).

Table 7.17: He, Ne and Ar[1] in (10.91 ± 0.03)mg **oxidised HF/HCl-resistant residue** of Grosnaja (**bulk** measurement HB09, 06/05/98-22/05/98).

Step	^{4}He	^{3}He/^{4}He (x 10^4)	^{20}Ne	^{20}Ne/^{22}Ne	^{21}Ne/^{22}Ne	^{36}Ar	^{36}Ar/^{38}Ar	^{40}Ar/^{36}Ar
600°C	427	7.7	3	10	0.05			
	17	1.6	3	7	0.04			
1800°C	49122	1.52	252	8.56	0.0413	369	5.4	2.70
	1904	0.08	4	0.06	0.0004	7	0.2	0.07
total	49549	1.57	254	8.57	0.0414			
	1904	0.08	5	0.14	0.0008			

Gas concentrations in 10^{-8} cm^3 STP/g residue; [1] 600°C step not measured to avoid too much background gas (chapter 2.1.2).

Table 7.18: Kr in the **HF/HCl-resistant residue** of Grosnaja (etch run).
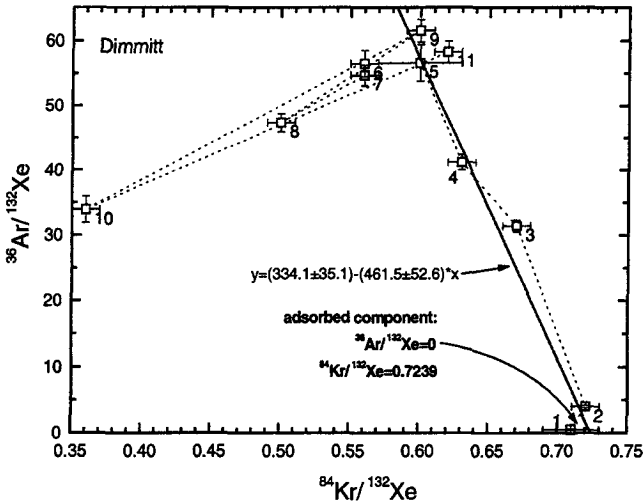
Step	^{84}Kr	^{78}Kr/^{84}Kr x 100	^{80}Kr/^{84}Kr x 100	^{82}Kr/^{84}Kr x 100	^{83}Kr/^{84}Kr x 100	^{86}Kr/^{84}Kr x 100
1	9027	0.43	3.94	20.05	20.10	30.77
	96	0.05	0.02	0.07	0.07	0.10
cor. [1]	0					
	0					
2[2]	11.71	0.579	3.36	20.25	20.16	30.84
	0.10	0.017	0.03	0.10	0.08	0.19

... Table 7.18 continued

Step	^{84}Kr	^{78}Kr/^{84}Kr x 100	^{80}Kr/^{84}Kr x 100	^{82}Kr/^{84}Kr x 100	^{83}Kr/^{84}Kr x 100	^{86}Kr/^{84}Kr x 100
3	3922	0.597	3.94	20.04	20.05	30.35
	29	0.003	0.02	0.06	0.05	0.13
cor. [1]	20					
	2					
4	1441	0.592	3.93	20.10	20.01	30.8
	14	0.008	0.03	0.13	0.13	0.2
cor. [1]	35					
	4					
5	1027	0.601	3.929	20.04	19.98	30.50
	7	0.004	0.011	0.09	0.05	0.09
cor. [1]	63					
	6					
6	719	0.596	3.94	20.09	20.17	30.66
	6	0.006	0.02	0.08	0.07	0.09
cor. [1]	51					
	5					
7	17.5	0.6061	3.93	20.18	20.32	30.84
	0.2	0.0011	0.02	0.10	0.09	0.12
8	26.5	0.616	3.949	20.06	19.93	30.88
	0.2	0.011	0.015	0.10	0.04	0.19
9	31.8	0.599	3.99	20.36	20.36	30.93
	0.2	0.010	0.03	0.07	0.11	0.12
10	42.6	0.579	3.86	19.96	20.17	30.14
	0.4	0.004	0.03	0.14	0.15	0.16
11	77.2	0.606	3.97	20.3	20.59	31.6
	0.6	0.006	0.03	0.2	0.17	0.3
12	85.6	0.607	3.927	20.09	20.14	30.78
	0.6	0.005	0.012	0.06	0.07	0.09
13	30.3	0.582	3.95	20.14	20.14	30.99
	0.2	0.010	0.02	0.07	0.06	0.09
14	36.1	0.603	3.93	20.05	20.05	30.65
	0.3	0.014	0.02	0.07	0.10	0.14
15	27.1	0.593	3.95	20.31	20.18	31.1
	0.2	0.018	0.03	0.13	0.12	0.2
total	16523	0.50	3.94	20.1	20.1	30.7
	102	0.03	0.04	0.2	0.2	0.3
cor. [1]	5449					

Gas concentrations in 10^{-10} cm^3 STP/g residue; [1] Steps 1 and 3-6 contain significant abundances of adsorbed Kr and Xe (see Figure 3.19). Steps 1-8 form a two-component-mixing line with pure Q in steps 2, 7 and 8 and an adsorbed component (^{36}Ar/^{132}Xe $= 0$; ^{84}Kr/^{132}Xe $= 6.5549$) as end members. These components were used to correct for adsorbed Kr and Xe (Figure 7.2). 10 % uncertainty are added; [2] Valve G2 (between sample and acid) closed.

Table 7.19: Kr in **bulk** Grosnaja.

Step	^{84}Kr	^{78}Kr/^{84}Kr x 100	^{80}Kr/^{84}Kr x 100	^{82}Kr/^{84}Kr x 100	^{83}Kr/^{84}Kr x 100	^{86}Kr/^{84}Kr x 100
1800°C[1]	36.0	267	6.9	20.18	19.94	31.3
	0.4	54	1.0	0.13	0.12	0.2

Gas concentrations in 10^{-10} cm^3 STP/g meteorite; [1] Total extraction without pre-step at 600°C.

Table 7.20: Kr[1] [2] in the **oxidised HF/HCl-resistant residue** of Grosnaja (**bulk measurement**).

Step	^{84}Kr	^{78}Kr/^{84}Kr x 100	^{80}Kr/^{84}Kr x 100	^{82}Kr/^{84}Kr x 100	^{83}Kr/^{84}Kr x 100	^{86}Kr/^{84}Kr x 100
1800°C	412	..	..	..	..	..
	18	..	..	..	..	..

Gas concentrations in 10^{-10} cm^3 STP/g residue; [1] 600°C step not measured to avoid too much background gas (chapter 2.1.2); [2] measurement corrupted by large amounts of reactive gases in the mass spectrometer.

Table 7.21: Xe in the **HF/HCl-resistant residue** of Grosnaja (etch run).

Step	^{132}Xe	^{124}Xe/^{132}Xe x 100	^{126}Xe/^{132}Xe x 100	^{128}Xe/^{132}Xe x 100	^{129}Xe/^{132}Xe x 100	^{130}Xe/^{132}Xe x 100	^{131}Xe/^{132}Xe x 100	^{134}Xe/^{132}Xe x 100	^{136}Xe/^{132}Xe x 100
1	1329	0.345	0.331	7.15	97.9	14.98	78.5	38.6	33.0
	16	0.004	0.005	0.07	0.6	0.13	0.7	0.2	0.3
cor. [1]	0								
	0								
2[2]	11.70	0.461	0.383	8.06	109.7	16.59	83.1	37.9	32.8
	0.14	0.011	0.015	0.11	0.9	0.16	0.7	0.3	0.6
3	616	0.365	0.329	7.33	100.7	15.17	80.0	38.7	32.9
	10	0.004	0.006	0.06	0.7	0.13	0.6	0.2	0.2
cor. [1]	30								
	3								
4	251	0.365	0.340	7.31	99.8	15.33	79.7	39.1	33.07
	3	0.006	0.006	0.05	0.3	0.13	0.4	0.2	0.14
cor. [1]	41								
	4								
5	213	0.378	0.343	7.47	100.7	15.44	79.4	38.8	32.6
	3	0.003	0.005	0.06	0.6	0.09	0.3	0.2	0.2
cor. [1]	58								
	6								
6	155	0.373	0.360	7.45	101.2	15.61	80.4	38.8	33.0
	2	0.006	0.005	0.06	0.7	0.15	0.6	0.3	0.2
cor. [1]	45								
	5								
7	16.3	0.435	0.407	8.13	104.5	16.15	81.4	37.9	32.1
	0.2	0.006	0.012	0.05	0.6	0.10	0.7	0.2	0.2
8	33.4	0.447	0.415	8.07	104.2	15.97	80.8	37.3	31.8
	0.4	0.008	0.004	0.07	0.8	0.15	0.7	0.3	0.2
9	36.9	0.460	0.408	8.11	105.3	16.21	81.4	37.6	31.0
	0.4	0.004	0.007	0.05	0.6	0.14	0.4	0.3	0.3
10	50.7	0.454	0.401	8.12	105.4	16.44	81.4	37.5	32.1
	0.6	0.006	0.004	0.06	0.8	0.13	0.9	0.3	0.2
11	98.7	0.451	0.411	8.22	104.2	16.04	82.0	37.6	30.8
	1.0	0.005	0.003	0.05	0.5	0.08	0.4	0.3	0.2

... Table 7.21 continued

Step	^{132}Xe	^{124}Xe/^{132}Xe x 100	^{126}Xe/^{132}Xe x 100	^{128}Xe/^{132}Xe x 100	^{129}Xe/^{132}Xe x 100	^{130}Xe/^{132}Xe x 100	^{131}Xe/^{132}Xe x 100	^{134}Xe/^{132}Xe x 100	^{136}Xe/^{132}Xe x 100
12	109.0	0.462	0.405	8.20	103.7	16.19	81.1	37.6	31.1
	1.1	0.005	0.003	0.06	0.5	0.08	0.6	0.2	0.2
13	39.1	0.451	0.400	8.23	103.8	16.09	81.5	37.4	31.2
	0.4	0.006	0.003	0.06	0.8	0.10	0.6	0.2	0.2
14	34.3	0.447	0.408	8.01	102.2	15.98	80.8	37.5	31.7
	0.4	0.007	0.008	0.05	0.5	0.12	0.5	0.3	0.7
15	31.3	0.458	0.411	8.21	106.3	16.34	82.4	38.1	31.7
	0.4	0.009	0.006	0.09	1.1	0.17	0.8	0.5	0.4
total	3025	0.371	0.345	7.39	99.9	15.29	79.5	38.5	32.7
	20	0.004	0.004	0.08	1.0	0.16	0.6	0.4	0.3
cor. [1]	623								
	9								

Gas concentrations in 10^{-10} cm^3 STP/g residue; [1] see footnote [1] of Table 7.18; [2] Valve G2 (between sample and acid) closed.
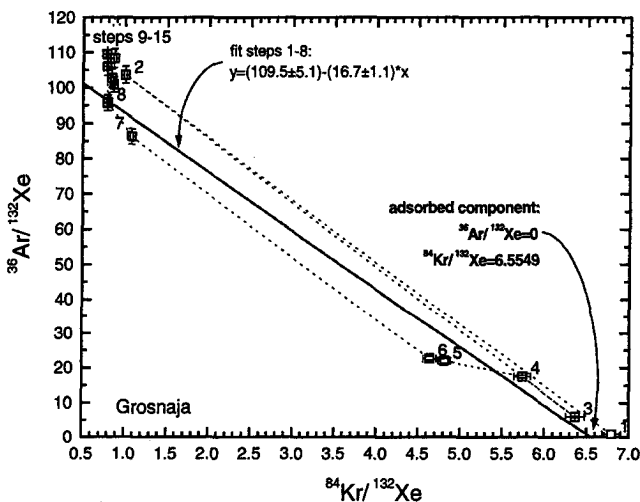
Figure 7.2: The ^{36}Ar/^{132}Xe vs. ^{84}Kr/^{132}Xe plot shows (in combination with the Xe three-isotope-plots of chapter 3.1.5) that steps 1-6 contain large amounts of adsorbed Kr and Xe.

Table 7.22: Xe in bulk Grosnaja.

Step	^{132}Xe	^{124}Xe/^{132}Xe x 100	^{126}Xe/^{132}Xe x 100	^{128}Xe/^{132}Xe x 100	^{129}Xe/^{132}Xe x 100	^{130}Xe/^{132}Xe x 100	^{131}Xe/^{132}Xe x 100	^{134}Xe/^{132}Xe x 100	^{136}Xe/^{132}Xe x 100
1800°C[1]	46.9	0.4	0.3	7.4	108	15.7	79	36.9	31.8
	1.6	0.4	0.3	0.3	3	0.6	2	1.3	1.0

Gas concentrations in 10^{-10} cm^3 STP/g meteorite; [1] Total extraction without pre-step at 600°C.

Table 7.23: Xe[1) 2)] in the **oxidised HF/HCl-resistant residue** of Grosnaja (**bulk** measurement).

Step	^{132}Xe	^{124}Xe/^{132}Xe x 100	^{126}Xe/^{132}Xe x 100	^{128}Xe/^{132}Xe x 100	^{129}Xe/^{132}Xe x 100	^{130}Xe/^{132}Xe x 100	^{131}Xe/^{132}Xe x 100	^{134}Xe/^{132}Xe x 100	^{136}Xe/^{132}Xe x 100
1800°C	509	0.53	0.54	7.69	104.9	15.55	81.9	41.1	36.3
	9	0.07	0.18	0.10	1.1	0.19	0.7	0.4	0.4

Gas concentrations in 10^{-10} cm^3 STP/g residue; [1)] 600°C step not measured to avoid too much background gas (chapter 2.1.2); [2)] measurement corrupted by large amounts of reactive gases in the mass spectrometer.

7.4 Noble gases in Chainpur

Table 7.24: He, Ne and Ar in the **HF/HCl-resistant residue** of Chainpur (etch run HB06, 23/06-18/11/97).

Step		^{4}He	^{3}He/^{4}He (x 10^4)	^{20}Ne	^{20}Ne/^{22}Ne	^{21}Ne/^{22}Ne	^{36}Ar	^{36}Ar/^{38}Ar	^{40}Ar/^{36}Ar
1	vap. 25h	5.71	17.2	0.0374	9.21	0.150	0.649	5.363	33.68
		0.12	0.6	0.0008	0.07	0.007	0.009	0.009	0.17
2	vap. 34h	8.98	15.5	0.0553	9.24	0.145	0.858	5.373	21.31
		0.18	0.5	0.0015	0.14	0.006	0.012	0.016	0.07
3	vap. 89h	30.6	12.5	0.189	9.36	0.147	2.00	5.39	10.24
		0.8	0.5	0.004	0.07	0.003	0.03	0.02	0.04
4	vap. 162h	53.6	10.3	0.392	9.04	0.138	5.62	5.379	8.58
		1.3	0.4	0.008	0.06	0.002	0.08	0.012	0.08
5	vap 136h	40.9	9.0	0.336	9.21	0.134	7.47	5.372	5.823
		1.0	0.3	0.007	0.08	0.002	0.09	0.013	0.019
6	vap. 570h	89	6.8	0.863	9.10	0.1156	34.7	5.362	3.184
		2	0.3	0.016	0.03	0.0011	0.4	0.015	0.012
7	25°C 48h	60.2	6.5	0.588	9.07	0.1120	22.4	5.38	9.38
		1.5	0.2	0.012	0.07	0.0014	1.1	0.02	0.07
8	25°C 114h	18.7	5.7	0.222	8.89	0.099	1)	1)	1)
		0.5	0.2	0.005	0.09	0.002			
9	25°C 112h	22.1	5.1	0.227	8.20	0.0901	9.04	5.366	40.3
		0.5	0.2	0.005	0.07	0.0014	0.12	0.011	0.2
10	25°C 48h	6.06	5.12	0.0600	8.25	0.099	2.48	5.395	52.0
		0.13	0.19	0.0015	0.11	0.003	0.03	0.019	0.4
11	25°C 231h	17.6	4.80	0.185	8.28	0.095	7.98	5.395	53.0
		0.4	0.18	0.004	0.07	0.002	0.10	0.013	0.2
12	35°C 61h	15.0	4.53	0.148	8.51	0.093	5.59	5.39	17.88
		0.4	0.18	0.004	0.10	0.003	0.07	0.02	0.07
13	45°C 88h	26.9	4.64	0.270	8.97	0.0982	1)	1)	1)
		0.7	0.18	0.005	0.06	0.0014			
14	55°C 75h	18.2	4.35	0.170	9.63	0.103	6.00	5.369	4.59
		0.4	0.17	0.004	0.08	0.002	0.08	0.018	0.03
15	65°C 96h	21.9	4.48[2)]	0.203	9.05	0.0967	7.35	5.37	8.77
		0.5	0.17	0.004	0.07	0.0011	0.10	0.02	0.07
16	75°C 70h	27.0	5.5[2)]	0.247	9.04	0.096	1)	1)	1)
		0.7	0.2	0.005	0.06	0.002			
17	85°C 100h	13.1	8.9[2)]	0.119	9.32	0.102	3.82	5.35	7.66
		0.3	0.3	0.002	0.06	0.004	0.05	0.02	0.09
18	95°C 122h	16.4	13.0[2)]	0.153	9.37	0.107	5.06	5.358	25.04
		0.4	0.5	0.003	0.08	0.002	0.07	0.016	0.10

... Table 7.24 continued

Step		^{4}He	^{3}He/^{4}He (x 10^4)	^{20}Ne	^{20}Ne/^{22}Ne	^{21}Ne/^{22}Ne	^{36}Ar	^{36}Ar/^{38}Ar	^{40}Ar/^{36}Ar
19	95°C 145h	0.057	1473	0.0004	10	-0.13	0.0325	5.12	136
		0.006	188	0.0002	4	0.33	0.0004	0.02	2
total[3]			492	7.56	4.46	9.00	0.1120	121.1	5.37	16.00
			4	0.09	0.03	0.08	0.0011	1.1	0.04	0.13

Gas concentrations in 10^{-8} cm^3 STP/g residue; [1] Ar not measured due to too high background; [2] corrected with ^{3}He blanks up to 41% of the measured values due to leakage in a calibration bottle; [3] without step 19 (almost no gas, no Q-like pattern).

Table 7.25: He, Ne and Ar[1] in (9.99 ± 0.02)mg **HF/HCl-resistant residue** of Chainpur (**bulk measurement HB09, 06/05/98-22/05/98**).

Step	^{4}He	^{3}He/^{4}He (x 10^4)	^{20}Ne	^{20}Ne/^{22}Ne	^{21}Ne/^{22}Ne	^{36}Ar	^{36}Ar/^{38}Ar	^{40}Ar/^{36}Ar
600°C	43	202	1	13	0.4			
	6	25	3	21	0.6			
1800°C	1442	7.3	10.9	8.0	0.163	75.5	5.36	9.02
	56	0.7	1.7	0.9	0.018	0.2	0.03	0.03
total	1485	13.3	12	8	0.17			
	56	1.0	3	2	0.06			

Gas concentrations in 10^{-8} cm^3 STP/g residue; [1] 600°C step not measured to avoid too much background gas (chapter 2.1.2).

Table 7.26: He, Ne and Ar[1] in (38.64 ± 0.10)mg **oxidised HF/HCl-resistant residue** of Chainpur (**bulk measurement HB09, 06/05/98-22/05/98**).

Step	^{4}He	^{3}He/^{4}He (x 10^4)	^{20}Ne	^{20}Ne/^{22}Ne	^{21}Ne/^{22}Ne	^{36}Ar	^{36}Ar/^{38}Ar	^{40}Ar/^{36}Ar
600°C	52	202	0.3	4	0.5			
	2	12	0.5	4	0.5			
1800°C	1026	4.7	5.9	7.4	0.166	10.59	5.45	22.39
	40	0.4	0.6	0.5	0.012	0.04	0.03	0.13
total	1079	14.3	6.2	7.0	0.20			
	40	0.7	0.8	1.2	0.08			

Gas concentrations in 10^{-8} cm^3 STP/g residue; [1] 600°C step not measured to avoid too much background gas (chapter 2.1.2).

Table 7.27: Kr in the **HF/HCl-resistant residue** of Chainpur (etch run).

Step	^{84}Kr	^{78}Kr/^{84}Kr x 100	^{80}Kr/^{84}Kr x 100	^{82}Kr/^{84}Kr x 100	^{83}Kr/^{84}Kr x 100	^{86}Kr/^{84}Kr x 100
1	1.714	0.614	4.02	20.45	20.10	30.4
	0.010	0.014	0.04	0.14	0.11	0.2
cor. [1]	0.9					
	0.5					
2	1.847	0.61	4.07	20.2	20.26	30.87
	0.010	0.03	0.07	0.2	0.09	0.12
cor. [1]	1.3					
	0.6					
3	3.20	0.59	3.98	20.14	20.24	30.9
	0.02	0.02	0.03	0.13	0.16	0.2
4	7.25	0.608	3.977	20.18	20.13	30.86
	0.04	0.010	0.015	0.08	0.09	0.11

... Table 7.27 continued

Step	^{84}Kr	^{78}Kr/^{84}Kr x 100	^{80}Kr/^{84}Kr x 100	^{82}Kr/^{84}Kr x 100	^{83}Kr/^{84}Kr x 100	^{86}Kr/^{84}Kr x 100
5	9.82	0.613	3.92	20.22	20.12	30.84
	0.05	0.009	0.03	0.10	0.09	0.13
6	49.0	0.588	3.89	20.0	20.09	30.6
	0.3	0.010	0.04	0.3	0.16	0.3
7[2)]	36	0.8	5.0	26	26	41
	7	0.2	1.3	7	7	10
8[2)]						
9	15.11	0.620	3.99	20.25	20.08	30.9
	0.10	0.011	0.06	0.16	0.18	0.3
10	3.65	0.596	3.99	20.3	20.09	30.94
	0.02	0.012	0.04	0.2	0.13	0.15
11	10.64	0.615	3.98	20.32	20.32	31.0
	0.07	0.009	0.02	0.14	0.17	0.2
12	6.41	0.617	3.94	20.13	20.21	30.85
	0.03	0.010	0.03	0.09	0.09	0.09
13[2)]						
14	6.43	0.601	3.93	20.28	20.34	31.05
	0.04	0.019	0.02	0.11	0.08	0.14
15	8.07	0.613	3.94	20.15	20.27	31.00
	0.04	0.011	0.02	0.08	0.05	0.14
16[2)]						
17	4.03	0.592	3.94	20.26	20.15	30.88
	0.02	0.016	0.02	0.09	0.09	0.13
18	5.53	0.617	3.96	20.33	20.24	31.0
	0.03	0.018	0.04	0.11	0.12	0.2
19	0.0594	0.37	2.6	18.0	19.5	31.6
	0.0008	0.07	0.2	0.6	0.5	0.9
total[3)]	169	0.63	4.1	21.2	21.3	33
	7	0.05	0.4	1.9	1.9	3
cor.[1)]	168					
	7					

Gas concentrations in 10^{-10} cm^3 STP/g residue; [1)] Steps 1-2 contain minor abundances of absorbed atmospheric Kr (see chapter 3.2, Figure 3.20). These contributions are corrected with ^{36}Ar abundances of these steps and the elemental ratio ^{36}Ar/^{84}Kr of steps 3-7 with adopted errors of 50 %; [2)] not measured due to too high background; [3)] without step 19 (almost no gas, no Q-like pattern).

Table 7.28: Kr[1)] in the **HF/HCl-resistant residue** of Chainpur (**bulk measurement**).

Step	^{84}Kr	^{78}Kr/^{84}Kr x 100	^{80}Kr/^{84}Kr x 100	^{82}Kr/^{84}Kr x 100	^{83}Kr/^{84}Kr x 100	^{86}Kr/^{84}Kr x 100
1800 °C	96.2	0.67	4.28	22.28	22.18	..
	0.5	0.02	0.10	0.13	0.14	..

Gas concentrations in 10^{-10} cm^3 STP/g residue; [1)] 600°C step not measured to avoid too much background gas (chapter 2.1.2).

Table 7.29: Kr[1] in the **oxidised HF/HCl-resistant residue** of Chainpur (**bulk measurement**).

Step	^{84}Kr	^{78}Kr/^{84}Kr x 100	^{80}Kr/^{84}Kr x 100	^{82}Kr/^{84}Kr x 100	^{83}Kr/^{84}Kr x 100	^{86}Kr/^{84}Kr x 100
1800°C	10.72	..	4.18	22.7	23.0	..
	0.07	..	0.15	0.3	0.3	..

Gas concentrations in 10^{-10} cm^3 STP/g residue; [1] 600°C step not measured to avoid too much background gas (chapter 2.1.2).

Table 7.30: Xe in the **HF/HCl-resistant residue** of Chainpur (etch run).

Step	^{132}Xe	^{124}Xe/^{132}Xe x 100	^{126}Xe/^{132}Xe x 100	^{128}Xe/^{132}Xe x 100	^{129}Xe/^{132}Xe x 100	^{130}Xe/^{132}Xe x 100	^{131}Xe/^{132}Xe x 100	^{134}Xe/^{132}Xe x 100	^{136}Xe/^{132}Xe x 100
1	1.56	0.427	0.376	7.68	106.7	15.67	81.3	37.3	31.6
	0.03	0.009	0.017	0.10	1.0	0.12	0.6	0.3	0.3
cor. [1]	1.1								
	0.6								
2	2.04	0.434	0.369	7.86	106.2	15.67	80.5	36.80	31.29
	0.04	0.012	0.010	0.06	0.4	0.11	0.8	0.13	0.19
cor. [1]	1.5								
	0.7								
3	4.31	0.442	0.393	7.94	106.9	16.29	81.7	37.4	32.2
	0.08	0.008	0.010	0.05	0.4	0.04	0.6	0.3	0.2
4	10.8	0.470	0.404	8.19	105.8	16.14	81.9	37.4	31.31
	0.2	0.006	0.004	0.05	0.7	0.08	0.5	0.2	0.14
5	13.5	0.453	0.393	8.22	104.6	16.13	82.7	37.9	32.0
	0.3	0.008	0.004	0.07	0.9	0.14	0.7	0.3	0.3
6	56.9	0.446	0.386	8.09	104.9	15.99	81.6	37.7	31.82
	1.1	0.004	0.007	0.04	0.5	0.06	0.4	0.3	0.11
7[2]	40	0.42	0.39	7.5	82	15.6	81	38	32
	3	0.05	0.05	1.0	15	1.8	9	4	7
8[2]									
9	15.5	0.447	0.405	8.15	103.2	16.06	82.0	37.91	31.70
	0.3	0.008	0.002	0.06	0.6	0.12	0.8	0.17	0.18
10	4.00	0.460	0.413	8.27	103.6	16.27	81.6	37.6	31.47
	0.07	0.006	0.009	0.06	0.4	0.09	0.4	0.2	0.15
11	12.1	0.452	0.409	8.22	104.1	16.34	82.2	37.9	31.49
	0.2	0.003	0.009	0.04	0.5	0.09	0.6	0.3	0.19
12	9.8	0.457	0.405	8.25	102.6	16.07	82.2	37.3	31.9
	0.2	0.008	0.008	0.04	0.5	0.12	0.6	0.2	0.3
13[2]									
14	10.3	0.455	0.414	8.28	104.3	16.12	82.1	37.1	31.9
	0.2	0.004	0.005	0.06	0.7	0.13	0.8	0.3	0.3
15	12.0	0.454	0.414	8.24	104.8	16.20	82.4	37.5	31.7
	0.2	0.007	0.007	0.06	0.7	0.11	0.6	0.2	0.2
16[2]									
17	6.40	0.449	0.405	8.21	105.5	16.18	82.0	37.0	32.06
	0.12	0.005	0.003	0.04	0.6	0.15	0.4	0.2	0.17
18	8.30	0.443	0.400	8.30	104.2	16.34	81.9	36.9	30.9
	0.11	0.009	0.010	0.11	0.6	0.10	0.5	0.3	0.3

... Table 7.30 continued

Step	^{132}Xe	^{124}Xe/^{132}Xe x 100	^{126}Xe/^{132}Xe x 100	^{128}Xe/^{132}Xe x 100	^{129}Xe/^{132}Xe x 100	^{130}Xe/^{132}Xe x 100	^{131}Xe/^{132}Xe x 100	^{134}Xe/^{132}Xe x 100	^{136}Xe/^{132}Xe x 100
19	0.135	0.43	0.46	8.1	104.7	15.9	81.9	39.9	34.4
	0.003	0.04	0.06	0.2	1.2	0.3	1.0	0.7	0.5
total[3]	207	0.444	0.396	8.1	101	16.0	82	37.7	31.9
	3	0.014	0.012	0.2	3	0.5	2	1.1	0.9
cor. [1]	206								
	3								

Gas concentrations in 10^{-10} cm^3 STP/g residue; [1] see footnote [1] of Table 7.27; [2] not measured due to too high background; [3] without step 19 (almost no gas, no Q-like pattern).

Table 7.31: Xe[1] in the HF/HCl-resistant residue of Chainpur (bulk measurement).

Step	^{132}Xe	^{124}Xe/^{132}Xe x 100	^{126}Xe/^{132}Xe x 100	^{128}Xe/^{132}Xe x 100	^{129}Xe/^{132}Xe x 100	^{130}Xe/^{132}Xe x 100	^{131}Xe/^{132}Xe x 100	^{134}Xe/^{132}Xe x 100	^{136}Xe/^{132}Xe x 100
1800°C	132	0.455	0.41	8.29	104.6	16.27	82.1	37.5	31.8
	2	0.013	0.02	0.12	0.7	0.11	0.5	0.3	0.3

Gas concentrations in 10^{-10} cm^3 STP/g residue; [1] 600°C step not measured to avoid too much background gas (chapter 2.1.2).

Table 7.32: Xe[1] in the oxidised HF/HCl-resistant residue of Chainpur (bulk measurement).

Step	^{132}Xe	^{124}Xe/^{132}Xe x 100	^{126}Xe/^{132}Xe x 100	^{128}Xe/^{132}Xe x 100	^{129}Xe/^{132}Xe x 100	^{130}Xe/^{132}Xe x 100	^{131}Xe/^{132}Xe x 100	^{134}Xe/^{132}Xe x 100	^{136}Xe/^{132}Xe x 100
1800°C	13.4	0.51	0.61	8.54	106.1	16.4	81.8	41.2	34.9
	0.2	0.03	0.05	0.14	0.9	0.2	0.7	0.4	0.4

Gas concentrations in 10^{-10} cm^3 STP/g residue; [1] 600°C step not measured to avoid too much background gas (chapter 2.1.2).

7.5 Noble gases in Cold Bokkeveld

Table 7.33: He, Ne and Ar in the HF/HCl-resistant residue of Cold Bokkeveld (etch run HB08, 13/01-07/06/98).

Step		^{4}He	^{3}He/^{4}He (x 10^4)	^{20}Ne	^{20}Ne/^{22}Ne	^{21}Ne/^{22}Ne	^{36}Ar	^{36}Ar/^{38}Ar	^{40}Ar/^{36}Ar
0[1]		67.7	1.70	0.393	9.55	0.0303	3.83	5.394	69.3
		1.1	0.04	0.009	0.07	0.0005	0.09	0.015	0.4
1	vap. 19h	42.9	1.46	0.209	10.28	0.0328	1.85	5.412	17.31
		0.7	0.03	0.004	0.04	0.0010	0.04	0.014	0.08
2	vap 48h	218	1.73	0.936	10.22	0.0388	9.2	5.41	8.70
		3	0.04	0.019	0.04	0.0004	0.2	0.03	0.04
3	vap 67.5h	197	1.48	1.02	10.10	0.0323	11.4	5.379	8.56
		3	0.03	0.02	0.03	0.0003	0.3	0.017	0.08
4	vap 91h	409	1.44	1.96	9.38	0.0275	21.8	5.375	6.57
		6	0.03	0.04	0.04	0.0002	0.5	0.011	0.04
5	vap 113h	419	1.43	2.04	8.09	0.0240	24.1	5.392	5.96
		6	0.03	0.04	0.04	0.0006	0.6	0.014	0.04
6	vap 136h	414	1.41	1.98	6.919	0.0206	23.8	5.38	7.74
		10	0.05	0.04	0.017	0.0004	0.6	0.02	0.05
7	vap 159h	450	1.39	2.28	6.099	0.01847	29.1	5.39	5.29
		7	0.03	0.05	0.014	0.00017	0.7	0.02	0.03

... Table 7.33 continued

Step		^{4}He	^{3}He/^{4}He (x 10^4)	^{20}Ne	^{20}Ne/^{22}Ne	^{21}Ne/^{22}Ne	^{36}Ar	^{36}Ar/^{38}Ar	^{40}Ar/^{36}Ar
8	vap 136h	387	1.40	1.95	5.775	0.0178	26.1	5.382	5.58
		6	0.03	0.04	0.019	0.0003	0.6	0.010	0.04
9	vap 109h	304	1.40	1.51	5.676	0.0179	20.2	5.354	7.34
		5	0.03	0.03	0.016	0.0002	0.5	0.013	0.06
10	vap 159h	366	1.40	1.94	5.45	0.0172	26.9	5.368	4.00
		6	0.03	0.04	0.02	0.0003	0.6	0.013	0.04
11	vap 85h	236	1.46	1.17	5.317	0.0169	16.4	5.398	7.96
		5	0.04	0.02	0.014	0.0003	0.4	0.012	0.07
12	vap 87h	237	1.43	1.27	5.27	0.0167	18.5	5.38	4.92
		4	0.03	0.03	0.02	0.0003	0.4	0.02	0.06
13[2)]	dest. 16h	97.6	1.45	0.548	5.26	0.0157			
		1.5	0.03	0.012	0.03	0.0004			
14	-25°C 308h	4.95	1.42	0.0356	5.68	0.0170	1.66	5.365	178.1
		0.04	0.11	0.0010	0.16	0.0011	0.03	0.017	1.4
15	25°C 19h	82.2	1.423	0.432	5.57	0.01813	7.64	5.346	30.1
		0.4	0.013	0.003	0.02	0.00012	0.11	0.017	0.4
16	25°C 42h	127.0	1.397	0.646	4.977	0.0168	9.57	5.36	16.88
		0.5	0.012	0.004	0.020	0.0002	0.14	0.02	0.13
17	25°C 88h	169.4	1.365	0.860	4.873	0.0149	12.12	5.370	6.63
		0.7	0.009	0.005	0.019	0.0002	0.18	0.014	0.10
18	25°C 141h	217.5	1.371	1.138	5.041	0.01532	16.3	5.368	3.50
		0.8	0.010	0.006	0.012	0.00012	0.2	0.015	0.04
19	35°C 41h	221.9	1.418	1.210	5.57	0.0168	18.5	5.352	2.51
		0.9	0.011	0.008	0.02	0.0003	0.3	0.014	0.03
20	45°C 93h	519	1.401	3.140	6.284	0.01834	52.3	5.28	1.50
		2	0.011	0.016	0.014	0.00017	0.9	0.05	0.02
21	55°C 84h	484.7	1.401	3.31	7.25	0.02068	60.8	5.38	1.353
		1.9	0.010	0.02	0.03	0.00015	1.1	0.05	0.017
22	65°C 66h	358.7	1.428	3.185	9.55	0.02775	54.9	5.29	1.288
		1.4	0.011	0.016	0.02	0.00019	0.9	0.04	0.012
23	75°C 70h	133.4	1.485	1.745	10.01	0.03058	23.5	5.365	1.05
		0.5	0.014	0.010	0.03	0.00016	0.3	0.015	0.02
24	85°C 65h	76.5	1.540	1.152	10.00	0.0310	15.0	5.338	7.99
		0.3	0.017	0.008	0.04	0.0005	0.2	0.015	0.09
25	95°C 76h	78.2	1.556	1.144	9.94	0.0312	14.6	5.366	1.71
		0.3	0.018	0.008	0.05	0.0007	0.2	0.016	0.06
26	95°C 99h	98.9	1.55	1.356	9.96	0.0304	19.3	5.369	4.02
		0.4	0.02	0.008	0.03	0.0003	0.3	0.018	0.05
27	85°C 140h	26.14	1.70	0.495	9.94	0.0317	5.38	5.40	2.80
		0.15	0.02	0.004	0.05	0.0008	0.08	0.03	0.13
28	85°C 125h	19.99	1.728	0.360	9.96	0.0324	3.82	5.358	3.31
		0.09	0.017	0.003	0.05	0.0007	0.06	0.016	0.09
29	85°C 186h	18.41	1.702	0.349	9.81	0.0315	3.47	5.34	3.72
		0.09	0.027	0.003	0.06	0.0007	0.05	0.02	0.09
30	85°C 137h	13.94	1.588	0.245	9.94	0.0342	2.83	5.382	4.42
		0.08	0.034	0.003	0.07	0.0005	0.04	0.016	0.11
total		6497	1.437	40.03	7.01	0.02141	555	5.36	5.78
		20	0.006	0.12	0.03	0.00011	2	0.03	0.04

Gas concentrations in 10^{-8} cm^3 STP/g residue; [1)] A first "gold blank" step without any fresh acid from the acid gold finger, but heated to 100°C contained significant amounts of Q-like gases, probably due to etching of remaining acid droplets from earlier experiments; [2)] not measured due to too high background.

Table 7.34: He, Ne and Ar in (a) (22.11 ± 0.02)mg and (b) (18.93 ± 0.02)mg **HF/HCl-resistant residues** of Cold Bokkeveld (**bulk** measurements (a) HB09, 06/05/98-22/05/98 and (b) HB10, 12/01/99-17/01/99).

	Step	^{4}He	^{3}He/^{4}He (x 10^4)	^{20}Ne	^{20}Ne/^{22}Ne	^{21}Ne/^{22}Ne	^{36}Ar	^{36}Ar/^{38}Ar	^{40}Ar/^{36}Ar
a)	600°C[1]	7588	1.69	36.3	7.71	0.0471			
		293	0.09	0.6	0.10	0.0008			
	1800°C	68681	1.45	212	7.70	0.0362	989	5.37	0.4001
		2647	0.07	4	0.09	0.0005	3	0.05	0.0011
	total	76269	1.48	248	7.70	0.0378			
		2663	0.06	4	0.14	0.0007			
b)	1800°C[2]	49937	1.477	179	7.81	0.0308	937	5.4	0.051
		226	0.015	3	0.08	0.0003	209	1.0	0.006

Gas concentrations in 10^{-8} cm^3 STP/g residue; [1] Ar, Kr and Xe could not be measured due to too much Teflon-induced background gas (chapter 2.1.2); [2] 600°C step not measured to avoid too much background gas (chapter 2.1.2).

Table 7.35: He, Ne and Ar in (a) (10.93 ± 0.05)mg and (b) (28.79 ± 0.05)mg **oxidised HF/HCl-resistant residues** of Cold Bokkeveld (**bulk** measurements HB10, 12/01/99-17/01/99).

	Step	^{4}He	^{3}He/^{4}He (x 10^4)	^{20}Ne	^{20}Ne/^{22}Ne	^{21}Ne/^{22}Ne	^{36}Ar	^{36}Ar/^{38}Ar	^{40}Ar/^{36}Ar
a)	1800°C[1]	66251	1.44	208	7.66	0.0548	965	5.39	2.760
		417	0.02	3	0.10	0.0004	8	0.06	0.007
b)	1800°C[1]	59678	1.450	179.1	8.00	0.0315	540	5.4	0.352
		280	0.015	1.6	0.06	0.0002	25	0.4	0.014

Gas concentrations in 10^{-8} cm^3 STP/g residue; [1] 600°C step not measured to avoid too much background gas (chapter 2.1.2).

Table 7.36: Kr in the HF/HCl-resistant residue of Cold Bokkeveld (**etch run**).

Step	^{84}Kr	^{78}Kr/^{84}Kr x 100	^{80}Kr/^{84}Kr x 100	^{82}Kr/^{84}Kr x 100	^{83}Kr/^{84}Kr x 100	^{86}Kr/^{84}Kr x 100
0[1]	21.29	0.604	3.87	20.18	19.98	30.5
	0.38	0.007	0.02	0.12	0.12	0.2
1	4.78	0.584	3.94	20.16	20.21	30.75
	0.08	0.019	0.04	0.17	0.09	0.17
2	16.64	0.603	3.91	20.24	20.20	30.97
	0.29	0.005	0.03	0.13	0.12	0.17
3	18.36	0.592	3.89	19.98	20.09	31.0
	0.33	0.006	0.03	0.11	0.12	0.2
4	31.75	0.591	3.880	20.08	20.01	30.73
	0.55	0.006	0.018	0.10	0.09	0.13
5	34.31	0.580	3.91	20.13	20.16	30.9
	0.59	0.006	0.03	0.14	0.12	0.2
6	32.89	0.587	3.872	19.90	20.04	30.50
	0.59	0.012	0.018	0.08	0.09	0.14
7	38.82	0.575	3.85	19.84	19.9	30.7
	0.68	0.008	0.03	0.16	0.2	0.3
8	34.37	0.591	3.88	20.1	20.02	30.9
	0.60	0.010	0.02	0.2	0.16	0.2
9	26.39	0.587	3.86	20.19	20.05	30.9
	0.44	0.006	0.03	0.14	0.13	0.2

... Table 7.36 continued

Step	^{84}Kr	^{78}Kr/^{84}Kr x 100	^{80}Kr/^{84}Kr x 100	^{82}Kr/^{84}Kr x 100	^{83}Kr/^{84}Kr x 100	^{86}Kr/^{84}Kr x 100
10	34.56	0.596	3.88	20.19	20.17	30.8
	0.57	0.004	0.02	0.14	0.14	0.2
11	21.04	0.608	3.93	20.12	20.12	30.9
	0.35	0.010	0.03	0.13	0.13	0.2
12	23.70	0.594	3.86	20.20	20.13	30.67
	0.41	0.006	0.03	0.11	0.13	0.18
13[2]						
14	0.91	0.65	4.05	20.12	20.39	31.14
	0.01	0.03	0.03	0.12	0.06	0.16
15	9.09	0.599	3.87	20.21	20.06	30.78
	0.06	0.008	0.02	0.14	0.12	0.14
16	11.21	0.602	3.888	19.98	20.09	30.87
	0.07	0.006	0.019	0.08	0.09	0.14
17	14.25	0.578	3.89	20.20	20.21	30.7
	0.09	0.009	0.02	0.09	0.11	0.2
18	19.00	0.607	3.90	20.02	20.15	31.03
	0.13	0.012	0.02	0.07	0.12	0.15
19	20.96	0.606	3.92	20.28	20.13	30.7
	0.15	0.004	0.02	0.13	0.15	0.2
20	56.27	0.610	3.960	20.05	20.15	30.98
	0.46	0.004	0.015	0.08	0.06	0.10
21	61.96	0.623	3.934	20.04	20.15	30.65
	0.55	0.005	0.018	0.09	0.11	0.16
22	47.78	0.617	3.951	20.27	20.21	31.09
	0.38	0.005	0.009	0.06	0.06	0.17
23	22.94	0.601	3.96	20.11	20.10	31.12
	0.14	0.004	0.04	0.07	0.07	0.10
24	17.13	0.599	3.941	20.24	20.28	30.77
	0.11	0.004	0.019	0.11	0.11	0.17
25	15.15	0.596	3.90	20.01	19.96	30.64
	0.10	0.009	0.02	0.09	0.07	0.14
26	22.01	0.593	3.93	20.22	20.16	30.69
	0.14	0.005	0.03	0.13	0.10	0.10
27	6.14	0.619	3.97	20.25	20.24	30.78
	0.04	0.008	0.02	0.08	0.07	0.10
28	4.31	0.579	3.923	20.36	20.17	30.90
	0.03	0.003	0.019	0.06	0.06	0.16
29	3.95	0.595	3.92	20.49	20.47	30.9
	0.03	0.010	0.03	0.14	0.13	0.2
30	3.51	0.560	3.96	20.11	20.11	30.77
	0.02	0.024	0.05	0.13	0.10	0.09
total	675.5	0.599	3.908	20.11	20.11	30.82
	1.9	0.003	0.014	0.07	0.07	0.11

Gas concentrations in 10^{-10} cm^3 STP/g residue; [1] see footnote [1] of Table 7.33; [2] not measured due to too high background.

Table 7.37: Kr[1] in the **HF/HCl-resistant residue** (a) of Cold Bokkeveld (**bulk measurement**).

Step	^{84}Kr	^{78}Kr/^{84}Kr x 100	^{80}Kr/^{84}Kr x 100	^{82}Kr/^{84}Kr x 100	^{83}Kr/^{84}Kr x 100	^{86}Kr/^{84}Kr x 100
1800°C	1186	..	4.04	20.45	20.33	30.83
	6	..	0.03	0.09	0.08	0.12

Gas concentrations in 10^{-10} cm^3 STP/g residue; [1] 600°C step not measured to avoid too much background gas (chapter 2.1.2).

Table 7.38: Kr[1] in the **oxidised HF/HCl-resistant residue** (a) of Cold Bokkeveld (**bulk measurement**).

Step	^{84}Kr	^{78}Kr/^{84}Kr x 100	^{80}Kr/^{84}Kr x 100	^{82}Kr/^{84}Kr x 100	^{83}Kr/^{84}Kr x 100	^{86}Kr/^{84}Kr x 100
1800°C	928	0.664	3.935	20.27	20.37	31.00
	9	0.005	0.019	0.07	0.07	0.12

Gas concentrations in 10^{-10} cm^3 STP/g residue; [1] 600°C step not measured to avoid too much background gas (chapter 2.1.2).

Table 7.39: Xe in the HF/HCl-resistant residue of Cold Bokkeveld (**etch run**).

Step	^{132}Xe	^{124}Xe/^{132}Xe x 100	^{126}Xe/^{132}Xe x 100	^{128}Xe/^{132}Xe x 100	^{129}Xe/^{132}Xe x 100	^{130}Xe/^{132}Xe x 100	^{131}Xe/^{132}Xe x 100	^{134}Xe/^{132}Xe x 100	^{136}Xe/^{132}Xe x 100
0[1]	26.9	0.358	0.335	7.30	100.2	15.05	78.3	37.8	32.7
	0.9	0.003	0.003	0.06	0.6	0.09	0.8	0.4	0.3
1	5.9	0.411	0.378	8.26	102.4	16.02	81.3	38.0	31.96
	0.2	0.007	0.006	0.07	0.5	0.13	0.6	0.2	0.18
2	23.8	0.434	0.392	8.12	103.7	16.06	81.1	37.3	31.7
	0.8	0.004	0.004	0.05	0.6	0.09	0.6	0.4	0.3
3	28.3	0.442	0.388	8.01	102.6	15.89	79.7	36.8	31.3
	1.0	0.009	0.007	0.08	0.9	0.16	0.8	0.4	0.5
4	49.9	0.450	0.408	8.20	104.1	15.95	80.9	37.4	31.19
	1.7	0.008	0.010	0.07	0.4	0.06	0.3	0.2	0.17
5	55.3	0.436	0.393	8.18	104.3	16.06	81.8	37.67	31.2
	1.8	0.006	0.003	0.05	0.6	0.10	0.3	0.17	0.2
6	52.6	0.436	0.394	8.18	103.7	16.04	82.0	36.9	31.2
	1.8	0.005	0.003	0.07	0.6	0.10	0.5	0.3	0.2
7	62	0.431	0.383	8.23	105.1	16.28	82.6	37.7	31.6
	2	0.007	0.005	0.09	1.3	0.17	0.7	0.5	0.4
8	55.9	0.434	0.384	8.11	103.7	16.00	81.4	36.93	30.96
	1.9	0.004	0.005	0.05	0.4	0.09	0.3	0.19	0.19
9	43.1	0.448	0.389	8.15	103.7	16.03	80.7	37.3	31.2
	1.4	0.006	0.006	0.06	0.6	0.12	0.6	0.2	0.2
10	56.9	0.429	0.380	8.17	103.7	15.93	81.6	37.0	31.2
	1.9	0.005	0.005	0.08	0.9	0.14	0.7	0.4	0.3
11	34.2	0.447	0.399	8.12	104.4	16.06	81.6	37.5	31.5
	1.1	0.004	0.003	0.09	0.7	0.08	0.4	0.3	0.2
12	39.3	0.435	0.380	8.08	104.4	16.1	81.7	36.2	31.3
	1.3	0.009	0.006	0.11	1.5	0.2	1.2	0.5	0.5
13[2]									
14	1.48	0.461	0.389	8.11	103.4	16.14	82.2	38.6	31.9
	0.02	0.010	0.008	0.09	0.8	0.15	0.7	0.4	0.3
15	14.93	0.451	0.406	8.20	103.2	16.26	81.3	36.57	30.7
	0.15	0.009	0.007	0.04	0.5	0.10	0.5	0.12	0.2

... Table 7.39 continued

Step	^{132}Xe	^{124}Xe/^{132}Xe x 100	^{126}Xe/^{132}Xe x 100	^{128}Xe/^{132}Xe x 100	^{129}Xe/^{132}Xe x 100	^{130}Xe/^{132}Xe x 100	^{131}Xe/^{132}Xe x 100	^{134}Xe/^{132}Xe x 100	^{136}Xe/^{132}Xe x 100
16	17.36	0.455	0.403	8.33	105.1	16.34	82.9	37.9	32.0
	0.20	0.007	0.005	0.09	1.0	0.15	0.8	0.3	0.3
17	22.3	0.447	0.400	8.23	103.5	16.03	81.7	37.4	31.0
	0.2	0.007	0.003	0.07	0.8	0.15	0.6	0.2	0.3
18	29.7	0.444	0.402	8.21	102.5	16.16	81.6	37.20	31.3
	0.3	0.004	0.004	0.04	0.5	0.06	0.2	0.19	0.2
19	33.3	0.443	0.395	8.14	103.0	16.08	80.8	37.37	31.4
	0.3	0.003	0.003	0.04	0.4	0.07	0.5	0.17	0.2
20	88.5	0.450	0.401	8.25	103.6	16.17	81.6	37.4	31.6
	1.0	0.004	0.004	0.05	0.5	0.08	0.5	0.2	0.3
21	95.4	0.458	0.398	8.20	104.6	16.26	82.6	37.3	32.2
	1.1	0.004	0.004	0.08	0.5	0.08	0.4	0.3	0.2
22	76.8	0.450	0.400	8.20	103.0	16.11	81.6	37.1	31.6
	0.9	0.004	0.004	0.05	0.5	0.07	0.3	0.3	0.2
23	35.9	0.440	0.379	8.34	103.4	16.38	84.3	39.1	32.8
	0.5	0.005	0.005	0.08	1.7	0.15	1.2	0.4	0.3
24	27.0	0.448	0.400	8.25	103.9	16.14	81.7	38.1	31.67
	0.3	0.004	0.004	0.05	0.5	0.11	0.5	0.2	0.14
25	23.7	0.444	0.400	8.14	104.3	16.21	82.5	37.2	31.83
	0.2	0.006	0.004	0.06	0.6	0.12	0.4	0.2	0.15
26	33.1	0.461	0.411	8.18	104.1	16.21	82.1	38.0	31.90
	0.4	0.004	0.003	0.05	0.5	0.07	0.4	0.2	0.17
27	10.98	0.445	0.399	8.17	104.0	16.03	81.1	37.6	31.5
	0.11	0.004	0.005	0.05	0.7	0.10	0.4	0.3	0.3
28	6.91	0.454	0.400	8.22	104.8	16.01	81.3	38.3	31.8
	0.07	0.006	0.005	0.09	0.5	0.08	0.6	0.3	0.2
29	6.30	0.454	0.397	8.16	103.5	16.05	82.4	37.2	32.0
	0.07	0.006	0.007	0.10	0.8	0.12	0.6	0.4	0.2
30	5.47	0.454	0.417	8.23	104.4	16.20	82.2	38.1	31.9
	0.05	0.006	0.006	0.05	0.6	0.10	0.5	0.3	0.2
total	1064	0.439	0.391	8.12	103.2	16.00	81.2	37.2	31.39
	6	0.003	0.002	0.05	0.6	0.09	0.5	0.2	0.19

Gas concentrations in 10^{-10} cm^3 STP/g residue; [1] see footnote [1] of Table 7.33; [2] see footnote [2] of Table 7.33.

Table 7.40: Xe[1] in the **HF/HCl-resistant residue** (a) of Cold Bokkeveld (bulk measurement).

Step	^{132}Xe	^{124}Xe/^{132}Xe x 100	^{126}Xe/^{132}Xe x 100	^{128}Xe/^{132}Xe x 100	^{129}Xe/^{132}Xe x 100	^{130}Xe/^{132}Xe x 100	^{131}Xe/^{132}Xe x 100	^{134}Xe/^{132}Xe x 100	^{136}Xe/^{132}Xe x 100
1800°C	1723	0.486	0.427	8.12	103.6	16.11	82.12	38.39	32.3
	28	0.007	0.005	0.05	0.6	0.07	0.19	0.14	0.2

Gas concentrations in 10^{-10} cm^3 STP/g residue; [1] 600°C step not measured to avoid too much background gas (chapter 2.1.2).

Table 7.41: Xe[1] in the **oxidised HF/HCl-resistant residue** (a) of Cold Bokkeveld (bulk measurement).

Step	^{132}Xe	^{124}Xe/^{132}Xe x 100	^{126}Xe/^{132}Xe x 100	^{128}Xe/^{132}Xe x 100	^{129}Xe/^{132}Xe x 100	^{130}Xe/^{132}Xe x 100	^{131}Xe/^{132}Xe x 100	^{134}Xe/^{132}Xe x 100	^{136}Xe/^{132}Xe x 100
1800°C	1172	0.457	0.405	8.29	104.0	16.19	81.9	38.31	32.32
	28	0.003	0.003	0.04	0.4	0.07	0.4	0.17	0.17

Gas concentrations in 10^{-10} cm^3 STP/g residue; [1] 600°C step not measured to avoid too much background gas (chapter 2.1.2).

7.6 Noble gases in Dhajala

The HF/HCl-resistant residue of H3.8 Dhajala (I) has been originally produced for the analysis with CSSE. Unfortunately, the first demineralisation attempt yielded only a very small residue probably largely polluted with unsolvable fluorides as indicated by large grey particles in the residue (chapter 2.1.2). For this reason, the residue has been measured completely by pyrolysis. The absolute concentrations are not reliable and amount to only 8-10 % of those obtained by Schelhaas *et al.* (1990). Nevertheless, since the ^{4}He concentration has never been measured before and Dhajala does not contain diamonds (Schelhaas *et al.*, 1990), the elemental and isotopic ratios are useful, e. g. for further CSSE examinations of a second residue produced later, and the values are given in the following tables. Most isotopic ratios are within the uncertainties identical with those obtained by pyrolysis at 1800°C (Schelhaas *et al.*, 1990).

Table 7.42: He, Ne and Ar[1] in (15.23 ± 0.05)mg **HF/HCl-resistant residue** of Dhajala (**bulk** measurement HB10, 12/01/99-17/01/99).

Step	^{4}He[2]	^{3}He/^{4}He (x 10^4)	^{20}Ne[2]	^{20}Ne/^{22}Ne	^{21}Ne/^{22}Ne	^{36}Ar[2]	^{36}Ar/^{38}Ar	^{40}Ar/^{36}Ar
1800°C	120.4	16	1.8	6.3	0.37	68.0	5.29	2.859
	0.7	5	0.6	1.5	0.08	0.5	0.02	0.012

Gas concentrations in 10^{-8} cm^3 STP/g residue; [1] 600°C step not measured to avoid too much background gas (chapter 2.1.2); [2] too small, see text above.

Table 7.43: Kr[1] in the **HF/HCl-resistant residue** of Dhajala (**bulk** measurement).

Step	^{84}Kr[2]	^{78}Kr/^{84}Kr x 100	^{80}Kr/^{84}Kr x 100	^{82}Kr/^{84}Kr x 100	^{83}Kr/^{84}Kr x 100	^{86}Kr/^{84}Kr x 100
1800°C	73.0	..	4.20	20.8	20.42	31.07
	0.7	..	0.08	0.3	0.15	0.14

Gas concentrations in 10^{-10} cm^3 STP/g residue; [1] 600°C step not measured to avoid too much background gas (chapter 2.1.2); [2] too small, see text above.

Table 7.44: Xe[1)] in the HF/HCl-resistant residue of Dhajala (bulk measurement).

Step	^{132}Xe[2)]	^{124}Xe/^{132}Xe x 100	^{126}Xe/^{132}Xe x 100	^{128}Xe/^{132}Xe x 100	^{129}Xe/^{132}Xe x 100	^{130}Xe/^{132}Xe x 100	^{131}Xe/^{132}Xe x 100	^{134}Xe/^{132}Xe x 100	^{136}Xe/^{132}Xe x 100
1800°C	128	0.487	0.44	8.38	104.7	16.25	82.3	38.1	31.57
	3	0.017	0.02	0.06	0.5	0.09	0.4	0.2	0.12

Gas concentrations in 10^{-10} cm^3 STP/g residue; [1)] 600°C step not measured to avoid too much background gas (chapter 2.1.2); [2)] too small, see text above.

7.7 Noble gases in 2 new Antarctic meteorites GRO95505 and WSG95300

The noble gas contents in some splits of two rather new Antarctic unequilibrated chondrites L3.6 *Grosvenor Mountains GRO95505* and H3.4 *Wisconsin Range - Scott Glacier Region WSG95300* (both found in 1995, preliminarily classified and kindly provided by NASA) were measured by total extraction pyrolysis (about 1800°C) in order to check if these samples may contain relatively large amounts of primordial noble gases and relatively low cosmogenic portions which would allow to use these samples for CSSE experiments.

Table 7.45: Primordial Ar and Xe and roughly estimated cosmic-ray exposure ages of the Antarctic meteorites GRO95505 (L3.6) and WSG 95300 (H3.4). For comparison, the classification intervals for primordial ^{36}Ar and ^{132}Xe in UOCs according to Anders and Zadnik (1985) are also given.

Sample	weight [mg]	^{36}Ar$_{prim}$ [10^{-8} cm^3 STP/g]	^{132}Xe [10^{-10} cm^3 STP/g]	$T_{exp}(^3$He) [Ma]	$T_{exp}(^{21}$Ne) [Ma]
GRO95505 split 7	100.16 ± 0.05	46.0	35.6	27.1	30.0
GRO95505 split 10	63.43 ± 0.05	46.6	35.3	30.7	34.0
GRO95505 split 11	70.18 ± 0.05	*26.3*	*17.0*	28.7	32.4
WSG95300 split 9	59.72 ± 0.05	60.5	40.3	30.2	35.4
WSG95300 split 11	76.66 ± 0.05	58.8	34.1	29.5	34.0
sub-type 3.6		32-36	16-18		
sub-type 3.4		40-46	20-23		

The noble gas data (Table 7.46-Table 7.48) are quite similar for splits 7 and 10 of GRO and splits 9 and 11 of WSG, respectively. Split 11 of GRO, however, shows significant deviations, both in the He, Ar, Kr and Xe concentrations, as well as in the *isotopic ratios* of He, Ne and Ar. While the Ar, Kr and Xe concentrations (48-53 % lower than the average of splits 7 and 10) as well as He and Ne (rather similar in all three splits) suggest losses during the Ar-Xe extraction procedure, the different isotopic ratios of split 11 rather point to an usual inhomogeneity of GRO.

The elemental ratios ^{4}He/^{36}Ar and ^{20}Ne/^{36}Ar are smaller than 77 and 0.32, respectively, for all measured splits. This indicates that no significant amounts of solar noble gases have been trapped. To determine the total primordial fraction (Q + HL +...) of Ar and Xe, the following simple assumptions were made: ^{132}Xe$_{total}$ = ^{132}Xe$_{prim}$, (^{38}Ar/^{21}Ne)$_{cosm}$ = 0.105 (Graf et al., 1990), (^{36}Ar/^{38}Ar)$_{cosm}$ = 0.65 (Eugster et al., 1998). ^{21}Ne has been corrected for ^{21}Ne$_{prim}$ assuming ^{20}Ne$_{total}$ = ^{20}Ne$_{prim}$ and (^{20}Ne/^{21}Ne)$_{prim}$ = 283. The contributions of ^{21}Ne$_{prim}$ amount to about 0.4 %. Table 7.45 shows the primordial ^{36}Ar and ^{132}Xe abundances in all splits. These two element concentrations were proposed as parameters for the petrographic sub-classification of unequilibrated ordinary chondrites according to their metamorphic history (Sears et al., 1980) and their accretion conditions in the solar nebula (Anders and Zadnik, 1985). Both meteorites seem to contain more primordial noble gas than is to be expected according to their petrographic type. The sub-classification intervals for ^{36}Ar and ^{132}Xe Ne in UOCs are

also listed in Table 7.45. Nevertheless, the meteorites are not very suitable to be analysed with CSSE since both have been exposed to cosmic rays for about $32-34$ Ma (Table 7.45), estimated by the ^{3}He and ^{21}Ne concentrations under the assumption ^{3}He$_{total} = {}^3$He$_{cosm}$, corrected for primordial ^{21}Ne and using the formulas of Eugster (1988). These exposure ages are even larger than that of Chainpur which has the longest exposure time (Table 2.1) among the samples analysed with CSSE in this study.

Table 7.46: He, Ne and Ar[1] in bulk GRO95505 and WSG95300 (**bulk** measurement HB07, 27/8/97-23/1/98).

Sample	^{4}He	^{3}He/^{4}He (x 10^4)	^{20}Ne	^{20}Ne/^{22}Ne	^{21}Ne/^{22}Ne	^{36}Ar	^{36}Ar/^{38}Ar	^{40}Ar/^{36}Ar
GRO95505/7	1689	253.3	8.20	0.998	0.822	46.5	5.00	113.2
	10	0.9	0.08	0.004	0.004	0.6	0.02	0.2
GRO95505/10	1719	263.0	8.83	1.008	0.821	47.2	4.79	105.7
	10	0.9	0.08	0.002	0.002	0.7	0.02	0.3
GRO95505/11	2062	219.0	8.51	0.925	0.836	26.9	4.81	221.9
	12	1.1	0.08	0.002	0.003	0.4	0.02	0.3
WSG95300/9	1755	268.5	10.67	1.049	0.853	61.1	4.95	56.1
	10	1.2	0.10	0.002	0.002	1.0	0.02	0.3
WSG95300/11	1701	270.7	10.73	1.043	0.867	59.4	4.92	41.3
	10	1.0	0.10	0.003	0.003	0.8	0.02	0.1

Gas concentrations in 10^{-8} cm^3 STP/g meteorite; [1] Total extraction at 1800°C without pre-step at 600°C.

Table 7.47: Kr[1] in bulk GRO95505 and WSG95300.

Sample	^{84}Kr	^{78}Kr/^{84}Kr x 100	^{80}Kr/^{84}Kr x 100	^{82}Kr/^{84}Kr x 100	^{83}Kr/^{84}Kr x 100	^{86}Kr/^{84}Kr x 100
GRO95505/7	29.7	..	4.06	20.36	20.43	31.17
	0.3	..	0.03	0.11	0.14	0.16
GRO95505/10	28.4	..	4.11	20.39	20.19	30.9
	0.3	..	0.03	0.17	0.17	0.2
GRO95505/11	15.05	..	4.10	20.43	20.45	31.1
	0.18	..	0.04	0.14	0.14	0.2
WSG95300/9	32.6	0.677	4.01	20.08	20.1	30.9
	0.4	0.013	0.04	0.19	0.2	0.3
WSG95300/11	33.4	..	4.04	20.16	20.26	31.1
	0.4	..	0.03	0.10	0.11	0.2

Gas concentrations in 10^{-10} cm^3 STP/g; [1] Total extraction at 1800°C without pre-step at 600°C.

Table 7.48: Xe[1] in bulk GRO95505 and WSG95300.

Sample	^{132}Xe	^{124}Xe/^{132}Xe x 100	^{126}Xe/^{132}Xe x 100	^{128}Xe/^{132}Xe x 100	^{129}Xe/^{132}Xe x 100	^{130}Xe/^{132}Xe x 100	^{131}Xe/^{132}Xe x 100	^{134}Xe/^{132}Xe x 100	^{136}Xe/^{132}Xe x 100
GRO/7	35.6	0.445	0.410	8.06	106.8	15.98	81.2	38.0	32.0
	1.2	0.005	0.005	0.06	0.8	0.09	0.5	0.2	0.2
GRO/10	35.3	0.457	0.400	8.02	107.2	15.90	81.3	37.9	32.1
	1.2	0.012	0.013	0.06	0.6	0.12	0.5	0.3	0.2
GRO/11	17.0	0.453	0.416	8.10	110.1	16.10	81.8	37.8	32.29
	0.6	0.013	0.013	0.06	0.7	0.09	0.4	0.2	0.15
WSG/9	40.3	0.449	0.407	7.97	105.7	15.92	81.5	37.7	31.6
	1.4	0.013	0.012	0.06	0.8	0.10	0.7	0.3	0.2
WSG/11	34.1	0.448	0.399	8.11	107.1	16.21	82.4	38.5	32.28
	1.1	0.007	0.002	0.04	0.3	0.10	0.4	0.2	0.17

Gas concentrations in 10^{-10} cm^3 STP/g; [1] Total extraction at 1800°C without pre-step at 600°C.

7.8 Technical remarks

7.8.1 Noble gas abundances of gold blanks

Table 7.49: Main noble gas isotopes measured for CSSE gold blanks (including sample).

"G1" closed		^{4}He [10^{-10}cm^3]	^{20}Ne [10^{-13}cm^3]	^{36}Ar [10^{-12}cm^3]	^{40}Ar [10^{-10}cm^3]	^{40}Ar/^{36}Ar	^{84}Kr [10^{-15}cm^3]	^{132}Xe [10^{-15}cm^3]
Lancé	41d	1.12	479	149	341	228.3	3336	465
		0.08	17	6	12		53	9
	20h 40'	-0.2	63	7.7	18.5	240.3	181	23.3
		-1.4	34	0.4	1.2		4	1.9
Dimmitt	49d 5h	5856	9305	2861	5819	203.4	119716	52299
		41	118	66	129		1463	968
	21h	182	250	64	129	200.1	2522	1064
		2	27	9	12		33	24
Grosnaja	288h	-3	17	1313	3821	291.0	83845	55474
		-10	11	26	52		640	730
	24h	0	70	69.6	203	291.1	3893	2449
		6	11	1.4	3		44	31
Chainpur	ca. 168h	0.6	21	71.2	194	272.1	1281	123
		0.2	8	1.0	2		15	8
Cold Bokkeveld	ca. 216h	2	31	59.1	116.4	196.9	11108	21790
		2	5	1.4	1.9		229	732
	24h	2	22	28.5	53.1	186.3	3426	4480
		6	8	0.7	0.9		114	174
	50h 100°C[1]	1872	10870	10589	7427	70.1	588975	743278
		29	242	247	118		10392	24916
	22h	2	28	714	123	17.2	4256	7459
		4	3	17	14		86	249

[1] A first "gold blank" step without any fresh acid from the acid gold finger, but after heating of the sample to 100 °C, contained significant amounts of Q-like gases, probably due to etching of remaining acid droplets from earlier experiments. The blank is adopted as "step 0".

7.8.2 Neonhydride interference

As stated before, the etch experiments HB03 (Lancé) and HB04 (Dimmitt) were affected by insufficient H$_2$-cleaning. During these experiments the "SAES"-getter connected directly with the mass spectrometer volume has been run at higher temperatures ($\approx$ 400°C / 70 units / 17 V) in order to provide a lower background of N, O, CO and other reactive gases. Unfortunately, this also resulted in a too high hydrogen background and thus in a higher probability for the formation of neon-hydride. Due to the small abundance of ^{21}Ne, this isotope was influenced by the interference with ^{20}NeH. This problem was discovered by an apparently higher mass discrimination for the ratio ^{21}Ne/^{22}Ne (measured ratio / standard ratio = 1.079 (HB03) and 1.049 (HB04), respectively) compared with the discrimination for ^{20}Ne/^{22}Ne (1.010, 1.004). The interference was corrected with the following simple procedure. During two dilution series, ^{22}Ne and ^{22}NeH were measured. The resulting ratios ^{22}NeH/^{22}Ne depending on the ^{22}Ne amounts are plotted in Figure 7.3. For reasons of simplicity, these values were

fitted by two suitable linear fits that intersect, somewhat arbitrarily, at the ^{22}Ne counting rate of 22716 Hz. Assuming that the probability of forming ^{20}NeH and ^{22}NeH should essentially be the same, these two fits were used to calculate and subtract the ^{20}NeH interference on ^{21}Ne.
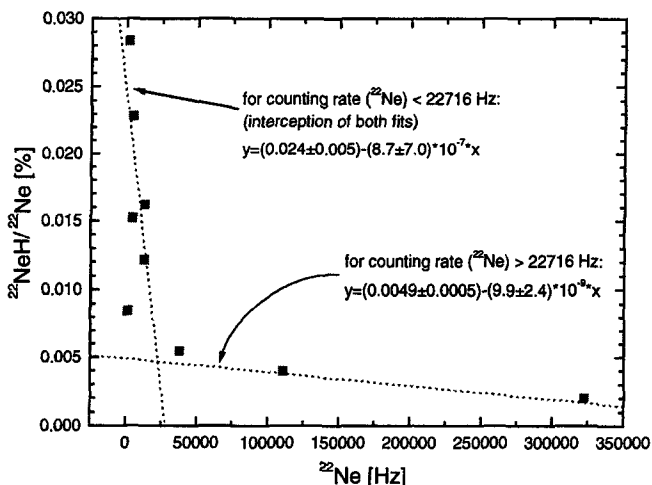

for counting rate (^{22}Ne) < 22716 Hz:
(interception of both fits)
$y = (0.024 \pm 0.005) - (8.7 \pm 7.0) \cdot 10^{-7} \cdot x$

for counting rate (^{22}Ne) > 22716 Hz:
$y = (0.0049 \pm 0.0005) - (9.9 \pm 2.4) \cdot 10^{-9} \cdot x$

Figure 7.3: The ^{22}NeH/^{22}Ne ratio depends on the ^{22}Ne concentration and is used to correct for the influence of ^{22}NeH on ^{21}Ne.

The corrections amount to 1-5 % of the measured ^{21}Ne in calibration steps ("Fast Calibrations") and 1-4 % in main gas-rich steps of runs HB03 and HB04. An error of 50% of the correction is added, which is enough to include the higher discrepancies in the mass discriminations mentioned above. However, this correction of interfering ^{20}NeH amounts to only 1.7% - 3.9% of the ^{21}Ne abundances in the gas-rich steps 1-8 of the etching of Lancé (step 9 contains almost no gas and is, thus, neglected). In the same way, 1.1% - 3.6% of the measured ^{21}Ne from Dimmitt are subtracted. All other experiments are executed with the getters at room temperature (0 units / 0 V) or 250°C (50 units / 12 V). No corrections have to be made for these experiments.

7.8.3 Atmospheric composition

Several sets of the atmospheric noble gas isotopic composition are known. We used data sets given in Table 7.50, Table 7.51 and Table 7.52 (bold values) for calibration. For Ne, the original atmospheric Ne data (Eberhardt *et al.* 1965) have been improved, since the commercial pure Ne used in our experiments is clearly composed distinctly . However, due to inconsistent mass discrimination that occurred during this work for the ratios ^{20}Ne/^{22}Ne and ^{21}Ne/^{22}Ne, respectively, I still suspect slight differences of the standard values to the real composition. This is discussed in chapter 7.8.4. Other data sets are also shown to allow re-calibration according to these atmospheric values.

Table 7.50: Atmospheric composition of He, Ne and Ar as used in this work.

^{3}He/^{4}He x 10^6	^{20}Ne/^{22}Ne	^{21}Ne/^{22}Ne	^{38}Ar/^{36}Ar	^{40}Ar/^{36}Ar	
1.399 ± 0.013	9.80 ± 0.08	0.0290 ± 0.0003	0.1880 ± 0.0004	295.5[1]	see references in Ozima
	9.72[2]	0.02887[2]			and Podosek (1983)
	9.7685 ± 0.0011	0.02871 ± 0.00008	5.34 ± 0.03	297.1 ± 0.3	Valkiers et al. (1994)
	9.786 ± 0.010	0.02920 ± 0.00011	5.325 ± 0.013	296.0 ± 0.5	Valkiers et al. (1994)

[1] adopted; [2] adopted after long-term analysis; [3] "IRMM 1992-93 MAT 271"; [4] "IUPAC selected best measurement 1989".

Table 7.51: Atmospheric composition of Kr.

^{78}Kr/^{84}Kr	^{80}Kr/^{84}Kr	^{82}Kr/^{84}Kr	^{83}Kr/^{84}Kr	^{86}Kr/^{84}Kr	source
0.609 ± 0.002	3.960 ± 0.002	20.217 ± 0.004	20.14 ± 0.02	30.52 ± 0.03	Basford et al. (1973)[1]
0.620 ± 0.002	4.001 ± 0.012	20.34 ± 0.06	20.18 ± 0.06	30.36 ± 0.06	Eugster et al. (1967a)[2]
0.618 ± 0.003	4.01 ± 0.02	20.50 ± 0.09	20.45 ± 0.09	30.98 ± 0.12	Eugster et al. (1967a)[3]
0.62032 ± 0.00013	4.0023 ± 0.0005	20.3251 ± 0.0015	20.1712 ± 0.0007	30.3539 ± 0.0008	Valkiers et al. (1994)[4]
0.632 ± 0.007	3.9975 ± 0.0071	20.330 ± 0.019	20.225 ± 0.019	30.372 ± 0.020	Valkiers et al. (1994)[5]

[1] used in this work; [2] uncorrected data "Atlas CH-4 spectrometer" used by Huss and Lewis (1994a) and Huss et al., (1996); [3] used by Eugster et al. (1967a) and Eugster et al. (1967b); [4] "IRMM 1992-93 MAT 271"; [5] "IUPAC selected best measurement 1989".

Table 7.52: Atmospheric composition of Xe (^{132}Xe = 100).

^{124}Xe/^{132}Xe	^{126}Xe/^{132}Xe	^{128}Xe/^{132}Xe	^{129}Xe/^{132}Xe	Source
0.3537 ± 0.0011	0.3300 ± 0.0017	7.136 ± 0.009	98.32 ± 0.12	Basford et al. (1973)[1]
0.3575 ± 0.0016	0.3331 ± 0.0015	7.14 ± 0.02	98.32 ± 0.35	Nier (1950b)[2]
0.3536 ± 0.0012	0.3308 ± 0.0007	7.099 ± 0.003	98.11 ± 0.04	Valkiers et al. (1998)[3]

Table 7.52: Atmospheric composition of Xe (^{132}Xe = 100).

^{130}Xe/^{132}Xe	^{131}Xe/^{132}Xe	^{134}Xe/^{132}Xe	^{136}Xe/^{132}Xe	Source
15.136 ± 0.012	78.90 ± 0.11	38.79 ± 0.06	32.94 ± 0.04	Basford et al. (1973)[1]
15.15 ± 0.05	78.76 ± 0.25	38.82 ± 0.11	32.98 ± 0.08	Nier (1950b)[2]
15.129 ± 0.005	78.906 ± 0.008	38.782 ± 0.007	32.916 ± 0.017	Valkiers et al. (1998)[3]

[1] used in this work; [2] used by Huss and Lewis (1994a); Huss et al., (1996) and Eugster et al. (1967b); [3] commercial Xe standard.

7.8.4 Mass discrimination

The determination of the Ne mass discrimination revealed a general trend: The mass discrimination (defined *only here* for Ne as standard ratio/measured ratio) obtained from the ^{21}Ne/^{22}Ne ratio has been relatively larger than that from the ^{20}Ne/^{22}Ne ratio (Table 7.53). This was observed in all experiments in both mass spectrometers (except for HB03 and HB04, where neonhydride *lowered* the mass discrimination, see chapter 7.8.2). This might suggest that the real standard (air) composition measured in this work is slightly different from the composition assumed prior to the experiments and given in chapter 7.8.3. The standard ^{20}Ne/^{22}Ne ratio should be larger or the ^{21}Ne/^{22}Ne ratio smaller, respectively. Several sets of data for atmospheric Ne are known. However, *commercial* one-element gas samples easily suffer fractionation. For our chosen value of $(^{20}$Ne/^{22}Ne$)_{std}$ = 9.72 (determined by comparison with air Ne according to Eberhardt et al., 1965 $(^{20}$Ne/^{22}Ne$)_{air}$ = 9.80), a 0.2 % lower value for ^{21}Ne/^{22}Ne (0.02882 instead of adopted 0.02887) would result in consistent mass discrimination for both Ne isotopic ratios. Especially in view of the new data by Valkiers et al. (1994), this seems possible. The

determination of the mass discrimination for the other elements according to the formula given in chapter 2.3.3 did not cause any problems. The values are given in Table 7.54.

Table 7.53: Ne mass discrimination (defined *here* as standard ratio/measured ratio) and calculated standard $^{21}Ne/^{22}Ne$ ratios for different choices[1] of $(^{20}Ne/^{22}Ne)_{std}$.

experiment	$(^{20}Ne/^{22}Ne)_{std}/_{msr}$	$(^{21}Ne/^{22}Ne)_{std/msr}$	$(^{21}Ne/^{22}Ne)_{std}$ for $(^{20}Ne/^{22}Ne)_{std} =$		
			9.72	**9.7685**	**9.80**
HB03	0.9897 ± 0.0009	*0.927 ± 0.003*[2]			
HB04	0.9963 ± 0.0011	*0.954 ± 0.004*[2]			
HB05	0.9917 ± 0.0009	1.004 ± 0.004	0.02877	0.02884	0.02889
HB06	0.9919 ± 0.0007	1.009 ± 0.003	0.02862	0.02869	0.02873
HB08I	0.9878 ± 0.0012	0.997 ± 0.003	0.02892	0.02899	0.02903
HB08II	0.9984 ± 0.0014	1.004 ± 0.003	0.02885	0.02892	0.02897
HB07	0.9568 ± 0.0004	0.985 ± 0.001	0.02880	0.02887	0.02891
HB09	0.9693 ± 0.0011	0.987 ± 0.004	0.02892	0.02899	0.02903
HB10	0.9708 ± 0.0013	0.991 ± 0.003	0.02885	0.02892	0.02896
average			**0.02882**	**0.02889**	**0.02893**

[1] see chapter 7.8.3; [2] NeH interference.

Table 7.54: Mass discrimination determined in this work [%/amu].

		"Albatros"			"Minneapolis"	
element	run	counter	Faraday cup	run	multiplier	Faraday cup
He	HB03	0.0 ± 0.0[1]	0.3 ± 0.2	HB07	-8.1 ± 0.5[1]	0.14 ± 0.03
	HB04	0.0 ± 0.0[1]	0.9 ± 0.2	HB09	-8.1 ± 0.5	0.20 ± 0.09
	HB05	0.0 ± 0.0[1]	0.4 ± 0.2	HB10	-10.9 ± 1.2	0.26 ± 0.09
	HB06	0.0 ± 0.0[1]	-0.0 ± 0.3			
	HB08/I	0.0 ± 0.0[1]	0.5 ± 0.3			
	HB08/II	0.0 ± 0.0[1]	0.6 ± 0.2			
Ne[2]	HB03	-0.52 ± 0.05	1.9 ± 0.8	HB07	-2.16 ± 0.02	0.09 ± 0.08
	HB04	-0.18 ± 0.06	1.7 ± 0.7	HB09	-1.54 ± 0.06	-0.2 ± 0.4
	HB05	-0.42 ± 0.05	0.0 ± 0.0[1]	HB10	-0.8 ± 0.6	-0.02 ± 0.05
	HB06	-0.40 ± 0.03				
	HB08/I	-0.08 ± 0.07	0.0 ± 0.0[1]			
	HB08/II	-0.61 ± 0.06				
Ar	HB03	0.65 ± 0.05	1.16 ± 0.10	HB07	0.07 ± 0.09	0.88 ± 0.03
	HB04	0.86 ± 0.07	0.88 ± 0.12	HB09	-0.15 ± 0.20	0.75 ± 0.07
	HB05	0.45 ± 0.08	1.09 ± 0.08	HB10	-0.24 ± 0.14	0.73 ± 0.07
	HB06	0.42 ± 0.05	0.93 ± 0.08			
	HB08/I	0.56 ± 0.10	1.49 ± 0.11			
	HB08/II	0.21 ± 0.05	1.28 ± 0.12			
Kr	HB03	-0.65 ± 0.08	0.0 ± 0.0[1]	HB07	-1.09 ± 0.04	
	HB04	-0.41 ± 0.06	-0.1 ± 2.5	HB09	-0.37 ± 0.15[1]	
	HB05	-0.53 ± 0.05	0.0 ± 0.0[1]	HB10	0.75 ± 0.06	
	HB06	-0.59 ± 0.03				
	HB08/I	-0.30 ± 0.05				
	HB08/II	-0.70 ± 0.04				
Xe	HB03	-0.25 ± 0.03	0.0 ± 0.0[1]	HB07	-0.65 ± 0.02	
	HB04	-0.02 ± 0.09	0.0 ± 0.0[1]	HB09	-0.37 ± 0.15	
	HB05	-0.13 ± 0.05	0.0 ± 0.0[1]	HB10	-0.45 ± 0.04	
	HB06	-0.27 ± 0.02				
	HB08/I	-0.09 ± 0.07				
	HB08/II	-0.29 ± 0.08				

[1] adopted value; [2] determined only from $^{20}Ne/^{22}Ne$, see text.

Curriculum Vitae

Henner Busemann

May 31, 1967	born in Hannover, Germany
1973-1977	Primary school Grundschule an der Uhlandstraße, Hannover
1977-1986	Gymnasium Lutherschule, Hannover
1988-1994	Study of Physics at the University of Hannover
1994	Diploma at "Zentrum für Strahlenschutz und Radioökologie der Universität Hannover" (Center for radiation protection and radioecology at the University of Hannover)
	Diploma thesis: "Experimentelle Bestimmung und theoretische Interpretation von Dünntarget-Wirkungsquerschnitten protonen-induzierter Reaktionen" (Experimental determination and theoretical interpretation of thin-target cross-sections of proton-induced reactions)
1994-1998	PhD. student and assistant position at Institute of Isotope Geology and Mineral Resources, ETH Zürich

Acknowledgements

Finally, a pleasant, but also very difficult task (since this is surely the most or only read page of this thesis) is to thank all the people that have accompanied, encouraged and supported me during the very interesting time of my PhD studies at ETH in Zürich. In more detail and first of all, I thank my supervisor Rainer Wieler for all the help and educating discussions (not exclusively about soccer...!) during four instructive years and, especially, for causing an extraordinarily enjoyable and motivating "low pressure" atmosphere in our lab. Merssi vielmal! In particular, I am grateful to Heiri Baur for his incredible patience and knowledge, for the technical support and the introduction into (some of) the mystic secrets of mass spectrometry. Furthermore, I thank Uli Ott for his -as usual- very careful, detailed and fast corrections and advice, as well as Alex Halliday for being very interested in this rather especial extraterrestrial "Q-stuff". The self-sacrificing Rainer Wieler, Suzan van der Lee and Jörg Schäfer spent a lot of time and thoughts on correcting and organising my first, second, and... drafts and finally brought this thesis into a (somewhat more) readable and English-resembling form. Laura Bruno, Jörg Schäfer, Ingo Leya, Britt Meyer and Veronika Heber contributed largely to the mostly very positive and always very intimate atmosphere in our noble gas group, allowing for a lot of fun and friendship, conversations, numerous nights of drinking and also very helpful and inspiring discussions.

I can not imagine what would have happened to me without thorough "how-to-get-used-to-Swiss-life introductions" and without the friendship I obtained by several (similarly alien) people as Berta Ordóñez-Casado, Roland Mundil, Ulrike Kastrup, Mara Cortes, Jörg Schäfer, Insa Neuweiler and Claudia Schmellentin. A special "Vielen Dank" for the "long-distance support" goes to all the Hanoverians, especially, to Anja-Alexandra Ziegler. Last but most importantly, I thank my parents, my sisters Karin and Heike, and Suzan for all their help, motivation and understanding.